ЖУРНАЛ
ЭКСПЕРИМЕНТАЛЬНОЙ И ТЕОРЕТИЧЕСКОЙ
ФИЗИКИ
АКАДЕМИЯ НАУК СССР

SOVIET PHYSICS

JETP

VOLUME 4 NUMBER 1

A Translation

of the

Journal of Experimental and Theoretical Physics

of the

Academy of Sciences of the USSR

FEBRUARY, 1957

Published by the

AMERICAN INSTITUTE OF PHYSICS
INCORPORATED

SOVIET PHYSICS
JETP

A translation of the Journal of Experimental and Theoretical Physics of the USSR.

A publication of the

AMERICAN INSTITUTE OF PHYSICS

Governing Board

Frederick Seitz, *Chairman*
Allen V. Astin
Robert F. Bacher
W. S. Baird
H. A. Bethe
R. T. Birge
Frank D. Dexter
I. C. Gardner
S. A. Goudsmit
Charles Kittel
Hugh S. Knowles
R. B. Lindsay
William F. Meggers
Harry F. Olson
R. R. Palmer
R. F. Paton
Eric Rodgers
Ralph A. Sawyer
H. D. Smyth
Mark W. Zemansky

Administrative Staff

Henry A. Barton,
Director
Mark W. Zemansky,
Treasurer
Wallace Waterfall,
Executive Secretary
Theodore Vorburger,
Advertising Manager
Ruth F. Bryans,
Publication Manager
Alice Mastropietro
Circulation Manager
Kathryn Setze,
Assistant Treasurer
Eugene H. Kone,
Director of Public Relations

American Institute of Physics Advisory Board on Russian Translations

Elmer Hutchisson, *Chairman*
Dwight Gray, Morton Hamermesh, Vladimir Rojansky,
Victor Weisskopf

Editor of Soviet Physics

Robert T. Beyer, Department of Physics, Brown University,
Providence, R.I.

Soviet Physics is a monthly journal published by the American Institute of Physics for the purpose of making available in English reports of current Soviet research in physics as contained in the Journal of Experimental and Theoretical Physics of the Academy of Sciences of the USSR. The page size of Soviet Physics will be 7⅞" x 10½", the same as other Institute journals.

Transliteration of the names of Russian authors follows the system employed by the Library of Congress.

This translating and publishing project was undertaken by the Institute in the conviction that dissemination of the results of researches everywhere in the world is invaluable to the advancement of science. The National Science Foundation of the United States encouraged the project initially and is supporting it in large part by a grant.

The American Institute of Physics and its translators propose to translate faithfully all the material in the Journal of EXPERIMENTAL AND THEORETICAL PHYSICS OF THE USSR appearing after January 1, 1955. The views expressed in the translated material, therefore, are intended to be those expressed by the original authors, and not those of the translators nor of the American Institute of Physics.

Two volumes are published annually, each of six issues. Each volume contains the translation of one volume of the Journal of EXPERIMENTAL AND THEORETICAL PHYSICS OF THE USSR. New volumes begin in February and August.

Subscription Prices:

Per year (12 issues)	
United States and Canada	$60.00
Elsewhere	64.00
Back Numbers	
Single copies	$ 6.00

Subscriptions should be addressed to the American Institute of Physics, 57 East 55 Street, New York 22, New York.

Copyright by American Institute of Physics 1957

SOVIET PHYSICS

JETP

The Translation Journals of the American Institute of Physics

Since the fall of 1955, the American Institute of Physics has been carrying out a program of translating Russian physics' journals. The present journal, now in its fourth volume, has recently been followed by three others:

Soviet Physics – Technical Physics

A translation of the "Journal of Technical Physics" of the Academy of Sciences of the U.S.S.R. Approximately 4,000 Russian pages per year. Annually, $90.00 domestic, $95.00 foreign.

Soviet Physics – Acoustics

A Translation of the "Journal of Acoustics" of the Academy of Sciences of the U.S.S.R. Four issues per year, approximately 500 Russian pages. Annually, $20.00 domestic, $22.00 foreign. The 1955 issues of "Journal of Acoustics" U.S.S.R. will also be published. This will consist of two volumes, approximately 500 pages, and the subscription price will be $20.00 for the set.

Soviet Physics – Doklady

A translation of the "Physics Section" of the Proceedings of the Academy of Sciences of the U.S.S.R. Six issues per year, approximately 900 Russian pages. Annually, $25.00 domestic, $27.50 foreign.

All of these journals can be subscribed to through the American Institute of Physics, 57 East 55th Street, New York 22, N. Y.

The response to Soviet Physics JETP has been excellent. The subscription list is above 800 and growing. Subscriptions to the other journals, however, have lagged far behind. The Institute would therefore like to call them to your attention, to recommend them as additions to the library of your school or laboratory. Increased support is mandatory if the project is to be maintained at its present level.

SOVIET PHYSICS JETP VOLUME 4, NUMBER 1 FEBRUARY, 1957

Direct Measurement of Molecular Attraction of Solid Bodies. II. Method for Measuring the Gap. Results of Experiments. *

I. I. ABRIKOSOVA AND B. V. DERIAGIN**
Institute of Physical Chemistry, Academy of Sciences, USSR

(Submitted to JETP editor, December 14, 1955)
J. Exptl. Theoret. Phys. (U.S.S.R.) 31, 3 - 13 (January, 1956)

Results are presented of measurements of molecular attraction for fused quartz for distances from 0.08 to 1 μ. The data are in good agreement with calculations using the formula of the theory of E. M. Lifshitz, which deals with the case of separations which are much greater than the wavelengths of the fundamental ultraviolet absorption bands, and which contains no undetermined empirical constants. The agreement obtained substantiates both Lifshitz' theory and the electromagnetic nature of the molecular forces which was already suggested by P. N. Lebedev in 1894.

The results of measurements of Overbeek and Sparnaay exceed the theoretical values by almost a factor of 10^4, apparently due to electrostatic effects.

1. METHOD OF MEASUREMENT OF SEPARATION

THE size of the minimum gap H between the lens L and plate P was calculated from the diameter of Newton's rings measured with a microscope provided with an ocular scale, when the gap was illuminated by light from a 300 watt lamp through a constant deviation monochromator and the vertical illuminator of the microscope (see Fig. 1). It is easy to find the relation between the gap H, the diameter d_m of the m th dark ring, the wave length λ of the monochromatic light, and the radius R of the spherical surface. The condition for producing the mth dark ring is

$$2\delta_m + 2H + \lambda/2 = (2m+1)\lambda/2. \quad (1)$$

From the geometry, it is clear that the part of the air gap which is denoted by δ_m in Fig. 2 is related to the diameter d_m of the m th ring by the relation

$$\delta_m = d_m^2 / 8R.$$

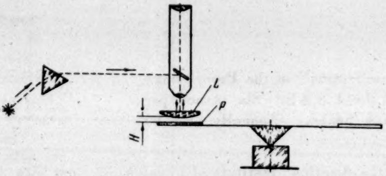

FIG. 1

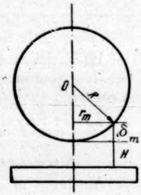

FIG. 2.

Substituting for δ_m in terms of d_m in Eq. (1), we obtain for the minimum distance H between the surfaces the expression

$$H = \frac{\lambda}{2}\left(m - \frac{d_m^2}{4R\lambda}\right), \quad (2)$$

from which it follows that to determine H we must know m, d_m, λ and R.

To determine the ring number m one can, while observing the rings, bring the surfaces into contact and thus compute the order number of the ring. Such a procedure is unsuitable when measuring molecular attraction, because of the possibility of contact electrification. We therefore used a different method based on the changes in the diameter of the interference ring when the number m and the wavelength λ of monochromatic light are varied for constant H.

We introduce the quantities $\Delta(d_m)^2$ and $\Delta(d_\lambda)^2$, defined by the following equations:

$$\Delta(d_m^2) = d_{\lambda+\Delta\lambda,\,m}^2 - d_{\lambda,\,m}^2 \quad (3)$$

---

*Cf. the literature references in Reference 1.

**F. B. Leib participated in the development of the technique.

and

$$\Delta (d_\lambda^2) = d^2_{\lambda,\, m+\Delta m} - d^2_{\lambda,\, m}. \qquad (3')$$

Using the relation (2), we can write

$$\Delta (d_m^2) / \Delta\lambda = 4Rm \qquad (4)$$

and

$$\Delta (d_\lambda^2) / \Delta m = 4R\lambda. \qquad (4')$$

Dividing (4) by (4 ′), we get for m the expression

$$m = \lambda \Delta (d_m^2)\, \Delta m / \Delta (d_\lambda^2)\, \Delta\lambda. \qquad (5)$$

Before starting the fundamental measurements, i. e., the measurement of the force of attraction F and the corresponding gap H, the number m of a particular ring was determined from (5), and from it the numbers of other rings. The radius R of the spherical surface was measured using the same optical system. According to (2), d_m^2 depends linearly on m for constant λ and H. If we plot d_m^2 as ordinate and m as abscissa, then if we divide the tangent of the angle between the line $d_m^2 = f(m)$ and the m axis by 4 λ, we get the radius R.

Since λ, m and R were always determined before the fundamental measurement, the latter reduced to measurement of a current i and the diameter of one (sometimes 2 – 3) interference ring. This last fact made possible the successful performance of the experiment, since it enabled us to concentrate our attention on the simultaneous measurement of only two quantities.

The precision of measurement of the gap H was almost entirely determined by the uncertainty in measurement of the diameter of the m th (usually the second) ring d_m, which amounted (for d_2) to ~ ± 1%, which guaranteed an accuracy in the measurement of the gap H of approximately $\pm 0.002\,\mu$.

2. CLEANING OF SURFACES

The method of cleaning the glass and quartz surfaces with which the interaction was studied was an essential point. For a successful experiment, the surfaces must be carefully cleaned of all films and dust particles.

The usual methods of chemical cleaning such as washing with chromic acid cleaner were not used, since they sometimes damage polished glass surfaces. We successfully used the following method for thorough cleaning of glass and quartz surfaces. We washed the plate and lens with distilled alcohol and ether, using cotton from which the grease had been removed in a Soxhlet extractor, and then processed them in a glow discharge under glass wool. The purity of the surface could be judged from the fact that after cleaning we always observed complete wetting of the glass surface by water.

It proved to be far more difficult to rid the surfaces of dust. Of all the methods tried by us (removal of dust particles with a grease-free brush, cotton, fabric, chamois, etc.), the best results were gotten when the surfaces (after cleaning in a glow discharge) were rubbed with grease-free cotton slightly moistened with pure ether. (This last step was, of course, for removal of dust and not for improving the cleanliness of the surface). The surfaces remained free of film after such treatment since, as was the case immediately after cleaning in the glow discharge, they were completely wet by water.

Before placing them on the balances, the surfaces were examined under a binocular microscope at 100 - fold magnification.

3. FUNDAMENTAL EXPERIMENTAL DIFFICULTIES AND THEIR ELIMINATION

The main experimental difficulties were associated with 1) sensitivity of the apparatus to vibrations of the support, 2) dust particles falling on the surfaces under investigation, 3) electrification of the surfaces during cleaning.

1) The true sensitivity of the apparatus for determining the interaction force depends essentially on the vibration of the support on which the apparatus is placed; we therefore carried out special experiments to study the vibration of the apparatus and the effect of various damping mechanisms.

Vibrations of the support result in fluctuations of the current in the feedback circuit. By eliminating in turn all the sources of current fluctuations, we established that their main cause is the presence of industrial and vehicular noises which are transmitted through the ground and which vary in time in both amplitude and frequency. To measure the damping properties of various supports, we removed the beam balance from our circuit, and put a mirror on the platform in its place (cf. Fig. 5, Ref. 1); we thus obtained a sensitive photoelectric indicator of vibrations of the support. Because of the fact that we had to come into direct contact with the equipment during preparation for measurement and during the measurement itself, damping mechanisms such as are used in setting up sensitive galvanometers were not suitable. We succeeded in obtaining the best results by placing the apparatus on a table with shock absorbers, which in turn was placed on a cement pedestal which was isolated from the foundation and embedded in the ground. (See Fig. 5, Ref. 1.)

To decrease the effect of vibration further, the optical relay system was improved: light reflected from mirror S_1 (Fig. 3) fixed on the beam balance was reflected once more from mirror S_2 which was coupled to the platform (cf. Fig. 5 of Ref. 1), which made the photocurrent independent of vibrations common to both the beam balance and the platform, and dependent only on the gap H.

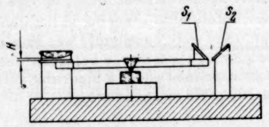

FIG. 3.

The angle between mirrors S_1 and S_2 was approximately 90°. By means of a screw brought out under the platform we could regulate the position of mirror S_2 for adjustment of the apparatus.

2) The preparation of samples for measurement is a very important part of the experiment, since during cleaning the surfaces of dust the samples become electrified, as a result of which they interact with a force which far exceeds the molecular attraction and masks it. To eliminate charges from the surfaces of the plate and lens, we had to separate them and, by some means, ionize the air around the apparatus. When this was done, dust particles from the air frequently fell on the surfaces, and we had once again to clean them and remove the charge, until we succeeded in removing both the dust particles and the electrostatic interaction. As the tests showed, dust does not enter the gap if the distance between plate and lens is very small, so that it is important to achieve simultaneous absence of dust and charge once, and then not separate the surfaces by more than 5 – 10 μ.

3) Electrical charges develop on clean dry surfaces very easily, from even the slightest contact with a clean brush or rubber gloves. Each time, before we succeeded in measuring the molecular attraction, we had to get rid of the surface charges by ionizing the air. We used the radioactive isotope S^{35} to remove the charges from the quartz surfaces. Removal of the charge turned out to be impossible when the surfaces were very close. Only for very large separations of the surfaces (1 mm and greater) was the action of the ionizer effective, which showed that the attractive forces observed previously were of electrical origin. The slow discharge when the gap between the surfaces is narrow is probably explained by the fact that very few ions enter such a gap.

As already mentioned, the sensitivity of the apparatus for measuring the attractive force is almost entirely determined by the current fluctuations in the feedback loop caused by vibrations of the support. For this reason, at the beginning, when we did not use all the methods described in this Section for preventing the vibration, the sensitivity proved to be insufficient for detecting and measuring the molecular attraction. After getting rid of the charges, no attraction between the surfaces was detected up to gaps of $H = {\sim}0.05\ \mu$, while the accuracy of the force measurement was $\pm 10^{-2}$ dyne.

4. RESULTS OF MEASUREMENT

The basic result of the work is the detection and quantitative measurement of the molecular attraction between samples of fused quartz separated by a gap of $10^{-5} - 10^{-4}$ cm.

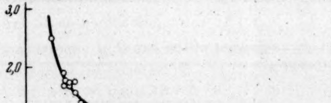

FIG. 4.

TABLE 1.

$R=10$ см (measurements in air)		$R=10$ см (measurements in air)	
H in μ	$F\cdot10^3$ in dynes	H in μ	$F\cdot10^3$ in dynes
0.09	1.5_0	0.17	0.5_6
0.13	0.9_0	0.19	0.3_7
0.13	0.8_0	0.32	0.1_9
0.13	0.7_0	0.59	0.0
0.14	0.7_0	0.64	0.0
0.16	0.7_5	0.82	0.0

In Fig. 4 and Table 1 we give the dependence of the force of attraction F on the separation H, as measured in air (the radius of the sphere was $R = 10$ cm).

This dependence $F(H)$ corresponds to the minimum of all the attraction effects observed by us with quartz glass samples. This last point, together with the satisfactory reproducibility of the effect in different experiments, made it possible for us to assume that the effect was of molecular origin. However, to convince ourselves completely of the validity of this assumption, we had to assure ourselves of the absence of spurious attraction effects in our experiments. The most important disturbing influence in measuring the molecular attraction was the electrostatic interaction of the samples. One might therefore suppose that the dependence shown in Fig. 4 includes an electrostatic contribution, and that the molecular attraction which we are trying to measure is only a part of what is measured in the experiment.

If the electrostatic charges are removed completely and the observed attraction between the objects is actually the molecular attraction, then it should be 1) insensitive to repeeated ionization of the air around the samples; 2) proportional to the radius of the spherical surface (cf. Eq. 9 of Ref. 1) ; 3) reproducible from experiment to experiment both with respect to magnitude and with respect to the manner in which the force falls off with distance; 4) reproducible in experiments where the surfaces are brought close to one another at various points; 5) unaffected by removal of air from the gap between the objects.

Further investigations were devoted to checking whether these points were fulfilled by the attraction which we claimed to be molecular. The measurements in vacuum proved to be the most exact and reproducible. The results of experiments in vacuum are given in Fig. 5 and Table 2. Curve I refers to a radius $R = 10$ cm, curve II to $R = 26$ cm. Within the limits of error of the measurements, these data satisfy all the requirements enumerated above.

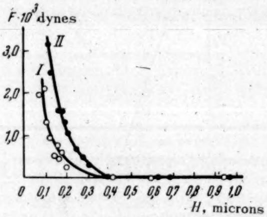

FIG. 5.

TABLE II.

$R=10$ см		$R=26$ см	
H in μ	$F\cdot10^3$ in dynes	H in μ	$F\cdot10^3$ in dynes
0,08	1.9_5	0,13	3.1_4
0,10	2.0_8	0,14	2.4_9
0,11	1.3_0	0,17	1.5_7
0,13	0.9_1	0,18	1.5_7
0,15	0.5_2	0,20	1.3_1
0,16	0.7_2	0,22	1.0_5
0,17	$0,4_6$	0.25	$0,6_6$
0,18	0.5_9	0,28	0.4_6
0.20	$0,2_6$	0.31	0.2_6
0.42	0	0,42	0
0,64	0	0,62	0
0,96	0	0.71	0
		0.96	0

In Fig. 6, we show on a log-log scale the results of a large number of experiments which were separated by large time intervals and were carried out with various quartz samples. The lens radius was $R = 11.1$ cm. The open circles show points which were gotten from measurements in air. Just before each of these measurements, the air around the samples was subjected to repeated ionization by strong sources. (The straight line shown in the figure was calculated from Lifshitz' theory, which we shall discuss later.)

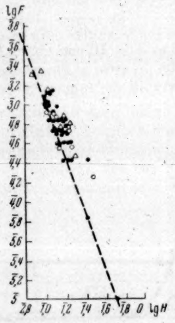

FIG. 6

According to Eq. (9) of Ref. 1, the quotient of $F(H)$ by $2\pi R$, where R is the radius of the spherical surface, is the energy of attraction, $U(H)$, of two infinite plates, per square cm of area. Figure 7 shows the dependence of the energy U on the separation H, where the dark circles refer to experiments with lens radius $R = 11.1$ cm, the triangles — $R = 10$ cm, and the open circles — $R = 25.4$ cm. This graph illustrates the linear dependence of the attractive forces on the sphere radius, and thus shows that the attractive energy $U(H)$ for the plane case does not depend on which lens was used for measuring the force of attraction.*

Thus all the points enumerated above are satisfied.

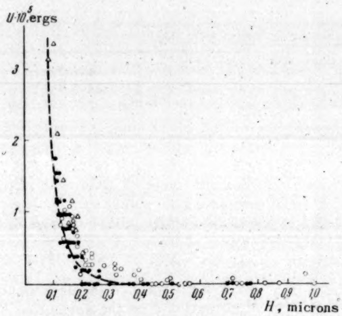

FIG. 7.

5. DISCUSSION OF RESULTS

Considering that the present work has as its purpose the detection and measurement of an effect whose existence could not be demonstrated previously by direct experiments, we feel that it is necessary to consider in more detail the analysis of the results of the measurements and the basis for their interpretation. Such an analysis requires us to look at two questions: the demonstration that the effect discovered in this work is not the consequence of some deficiency in the method of measurement, and the demonstration that the attraction measured in the present work is not associated with some other non-molecular attraction.

The agreement between measurements done in air and in vacuum indicates that they are independent of convection currents; radiometer effects, the presence of a viscous air layer between the bodies, and of the presence of water vapor in the air.

To avoid errors in the measurements due to various mechanical effects of parts of the apparatus, for example elastic forces in the wires carrying current to the coil, friction between the knife edge and its bearing, dust particles remaining on the surfaces of the bodies, etc., we took the following precautions. The elastic effect of the conductors was reduced to a minimum by using very thin wollaston wire annealed over a gas flame. The agate prism and its agate bearing satisfied all the requirements which are imposed on such components in the best types of microanalytic balances. In good microanalytic balances having a balance arm and pans weighing several tens of grams, friction does not hinder weighing to $10^{-5} - 10^{-6}$ gm. Since friction is proportional to load, it is understandable why with our balance, where the beam weighed 0.1 gm, we could completely neglect the friction between the prism and its support in measurements with an accuracy of $1 - 2 \times 10^{-7}$ gm.

---

*We have not been able to increase the number of different radii R, since for $R < 10$ cm the attractive forces are small, while for $R > 26$ cm it is very hard to avoid the effects of dust particles.

The presence of dust on the surfaces, which could influence the measurements, was always detected by observing the appearance, as the gap was decreased, of repulsive forces which could be recorded by our equipment with the same sensitivity as were the attractive forces, and which never varied smoothly with varying distance. The measurements were taken only if, when the gap was decreased to 0. 05 – 0.1 μ, no forces other than the attractive forces were observed.

We also believe that the observed attraction cannot be explained by the presence of films remaining on the surfaces after cleaning. The presence on the quartz surfaces of adsorbed water layers, which is unavoidable when measurements are made in air or in poor vacuum, did not affect the results of the measurement since, first of all, the separation between the objects was much greater than the possible thickness of such layers, and, secondly, the dielectric constant, which is closely related to the magnitude of the molecular attraction, is approximately the same for adsorbed layers of water as it is for quartz.

If the dielectric constants of the layer and the quartz are almost the same, then the presence of an adsorbed layer of thickness, say, 10 A, is equivalent to a change of the gap by an amount of the same order, i. e., by 10 A, which for an accuracy in measurement of H of ~ 100 A has no effect whatsoever on the results. The assumption that an adsorbed water layer has about the same dielectric constant as quartz is supported by experiments of Kurbatov[2] who finds that even for a thickness of 4 – 5 monolayers the dielectric constant of an adsorbed water layer is lower by an order of magnitude than that of the volume phase.

Different cleaning methods were used in various experiments. For example, the curve of Fig. 4 refers to experiments where the dust particles were removed with a grease-free brush, whereas the graphs of Figs. 5 and 6 are for cases where ether and grease-free cotton were used for cleansing. If we should claim that the attraction is associated with the surface films, then the agreement of the results of so many experiments would make it necessary to assume that the same surface film was present in all cases, which is altogether improbable.

The absence of a possible effect of contact electrification of the quartz surfaces on the results of the measurements was verified in the experiment.

Even without making the appropriate computations, we can say that the attractive forces shown, for example, in Fig. 5 are not gravitational forces, since the latter cannot show such a marked change when the gap is changed by an amount small compared to the separation of the centers of mass of the bodies.

There is no need to discuss magnetic forces for the case where quartz samples are used. As for attractive forces between the bodies due to their electrification, these were discussed in detail earlier.

6. COMPARISON WITH THEORY

1) Comparison with the results of computations based on summation of interactions of all pairs of molecules.

If we follow the method of summation of interactions of all pairs of molecules, which is the one used until recently,[1] then for the case of a sphere and a plane we must use the formula

$$F = AR/6H^2.$$

Substituting the results of our experiments in this formula, we get for the constant A the value 5×10^{-14} ergs. But the constant A for quartz is approximately 10^{-12} ergs, i.e., 20 times greater than the value given by the experiment.

Such a comparison shows the unsuitability of the computational methods used up to now (at least, for the case of distances of order 10^{-5} cm). We may therefore assert that the results of the experiments have quite general significance, despite the fact that only one material was measured.

If we use the same summation method, but include the correction of Casimir and Polder (cf. Ref. 1), then we should use the formula

$$U = A_1/30\pi H^3.$$

for the energy $U(H)$.

Substituting our experimental results, we obtain for the constant A_1 a value of approximately 3×10^{-18} erg – cm. Using the formula $A_1 = \pi^2 q^2 c_1$ we get $A_1 = 1 \times 10^{-18}$ erg – cm (the value of the polarizability α being taken from the work of Margenau[3]).

Thus here too there is disagreement between theory and experiment, but the discrepancy is much less than for the case where the London forces are summed.[1]

2) Comparison with the theory of E. M. Lifshitz.

Precise comparison with the theory of Lifshitz[4] requires adequate knowledge of the optical properties of the material within its absorption regions. However the character of the absorption of quartz (its transparency for wavelengths equal to the gaps H used in the experiments) enables us to make an approximate theoretical estimate.

The theoretical value of the force per cm ^{2} for two plates is given for quartz by the formula

$$f(H) = \frac{\hbar c}{H^4}\frac{\pi^2}{240}\left(\frac{\varepsilon_0 - 1}{\varepsilon_0 + 1}\right)^2 \varphi(\varepsilon_0),$$

where ϵ_0 is taken equal to the square of the refractive index in the optical region, and $\varphi(\epsilon_0)$ is given by the table presented in Reference 1.

In order to compare the theoretical values with directly measured experimental quantities, we carry out a series of transformations. By integrating the expression for $f(H)$, we get a formula for the energy of attraction, per cm ^{2}, for two plates, in the form

$$U(H) = \frac{-\hbar c}{3H^2}\frac{\pi^2}{240}\left(\frac{\varepsilon_0 - 1}{\varepsilon_0 + 1}\right)^2 \varphi(\varepsilon_0).$$

The dotted curve in Fig. 7 shows $U(H)$ as computed from this formula, where ϵ_0 was taken equal to the square of the index of refraction in the optical region.

To go over from the energy $U(H)$ to the force $F(H)$ between a sphere of radius R and a plane, we make use of the relation given earlier:

$$F(H) = 2\pi R U(H).$$

The dependence of $F(H)$ calculated in this fashion is given in log-log plot in Fig. 6 (for R = 11. 1 cm).

Considering the roughness of the estimate as well as the uncertainties in the measurements, such agreement can be regarded as altogether satisfactory.

The agreement of experiment and theory shown in the graphs (cf. Figs. 6 and 7) should be regarded on the one hand as support of the validity of the theory of E. M. Lifshitz, and on the other hand as one of the essential proofs of the molecular nature of the attractive effect measured in the experiment.

The agreement of the results of experiment with a theory which explains the molecular interaction as the effect of electromagnetic fields, which exist within every absorbing medium and extend beyond its boundaries, enables us to answer a question which was posed by P. N. Lebedev in 1894 (cf. Ref. 1). Molecular attraction actually does " reduce to electromagnetic forces " and "no other forces of presently unknown origin " enter into its description.

We note that in the experiments of Overbeek and Sparnaay,[5] results differing from ours were obtained. Overbeek and Sparnaay measured the attractive forces between plates of fused quartz by means of a special dynamometer in which the shift of the spring was measured by an electric capacitor method; the separation of the plates was determined from the interference fringes produced by the narrow slit; in the discussion of the Faraday Society in 1954, this work was presented at the same time as ours.[6] The results of the Dutch workers were given in the form of a graph, on a logarithmic scale, of the dependence of the attractive force on distance, and a computation of the experimental value of the constant A which was found to be 3.8×10^{-11} erg.

If we make the computation according to Lifshitz' theory, then we obtain, for a separation of 1200 A between quartz plates, an attractive force of approximately 2×10^{-4} dynes / cm ^{2}, whereas this distance corresponded to a force of 1 dyne in the experiments of Overbeek and Sparnaay. Thus the experimental data are higher than theory by about a factor of 10.[4]

The poor reproducibility of the data of Overbeek and Sparnaay as well as the too high value of the attractive effect found in their experiments are probably associated with surface electrification.

3) Application to the theory of Coagulation.

According to the theory of Fuchs[7] the rate of coagulation of a disperse system whose particles of radius r attract one another with an energy $U(x)$ as a function of the distance x between their centers, is increased relative to the case where $U(x) = 0$ which was treated by M. Smoluchowski by a factor of

$$1 : 2r \int_{2r}^{\infty} \frac{\exp\{-U(x)/kT\}\,dx}{x^2} \qquad (6)$$

$$= 1 : \int_{0}^{\infty} \frac{\exp\{-U/kT\}\,d\tau}{(1+\tau)^2},$$

where

$$\tau = (x - 2r)/2r.$$

If τ is sufficiently small (compared to the wavelengths of the fundamental bands in the absorption spectrum of the particles) then, for values satisfying the condition $x - 2r \ll 2r$, U can be expressed as

$$U = \frac{A\,2r}{24\,(x-2r)} = \frac{1}{24}\,\frac{A}{\tau}.$$

Considering that $A / 24$ and kT are quantities of the same order of magnitude, we see that the coefficient of acceleration of coagulation will be considerably greater than unity * , since U / kT will have sizable values over quite a wide range of values of τ starting from zero, so the acceleration coefficient will be independent of r. However if r is made sufficiently large, this result is changed. In fact, for sufficiently large r, the main part of the integral in (6) comes from values of x for which we must introduce corrections for electromagnetic retardation, which reduces U and consequently also decreases the acceleration of the coagulation. So, for example, for aerosols with particles having $r > 0.3\ \mu$, the acceleration of the coagulation due to the effects of molecular forces will be extremely small.

The situation is different in the case of lyophobic sols, where in addition to the attractive energy there is an energy of repulsion caused by the overlap of the ion clouds of the two particles. In this case, for sufficiently coarse particles both terms in the interaction energy will (at those distances for which they are sizable) be proportional to the radius; therefore the presence or absence of an energy barrier for the resultant interaction, which essentially determines the stability of the system, will not depend on the radius of the particles but only on the law of falloff with gap width of the two terms in the interaction energy. It is therefore obvious that for small thicknesses of the ion atmospheres (i. e. for medium and high concentrations of electrolyte) less than 10^{-6} cm, the behavior of the molecular forces is important for distances where corrections for electromagnetic retardation are not necessary, so that the previously developed theory of the stability of sols, and in particular the sixth power law[9] for the coagulating effect of ions of opposite sign, (the Hardy – Schulze law), remains valid. The limit of applicability of this law is therefore not determined by the particle radius** but by the concentration: for very low concentrations, because of the more rapid dropoff of the attractive force at large distances (because of the extra power of the gap width), it is easy to show that the 6 th power law should go over into an 8 th power law. Since very small coagulant concentrations can be observed only for highly charged (tri – or quadrivalent) ions, such an effect is to be expected only for these cases.

CONCLUSIONS

1. A method is developed which enables one to measure the interaction between very smooth, solid, transparent bodies as a function of their separation. The force is measured by means of a special beam microbalance with photocell-magnet negative feedback. The separation of the bodies is computed from the diameters of Newton's rings. The range of forces measured is $1 - 2 \times 10^{-4} - 20$ dynes, and the separations $10^{-5} - 10^{-3}$ cm.

2). The molecular attraction of samples of quartz glass was detected and measured. The energy of attraction per cm^2, $U(H)$, between two plates varies with separation H approximately as H^{-3}, and is approximately 1×10^{-5} ergs for $H = 1.5 \times 10^{-5}$ cm.

3.) It is shown experimentally that the attractive force between a spherical and a plane surface is proportional to the radius of the sphere, which is in accord with the molecular nature of these forces.

4.) The work described is the first direct experimental test of the theory of molecular attractive forces between condensed bodies.

5.) An analysis is made of the present state of the problem of molecular attraction. It is indicated that the usually accepted notion of additivity of molecular attractive forces in condensed media has no basis either theoretically or experimentally.

6.) We demonstrate experimentally that computations of the molecular attraction of macroscopic bodies by summing the interaction computed from London 's formula over all pairs of molecules are inapplicable when the separation of surfaces is 1×10^{-5} cm or greater. Better results are gotten if the electromagnetic retardation is included.

7.) The experimental data are found to be in accord with Lifshitz' theory. This agreement supports P. N. Lebedev 's hypothesis of the electromagnetic nature of molecular forces.

8.) Since the London – Hamaker H^{-2} law for $U(H)$ appears as the particular limiting case of Lifshitz ' theory for small distances, for which there is no electromagnetic retardation, the

---

*This conclusion was already drawn in Ref. 8.

**Thus we cannot agree with the assertion of Verwey and Overbeek[10] that this law requires correction for retardation effects in the case of large particle size and *only* in that case.

confirmation of this theory gives a basis for using the H^{-2} law at small distances.

9.) The observed deviation from the H^{-2} law, toward lower values, for large distances (10^{-5} cm) indicates (as is easily seen) a small effect of molecular forces on the rate of coagulation of aerosols with particle diameters greater than 3×10^{-5} cm.

10.) The data obtained demonstrate the existence of molecular forces of long range surface interaction, which is one of the corner stones of the contemporary theory of the stability and coagulation of colloids.

11.) The data show that deviations from the 6th power law of the charge, which occurs in the Hardy — Schulze rule, are to be expected for very low concentrations of electrolyte and highly charged ions of opposite sign.

12.) It is pointed out that the measured values of molecular attractive forces in the experiments of Overbeek and Sparnaay exceed both the theoretical values as well as our results by 3 — 4 orders of magnitude, apparently because effects not related to molecular forces played a part in their measurements.

We express our sincere thanks to Prof. E. M. Lifshitz for discussion of theoretical questions, to laboratory worker I. V. Zhadovska for help with the measurements, and to N. I. Butuzov for polishing the samples.

---

[1] B. V. Deriagin and I. I. Abrikosova, J. Exptl. Theoret. Phys. (U.S.S.R.) **30**, 993 (1956).

[2] L. N. Kurbatov, Zh. Fiz. Khim **28**, 287 (1954).

[3] H. Margenau, Rev. Mod. Phys., **11**, 1 (1939).

[4] E. M. Lifshitz, J. Exptl. Theoret. Phys. (U.S.S.R.) **29**, 94 (1955) ; Soviet Phys. JETP **2**, 73 (1956).

[5] J. Th. Overbeek and M. J. Sparnaay, J. Colloid Sci., **7**, 343 (1952).

[6] Discussion Faraday Society, **18**, 12 (1954), Coagulation and Flocculation.

[7] N. Fuchs, Z. Physik **89**, 736 (1934).

[8] I. V. Petrianov, N. N. Tunitskii, J. Phys. Chem. USSR **17** 408 (1943); Acta Physicochim. USSR **18**, 185 (1942).

[9] B. V. Deriagin and L. D. Landau, J. Exptl. Theoret. Phys. (U.S.S.R.) **11**, 802 (1941); **15**, 662 (1945); Acta Physicochim. USSR **14**, 633 (1941).

[10] E. Verwey and J. Th. Overbeek, *Theory of the Stability of Lyophobic Colloids* . Elsevier, Amsterdam, 1948.

Translated by M. Hamermesh
1

SOVIET PHYSICS JETP VOLUME 4, NUMBER 1 FEBRUARY, 1957

Elastic Scattering of 310 Mev π^+ Mesons from Protons

E. L. GRIGORIEV AND N. A. MITIN

(Submitted to JETP editor March 6, 1956)
J. Exptl. Theoret. Phys. (U.S.S.R.) 31, 37-39 (1956)

The angular distribution of 310 mev π^+ mesons elastically scattered by protons in photoemulsions has been measured. The differential scattering cross section based on 427 observed cases has been obtained in the center-of-mass system.

The phase analysis, taking into account only the *S* and *P* states, and assuming the Fermi solution, gave the following values for the phase shifts: $\alpha_3 = -23°$, $\alpha_{33} = 132°$, $\alpha_{31} = -9°$. The *D* state, apparently, contributes little to scattering in comparison with the *S* and *P* states.

EXPERIMENTS conducted in recent years for studying the scattering of π mesons have made possible the development of a series of essential laws of interaction of π mesons with nucleons. These experiments have shown that the scattering cross section attains a maximum value for energies of π mesons near 200 mev[1,2] Attempts have been made to associate this maximum with the existence of an excited state of the nucleon.[3] Theoretical estimates for such an assumption lead to a satisfactory agreement with experiment over a significant range of meson energies.

The combined available evidence for total and differential cross sections for meson nucleon scattering gives reason to think that the experimental results for meson scattering down to an energy of 230 mev could be satisfactorily explained on the supposition that only *S* and *P* states participate in the scattering. It might be expected that even at meson energies of 200-250 mev the *D* states likewise should take part in the scattering; however, the poor accuracy of the measurements does not permit evaluation of the role in the scattering played by the states with the higher values of the orbital momentum. For π mesons with energies greater than 230 mev there are no reliable measurements at all of the differential cross section for meson-nucleon scattering.*

In the present work the differential cross section for elastic scattering of 310 mev π^+ mesons from hydrogen has been measured with the help of photoemulsions. Electron-sensitive photographic plates with an emulsion layer thickness of 400 μ were exposed to a beam of π^+ mesons emerging from the meson magnetic spectrometer.[5] The mesons originated from the paraffin target on bombarding it with a beam of 660 mev protons emerging from the synchrocyclotron chamber; the π^+ mesons, proceeding from the target at an angle of 7.3°, were deflected by the magnetic field after an initial collimation, and in the form of a narrow converging beam fell on the second collimator, to the rear of which were installed the photographic plates. The meson energy at the collimator was equal to 338 mev. A copper absorber having a thickness of 2 cm was placed to the rear of the collimator to protect the plates from protons falling on them. The energy possessed by the mesons after passage through the absorber was estimated to be 310 ± 10 mev.

The search for cases of scattering was carried out by examining the surface of the photographic plates using immersion objectives, the microscope having a total magnifying power of 450 x. A second survey was made of the entire surfaces of the photographic plates for the most complete recording of the scattering events. In order to determine the recording efficiency, which is somewhat different for various scattering angles, a portion of the surface of the photographic plates was carefully examined under a higher magnification (~ 630 x). The corrections which were introduced on the basis of the results obtained from such a survey decreased for angles greater than 110° in the center-of-mass system, and did not exceed 4–5%.

The elastically scattered events were identified with the aid of the following criteria, derived from the laws of conservation of energy and momentum:

1. The angular correlation between the scattered meson and the proton recoil. Cases in which the angular correlation differed from the calculated value by more than 1° were discarded.

2. Coplanarity. The condition for coplanarity is fulfilled for the case when

$$\sin \Phi = \frac{\cos \delta_0 \cos \delta_1 \cos \delta_2}{\sin \vartheta}$$

$$\times [\sin \vartheta_2 \operatorname{tg} \delta_1 - \sin \vartheta_1 \operatorname{tg} \delta_2 + \operatorname{tg} \delta_0 \sin (\vartheta_1 - \vartheta_2)]$$

$$= 0,$$

where δ_0, δ_1, δ_2 are the angles of inclination of the tracks of the incoming meson, the scattered meson, and the proton recoil with respect to the plane of the emulsion, respectively; θ_1 and θ_2 are the scattering angles of the meson and of the proton recoil, respectively, in the plane of the emulsion; θ is the angle between the scattered meson and the proton recoil in the plane of the emulsion; and Φ is the angle between the track of the incident meson and the plane passing through the tracks of the scattered meson and the proton recoil.

Cases for which $\Phi > 1°$ were discarded, being regarded as not satisfying the condition for coplanarity.

3. For cases of scattering through small angles for which the proton recoil stopped in the emulsion, corresponding to a low energy, it was required that the energy be equal to the calculated value.

Scattering events caused by mesons whose tracks in the photoemulsion were deflected from the primary direction of the meson beam through angles greater than 3°, corresponding to the average angle of multiple scattering in the copper absorber, were not counted.

Altogether 427 scattering events were found in the angle interval 10° – 170° in the center-of-mass system. The differential scattering cross section, calculated on the basis of the observed results, is presented in the diagram. It was assumed that the total scattering cross section of mesons from hydrogen for an energy of 310 mev was equal to 70×10^{-27} cm^2.[6] The interval of summation is 20°

The representation of the experimental results in the form of an analysis into a series of Legendre polynomials showed that the most important terms are those of the zeroth, first, and second orders.

Noting this circumstance, and taking into account the fact that the curve, evaluated without the presence of the higher terms, agrees entirely satisfactorily with the experimental results, it then becomes possible to express the differential cross section in the form of a decomposition involving only the first three polynomials. The final expression for the differential cross section then becomes

---

*There exists a short communication [4] regarding the scattering of mesons at energies of 260, 300, and 400 mev. In this work, utilizing a diffusion chamber, 100, 151, and 47 $\pi^+ - p$ scattering events, respectively, are analyzed for mesons with the indicated higher energies.

$$d\sigma/d\Omega = [(2.4 \pm 0.2) + (4.9 \pm 0.4)\cos\vartheta + (9.3 \pm 0.7)\cos^2\vartheta]\cdot 10^{-27}\ \mathrm{cm}^2/\mathrm{ster.}$$

The solid curve *a* on the drawing is obtained using this formula.

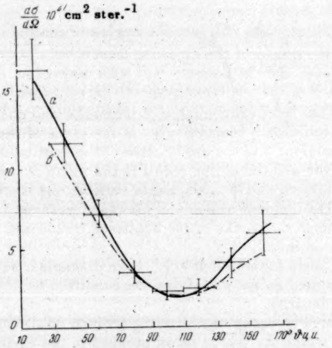

Differential cross section for 310 mev π mesons elastically scattered from protons. *a* – experimental curve, *b* – curve calculated on the supposition of an excited nucleon state.

Thus, the results of our experiments indicate that the scattering of 310 mev π^+ mesons can be satisfactorily explained in the first approximation if it is assumed that only *S* and *P* states participate in the scattering. An insufficiently high accuracy in the observed results does not afford an opportunity of making definite conclusions concerning the magnitude of the *D* state contribution to the scattering. However, one can expect that the *D* state plays a comparatively smaller role in scattering than the *S* and the *P* states.

The phase analysis for scattering was carried out for the Fermi solution[7] using graphical methods. The phase shifts for the S, $P_{3/2}$, and $P_{1/2}$ states with an isotopic spin of $T = 3/2$ were found to be $\alpha_3 = -23°$, $\alpha_{33} = 132°$, and $\alpha_{31} = -9°$.

Experimental data show that the phase α_{33} passes through 90° in the region of meson energies about 200 mev. This fact indicates the presence of resonance interactions of π mesons with nucleons in states with total and isotopic spins equal to 3/2. The value $\alpha_{33} = 132°$ for a meson energy of 310 mev does not contradict the supposition concerning the existence of such a resonance interaction.

It is interesting to compare the observed results with the calculations based on the assumption of the existence of an excited nucleon state.[3] Such calculations (curve *b* in the drawing) were carried out on the supposition that only *S* and *P* states take part in the scattering. The validity of neglecting the contributions of the higher states is confirmed by our measurements. As is seen from the drawing, the calculated curve reproduces well the general character of the angular distribution of elastically scattered π^+ mesons.

In conclusion we would like to express our gratitude to Prof. M. G. Meshcheriakov for his guidance of the work, as well as to B. C. Neganov and V. P. Zrelov for assistance in conducting the experiment.

Note added in proof: With the help of the high-speed electron calculating machine (BECM) a more rigorous analysis of the results was undertaken. Taking into account only the *S* and *P* waves, the following values for the phase shifts were obtained: $\alpha_3 = -22.7°$, $\alpha_{33} = 130.9°$, $\alpha_{31} = -7.0°$. Taking into account the *D* wave also, the phase shifts have the values $\alpha_3 = -16.8°$, $\alpha_{33} = 129.6°$, $\alpha_{31} = -2.0°$, $\delta_{33} = 2.6°$, $\delta_{35} = -6.5°$, ... , where δ_{33} and δ_{35} are the phase shifts corresponding, respectively, to the $D_{3/2}$ and the $D_{5/2}$ states for an isotopic spin of $T - 3/2$.

[1] Ignatenko, Muhin, Ozerov and Pontecorvo, Dokl. Akad. Nauk SSSR **103**, No. 1(1955).

[2] Ashkin, Blaser et al, Phys. Rev. **96**, 1104 (1954).

[3] Tamm, Gol 'fand and Feinberg, J. Exptl. Theoret. Phys. (U.S.S.R.) **26**, 649 (1954).

[4] R. S. Margulies, Bull. Am. Phys. Soc. **30**, 28 (1955).

[5] Meshcheriakov, Zrelov, Neganov, Vzorov, and Shabulin. Report (Otchet) Institute for Nuclear Problems, Academy of Sciences, USSR (1955).

[6] Ignatenko, Muhin, Ozerov and Pontecorvo, Dokl. Akad. Nauk SSSR **103**, 395 (1955).

[7] J. Ashkin and S. H. Vosko, Phys. Rev. **91**, 1248 (1953).

[8] H. A. Bethe and F. Hoffman, Phys. Rev. **96**, 1100 (1954).

Translated by E. V. Ivash
6

SOVIET PHYSICS JETP VOLUME 4, NUMBER 1 FEBRUARY, 1957

On the Problem of Unquantized Relativistically Invariant Renormalized Equations for a Three-Dimensional Extended Particle

IU. M. SHIROKOV AND D. G. SANNIKOV
Moscow State University

(Submitted to JETP editor April 18, 1955)
J. Exptl. Theoret. Phys. (U.S.S.R.) 31, 113-120 (January, 1956)

A system of relativistically invariant equations for a smeared-out particle interacting with a field has been obtained by using the method previously proposed (see Ref. 1) for constructing a three-dimensional extended particle. The conservation laws for the total energy-momentum four-vector are formulated. The particle is stable without the necessity for introducing additional forces (of the Poincare pressure type). An exact mass renormalization is carried out. For comparison with earlier equations, a rigorous limiting transition to the case of a point particle is made. Interaction with the electromagnetic field and with a scalar meson field are considered.

1. THE theory of elementary particles is basically a quantum theory. However, many difficulties of the quantized theory have a classical origin, so that it appears worthwhile to consider some questions in classical theory, especially since it is simpler and more pictorial, and may suggest the way to construct a quantized theory. Among the fundamental questions which have been discussed in recent times from both points of view, the foremost are the problem of the intrinsic mass and the derivation of the equation of motion of the particle.

Historically, the first elementary particle equation was Lorentz's equation for the three-dimensionally extended spherical electron. The decisive shortcoming of this equation is its noncovariance and the need for invoking forces of nonelectromagnetic origin (Poincare pressure) to stabilize the electron. The fundamental difficulty in constructing a theory of point particles on a classical basis is associated with the appearance of infinite intrinsic masses. One can avoid this difficulty in the classical theory by taking the point of view that all the particle mass is mechanical in origin, and eliminating all sources of electromagnetic mass.

Dirac[2] obtained an equation for a point electron by calculating the flux of energy and momentum from a world tube and using an artifice for eliminating the field-mass: the solution of the equation for the proper field of the electron was taken to be half the difference between the advanced and retarded potentials. Later other attempts were made to eliminate the infinite electromagnetic mass of the point particle and to derive an equation of motion for it. The electron, and also a nucleon interacting with meson fields, was considered (cf., for example, Refs. 3 and 4), but in all cases the use of half the difference between retarded and advanced potentials is a fixed requirement in deriving the equation of motion.

Attempts have been made[1,5] to construct a theory of a three-dimensionally extended relativistically invariant particle. The equation of motion of such a particle in an external field was obtained[1], and it was shown that relativistic invariance is achieved, and that the difficulties associated with Laue's theorem (instability of the electron, nonuniqueness of the 4-momentum) are removed if a covariant form of the Poincare pressure is introduced.

We make use of the method proposed in Ref. 1 for constructing a three-dimensional invariant "smearing". However, in contrast to Ref. 1, we shall smear the interaction and not the charge, as a result of which the particle will be stable without the introduction of the Poincare pressure.

2. We consider first the case of an electron interacting with the electromagnetic field. By analogy with ordinary electrodymanics, we choose the action S in the form

$$S = S^m + S^f + S^{int}; \tag{1}$$

$$S^m = -m\int d\tau; \tag{2}$$

$$S^f = -\frac{1}{8\pi}\int d\Omega\left\{\frac{1}{2}F_{ik}^2(x) + \left(\frac{\partial A_i(x)}{\partial x_i}\right)^2\right\}; \tag{3}$$

$$S^{int} = \int d\Omega\, A_i(x)\, j_i(x), \tag{4}$$

where S^m and S^f refer to the free particle and the field, respectively, and S^{int} to the interaction.

Here, in contrast to the usual electrodynamics

$j_i(x)$ is the current of a three-dimensional extended particle and not of a point particle. As shown in Ref. 1, the conserved current for such a particle has the form

$$j_i(x) = \int d\tau \rho(r_l)\,\delta(r_k u_k)(1 + r_j w_j)\,u_i. \tag{5}$$

The notation used here and in the sequel is the same as in Ref. 1.

Varying S with respect to the coordinates of particle and field we obtain, respectively, the equations of motion and the field equations:

$$mw_i = \int d\Omega\rho(r)\,\delta(r_k u_k)(1 + r_l w_l)\,F_{ij}(x)\,u_j \tag{6}$$

$$- \frac{d}{d\tau}\int d\Omega\rho(r)\,\delta(r_k u_k)\{A_j(x)\,u_j u_i r_l w_l$$

$$+ A_i(x)\,r_l w_l - A_j(x)\,r_i w_j\};$$

$$\Box A_i(x) = -4\pi j_i(x). \tag{7}$$

By direct substitution of $A_k + \partial\varphi/\partial x_k$ for A_k, one can verify that Eq. (6) is gauge invariant.

The equation of motion (6) is not identical with Eq. (28) of Ref. 1, differing from it by the term

$$\frac{d}{d\tau}\int d\Omega\rho(r)\,\delta(r_k u_k)\,\{A_j(x)\,u_j u_i r_l w_l \tag{8}$$

$$+ A_i(x) r_l w_l - A_j(x)\,r_i w_j\}.$$

This term is connected with the Thomas precession: a particle displaced relativistically along a closed contour will, when it returns to its initial position, turn out to have rotated through some angle about its axis. This is unimportant for a point particle, and in fact Eq. (8) goes to zero for $r_k \to 0$. For rectilinear motion, even if accelerated, this term again gives zero. It describes forces which appear only during curvilinear motion and are associated with rotation of the particle about its axis. Thus, for a rigid relativistic particle in a field there appears, so to speak, an additional degree of freedom, so that initially we must assign not only the coordinates and velocities, but also the angular velocity of the Thomas precession, which is uniquely determined by the normal component of the acceleration. This is the reason why the term (8) contains $\dot{w}_k$, the third derivative with respect to τ. If the particle is initially free, then (8) vanishes and the assignment of the auxiliary initial condition is unnecessary.

3. To obtain the total conserved 4-momentum P_i, we use a method developed by Pauli[6]. In this paper there was obtained for the first time an explicit expression for the energy-momentum integral in a quantized nonlocal theory. It satisfies exact conservation laws, and not asymptotic ones as previously supposed. Thus one can at any stage of the computation make the transition to a local theory which coincides with the usual theory.

Although we are not considering the interaction of fields, but rather of a field and particle, we shall also use the method proposed in Ref. 6. As a result of computations similar to those of Ref. 6, the total 4-momentum is obtained in the form

$$P_i(t) = P_i^m(t) + P_i^f(t) + P_i^{int}(t); \tag{9}$$

$$P_i^{int}(t)$$

$$= \int d\Omega' j_l(x') \frac{\partial A_l(x')}{\partial x_i'} \frac{1}{2} \{\varepsilon(t - T) - \varepsilon(t - t')\}$$

$$- \int d\Omega' j_l(x') \frac{\partial A_i(x')}{\partial x_l'} \frac{1}{2} \{1 + \varepsilon(t - t')\}$$

$$+ \int d\Omega' \int dT \delta(T - t)\,\{A_j(x')\,u_j u_i r_l' w_l \tag{10}$$

$$+ A_i(x')\,r_l' w_l - A_j(x')\,r_i' w_j\};$$

$$P_i^m(t) = m\int dT u_i \delta(T - t); \tag{11}$$

$$P_i^f(t) = \frac{1}{4\pi i}\int d\Omega' \delta(t - t') \tag{12}$$

$$\times \left\{F_{il}(x')\,F_{4l}(x') - \frac{\delta_{i4}}{4} F_{jl}^2(x')\right\},$$

where

$$\varepsilon(\tau) = +1 \quad \text{for} \quad \tau > 0$$

$$\text{and} \quad -1 \quad \text{for} \quad \tau < 0; \quad T(\tau) = -iX_4(\tau).$$

One can verify by direct test that the 4-momentum defined by Eqs. (9)-(12) is conserved, i.e.,

$$dP_i(t)/dt = 0. \tag{13}$$

4. Using the expression for $P_i(t)$, we get the completely renormalized particle mass M. For this purpose we solve the system of Eqs. (6) and (7) for an electron at rest in the absence of external fields and substitute the solution into the expression $-iP_4 = M$; we get

$$\varphi = -iA_4 = \int dV\rho(\mathbf{r})\frac{1}{|\mathbf{r}-\mathbf{r}'|}; \tag{14}$$

$$u_l = (0, 0, 0, i); \quad \mathbf{A} = 0;$$

$$M = m + m^f;$$

where

$$m^f = \frac{1}{2}\int dV\rho(\mathbf{r})\int dV\rho(\mathbf{r}')\frac{1}{|\mathbf{r}-\mathbf{r}'|} \tag{15}$$

is the finite electromagnetic mass of the electron. In the special case where the charge is distributed over the surface of a sphere of radius r_0, $m^f = e^2/2r_0$, while for a volume distribution, $m^f = 3e^2/5r_0$. m is the primitive mechanical mass, which enters explicitly into the equation of motion (6), M is the renormalized or experimental mass. In contrast to the quantum mechanical case, the renormalization is exact.

From consideration of the stationary case and using condition (13) it follows that the electron is stable without introducing any additional forces of the Poincare pressure type.

We can introduce the completely renormalized mass M into the equation of motion (6) in place of the primitive mass m. The equation of motion with the renormalized mass takes the form:

$$\begin{aligned} Mw_i &= m^f w_i \\ &+ \int d\Omega\rho(r)\,\delta(r_k u_k)(1 + r_l w_l)F_{ij}(x)u_j \\ &- \frac{d}{d\tau}\int d\Omega\rho(r)\,\delta(r_k u_k) \\ &\times \{A_j(x)u_j u_i r_l w_l + A_i(x)r_l w_l - A_j(x)r_i w_j\}, \end{aligned} \tag{16}$$

where m^f is to be taken from (15).

But this does not complete the renormalization process. We must similarly renormalize the field, i.e., eliminate from the right side of the equation of motion that part of the proper field of the particle which is already included in m^f.

In (16), $A_i(x)$ is the sum $A_i + A^s_i$, where A_i is the electromagnetic field external to the particle; A^s_i is the field produced by the particle. The latter consists of two parts: the field A^s_{ir} radiated by the particle, and the field A^s_{ia} permanently attached to it. A^s_{ia} is just that part of the field which must be taken out to get complete renormalization. Obviously we must require that in the stationary case A^s_{ia} coincide with the field of the free particle. However, the choice of A^s_i is not unique.

We shall take for A^s_i a solution of Eq. (7) in the form of a retarded potential, which corresponds to the natural physical description:

$$A^s_i(x) = \int d\Omega' 4\pi G^{ret}(x-x')\,j_i(x'); \tag{17}$$

$$\begin{aligned} G^{ret}(x-x') &= (1/4\pi)\,\delta \\ &\times \{|\mathbf{x}-\mathbf{x}'| - (t-t')\}/|\mathbf{x}-\mathbf{x}'|, \end{aligned} \tag{18}$$

where G^{ret} is the familiar Green's function for the retarded solution of the d'Alembert equation.

Substituting $A^s_i(x)$ into the right side of (6), we get the self-force

$$\begin{aligned} F^s_i(\tau) &= \int d\Omega\rho(r)\,\delta(r_k u_k) \\ &\times (1 + r_l w_l)\int d\Omega' 4\pi G^{ret}(x-x') \\ &\times \int d\tau'\delta(r'_n u'_n)\Big\{u_j(w'_i u'_j - w'_j u'_i)\rho(r') \\ &+ u_j\Big(u'_j\frac{\partial\rho(r')}{\partial x'_i} - u'_i\frac{\partial\rho(r')}{\partial x'_j}\Big)(1 + r'_m w'_m)\Big\} \\ &- \frac{d}{d\tau}\int d\Omega\rho(r)\,\delta(r_k u_k)\{r_l w_l(u_i u_j + \delta_{ij}) - r_i w_j\} \\ &\times \int d\Omega' 4\pi G^{ret}(x-x')\int d\tau'\delta(r'_n u'_n) \\ &\times (1 + r'_m w'_m)\rho(r')u'_j, \end{aligned} \tag{19}$$

where $r' = x' - X'$; $X' = X(\tau')$.

The equation then takes the form

$$Mw_i = m^f w_i + F_i + F^s_i, \tag{20}$$

where m^f is taken from (15), F^s_i from (19), and F_i from the right side of Eq. (6), where it is understood that now $A_i(x)$ includes only external fields satisfying the free-field equation

$$\Box A_i(x) = 0. \tag{21}$$

The system of equations (20 and (21) is a complete system of exactly renormalized equations describing an extended electron in interaction with the electromagnetic field. The total 4-momentum of the system is conserved despite the presence of odd time derivatives in the equation of motion.

5. The self-force F^s_i can be integrated approximately under the condition on the smallness of the acceleration

$$wr_0 \ll 1, \tag{22}$$

where r_0 is the size of the particle.

Multiplying (22) by M we get a simple interpretation: the change in energy (or momentum) along the path r_0 must not exceed the self-energy of the particle. For r_0 approaching zero and the point particle, the condition (22) drops out.

We carry out the computation in the rest system. In the final result we transform to an arbitrary system. We integrate in turn with respect to t, t', τ', using the three δ-functions

$$\delta(r_k u_k), \quad \delta(r'_n u'_n), \quad \delta\{|\mathbf{x}-\mathbf{x}'|-(t-t')\}$$

and make use of the normalization condition $\int dV\rho(\mathbf{r}) = 1$. The τ' integration is approximate. Introducing the new integration variable $s = \tau' - \tau$, we expand the integrand in series subject to the conditions

$$ws \ll 1 \tag{23}$$

and (22). But because of the δ-function in the integrand, s is of the same order of smallness as r_0. Therefore, conditions (22) and (23) are equivalent. As a result of the integration we get a series in powers of r_0. The first term of this series (of degree minus one in r_0),

$$\frac{1}{2}e^2 w_i \int dV\rho(\mathbf{r}) \int dV'\rho(\mathbf{r}') \frac{1}{|\mathbf{r}-\mathbf{r}'|} \tag{24}$$

corresponds to $A^s_{i\,a}$ [the Green's function is taken in the form ½$(G^{ret} + G^{adv})$]. In the equation, it combines with $m^f w_i$ from (15).

The second term of the series (of zero degree in r_0) is

$${}^2/_3 e^2 (\dot{w}_i + \dot{w}_k u_k u_i) \tag{25}$$

and is the well-known term for the self-force or reaction of the radiation from a point electron interacting with the electromagnetic field. It corresponds to $A^s_{i\,r}$ (here the Green's function is ½$(G^{ret} - G^{adv})$,

$$A^s_{i\,ir} + A^s_{i\,ia} = A^s_i \tag{26}$$

and correspondingly,

$$^1/_2(G^{ret} - G^{adv}) + {}^1/_2(G^{ret} + G^{adv}) = G^{ret}.$$

The remaining terms of the series (first and higher degree in r_0) are small under the condition $wr_0 \ll 1$, and can simply be dropped. For large accelerations they cease to be small, and the series expansion and integration of the self-force lose their meaning.

The final form of the renormalized equation of motion is

$$Mw_i = \int d\Omega\rho(r)\,\delta(r_k u_k)(1 + r_l w_l) F_{ij}(x) u_j \tag{27}$$

$$+ \frac{2}{3}e^2(\dot{w}_i + \dot{w}_k u_k u_i) + \ldots,$$

where terms of first and higher degree in r_0 have been dropped (they are expressed in the form of integrals). Equation (27) reminds one of Lorentz's equation but differs from it in being relativistically invariant. In addition, the electron is stable without the introduction of auxiliary forces (Poincare pressure). Together with Eq. (21) for the free external field, Eq. (27) gives a complete system of exactly renormalized equations for a three-dimensional extended particle interacting with the electromagnetic field. We have already given the conservation law (13) for the 4-momentum P_i defined by Eqs. (9)-(12).

For comparison with Dirac's equation, we go to the limit of a point particle. Then the terms of first and higher degree in r_0 vanish. The condition $wr_0 \ll 1$ no longer restricts the acceleration, and the equation of motion takes the form

$$Mw_i = e^2 F_{ik}(X)\, u_k + {}^2/_3 e^2 (w_i + w_k u_k u_i). \tag{28}$$

In this form, the equation of motion coincides with Dirac's equation. However, unlike Ref. 2, the physical interpretation of Eq. (28) is clear. Throughout the whole computation, we used finite quantities, considered the physically understandable case of retarded potentials, achieved exact mass renormalization, and also obtained rigorous conservation laws (9)-(13).

6. Let us now consider the case of a nucleon interacting with a scalar meson field. We proceed in complete analogy to the calculation for the electromagnetic field, so that everything previously stated also applies here. We shall only note the differences and peculiarities in the present case, and give the final results.

We choose the action function S in the form

$$S^m = -m\int d\tau; \tag{29}$$

$$S^f = -\frac{1}{8\pi}\int d\Omega\,\{\varphi_k^2(x) + \chi^2\varphi^2(x)\}; \tag{30}$$

$$S^{int} = -g\int d\tau\int d\Omega\rho(r)\,\delta(r_k u_k)\,(1 + r_l w_l)\,\varphi(x), \tag{31}$$

where $\varphi(x)$ is the potential of the meson field, $\varphi_k(x) = \partial\varphi(x)/\partial x_k$, χ is a constant numerically equal to $\mu/\hbar$, μ is the meson mass, g is the scalar coupling constant (the nuclear "charge").

We then get the equation of motion

$$mw_i = -g\int d\Omega\varphi_i(x)\,\rho(r)\,\delta(r_k u_k)\,(1 + r_l w_l) - g\int d\Omega\,\frac{d}{d\tau}\{\rho(r)\,\delta(r_k u_k)\,\varphi(x)\,u_i\} \tag{32}$$

and the field equation

$$(\Box - \chi^2)\,\varphi(x) = 4\pi g\int d\tau\rho(r)\,\delta(r_k u_k)\,(1 + r_l w_l). \tag{33}$$

It is interesting to note that the equation of motion (32) contains no derivatives with respect to τ higher than the second.

The action for vector coupling is

$$S_f^{int} = -f\int d\Omega\,\frac{\partial\varphi}{\partial x_k}\,f_k(x) = -f\int d\Omega\,\frac{\partial}{\partial x_k}\,(\varphi j_k)$$

because the divergence of the current vanishes identically, and is thus the integral of a divergence and therefore gives no contribution to the equation.

The total conserved 4-momentum has the form

$$P_i^{int}(t) = g\int d\Omega'\varphi_i(x')\int d\tau\rho(r')\,\delta(r_k' u_k)(1 + r_l' w_l) \times \frac{1}{2}\{\varepsilon(t - T) - \varepsilon(t - t')\} + g\int d\Omega'\varphi(x')\int dT\rho(r')\,\delta(r_k' u_k)\,u_i\delta(T - t);$$

$$P_i^m(t) = m\int dT u_i\delta(T - t);$$

$$P_i^f(t) = \frac{1}{4\pi i}\int d\Omega'\delta(t - t') \times \left\{\varphi_i(x')\,\varphi_4(x') - \frac{1}{2}\,\delta_{i4}\,(\varphi_l^2(x') + \chi^2\varphi^2(x'))\right\}. \tag{34}$$

The renormalized equation of motion is

$$Mw_i = m^f w_i + F_i(\varphi) + F_i^s, \tag{35}$$

where m^f is the finite field-mass of the nucleon, equal to

$$m^f = -\frac{1}{2}\,g^2\int dV\rho(\mathbf{r})\int dV'\rho(\mathbf{r}')\,\frac{e^{-\chi|\mathbf{r}-\mathbf{r}'|}}{|\mathbf{r}-\mathbf{r}'|}, \tag{36}$$

$F_i(\varphi)$ is the right side of Eq. (32), where $\varphi(x)$ now includes only external fields, satisfying the free-field equation

$$(\Box - \chi^2)\,\varphi(x) = 0. \tag{37}$$

F_i^s, the self-force, is equal to

$$F_i^s(\tau) = g^2\int d\Omega\delta(r_k u_k)\,\rho(r)\,(1 + r_l w_l) \times \int d\Omega'\cdot 4\pi G^{ret}(x - x') \times \int d\tau'\delta(r_n' u_n')(1 + r_m' w_m') \times \left\{\frac{\partial\rho(r')}{\partial x_k'}\,(\delta_{ik} + u_i u_k) + \rho(r')\,w_i\,(1 + r_l w_l)^{-1}\right\}. \tag{38}$$

In contrast to the electron case, F_i^s consists of two parts--a singular part $\tilde{F}_i^s$ and a nonsingular part F_i^χ

$$F_i^s = \tilde{F}_i^s + F_i^\chi, \tag{39}$$

corresponding to two parts of the Green's function

$$G^{ret} = \tilde{G}^{ret} + G^{\chi\,ret}, \tag{40}$$

where the singular part $\tilde{G}^{ret}$ is given by (18) while the nonsingular part $G^{\chi\,ret}$ is

$$G^{\chi\,ret}(x - x') = \begin{cases} -\frac{1}{4\pi}\,\frac{\chi J_1(\chi\sqrt{(t - t')^2 - (x - x')^2})}{\sqrt{(t - t')^2 - (x - x')^2}} \\ 0 \end{cases} \tag{41}$$

$$\times\quad \begin{matrix} t - t' > |x - x'| \\ t - t' < |x - x'| \end{matrix}$$

The singular part of the self-force $\tilde{F}_i^s$ is integrated, subject to the condition (22) just as in the case of the electron. The nonsingular part F can be expanded in series with respect to r_0 and approximately integrated only if we impose on the acceleration the new condition

$$w \ll \chi. \tag{42}$$

The integrand is expanded in series subject to conditions $wr_0 \ll 1$ and $ws \ll 1$. However, in contrast to the case of $\tilde{F}_i^s$ and that of the electron, here s is a variable taking on values from R to ∞ (the limits of the s integration). It proves to be sufficient to integrate, not to ∞, but to some s_0 such that $\chi s_0 \gg 1$, while $ws_0 \ll 1$, so that the expansion in series can be accomplished. These two conditions together give $w \ll \chi$. This new condition which did not occur for $\tilde{F}_i^s$ gives a stronger bound on the acceleration than the earlier $wr_0 \ll 1$ (for the chosen values of the constants $1/\chi = \hbar/\mu \sim 1.4 \times 10^{-11}$ cm) and is not eliminated when we go to the limit of a point particle.

The renormalized equation of motion (35) under the conditions $w \ll \chi$, $w \ll 1/r_0$ has the form

$$Mw_i = F_i(\varphi) - {}^1/_3\, g^2 (\dot{w}_i + \dot{w}_k u_k u_i) + \ldots, \tag{43}$$

where terms of first degree and higher in r_0 have been dropped and $F_i(\varphi)$ is the same as in (35).

For accelerations limited only by the one condition $w \ll 1/r_0$, the self-force F_i^χ cannot be expanded in series and integrated. In this case the equation of motion is expressible in the form

$$Mw_i = F_i(\varphi) + {}^1/_3\, g^2 (\dot{w}_i + w_k u_k u_i) + F_i^\chi - {}^1/_2\, g^2 \chi w_i + \cdots \tag{44}$$

Together with the Eq. (37) for the free external field, the equation of motion (35) [or, in the special cases, Eqs. (43) and (44)], gives the complete system of exactly renormalized equations for a three-dimensionally smeared nucleon interacting with a scalar meson field.

From Eq. (43), we obtain by rigorous transition to the point charge:

$$Mw_i = -g\,\{\varphi_i(X) + (d/d\tau)(\varphi(X)\,u_i)\} - {}^1/_3\, g^2 (\dot{w}_i + \dot{w}_k u_k u_i). \tag{45}$$

This is the equation for a point nucleon interacting with scalar meson fields, subject to the condition $w \ll \chi$. The constant χ does not appear explicitly in this equation (although the equation would be different, if $\chi = 0$.

For arbitrary accelerations, by making the limiting transition we obtain from Eq. (44)

$$\begin{aligned} Mw_i = &-g\left\{\varphi_i(X) + \frac{d}{d\tau}(\varphi(X)\,u_i)\right\} \\ &+ \frac{1}{3} g^2 (\dot{w}_i + \dot{w}_k u_k u_i) - \frac{1}{2} g^2 \chi w_i \\ &+ \frac{1}{2} g^2 \chi^2 u_i - g^2 \chi^2 \int_{-\infty}^{\tau} \frac{Y_i}{Y^2} J_2(\chi Y)\, d\tau' \\ &- g^2 \chi \frac{d}{d\tau}\left\{u_i \int_{-\infty}^{\tau} \frac{1}{Y} J_1(\chi Y)\, d\tau'\right\}, \end{aligned}$$

where $Y_k - X_k - X_k'$, $Y = \sqrt{-(X_k - X_k')^2}$.

Comparison of Eq. (46) with earlier equations for a point nucleon interacting with a scalar meson field shows that for the case of $w \ll \chi$ Eq. (46) leads to the well-known form of the equation (cf., for example, Eq. (50c) in Ref. 7], which is obtained using G^χ in the form $\frac{1}{2}(G^{\chi\,ret} - G^{\chi\,adv})$. But in the general case, (46) differs from Eq. (50c) of Ref. 7. In addition, precisely for the case of $w \ll \chi$, Eq. (46) was obtained by us in the entirely new form (45) where its interesting feature (opposite sign of the self-force) is explicitly clear.

Equation (46) differs from the equation obtained by using for G^χ the retarded solution $G^{\chi\,ret}$ [cf., for example, Eq. (21c) in Ref. 7] by having the additional term $-\frac{1}{2} g^2 \chi w_i$ on the right side of the equation. The effective mass correction $-\frac{1}{2} g^2 \chi$ obtained in Refs. 8 and 9 combined with our additional term, so that the results of these papers concerning changes of effective mass are incorrect.

7. The fundamental problem facing the present relativistic quantum theory is to obtain in closed form a system of renormalized equations not containing infinities. This problem is solved in the quantum theory of fields in the weak coupling approximation. The solutions (or the renormalized equations) are obtained in the form of series in the fine structure constant. It is of interest to try to solve the problem in another way: by first renormalizing the classical equations and then quantizing them. In this paper the first step along this path is carried out: systems of completely renormalized classical equations are obtained for particles interacting nonlocally with electromagnetic fields (20,21), (27,21) and meson fields (35,37), (43,37) and (44,37). It is important to note that the exact renormalization was carried out for a smeared interaction and is finite. The transition to the point particle is accomplished after the renormalization so that infinite expressions are absent not only from the final equations (28,21) and (45,37), (46,37), but also from every stage of the calculation. The attempt to quantize the renormalized equation is a fascinating, but obviously not simple, problem.

---

[1] Iu. M. Shirokov, J. Exptl. Theoret. Phys. (U.S.S.R.) **24**, 47 (1953).

[2] P. A. M. Dirac, Proc. Roy. Soc. (London) **167A**, 148 (1938).

[3] H. J. Bhabha, Proc. Roy. Soc. (London) **172A**, 384 (1939); **178A**, 314 (1941).

[4] H. J. Bhabha and Harish-Chandra, Proc. Roy. Soc. (London) **185A**, 250 (1946); Harish-Chandra, Proc. Roy. Soc. (London) **185A**, 269 (1946).

[5] Iu. M. Shirokov, J. Exptl. Theoret. Phys. (U.S.S.R.) **22**, 539 (1952).

[6] W. Pauli, Nuovo Cimento **10**, 648 (1953).

[7] P. Havas, Phys. Rev. **87**, 309 (1952).

[8] Harish-Chandra, Ind. Acad. Sci. **21**, 135 (1945).

[9] P. Havas, Phys. Rev. **93**, 882 (1954).

Translated by M. Hamermesh
14

SOVIET PHYSICS JETP VOLUME 4, NUMBER 1 FEBRUARY, 1957

Temperature Dependence of the Viscosity of Liquid Nitrogen At Constant Density

N. F. Zhdanova
Khar'kov State University

(Submitted to JETP editor January 25, 1956)
J. Exptl. Theoret. Phys. (U.S.S.R.) 31, 14-17 (July, 1956)

The results of measurements on the temperature dependence of the viscosity of liquid nitrogen at constant density are presented. These measurements were conducted over the density interval from $\rho = 0.38$ to $\rho = 0.86$ gm/cm^3 for temperatures ranging from the condensation temperature at each density to 300° K. The gas-like character of the variation of viscosity with temperature in liquid nitrogen at low densities is revealed for the first time.

IN 1950 Verkin and Rudenko[1] first investigated the temperature dependence of the viscosity of liquefied nitrogen and argon for constant values of the density. These experiments, in which it proved possible to distinguish quite fully the effects of the two factors of temperature and variation in molar volume upon the coefficient of viscosity, were conducted over a narrow density range.

The purpose of the present experiment has been to extend such an investigation to cover a wide range of densities--from a value of the density near that at the triple point to the value at the critical point. Liquid nitrogen was selected as the subject of the experiment, inasmuch as it belongs to the class of simple liquids; i.e., nonpolar, nonassociative liquids consisting of particles having spherical or nearly spherical symmetry. The full and systematic study of the properties of such substances is of great interest in connection with the problem of constructing a theory of the liquid state.

APPARATUS AND METHOD OF MEASUREMENT

In investigating the viscosity of this liquid use was made of the viscometer constructed by Verkin and Rudenko[1] and loaned for the present experiment by the Low-Temperature Laboratory of the Physico-Technical Institute, Academy of Sciences, Ukrainian SSR. The viscosity was determined from the time required for a cylindrical weight to fall along a tube of slightly greater diameter filled with the liquid to be investigated. Since pressures as high as 3000-4000 kg/cm^2 are developed as the temperature is increased with the density held constant, the tube and its contents were enclosed in a thick-walled bomb. Tube, weight and bomb were all made from the same material--beryllium bronze--and were placed within a metal Dewar flask. A core of iron-nickel magnetic alloy was pressed into the weight. Two pairs of induction coils were slipped onto the bomb, and their leads were connected in series either to a galvanometer or to an amplifier and oscillograph, with which it was possible to follow the motion of the weight down the tube through the liquid being studied, and to record the time of fall of the weight between two predetermined sections of the coils.

The experimental arrangement was such that the weight moved between the induction coils at a constant velocity, while no effect on the time of fall due to the ends of the bomb could be detected within the limits of accuracy of the measurement.

The measurement of the coefficient of viscosity of liquid nitrogen was made by means of a relative method. The value of the viscosity coefficient at the experimental temperature was determined from the formula

$$\eta_t = \eta_0 \tau_t (\rho - \rho_t) / \tau_0 (\rho - \rho_0), \qquad (1)$$

where η_0 and τ_0 are, respectively, the viscosity of nitrogen and the time of fall at $T = 18°\,\mathrm{C}$ and $P = 1$ atm, τ_t is the time of fall of the weight in the liquid being studied, ρ_t is the density of the liquid, ρ_0 is the density of nitrogen at $T = 18°\,\mathrm{C}$ and $P = 1$ atm, and ρ is the density of the weight.

Since $\rho_0 \ll \rho$, we have

$$\eta_t = \eta_0 \tau_t (\rho - \rho_t) / \tau_0 \rho.$$

The maximum error in the determination of η_t did not exceed 6%.

Before being condensed into the viscometer, the liquid nitrogen was subjected to repeated distillation to eliminate solidified contaminants. The density of the liquid was determined from tabular data on the dependence of ρ upon T under equilibrium vapor pressure as it was condensed into the apparatus and sealed into the bomb.

EXPERIMENTAL RESULTS

The results of the measurements on the viscosity of liquid nitrogen are represented in Fig. 1; the fluidity φ is measured in CGS units along the y-axis, and the temperature is measured along the x-axis. Curves *1, 2, 3* and *4* are taken from the work of Verkin and Rudenko; the points along curve *4*, which were obtained in the present experiment, agree well with the values found previously[1] The remaining curves (*5, 6, 7, 8, 9, 10, 11*) have been determined here for the first time*.

On the basis of the character of their curves and their work on the viscosity of compressed nitrogen[2,3], Verkin and Rudenko suggested that "the temperature coefficient of fluidity (viscosity) for A and N_2 changes sign as the density region near the critical density is approached." This prediction has received experimental verification in the present work; the change in the character of the temperature dependence of the viscosity of liquid nitrogen, however, does not take place in the vicinity of the critical density, but rather at a density having approximately twice the value at the critical point, as may be seen from the graph above.

From consideration of Fig. 1 it is evident that there are two regions in liquid nitrogen, in which the temperature dependence of the viscosity (fluidity) has different characteristics.

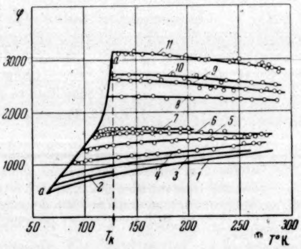

FIG. 1. Temperature dependence of viscosity in liquid nitrogen: *a* – under equilibrium vapor pressure; ρ equal to: *1* – 0.861, *2* – 0.832, *3* – 0.798, *4* – 0.746, *5* – 0.69, *6* – 0.63, *7* – 0.60, *8* – 0.50, *9* – 0.47, *10* – 0.43, *11* – 0.38 gm/cm³.

For liquid nitrogen of density $\rho > 2\rho_c$, where ρ_c is the density at the critical point, the viscosity decreases with increasing temperature, as is usual for liquids. For densities $\rho < 2\rho_c$ the viscosity increases with temperature, as is characteristic of gases.

In Fig. 1, curve *7* is distinguished by the fact that for the corresponding liquid nitrogen density $\rho \sim 2\rho_c$ the fluidity is independent of the temperature. From this same Figure it can be seen that the fluidity of liquid nitrogen under equilibrium vapor pressure does not yield a straight line in the coordinates $\varphi - T$, as was suggested by Rudenko[4]. For $\rho < 0.6$ gm/cm³, the experimental points diverge from a straight line, the fluidity varying with temperature more rapidly than would be the case for a linear dependence.

---

* A. Voronel' took part in the measurements for curves *4, 5, 6* and *7*.

The family of viscosity isotherms is plotted in Fig. 2. Values of the density ρ are given along the x-axis, and those of η, in CGS units, along the y-axis (these isotherms were obtained by rearrangement of the data of Fig. 1). It can be seen from the Figure that all of the isotherms intersect approximately in a point which for liquid nitrogen corresponds to a value for the density $\rho \approx 2\rho_c$.

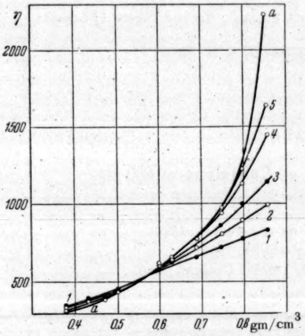

FIG. 2. Isotherms of nitrogen viscosity against density. Density in gm/cm^3 along the x-axis, viscosity, multiplied by 10^6, in CGS units along the y-axis. T equals: $1 - 273°$, $2 - 200°$, $3 - 150°$, $4 - 100°$, $5 - 85°$ K; $a - a$ under equilibrium vapor pressure.

Theoretical investigation of the viscous properties of liquids in the neighborhood of the triple point[5] leads to the dependence

$$\eta = Ae^{U/kT}, \tag{2}$$

where U, the activation energy, is a characteristic of the interaction between the liquid particles. U is usually taken to be independent of the temperature. It appeared desirable to investigate the applicability of Eq. (2) as a description of the experimental data for liquid nitrogen in the range $2\rho_c < \rho < \rho_{tr}$; i.e., in the region over which

$$\partial\varphi/\partial T\,|_{\rho = \mathrm{const}} > 0,$$

this being regarded as the fundamental feature of the viscous properties of liquids. From the given data it is possible to compute the magnitude of the activation energy U for various values of the liquid density. The values for U can be determined from the relation $\ln\eta = A + U/kT$, which, generally speaking, is correct only for values of the viscosity determined under conditions of constant molar volume.

In Fig. 3, $\ln\eta$ is plotted along the y-axis against $1/T$ along the x-axis. It is evident from the Figure that within the region for which $\partial\varphi/\partial T\,|_{\rho = \mathrm{const}}$ a linear dependence of $\ln\eta$ upon $1/T$ holds over the entire temperature range in which nitrogen exists in the liquid state. As they pass through the critical temperature, these straight lines merge smoothly into curves bending towards the x-axis. It is impossible to determine precisely the temperature at which the curvature begins, but it is clearly close to T_c. Thus, the temperature dependence of the viscosity of liquid nitrogen for constant values of the density $\rho > 0.6$ gm/cm$^3 \simeq 2\rho_c$ can be described by use of Eq. (2).

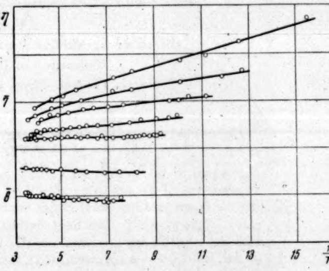

FIG. 3. Dependence of $\ln\eta$ on $1/T$ for liquid nitrogen at constant density.

The values obtained for the activation energy U show that it decreases with increasing molar volume for $U = 140$ cal/mol at $V = 32.6$ cm^3/mol to $U = 60$ cal/mol at $V = 40.6$ cm^3/mol.

The results cited above for the measurement of the temperature dependence of the viscosity of liquid nitrogen for constant values of the density permit the following conclusions to be drawn:

1. The viscosity (fluidity) of liquid nitrogen for constant values of the density depends very strongly upon the temperature. For $\rho > 2\rho_c$ the temperature dependence of the viscosity can be described by an exponential law, up to temperatures in the vicinity of T_c.

2. For liquid nitrogen

$$\text{for} \quad \rho > 2\rho_\kappa \quad (\partial\varphi/\partial T)_\rho > 0,$$

$$\text{for} \quad \rho < 2\rho_\kappa \quad (\partial\varphi/\partial T)_\rho < 0.$$

It may be suggested that the change in the character of the temperature dependence of the viscosity of nitrogen at a density near $2\rho_c$ is connected with a change in the mechanism of the viscosity. For $\rho > 2\rho_c$ the mechanism (liquid-like) prevails, while a different (gas-like) mechanism prevails for $\rho < 2\rho_c$.

In conclusion, I regard it as a pleasant duty to thank B. I. Verkin and I. S. Rudenko for directing this work.

---

[1] B. I. Verkin and I. S. Rudenko, J. Exptl. Theoret. Phys. (U.S.S.R.) 20, 523 (1950).

[2] A. Michels and R. O. Gibson, Proc. Roy. Soc. (London) A134, 288 (1931).

[3] N. F. Golubev and V. A. Petrov, *Nitrogen Handbook*, ONTIKhL, 1944.

[4] N. S. Rudenko, J. Exptl. Theoret. Phys. (U.S.S.R.) 18, 1123 (1948).

[5] I. I. Frenkel, *Kinetic Theory of Liquids*.

Translated by S. D. Elliott
2

SOVIET PHYSICS JETP VOLUME 4, NUMBER 1 FEBRUARY, 1957

Production of Positive Pions in (p− p) Collisions at 660 Mev

V. M. SIDOROV
Institute for Nuclear Problems, Academy of Sciences, USSR

(Submitted to JETP editor, March 24, 1956)
J. Exptl. Theoret. Phys. (U.S.S.R.) 31, 178-187 (August, 1956)

Using nuclear emulsions the energy spectra of positive pions produced in the reaction $p + p \to \pi^+ + \left\{ \begin{matrix} d \\ p+n \end{matrix} \right.$ at an energy of 657 ± 8 mev have been measured at angles, θ_π equal to 60°, 75°, 90°, 105° and 120° in the laboratory system. The angular dependence of the cross section $d\sigma/d\omega\,(\theta^*)$ in the center-of-mass system of the colliding nucleons and the total cross section for the reactions: $p + p \to \pi^+ + \left\{ \begin{matrix} d \\ p+n \end{matrix} \right.$ and $p + p \to p + n + \pi^+$ has been determined. The results are consistent with the assumption that the mesons are produced chiefly in *p*-states. In addition to transitions to the *S*-state of the final $(n - p)$ system, it is found that an important contribution is made by transitions in which the final state is a *P*-state.

1. INTRODUCTION

In $(p-p)$ collisions at an incident energy of 660 mev there is a strong probability for meson production in addition to elastic scattering. Experiments in which elastic proton-proton scattering has been studied[1] and measurements of the total cross section for $(p-p)$ interactions[2] indicate that in this energy region the probability for meson production is only slightly smaller than that for elastic scattering. Meson production can occur via the three following reactions:

$$p + p \to d + \pi^+; \qquad (1)$$

$$p + p \to + p + n + \pi^+; \qquad (2)$$

$$p + p \to p + p + \pi^0. \qquad (3)$$

Experimental studies in which (1) has been investigated[1] yield an angular dependence* of the cross section in the form $A + B\cos^2\theta^*$ which remains substantially constant over the energy range E_p =460-660 mev[3,4]. Possible transitions to the $^3S_1$ state of the final $(n-p)$ system are

$$^1S_0 \to {}^3S_1p_0; \quad {}^1D_2 \to {}^3S_1p_2; \quad {}^3P_1 \to {}^3S_1s_1.$$

(Here we are using the nomenclature given by Rosenfeld[5] in designating the final state of the system and it is assumed that the mesons are emitted only in *s*-states and *p*-states.) Analysis of the angular distribution and the energy dependence of the meson yield shows that these are consistent with the assumption that in (1) the mesons are produced chiefly in the *p*-state and that the transition of most importance is $^1D_2 \rightarrow {}^3S_1P_2$.

---

* The asterisk denotes quantities measured in the center-of-mass system (c.m.) of the colliding nucleons.

In (2), at an incident proton energy $E_p = 660$ mev, in addition to those indicated above, transitions to the *P*-state of the final nucleon system are energetically possible. The angular and energy distributions associated with the mesons will be determined to a considerable extent by the relative intensities of the corresponding transitions.

It is well known that the probability for neutral pion production in $(p-p)$ collisions is small close to threshold; at 460 mev the cross section $\sigma(p+p\rightarrow\pi^0)$ is as much as 3 – 4 times smaller than the cross section $\sigma(p+p\rightarrow d+\pi^+)$. However, as the energy of the incident proton is deccreased[6,7], a sharp rise is observed in the quantity $\sigma(p+p\rightarrow\pi^0)$. The extremely small cross section for the production of neutral pions close to threshold has been explained by the fact that the production of a pseudoscalar meson in an *Sp*-state is strictly forbidden. At the higher energies the *Pp*-state becomes available and this restriction no longer holds.

Thus, in meson-production, processes in which the relative nucleon energy is small at the end of the reaction the nature of the reaction is determined to a large extent by the nucleon final states. The present paper is devoted to an experimental investigation, using nuclear emulsions, in which the energy spectra and angular distributions for positive pions produced in reactions (1) and (2) were examined.

2. EXPERIMENTAL METHOD

This work on the production of mesons in hydrogen by protons was carried out at the synchrocyclotron of the Institute for Nuclear Problems, Academy of Sciences, USSR. Because of the high intensity of the external proton beam it was possible to make the measurements behind a four-meter concrete shield at a considerable distance from the machine; this arrangement resulted in extremely favorable background conditions. The proton beam was passed through a three-meter steel collimator by means of which a beam 120 mm in diameter was defined. The proton energy was 657 ± 8 mev.[8] A container filled with liquid hydrogen was placed in the beam. The diameter of the liquid hydrogen container was 12 cm. The positive pions produced in the $(p-p)$ collisions were emitted from the target through the glass walls of the container, which were 2 mm thick. Using a system of slit-collimators 20 cm long and 1 × 3 cm in cross section cut into the copper block, it was possible to select mesons emitted from given points of the target at angles, θ_π, 60°, 75°, 90°, 105°, and 120° with respect to the beam; these mesons were recorded in photographic emulsions. The detector angular resolution was 1.5°. The experimental arrangement is shown in Fig. 1. The emulsions were disposed in a copper block at an angle of 10° with respect to the incident mesons. The meson energy was determined by the range in the emulsion. The path length in the copper block was measured from the end of the meson track. The developed emulsions were scanned under a microscope with a magnification of 450 x. The positive pions stopped in the emulsion were identified by the character of the $\pi\rightarrow\mu$ decay. The background was determined by exposing the plates under these same geometrical conditions.

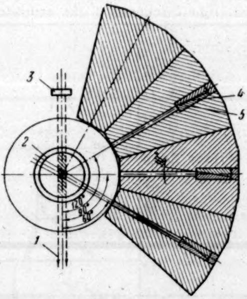

FIG. 1. Experimental set-up: *1* – proton beam, *2* – container with liquid hydrogen, *3* – monitor, *4* – photographic emulsion, *5* – copper absorber.

In plotting the positive pion spectra approximately 2000 $(\pi\rightarrow\mu)$ decays were studied at each angle.

3. DETERMINATION OF THE CROSS SECTION

The differential cross section for pion production is given by the expression

$$\frac{d^2\sigma}{d\omega dE} = \frac{N}{nN_p t\,[dE/dR]_E}\,\frac{r^2}{S}\,\frac{\eta_1\eta_2}{\eta_3},$$

where N_p is the number of protons which traverse the target, measured in the direction of the incident beam; N is the number of pions found in an area of the emulsion S ; r is the distance from the target to the emulsion surface; t is the thickness of the emulsion; $[\, dE/dR \,]_E$ is the energy lost in the emulsion by mesons having an energy E ; η_1 is a factor which takes into account mesons which are deflected from the beams by nuclear reactions; η_2 is a factor which denotes the mesons undergoing $\pi \to \mu$ decay before stopping in the emulsion; η_3 is the scanning efficiency for π - μ decay.

The proton number N_p was determined within an accuracy of 3 percent by means of a calibrated ionization chamber. The meson energy loss was determined from the expression [9]

$$[dE/dR]_E = 0.067 R_\pi^{0.419},$$

which is derived from the range-energy relation for protons. The thickness of the emulsion prior to development, t^*, was determined within an accuracy of 6 percent. In calculating the factor η_1 the mean -path-length for mesons in copper was taken to be 104.4 gm / cm^2 and its value varied within the limits 1.02 to 2.35 for meson energies ranging from 30 mev to 175 mev. The correction for the decay of positive pions in flight was small; the factor η_2 varied within the limits 1.04 and 1.10. The scanning efficiency was estimated by repeated scannings and found to be ~ 0.92.

4. EXPERIMENTAL RESULTS

In Fig. 2 are shown the meson energy distributions at angles of 60° , 75° , 90° , 105° , 120° in the laboratory system (l.s.). For all angles, with the exception of 60° , the energy distributions have clearly defined maxima in the hard part of the spectrum. The locations of these maxima correspond to values obtained from kinematic considerations in the reaction $p + p \to d + \pi^+$.

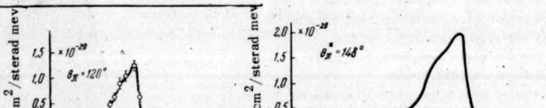

FIG. 2. Energy distributions for positive pions produced by 657 mev protons in hydrogen; θ_π refers to the laboratory system, θ_π^* refers to the c.m. system.

In these cases the spread about a monoenergetic line appears as a result of the following: a) limited angular resolution of the detector, b) energy spread in the proton beam, c) multiple scattering of mesons, d) spread due to fluctuations in the ionization losses. The calculated values for the energy spread are in agreement with the experimental results.

The smooth spectrum in the region of lower energy is attributed to mesons produced in the reaction $p + p \rightarrow p + n + \pi^+$. It was found possible at angles of 75 °, 90°, 105° and 120° (in the laboratory system) to separate out the contribution due to mesons produced in the reaction $p + p \rightarrow d + \pi^+$; the remainder is taken to be the energy distribution for the mesons from the reaction $p + p \rightarrow p + n + \pi^+$.

TABLE I

$\frac{d\sigma}{d\omega} \cdot 10^{28}$ in cm^2/sterad for the reaction	θ				
	60	75	90	105	120
$pp \rightarrow \pi^+ + \left\{ \begin{matrix} d \\ pn \end{matrix} \right.$ . . .	14.6 ± 1.6	8.9 ± 0.9	6.4 ± 0.7	$3.5 \pm 0,5$	$3,2 \pm 0.4$
$pp \rightarrow d\pi^+$	1.4 ± 0.1*	1.7 ± 0.4	1.8 ± 0.3	$1.4 \pm 0,3$	1.2 ± 0.2
$pp \rightarrow pn\pi^+$	13.2 ± 1.6	7.2 ± 1.3	4.6 ± 1.0	$2,1 \pm 0,8$	$2,0 \pm 0.6$
$\frac{(d\sigma/d\omega)_{pp \rightarrow pn\pi^+}}{(d\sigma/d\omega)_{pp \rightarrow d\pi^+}}$	9.4	4.2	2.6	1.5	1.7

---

* The value $(d\sigma/d\omega)^{60°}_{pp \rightarrow d\pi^+} = (1,4 \pm 0,1) \cdot 10^{-28}$ cm^2/sterad is taken from Ref. 4.

In Table 1 are shown the cross sections for positive pion production at the indicated angles in the laboratory system. At 60 °, because of the excessive energy spread, it was not possible to distinguish the contribution due to the reaction $p + p \rightarrow d + \pi^+$ and in the present experiment it was possible to measure only the combined cross section $d\sigma / d\omega \left(p + p \rightarrow \pi^+ + \left\{ \begin{matrix} d \\ p + n \end{matrix} \right. \right)$ at this angle. Combining the magnitude of the cross section $d\sigma / d\omega \left(p + p \rightarrow \pi + \left\{ \begin{matrix} d \\ p + n \end{matrix} \right. \right)$ at 60 ° with the results of Ref. 4 for reaction (1) we find that the magnitude of the cross section $d\sigma / d\omega \, (p + p \rightarrow d + \pi^+)$ is approximately 10 percent of the cross section $d\sigma / d\omega \times \left(p + p \rightarrow \pi^+ + \left\{ \begin{matrix} d \\ p + n \end{matrix} \right. \right)$. Hence, it may be assumed that the spectrum measured at 60 ° is determined chiefly by mesons produced in reaction (2).

5. TRANSFORMATION OF THE ENERGY DISTRIBUTIONS FROM THE LABORATORY SYSTEM TO THE CENTER-OF-MASS SYSTEM

In order to make a theoretical interpretation of these results it is neccessary to find the meson energy distribution and the cross section in the center-of-mass system (c. m. s.) of the colliding nucleons.

In converting the cross section from the laboratory system to the cm system use is made of the relation

$$\frac{d^2\sigma^*}{d\omega^* dE^*} = \frac{P^*}{P} \frac{d^2\sigma}{d\omega dE},$$

where $d^2\sigma^* / d\omega^* dE^*$; P^* and $d^2\sigma / d\omega dE$; P are the differential cross sections and the meson momenta in the c. m. system and laboratory system respectively. The ratio P^* / P is determined from the formula

$$E = E^* \gamma_c + P^* \beta_c \gamma_c \cos\theta^*,$$

where $\gamma_c = 1 \, (1 - \beta_c^2)^{1/2}$ and $\cos\theta^*$ are determined from the following relations[10]:

$$\cos\theta^* = \frac{1}{1 - \beta_c^2 \cos^2\theta} \left\{ - \gamma_\pi \sin^2\theta + (1 - \beta_c^2) \times \left(1 - \frac{\gamma_\pi^2 - \gamma_c^2}{1 - \beta_c^2} \sin^2\theta \right)^{1/2} \cos\theta \right\}.$$

In Fig. 3a is shown the ratio D^* / D as a function of meson anergy at angles. θ of 60° 75°, 90°, 105° and 120° for E_p = 657 mev.

The expression given for cos θ^* indicates that mesons emitted at a given angle, which have different energies, correspond to mesons emitted at different angles. In Fig. 3b is shown the dependence of the meson emission angle θ^* on the kinetic energy E^* for the experimental angles in the laboratory system. It is apparent from this curve that mesons with a kinetic energy E^* in the region from 30 to 150 mev and emitted, for example, at an angle $\theta = 90°$, correspond to mesons emitted in the region $125° < \theta^* < 135°$ in the center-of-mass system. Thus the angular spread in the c. m. system will cause a substantial distortion of the results in the conversion relation unless the mesons are concentrated in a narrow energy interval or the angular dependence of $d^2 \sigma / d\omega^* \cdot dE^*$ is close to isotropic. Since the mesons have a broad energy distribution and the angular dependence at different energies is not known beforehand, the situation noted above had to be taken into account in transforming the energy distributions into the center-of-mass system. Forthis purpose the values $d^2 \sigma / d\omega\, dE$ multiplied by the appropriate factor P^* / P are plotted in Fig. 3b. The points corresponding to the same value of meson kinetic energy E^* are connected by the smooth curves over the entire range of θ^*. In plotting the spectra in the center-of-mass system the values used were for $d\sigma^* / d\omega^* dE^*$ at angles θ^* of 5°, 112°, 125°, 137°, and 148°. These angles correspond to mesons produced in the reaction $p + p \rightarrow d + \pi^+$ with kinetic energies E^* = 149 mev and emitted at corresponding angles θ of 60°, 75°, 90°, 105° and 120° in the laboratory system.

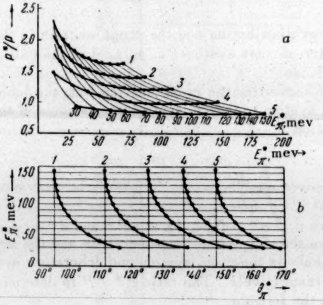

FIG. 3. a – the ratio P^*/P as a function of meson energy for the following values of θ_π: 1 – 120°, 2 – 105°, 3 – 90°, 4 – 75° and 5 – 60°; b – dependence of the meson emission angle θ^*_π on kinetic energy E^*_π for the same angles in the laboratory system.

6. MESON ANGULAR DISTRIBUTIONS IN THE CENTER-OF-MASS SYSTEM

In Figs. 2 and 4 are shown energy spectra for mesons produced in reactions (1) and (2) for incident proton energies E_p = 657 mev at the c.m. angles indicated above. In Table II are shown the cross sections for positive pion production, obtained by integrating the spectra, and the ratio for positive-pion yield produced in reactions (1) and (2). The total pion-production cross sections and the ratio of the total cross sections for reactions (1) and (2) are shown at the top.

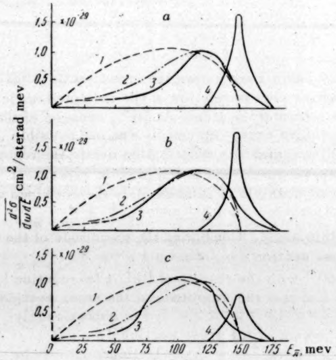

FIG. 4. Energy distributions for positive pions produced in $(p-p)$ collisions at proton energy E_p = 657 mev. a – θ^*_π = 137°; b – θ^*_π = 125°; c – θ^*_π = 112°. Curve 1 is a theoretical curve taken from Ref. 12; curve 2 is a theoretical curve taken from Ref. 13; curve 3 is the experimental curve for the reaction $p + p \rightarrow d + \pi^+$,

TABLE II

$\frac{d\sigma^*}{d\omega^*}\cdot 10^{28}$ in cm^2/sterad for the reaction	θ^* in degrees				
	95	112	125	137	148
$pp \to \pi^+ + \left\{ \begin{matrix} d \\ pn \end{matrix} \right.$ . . .	10.5±1.3	9.7±1.1	11.3±1.2	10.7±1.6	11.0±1.3
$pp \to d\pi^+$	1.0±0.07	1.9±0.5	3.0±0.5	3.5±0.7	4.2±0.6
$pp \to pn\pi^+$	9.5±1.3	7.8±1.2	8.3±1.3	7.2±1.7	6.8±1.4
$\frac{(d\sigma^*/d\omega^*)_{pp \to pn\pi^+}}{(d\sigma^*/d\omega^*)_{pp \to d\pi^+}}$	9.5	4.1	2.8	2.1	1.6

The data obtained in the present work indicates that the angular distribution of positive pions produced in (p-p) collisions at a proton energy $E_p = 657$ mev is virtually isotropic in the angular region from 95° to 148° in the c.m. system. The dependence of $d\sigma^*/d\omega^*(p + p \to \pi^+ + {}^{\,d}_{p+n})$ on the function $\cos^2\theta^*$ is shown in Fig. 5. Expressing the experimental results in the form of an empirical relation of the form $A(1 + B\cos^2\theta^*)$, using a least-squares fit, we find the angular distribution is given by the expression

$$(d\sigma^*/d\omega^*)_{pp \to \pi^+ + \left\{ {d \atop pn} \right.} = (10.3 \pm 1.8)\,[1 + (0.1 \pm 0.2)\cos^2\theta^*] \times 10^{-28}\ \text{cm}^2/\text{sterad}.$$

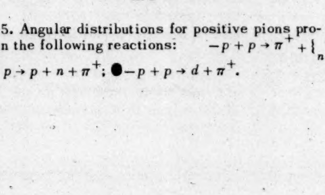

FIG. 5. Angular distributions for positive pions produced in the following reactions: $-p + p \to \pi^+ + \left\{ {d \atop n+p} \right.$; O$-p + p \to p + n + \pi^+$; ●$-p + p \to d + \pi^+$.

Using a least-squares fit for mesons produced in the reaction $p + p \to d + \pi^+$, the following angular dependence is found: $d\sigma^*/d\omega^*(p + p \to d + \pi^+) = (4.7 \pm 1.3)[(0.23 \pm 0.13) + \cos^2\theta^*] \cdot 10^{-28}$ cm^2/sterad which is in agreement, within experimental errors, with the results in Ref. 4 (the dotted line in Fig. 5 indicates the angular distribution for mesons from the reaction $p + p \to d + \pi^+$, as measured in Ref. 4).

Subtracting the mesons due to reaction (1) from the above quantity we obtain the meson angular distribution due to reaction (2)

$$(d\sigma^*/d\omega^*)_{pp \to pn\pi^+} = (9.2 \pm 1.8)\,[1 - (0.4 \pm 0.3)\cos^2\theta^*] \times 10^{-28}\ \text{cm}^2/\text{sterad}$$

In interpreting the results we shall consider the reaction $p + p \to p + n + \pi^+$ in detail. In the following we will assume that the important role is played by s and p meson states with respect to the two-nucleon system. Moreover, we will assume that at the energies being considered here both S and P nucleon states are involved at the end of the reaction. In this case the following are possible as final states for the system consisting of the two nucleons and the pion:

1) ${}^1S_0$; ${}^3S_1$ (Ss);
2) ${}^1S_0$; ${}^3S_1$; ${}^5S_2$ (Ps);
3) ${}^1P_1$; ${}^3P_{0,1,2}$ (Sp);
4) ${}^1P_1$; ${}^3P_{0,1,2}$; ${}^5P_{1,2,3}$ (Pp).

Here states 1) and 2) correspond to pions with orbital momentum $l = 0$, 3) and 4) orbital momentum $l = 1$. The final nucleon and meson states (in the nomenclature of Ref. 5) are shown in brackets.

According to Ref. 11, if a polarized proton beam is incident on an unpolarized target, the initial state of the system is described by the wave functions

$$\psi_1 = q_1\chi_{11}(\varphi_{10} + \varphi_{30} + \cdots)$$

$$+ (q_2/\sqrt{2})\,\chi_{10}(\varphi_{10} + \varphi_{30} + \cdots)$$

$$+ (q_2/\sqrt{2})\,\chi_{00}(\varphi_{00} + \varphi_{20} + \cdots);$$

$$\psi_1' = q_2\chi_{1-1}(\varphi_{10} + \varphi_{30} + \cdots)$$

$$+ (q_1/\sqrt{2})\,\chi_{10}(\varphi_{10} + \varphi_{30} + \cdots)$$

$$- (q_1/\sqrt{2})\,\chi_{00}(\varphi_{00} + \varphi_{20} + \cdots),$$

where $q_1 = \cos(\vartheta/2)\exp(-i\delta/2)$, $q_2 = \sin(\vartheta/2)\exp(i\delta/2)$ (ϑ, δ are the polarization angles): $\chi_{s\mu}$ is the spin wave function and φ_{lm} is the spherical function. Combining the orbital and spin moments, we obtain the initial states for the system

$$^3P_{1,2};\quad ^3F_{2,3}\qquad (M = \pm 1);$$

$$^3P_{0,2};\quad ^3F_2\qquad (M = 0);$$

$$^1S_0;\quad ^1D_2\qquad (M = 0).$$

Here we have given only those states of the initial system which can feed the final states being considered. The possible transitions in the reaction $p + p \to p + n + \pi^+$ are shown in Table III.

The amplitude of the final state is given by the expression

$$f = \sum A_{lsjM}\, I_{lsjM}.$$

TABLE III

Type	Initial state of the system	Final state of the system	Transition	Projection of total momentum
Sp	$^1S_0$	$^3S_1p_0$	$^1S_0 \to {}^3P_0$	0
Sp	$^1D_2$	$^3S_1p_2$	$^1D_2 \to {}^3P_2$	0
Ss	$^3P_1$	$^3S_1s_1$	$^3P_1 \to {}^3S_1$	±1
Ss	$^3P_0$	$^1S_0s_0$	$^3P_0 \to {}^1S_0$	0
Ps	$^1S_0$	$^3P_0s_0$	$^1S_0 \to {}^1S_0$	0
Ps	$^1D_2$	$^3P_2s_2$	$^1D_2 \to {}^5S_2$	0
Pp	$^3P_0$	$^3P_1p_0$	$^3P_0 \to {}^3P_0$	0
Pp	$^5P_1$	$^3P_1p_1$	$^3P_1 \to {}^3P_1$	±1
Pp	$^3P_1$	$^3P_0p_1$	$^3P_1 \to {}^1P_1$	±1
Pp	$^3P_1$	$^3P_2p_1$	$^3P_1 \to {}^5P_1$	±1
Pp	$^3P_2$	$^3P_1p_2$	$^3P_2 \to {}^3P_2$	±1;0
Pp	$^3P_2$	$^3P_2p_2$	$^3P_2 \to {}^5P_2$	±1;0
Pp	$^3F_2$	$^3P_1p_2$	$^3F_2 \to {}^3P_2$	±1;0
Pp	$^3F_2$	$^3P_2p_2$	$^3F_2 \to {}^5P_2$	±1;0
Pp	$^3F_3$	$^3P_2p_3$	$^3F_3 \to {}^5P_3$	±1

where the summation is carried out over all final states being considered, (A_{lsjM} is the transition probability, I_{lsjM} are the spherical functions).

The differential cross section $d\sigma^*/d\omega^*(\theta^*)$ is expressed in terms of the amplitude of the final state by

$$d\sigma^*/d\omega^* = f^+f. \tag{I}$$

Substituting the expression for f in Eq. (1) we obtain the meson angular distribution

$$d\sigma^*/d\omega^* = a' + b'\cos^2\theta^* + c'\sin^2\theta^*,$$

where a', b' and c' are expressed in terms of A_{lsjM} or

$$d\sigma^*/d\omega^* = a + b\cos^2\theta^*,$$

where $a = a' + c'$, $b = b' - c'$.

We may note that terms containing $\sin^2\theta^*$ in the angular distribution arise from transitions of the P_p class and from interference between the transitions ${}^1S_0 \to {}^3S_1p_0$ and ${}^1D_2 \to {}^3S_1p_2$. The meson angular distribution in reaction (1) is almost the same as the theoretical distribution for the transition ${}^1D_2 \to {}^3S_1p_2$ and indicates that the contribution of terms proportional to $\sin^2\theta^*$ due to interference of the indicated transitions, is small. It is also possible that this applies in reaction (2) since at an energy $E_p = 440$ mev [12] there was no noticeable change in the angular distribution with regard to an increase in the constant term for reactions (1) and (2) as compared with reaction (1).

Thus we see that the angular distributions for the reactions $p + p \to d + \pi^+$ (Sp and Ss transitions) and $p + p \to p + n + \pi^+$ (Sp; Ss; Pp and Ps transitions) can be given in the form $a + b\cos^2\theta$; however, if transitions of the Pp type participate in the meson production process and their contribution cannot be neglected, the coefficient $b = b' - c'$ in reaction (2) may be smaller. Under these conditions the value of the coefficient a in the same reactions may become larger; this increase, however, may be due to other causes as well as Pp transitions.

The angular distributions for positive pions produced in reactions (1) and (2), measured in the present work, indicate that the coefficients b' and c' are approximately equal; hence, it would seem that a considerable contribution is made by transitions of the Pp type in reaction (2) for proton energies of 657 mev. This effect is also found in the angular distributions in the reaction $p + p \to p + n + \pi^+$ in which the coefficient b becomes negative.

7. ANALYSIS OF THE POSITIVE PION PRODUCTION IN THE REACTION $p + p \to p + n + \pi^+$

From kinematic considerations it follows that mesons produced in the reaction $p + p \to p + n + \pi^+$ have a continuous distribution in energy over the range from zero to 150 mev in the center-of-mass system. The experimental energy spectra, however (cf. Figs. 2 and 4) extend to an energy of 175 mev; this may be explained by errors in the detector (some mesons may traverse only part of the path in the emulsion or in the wall). The energy distributions measured at angles of 95°, 112° and 125° would seem to indicate the meson spectra associated with reaction (2) have maxima in the region 100-125 mev. An analysis of the energy distributions in the measured regions of angle leads one to believe that mesons emitted an angles close to $\theta^* = 180°$ are concentrated in the higher energy region. Because of this deformation in the spectra, the angular distributions for different energy integrals have the form

$$E_\pi = 75 \div 100 \text{ mev}, \quad d\sigma^*/d\omega^* = 1 - \cos^2\theta^*;$$
$$E_\pi = 125 \div 150 \text{ mev}, \quad d\sigma^*/d\omega^* = 0.2 + \cos^2\theta^*.$$

This result is in agreement with the assumption of important contributions due to transitions of the Pp type in the production of positive pions at high energies. As a matter of fact, it was indicated above that Pp transitions tend to reduce the coefficient b in the expression for the angular dependence of the meson yield and to increase the constant term. This effect should be more noticeable for low meson energies which leave a considerable energy in the relative motion of the nucleons. In the region of high meson energy, Pp transitions should play a diminishing role and the angular dependence in the meson yield should be determined chiefly by Sp transitions; hence, in this energy region we should have a more intense production of mesons at angles close to 180° as compared with angles around 90°.

Thus the shape of the positive-pion energy distributions at different angles in the center-of-mass system as well as the angular distributions leads us to the conclusion that transitions of the Pp type make a large contribution to the cross section for meson production at $E_p = 657$ mev.

For comparison with the experimental results, Fig. 4 shows theoretical curves which describe the meson spectrum in reaction (2). Curves *1* and *2* are taken from Ref. 13 and correspond to the case $H \sim$ const and $H \sim P^*$, where H is the matrix element for the interaction. The statistical weight was computed for the case in which all particles appearing in the final state are relativistic. Comparison with the experimental data indicates that a better approximation results if the assumption is made that the matrix element depends linearly on meson momentum (curve *2*). The dependence indicated for the matrix element may indicate that in the reaction being considered mesons are produced with an angular momentum $l = 1$. Better agreement for the theoretical curve *2*, with the experimental data was observed at an angle $\theta^* = 125°$. At other angles there was a discrepancy which was attributed to the deformation of the positive pion spectrum with changing angle. The change in the shape of the spectrum, as was indicated above, occurs because in the final state the nucleons can have an angular momentum $l = 0$ or $l = q$ and the relative contributions of the associated transitions are different at different angles. Consequently, one expects that satisfactory agreement between theory and experimental results can be found at all angles only when account is taken of the nucleon interaction in the final states.

8. TOTAL CROSS SECTION FOR POSITIVE-PION PRODUCTION IN $(p-p)$ COLLISIONS

The total cross section for positive pion production in $(p-p)$ collisions at an energy of 675 mev is

$$\sigma_{pp\to\pi^+ + \left\{\begin{smallmatrix} d \\ pn \end{smallmatrix}\right.} = (13.4 \pm 2.2)\cdot 10^{-27}\ \text{cm}^2.$$

It is apparent that among the inelastic processes which occur in proton collisions at energies of 660 mev, an important part (80 percent) is played by the production of positive pions. Using the value $\sigma_{pp}^{\text{total}} = (41.4 \pm 0.6)$ mb taken from Ref. 2 and $\sigma_{pp}^{\text{elas}} = (24.7 \pm 1.2)$ mb from Ref. 14, we have for $\sigma_{pp}^{\text{inelas}}$ the value (16.7 ± 1.3) mb. Hence, it may be considered that $\sigma(p + p \to \pi^0) = (3.3 \pm 2.5)$ mb which is in agreement with the value for this quantity as measured in Ref. 6.

The value $\sigma(p + p \to p + n + \pi^+) = (10.1 \pm 2.3)$ mb is corroborated by Refs. 1 and 2. For the ration of the cross sections of these reactions we find

$$\dot{\sigma}_{pp\to pn\pi^+} / \dot{\sigma}_{pp\to d\pi^+} = 3.1.$$

We wish to take this opportunity to express our gratitude to Professor M. G. Meshcheriakov for his guidance. We are also indebted to S. M. Bilen'kii and Iu. A. Iappa for assistance.

---

[1] Meshcheriakov, Bogachev and Neganov, Izv. Akad. Nauk SSSR, Ser. Fiz. 19, 548 (1955).

[2] Dzhelepov, Moskalev and Medved', Dokl. Akad. Nauk SSSR 104, 382 (1955).

[3] Meshcheriakov, Neganov, Bogachev and Sidorov, Dokl. Akad. Nauk SSSR 100, 673 (1955).

[4] M. G. Meshcheriakov and B. S. Neganov, Dokl. Akad. Nauk SSSR 100, 677 (1955).

[5] A. H. Rosenfeld, Phys. Rev. 96, 139 (1954).

[6] Tiapkin, Kozodaev and Prokoshkin, Dokl. Akad. Nauk SSSR 100, 689 (1955).

[7] L. M. Soroko, J. Exptl. Theoret. Phys. (U.S.S.R.) 30, 296 (1956); Soviet Phys. JETP 3, 184 (1956).

[8] V. P. Zrelov, Report (Otchet) of the Inst. Nuclear Problems (1954).

[9] Bradner, Smith, Barkas and Bishop, Phys. Rev. 77, 462 (1950).

[10] J. Blaton, Det. Kgl. Danske Vidensk. Selsk. Matt-fys. Medd. 24, No. 20 (1950).

[11] V. B. Berestetskii, Dokl. Akad. Nauk SSSR 94, 130 (1954).

[12] A. H. Rosenfeld, Phys. Rev. 96, 130 (1954).

[13] Iu. A. Iappe, Report (Otchet) Inst. Nuclear Problems (1955).

[14] N. P. Bogachev, Dokl. Akad. Nauk SSSR 108, 806 (1956).

Translated by H. Lashinsky
37

Investigation of the (*d, p*) Reaction in Phosphorous and Chlorine

I. B. TEPLOV
Moscow State University

(Submitted to JETP editor February 24, 1956)
J. Exptl. Theoret. Phys. (U.S.S.R.) 31, 25-30 (July, 1956)

Proton angular distributions are determined for the $P^{31}(d,p)P^{32}$ and the $Cl^{35}(d,p)Cl^{36}$ reactions using thick nuclear photographic plates. The analysis of the observed experimental results permits a number of conclusions to be made regarding the excited states of the residual nuclei.

IT is well known that nuclear reactions of the (d,p) or the (d,n) types can proceed either with or without the formation of an intermediate nucleus. In the latter event, it is not the entire deuteron which interacts with the target nucleus, but rather, only one of its nucleons. A distinguishing characteristic of such a reaction mechanism---usually referred to as a stripping process---appears to be the presence of narrowly shaped maxima in the angular distribution of the outgoing particles, the positions of these maxima being characterized by the orbital momentum l with which the nucleon (a neutron for the case of the (d,p) reaction) is captured by the nucleus[1]. Consequently, a comparison of the experimental with the theoretical angular distributions makes possible the determination of a set of physical data for the various states of the residual nucleus. Of special importance is the circumstance that it is possible to investigate the excited states of the atomic nuclei using these methods, and, in particular, to verify the correctness of the shell model description of the properties of the low-lying excited levels.

The purpose of the present work, which was completed in 1954, was to determine the excited level characteristics of the P^{32} and Cl^{36} nuclei by an investigation of the energy and angular distributions of the protons formed in reactions of the (d,p) type in phosphorous and in chlorine. Detailed studies of the angular distributions produced in these proton reactions have not yet been published. Only angular distributions for the formation of residual nuclei in the ground states have been dealt with in several investigations[2-4], it being shown that the transferred orbital momentum in this case is equal to 2. In addition, a brief communication[5] has appeared concerning an investigation of the angular distribution of particles for a number of excited levels of P^{32}.

A cyclotron output, consisting of a focussed deuteron beam of energies near 4 mev, was used for studying the reactions. The energy spread in the beam did not exceed 1%, and the absolute value of the average energy was known with an accuracy of 3%. For the case of the $P^{31}(d,p)P^{32}$ reaction a thin layer (0.16 ± 0.05 mg/cm^2) of zinc sulfide, deposited on tinsel by evaporation in a vacuum, served as a target. For investigating the $Cl^{35}(d,p)Cl^{36}$ reaction the target was a layer of barium chloride (0.51 ± 0.09 and 0.27 ± 0.08 mg/cm^2), prepared in the same way. The protons produced in the nuclear reactions were detected with the help of thick-layered photographic plates of type Z-2 (having an emulsion thickness of $100\,\mu$) oriented at various angles to the direction of the incoming deuterons. An aluminum absorber of thickness $320\,\mu$ was inserted between the target and the photographic plates to absorb the elastically scattered deuterons.

The $P^{31}(d,p)P^{32}$ Reaction. The distribution of the proton tracks is shown in Fig. 1 for protons emerging from the target at an angle of 20° to the direction of the deuteron beam. The energies of excitation for various states of P^{32} obtained from the histogram are presented in the Table together with the data proceeding from a magnetic analysis of the products of the $P^{31}(d,p)P^{32}$ reaction. The results obtained by these two methods agree well among themselves considering, of course, the poor resolving power of the photographic plate method. In all, 18 photographic plates, exposed at various angles, were processed. Angular distributions obtained from an analysis of all the histograms for four groups of protons are presented in Figs. 2-4, the statistical errors only being indicated. The angle of scattering in the center-of-mass system for the proton is indicated along the abscissa axis, while the differential cross section in millibarns per steradian is along the ordinate axis (it is important to note that the accuracy of the determination of the absolute cross section is very poor---several tens of percent). The isotropic contributions of the angular distributions, obviously corresponding to the formation of the compound nucleus, are separated off by horizontal dashed lines. Curves on these same diagrams are presented which have been calculated using the theoretical formulas of Ref. 1, the values of the orbital momenta being selected so as to achieve optimum agreement between the experimental points and the calculated curves.

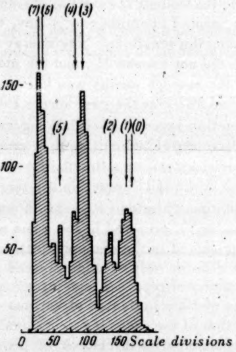

FIG. 1. Spectrum of protons emitted at an angle of 20° to the deuteron beam for the $P^{31}(d,p)P^{32}$ reaction. The divisions of the microscope ocular scale are indicated along the abscissa (1 division = 1.41μ).

Comparison of the experimental with the theoretical angular distributions indicates that it is possible to explain satisfactorily the observed results, provided that it is assumed that the transferred orbital momentum is equal to 2 for the case in which P^{32} is formed in the ground state (in agreement with the results of Refs. 2 and 3), and 0 for state (2). The angular distribution of the groups of protons corresponding to levels (3) and (4) can be explained by assuming that two orbital momenta, 0 and 3, contribute. Evidence in favor of the orbital momentum 0 corresponding to level (3) and the orbital momentum 3 to level (4) is given by the form of the peak of this group of protons on certain histograms, that of Fig. 1, for example. It is not possible to give any definite value at all for the orbital momentum of group (5), since the angular distribution of this group is practically isotropic (within limits of an average error of ±7%). In the Table are listed all the values obtained for the orbital momenta together with the parities and possible spin values of the observed nuclear levels ($|J_0 + 1 + s_n|_{min} \le J \le J_0 + l + ½$, where J_0 is the spin of P^{31}, equal to ½).

It is known from other evidence that the spin of the ground level of P^{32} is 1. Comparing the relative intensities obtained by the method of magnetic analysis[6] for the proton groups corresponding to capture by levels (0) and (1), it can be concluded that the spin of level (1) is equal to 2[7]. From the point of view of the nuclear shell model both of these levels correspond to the state $1d_{3/2}$ of the last neutron.

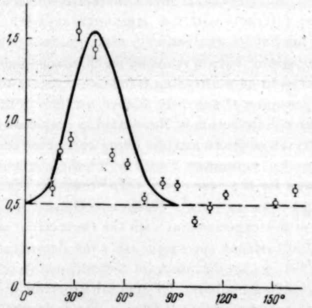

FIG. 2. Angular distribution of protons for the nuclear states (0 – 1) of P^{32}. The solid curve is plotted for $l = 2$.

The following discussion is based on the observation that if the probability of capture of the neutron into some excited level is comparable with the probability of capture into the ground state, then this excited level is formed by one particle excitation. If the capture probability for some level is considerably less than for the ground level, then the excited level which is formed involves excitation of the initial nucleus. As theory shows[1], the probability of neutron capture into a given state is proportional to $\sigma(\theta)f(E_d, E_p, \theta)/(2J + 1)$, where f is a known function of the angle and the deuteron and the proton energies, and σ is the differential cross section for the process. The capture probability of the neutron (in relative units) obtained in this manner is

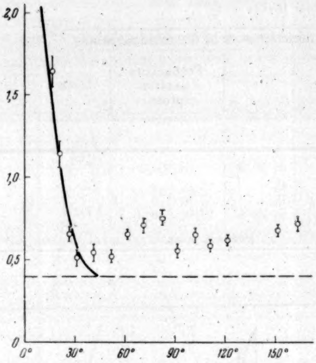

FIG. 3. Angular distribution of protons for the nuclear state (2) of P^{32}. The solid curve is plotted for $l = 0$.

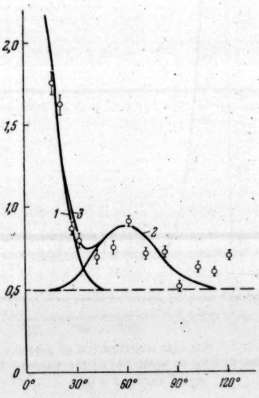

FIG. 4. Angular distribution of protons for the nuclear states (3–4) of P^{32}. Curves *1*, *2* and *3* are plotted for $l = 0$, 3 and 0 + 3, respectively.

indicated in one of the columns of the Table, the calculation for the doublet (0) – (1), making use of the fact that the spin of the ground state is 1 and the spin of state (1) is 2. The capture probability for excited states is evaluated for each allowable value of J. As is seen from the Table, level (4) corresponds to one particle excitation, namely, to the state $1f_{7/2}$ of the last neutron, while levels (2) and (3) are associated with excitation of the initial nucleus. If this interpretation is correct, then the number of possible values for the spin of state (4) is limited, since the combination of the proton in the state $2s_{1/2}$ and the neutron in the state $1f_{7/2}$ can only lead to the values 3 and 4 for the spin. The circumstance that several of the low-lying states of P^{32} can be described with the help of the shell model is quite understandable, since in this nucleus the last neutron alone occupies the new level.

It should be noted that the values of the orbital momenta for the excited nuclear states of P^{32} obtained in the present work are different from those communicated in Ref. 5. In agreement with the data presented there, however, the angular distributions of the proton groups for the formation of the nucleus in states (2), (3) and (4) are describable using a mixture of $l = 0$ and $l = 2$. No estimate of the degree of certainty of these results can be made at the present time, inasmuch as a detailed description of the experiments has not yet been published.

The $Cl^{35}(d,p)Cl^{36}$ Reaction. The nuclear level scheme of Cl^{36} obtained as the result of analyzing the distribution of proton tracks in photographic plates is presented in Fig. 5. In the same figure are indicated the level scheme determined from the γ–ray energies for the (n,γ) reactions[7], as well as the levels found by Innis[8], who investigated the $Cl^{35}(d,p)Cl^{36}$ reaction (see also Ref. 9).

Our measurements are found to be in satisfactory agreement with the results of these investigations as a result of our success in resolving all groups of protons corresponding to the known nuclear levels. The only exception is the 5.57 mev level, since in this case the protons corresponding to it are masked by the protons from the $O^{16}(d,p)O^{17}$ reaction. Groups (1) and (12), which previously have been unobserved, have very weak intensities and, possibly, are associated with the existence of foreign admixtures in the target.

Angular distributions were plotted for ten groups of protons, two of which are shown in Figs. 6 and 7. The orbital angular momentum values obtained by the comparison of the experimental results with the theoretical curves are indicated in Fig. 5 for all the levels for which angular distributions were plotted. In those cases in which the magnitude of the orbital momentum is not reliably

TABLE. Excited nuclear levels of P^{32}.

Level No.	Energy of excitation: Result of magnetic analysis in mev[7]	Energy of excitation: isotropic distribution in mev	l	Parity	J	Probability of neutron capture	State
(0)	0						$1d_{3/2}$
(1)	0,077	0	2	+	1; 2; 3	7.9	$1d_{3/2}$
(2)	0,515	0.48	0	+	0; 1	2.3; 0.8	
(3)	1.154	1.24	0	+	0; 1	3.8; 1.3	
(4)	1,316		3	—	2; 3; 4	12.0; 8.6; 6.7	$1f_{7/2}$
(5)	1.750	1.84					
(6)	2.177	2,23					
(7)	2.227						

Present work

determined--that is, whenever the agreement of the theoretical curve with the experimental points is not sufficiently good---a question mark has been placed opposite the dubious value. The parity and the allowed values of the spin J for the nuclear states of Cl^{36} observed in the reaction are indicated in the last two columns of Fig. 5. The results obtained for the longest track group agree with the published data[4]. The analysis which can be carried out for the case of the $Cl^{35}(d,p)Cl^{36}$ reaction, using the probability of neutron capture, does not lead to definite results, as is fully apparent, since the presence of levels with clearly manifested one particle excitation is not to be expected in Cl^{36}.

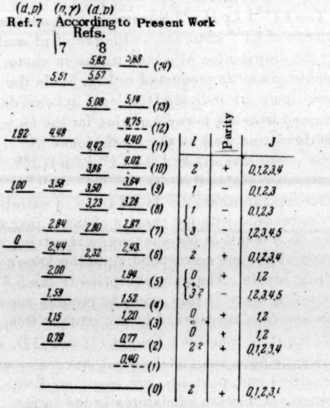
Cl38 (d,p) Ref. 7
Cl36 (n,γ) According to Refs. 7 8
(d,p) Present Work
5.82
5,68 (14)
5.51
5.57
5,08
5,14 (13)
4,75 (12)
1.92
4.48
4.42
4.40 (11)
3.86
4.02 (10)
1.00
3.58
3.50
3.64 (9)
3,23
3.28 (8)
2.84
2.80
2.87 (7)
0
2,44
2.32
2.43 (6)
2.00
1.94 (5)
1.59
1.52 (4)
1.15
1.20 (3)
0.79
0.77 (2)
0.40 (1)
(0)
l
Parity
J
2 + 0,1,2,3,4
1 - 0,1,2,3
1 - 0,1,2,3
3 - 1,2,3,4,5
2 + 0,1,2,3,4
0 + 1,2
3? - 1,2,3,4,5
0 + 1,2
0 + 1,2
2? + 0,1,2,3,4
2 + 0,1,2,3,4

FIG. 5. Nuclear level diagram for Cl^{36}.

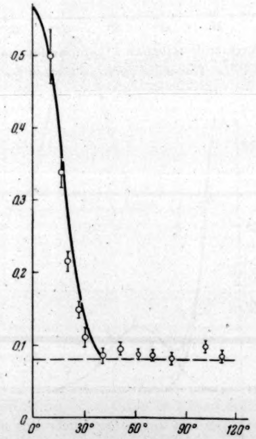

FIG. 6. Angular distribution of protons, corresponding to state (4) of the nucleus C^{36}. Solid curve: $l = 0$.

As an examination of the energy and angular distribution reveals, it is entirely probable that levels of Cl^{36} which cannot be resolved by the photographic plate method exist between levels (7) and (8) and near states (5) and (6). In evidence of this there is, first, the shape of the peaks of these proton groups, second, the very large differential cross section for the production of the protons composing these groups, and, third, the angular distributions for levels (5) and (7) – (8), which can be explained only if it is assumed that two values of the orbital momentum are transferred.

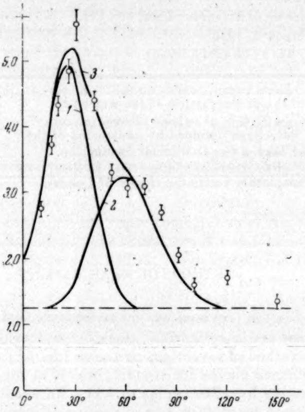

FIG. 7. Angular distribution of protons; corresponding to states (7) - (8) of the nucleus Cl^{36}, 1: $l = 1$; 2: $l = 3$, 3: $(l = 1) + (l = 3)$.

It should be noted that in constructing the energy level diagram of Cl^{36} it has been assumed that all of the groups of protons detected belong to the $Cl^{35}(d,p)Cl^{36}$ reaction. Some of the groups, however, could result from a reaction involving the heavy isotope Cl^{37} (25% in a natural mixture). The relative distribution of known[7] energy levels of Cl^{38} is shown in the left portion of Fig. 5.

In conclusion, I wish to express my gratitude to S. S. Vasiliev for his guidance, and to T. N. Markelov for assistance with the work.

Note added in proof: After submitting this article for publication, the work of Paris, Buechner and Endt[10] appeared in which the chlorine (*d,p*) reaction was investigated with the help of a magnetic spectrometer. A series of new nuclear energy levels of Cl^{36} in the range from 2.5 to 4 mev for the excitation energies (that is, in the region of levels (6) – (10)) were discovered, confirming the conclusions of the present article. The existence of level (1) with an energy of excitation 0.40 mev, however, was not confirmed.

[1] R. Huby, Prog. Nucl. Phys. **3**, 177 (1953).

[2] Parkinson, Beach and King, Phys. Rev. **87**, 387 (1952).

[3] C. F. Black, Phys. Rev. **90**, 381 (1953).

[4] J. S. King and W. C. Parkinson, Phys. Rev. **88**, 141 (1952).

[5] B. B. Kinsey and G. A. Bartholomew, Phys. Rev. **93**, 1260 (1954).

[6] Van Patter, Sperdutto, Endt, Buechner, and Enge, Phys. Rev. **86**, 502 (1952).

[7] P. M. Endt and I. C. Kluyver, Rev. Mod. Phys. **26**, 131 (1954).

[8] W. W. Ennis, Phys. Rev. **82**, 304 (1951).

[9] Groshev, Adiasevich and Demidov, *Report on the International Conference on the Peaceful Uses of Atomic Energy*, 1955.

[10] Paris, Buechner and Endt, Phys. Rev. **100**, 1317 (1955).

Translated by E. V. Ivash
4

SOVIET PHYSICS JETP VOLUME 4, NUMBER 1 FEBRUARY, 1957

The Coefficient of Volume Absorption of Second Sound and the Viscosity of the Normal Component of Helium II down to 0.83° K.

K. N. ZINOV'EVA
Institute for Physical Problems, Academy of Sciences, USSR

(Submitted to JETP editor March 2, 1956)
J. Exptl. Theoret. Phys. (U.S.S.R.) **31**, 31-36 (July, 1956)

Measurements of the absorption of second sound[1] have been extended to 0.83° K for frequencies from 200 cycles to 4 kc by the method of the determination of the width of resonance curves in standing waves. Values of the coefficient of volume absorption α/ω^2 and of viscosity η of the normal component of He II have been obtained by separation of the volume and surface losses. It is established that the losses due to thermal conduction predominate in the volume absorption. The analogue of the thermal conductivity in He II has been computed. The results of the experiment completely verify the theory of Landau and Khalatnikov for He II kinetic coefficients.

INTRODUCTION

THE absorption of second sound increases rapidly with drop in temperature, as was shown in a previous paper[1], and in other confirmatory researches[5,6]; in this case the surface absorption is due primarily to the viscosity, and the volume absorption to the thermal conductivity of He II.

The theoretical temperature dependence of the absorption coefficient has been computed by Khalatnikov[3,4], who showed that the absorption effect increased in the direction of low temperature; here the losses in second sound due to thermal conductivity are significantly greater than the losses determined by the first and second viscosity.

For the total coefficient of volume absorption, Khalatnikov obtained the expression

$$\frac{\alpha}{\omega^2} = \frac{1}{2\rho u_2^3}\left\{\frac{\rho_s}{\rho_n}\left[\frac{4}{3}\eta + \zeta_2 - \rho(\zeta_1 + \zeta_4) + \rho^2\zeta_3\right] + \frac{\varkappa}{c}\right\}, \qquad (1)$$

where η is the first viscosity coefficient, ζ_1, ζ_2, ζ_3, ζ_4 are the coefficients of second viscosity, c the heat capacity and $\varkappa$ the analogue of thermal conductivity in He II. Previous measurements of (1) did not permit a complete comparison of experiment with theory, since the experimental values of α/ω^2 were obtained in a comparatively narrow temperature range (1.0 – 1.2° K.).

In the present work, we have carried out measurements down to 0.83° K, using methods previously developed. In an attempt to make more precise the values and the temperature dependence of the kinetic coefficients we have also carried out more accurate measurements from 1 to 1.3° K.

METHODS OF MEASUREMENT

As in the previous work, the measurements were carried out in cylindrical glass resonators by the method of investigating the widths of the resonance curves for standing waves at frequencies from 200 cycles to 4 kc. We used three different resonators; two of them had internal diameters of 5.8 mm and lengths 91.2 and 44.5 mm, the third had an internal diameter 5.35 mm and length 86.2 mm. The plates at the ends of the resonator were made of glass instead of the plexiglass used previously, and were attached through a thin layer of oil to the polished faces of the resonator by means of a spring. A heater of constantan wire (50 μ) and a resistance thermometer of phosphor bronze (30 μ) were prepared in the form of flat, single-layered spools with bifilar windings, and were fastened to the disks. Replacement of the plexiglass reflectors by glass improved the frequency characteristics of the resonator in the region of the first transverse types of vibration, where earlier one had always observed an additional increase in the damping. The frequencies of the transverse resonances are given by[7]

$$(\omega/u_2)^2 = (l\pi/l_0)^2 + (r'_{nm}/a)^2, \qquad (2)$$

where $l = 1, 2, 3, \ldots$, r'_{nm} = roots of the derivatives of the Bessel functions, l_0 is the length and a the radius of the resonator. At the minimum velocity of second sound (at $T = 1.1$° K) two such transverse resonances exist up to 4 kc in the resonator of diameter 5.35 mm ($\nu' = 2000$ cycles and $\nu'' = 3620$ cycles), and in the resonator of diameter 5.8 mm, three ($\nu' = 1800$, $\nu'' = 3010$ and $\nu''' = 3840$ cycles). (The frequencies of transverse resonances increase with increase in the sound velocity.) Testing of the width of the resonance curves in regions close to transverse resonances showed that no noteworthy increase in the absorption of second sound could be observed at the fundamental resonances. This permitted us to extend the range of measurement (at not too low temperatures) to 4 kc. As in the previous research, the second sound was excited by the passage of current from the generator through the heater, and was detected by a resistance thermometer. The circuit described in Ref. 1 was used as an amplifier and was capable of measuring signals of ~ 0. 1 μ V with ease.

Temperatures below 1 ° K were obtained by removing the helium vapor through two diffusion pumps in series. The arrangement was similar to that described in Ref. 1. Temperatures of the helium inside the resonator above 1° K were measured with a resistance thermometer calibrated in terms of the helium vapor pressure. Below 1 ° K (down to 0.85 ° K), the temperature was determined from the velocity of second sound as measured by Peshkov[8] with a high degree of accuracy. The lowest temperature of 0.83 ° K obtained in the present work corresponded to a second sound velocity of 22.9 m / sec.

RESULTS

Measurements of the width of the resonance curves were carried out for minimum heat flow densities, usually not exceeding $3-5 \times 10^{-3}$ W/cm^2 since, for greater loading, a dependence of absorption on amplitude was observed. The graph of this dependence at T = 1. 27 ° K is shown in Fig. 1. As is evident from the drawing, the damping of second sound, relative to the damping at infinitesimal amplitude, was proportional to the power for three different frequencies. We did not make any special investigation of this problem and limited the region of measurement to small amplitudes, where the nonlinear effects are small.

To separate the volume and surface loss of second sound, proportional, respectively, to the square and square root of the frequency, the observed dependence on the frequency of the resonance width for different temperatures was plotted in coordinates $\Delta\ \nu/\sqrt{\nu}$; $\nu\sqrt{\nu}$, where ν is the frequency and $\Delta\ \nu$ is the resonance width in cycles. This dependence is plotted in Fig. 2 for the resonator d = 5. 8 mm, l_1 = 44.5 mm, l_2 = 91.2 mm. The intercepts on the ordinate determine the surface absorption of second sound, while the slope of the lines is proportional to the volume absorption. Above 1. 3 ° K, the accuracy of measurement was insufficient to determine the slope of the lines — they become virtually horizontal, which testifies to the predominant role of surface absorption at these frequencies.

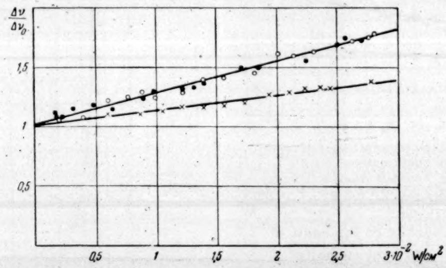

FIG. 1. Dependence of the absorption of second sound on power for T = 1.27 ° K in the resonator d = 5.35 mm and l = 86.2 mm ; O — 984, ● — 2750, × — 3960 cycles.

Boundary losses in the resonator, which amount to several per cent at high temperatures (1.6 – 2.0 ° K) are negligible at low temperatures, in comparison with the true absorption. While the absorption was always higher (at high temperatures) in the short resonator than in the long one (because of wall losses), at low temperatures, beginning about T ~ 1. 3 ° K, the absorption no longer depends on the length of the resonator.

We note that below 0.95 ° K, measurements are not possible in the longer resonator since the resonances for adjacent frequencies begin to overlap, due to the high damping.

The viscosity η of the normal component of He II can be computed from the magnitude of the surface absorption by the formula

$$\eta = \left(\frac{\Delta\nu}{\sqrt{\nu}}\right)_0^2 \frac{\pi r^2\rho^2\rho_n^2}{\rho_s^2}, \tag{3}$$

where r is the radius of the resonator, $(\Delta\nu/\sqrt{\nu})_0$ is the ordinate intercept in Fig. 2. The data for ρ_n/ρ, computed by Peshkov on the basis of second sound velocity[8] and heat capacity[9] measurements, were employed in this formula. The values of η computed from Eq. (3) down to the temperature $T = 0.83$ ° K, along with earlier measurements in the interval 1.4 – 2.1 ° K,[1] are shown by the circles in Fig. 3. We note that, in comparison with the earlier data, the values of η in the region 1.0 – 1.3 ° K are 20 to 30 per cent higher, which barely goes beyond the limits of error in the determination of η ($\sim$ 20 to 25 per cent). For comparison, the results of the measurement of viscosity by means of a rotating disk (Andronikashvili and others [10-12]) and the data of Heikkila and Hollis-Hallet[13], obtained by the rotating cylinder method, are plotted in the Figure. The solid line indicates the theoretical curve of Khalatnikov.[4] As is evident from the Figure, the experimental values of the viscosity agree quite satisfactorily, down to 0.83 ° K, with the theoretical values of Khalatnikov. At the lower temperature, the divergence can be explained by the extraordinarily steep dependence of η on T. It is interesting to note that the viscosity according to the measurements of Heikkila and Hollis-Hallet by the method of the rotating cylinder, which does not require knowledge of ρ_n/ρ, agrees well with our measurements, while the method of the rotating disk[10-12] gives essentially different results in the low temperature region. One cannot supply the reason for the divergence, which follows from our experiments, by errors in the determination of ρ_n/ρ at low temperatures, as has been assumed earlier by several authors. Evidently, in the region of low temperatures, where the concentration of the normal component is small, the dissipation of energy by the method of the rotating disk can increase appreciably, becuuse of the nonideality of the suspension system, which leads to an entrainment of superfluid along with the normal.

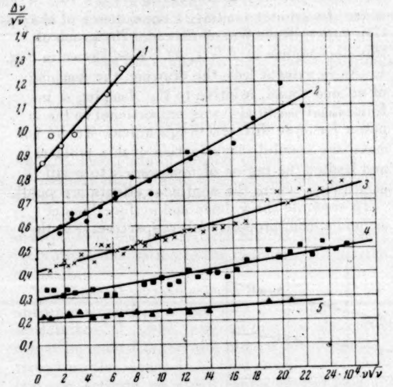

FIG. 2. Dependence of the absorption of second sound on frequency, in the coordinates $\Delta\nu/\sqrt{\nu}$, $\nu/\sqrt{\nu}$, O ● — resonator, $l = 44.5$ mm, $d = 5.8$ mm; × ■ ▲ — resonator, $l = 91.2$ mm, $d = 5.8$ mm; T is equal to: 1 – 0.86, 2 – 0.9, 3 – 0.95, 4 – 1.01, 5 – 1.1 ° K.

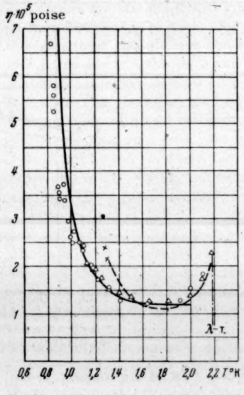

FIG. 3. Viscosity of the normal component of He II from the data: O = present measurements; ● = Ref. 12; × = Ref. 11; Δ = Ref. 13; broken line = Ref. 10; solid line = Ref. 4.

The coefficient of volume absorption α/ω^2 was computed from the magnitude of the volume loss of second sound in the temperature range 0.83 – 1.3 ° K. Computations were made according to the formula

$$\frac{\alpha}{\omega^2} = \frac{\Delta\nu/\nu^2}{4\pi\mu_2}, \tag{4}$$

where $\Delta\nu/\nu^2$ is the slope in Fig. 2, u_2 is the velocity of second sound. The temperature dependence of α/ω^2 is represented in a semi-logarithmic plot in Fig. 4. Here we have plotted the mean results of Hanson and Pellam [5] and the data of Atkins and Hart,[6] along with the theoretical curve of Khalatnikov[4] (solid line). It is easy to see that our experimental values of α/ω^2, determined to within 20 per cent, agree both with the theoretical values of Khalatnikov and with the values obtained by other authors at higher temperatures.

An estimate of the viscous loss in volume absorption of second sound according to values of the coefficient of first viscosity η, taken from our experiments (see Fig. 3), gives the broken curve in Fig. 4. As is evident from the Figure, viscosity losses are smaller by an order of magnitude than the total losses, and the relative contribution of the viscous loss decreases with decreasing temperature. Neglecting losses from second viscosity (in order of magnitude, they are comparable with losses from first viscosity), and attributing the remaining amount of absorption to the thermal conduction losses, we can estimate the coefficient of heat conductivity $\varkappa$ of He II to within 25 to 30 per cent. In this estimate, the values of the heat capacity were taken from the recent measurements of Kramers, Wasscher and Görter[14] which agree well with those of Ref. 9.

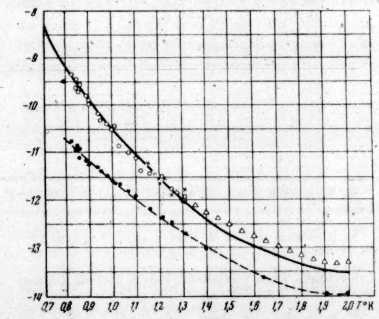

FIG. 4. Temperature dependence of the coefficient of volume absorption of second sound according to: O — present work, Δ — Ref. 5; × — Ref. 6; solid line — Ref. 4; ● — computed value of volume absorption of second sound, obtained from first viscosity.

The temperature dependence of $\varkappa$ is plotted in Fig. 5 on a semi-logarithmic scale. The solid line denotes the theoretical curve of Khalatnikov. The agreement of the experimental data with the theoretical is excellent. The high values of $\varkappa$ in the previous measurements[1] must evidently be explained by the additional increase in damping at high frequencies because of the effect of transverse vibrations.

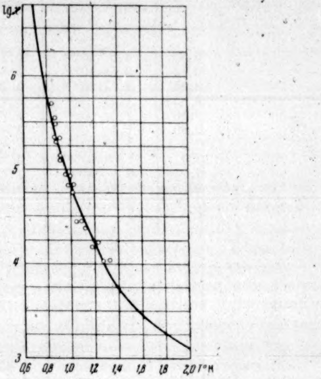

FIG. 5. Temperature dependence of the coefficient of thermal conductivity $\varkappa$ in He II: O = data of present work; solid curve = Ref. 4.

The experimental values of α/ω^2, η and $\varkappa$, taken from several experiments on different resonators, together with the data on u_2, ρ_n/ρ and c used by us are given in the Table. (Values of η above 1.4 °K are taken from the previous measurements.) From the values of $\varkappa$ it is not difficult to estimate the mean free path length of the phonons, making use of the classical formula in the quantum gas: $\varkappa = 1/3\, l_{ph}\, c_{ph}\, v_{ph}$. For the lowest temperature of our measurements, 0.83 °K, the mean free path length of the phonons was ~ 0.1 mm.

CONCLUSIONS

1. Experiments on the absorption of second sound down to 0.83 °K entirely confirm the validity of the theory of kinetic coefficients of He II of Landau and Khalatnikov.[2-4]

2. The volume absorption for second sound below 1 °K increases rapidly with decreasing temperatures, in full agreement with the theory. The losses due to the thermal conductivity of He II exceed the viscous losses by an order of magnitude.

3. The viscosity of the normal component of He II below 1 °K increases extremely rapidly with decrease in temperature. In absolute

T °K	α/ω^2, sec^2/см	$\eta \times 10^5$ poise	$\varkappa$ $\frac{\text{cal}}{\text{deg-cm-sec}}$	u_2, m/sec	ρ_n/ρ	c $\frac{\text{cal}}{\text{gm - deg}}$
0,83	$4.5 \cdot 10^{-10}$	6.7	$1.21 \cdot 10^{-2}$	22.9	$1.5 \cdot 10^{-3}$	$8.0 \cdot 10^{-2}$
0.85	$3.58 \cdot 10^{-10}$	5.8	$8.7 \cdot 10^{-3}$	22.0	$1.95 \cdot 10^{-3}$	$8.2 \cdot 10^{-3}$
0.85	$2.17 \cdot 10^{-10}$	5.26	$5.2 \cdot 10^{-3}$	22.0	$1.95 \cdot 10^{-3}$	$8.2 \cdot 10^{-3}$
0.855	$1,95 \cdot 10^{-10}$	5.6	$5,05 \cdot 10^{-3}$	21,95	$2.08 \cdot 10^{-3}$	$9.0 \cdot 10^{-3}$
0.86	$2.62 \cdot 10^{-10}$	3.7	$7.4 \cdot 10^{-3}$	21.6	$2.2 \cdot 10^{-3}$	$1.0 \cdot 10^{-3}$
0.89	$1.64 \cdot 10^{-10}$	3.66	$5.5 \cdot 10^{-3}$	20.6	$3.0 \cdot 10^{-3}$	$1.2 \cdot 10^{-3}$
0.9	$1.23 \cdot 10^{-10}$	3.42	$3.46 \cdot 10^{-3}$	20.3	$3.3 \cdot 10^{-3}$	$1.22 \cdot 10^{-2}$
0.9	$1.08 \cdot 10^{-10}$	3.55	$3.0 \cdot 10^{-3}$	20.3	$3.3 \cdot 10^{-3}$	$1.22 \cdot 10^{-2}$
0.94	$6.5 \cdot 10^{-11}$	3.72	$2.2 \cdot 10^{-3}$	19.5	$4.8 \cdot 10^{-3}$	$1.7 \cdot 10^{-2}$
0.95	$4.8 \cdot 10^{-11}$	3.38	$1.63 \cdot 10^{-3}$	19.35	$5.2 \cdot 10^{-3}$	$1.78 \cdot 10^{-2}$
0.98	$4.2 \cdot 10^{-11}$	2.96	$1.59 \cdot 10^{-3}$	18.9	$6.5 \cdot 10^{-3}$	$2.1 \cdot 10^{-2}$
1.0	$3.2 \cdot 10^{-11}$	2.61	$1.39 \cdot 10^{-3}$	18,7	$7.5 \cdot 10^{-3}$	$2.5 \cdot 10^{-2}$
1.01	$3.75 \cdot 10^{-11}$	2.5	$1.72 \cdot 10^{-3}$	18.7	$7.7 \cdot 10^{-3}$	$2.6 \cdot 10^{-2}$
1.03	$1.43 \cdot 10^{-11}$	2.74	$6.6 \cdot 10^{-4}$	18.5	$9.2 \cdot 10^{-3}$	$3.0 \cdot 10^{-2}$
1.07	$1.09 \cdot 10^{-11}$	2.49	$6.6 \cdot 10^{-4}$	18.35	$1.19 \cdot 10^{-2}$	$4.0 \cdot 10^{-2}$
1.1	$8.35 \cdot 10^{-12}$	2.45	$5.7 \cdot 10^{-4}$	18.30	$1.45 \cdot 10^{-2}$	$4.56, 10^{-2}$
1.16	$3.76 \cdot 10^{-12}$	2.02	$3.6 \cdot 10^{-4}$	18.4	$2.3 \cdot 10^{-2}$	$6.4 \cdot 10^{-2}$
1.21	$3.2 \cdot 10^{-12}$	1.72	$4.1 \cdot 10^{-4}$	18.55	$2.9 \cdot 10^{-2}$	$8.0 \cdot 10^{-2}$
1.25	$1.76 \cdot 10^{-12}$	1.8	$2.6 \cdot 10^{-4}$	18.85	$4.0 \cdot 10^{-2}$	$1.0 \cdot 10^{-1}$
1.31	$1.24 \cdot 10^{-12}$	1.56	$2.7 \cdot 10^{-4}$	19.2	$5.3 \cdot 10^{-2}$	$1.28 \cdot 10^{-1}$
1.4		1.3				
1.64		1.25				
1.91		1.3				
2.0		1.55				
2.1		1.8				

magnitude, the values of the viscosity agree with the results of the measurements of Heikkila and Hollis-Hallet[13], obtained by the rotating cylinder method, while a considerable divergence is observed from the results of Andronikashvili and others [10-12], observed by means of the rotating disk method below 1.5 ° K.

4. The analogue to the coefficient of thermal conductivity in He II, $\varkappa$, increases rapidly with drop in temperature, ranging in the interval 0.83 – 1.31° K from 1.2×10^{-2} to 2.7×10^{-4} cal/deg-cm-sec.

I take this opportunity to express my deep gratitude to V. Peshkov for valued advice and constant interest in the work, and also to N. I. Iakovlev, who helped in setting up the apparatus and carrying out the experiments.

---

[1] K. N. Zinov'eva, J. Exptl. Theoret. Phys. (U.S.S.R.) 25, 235 (1953).

[2] L. D. Landau and I. M. Khalatnikov, J. Exptl. Theoret. Phys. (U.S.S.R.) 19, 637, 709 (1949).

[3] I. M. Khalatnikov, J. Exptl. Theoret. Phys. (U.S.S.R.) 20, 243 (1950).

[4] I. M. Khalatnikov, J. Exptl. Theoret. Phys. (U.S.S.R.) 23, 8, 21 (1952).

[5] W. B. Hanson and J. R. Pellam, Phys. Rev. 95, 321 (1954).

[6] K. R. Atkins and K. H. Hart, Canad. J. Phys. 32, 381 (1954).

[7] Rayleigh, *Theory of Sound*, vol. 2, 295 (in Russian translation).

[8] V. P. Peshkov, J. Exptl. Theoret. Phys. (U.S.S.R.) 23, 686 (1952).

[9] Hull, Wilkinson and Wilks, Proc. Phys. Soc. (London) 64A, 379 (1951).

[10] E. Andronikashvili, J. Exptl. Theoret. Phys. (U.S.S.R.) 18, 429 (1948).

[11] deTroyer, van Itterbeek and Van den Berg, Physica 17, 50 (1951).

[12] A. C. Hollis-Hallet, Proc. Roy. Soc. (London) 210A, 404 (1952).

[13] W. J. Heikkila and A.C. Hollis-Hallet, Canad. J. Phys. 33, 420 (1955).

[14] Kramers, Wasscher and Gorter, Physica 18, 329 (1952).

Translated by R. T. Beyer
5

SOVIET PHYSICS JETP VOLUME 4, NUMBER 1 FEBRUARY, 1957

The Theory of Galvanomagnetic Effects in Metals

I. M. LIFSHITZ, M. IA. AZBEL' AND M. I. KAGANOV
Physico-technical Institute, Academy of Sciences, Ukrainian SSR

(Submitted to JETP editor December 15, 1955)
J. Exptl. Theoret. Phys. (U.S.S.R.) 31, 63-79 (July, 1956)

The theory of galvanomagnetic effects in metals in large magnetic fields is developed, without any restrictive assumptions concerning the dispersion law of electrons or the collision integral[1].

A LARGE number of experimental and theoretical studies have been devoted to the behavior of metals in electric and magnetic fields. After the discovery of Kapitza[2] of a linear increase of resistivity with field in a number of metals, it was shown by Justi[3] that all metals can be divided into two groups. In the first group (Cu, Na, In, Al,..) the resistivity in large magnetic field tends to a saturation value; in the second group (Bi, Be, Zn, Mg, ...) it grows without limit as the square of the magnetic field ($\rho \sim H^2$). Borovik[3] moreover showed that there is a characteristic difference in the behavior of the Hall field between these two groups. He also showed[3] that the linear growth of resistivity (Kapitza law) is observed in the transition region between two regions of quadratic growth.

In previous theories of the galvanomagnetic effects, it has been usual to start with some specific assumption about the form of the electron energy spectrum and of the metal and about the electron-lattice interactions. In order to explain an unlimited growth of resistivity, it has been usual to introduce "holes" (positively charged current carriers) somewhat artificially as well as electrons (negatively charged current carriers), and the precise physical meaning of the holes was obscure.

In the present work, a theory of galvanomagnetic effects is developed which involves no special assumptions beyond the use of the Fermi distribution for the electrons in the metal.

1. CONDUCTION ELECTRONS IN A MAGNETIC FIELD

The current carriers in a metal--the elementary excitations usually called metallic electrons or conduction electrons--are characterized by quasi-momentum p, energy ϵ, charge e and spin ½. The periodicity of the crystalline lattice leads to a periodic dependence of the energy ϵ on the quasi-momentum $\mathbf{p}$ with the period of the reciprocal lattice[4]. $\epsilon = \epsilon(\mathbf{p})$ is a many-valued function, so that more exactly we have $\epsilon = \epsilon_n(\mathbf{p})$, where n denotes the number of the energy band ("zone"); in what follows we shall omit the subscript n. Close to points of minimum or maximum energy, the constant-energy surfaces are clearly closed, and moreover, in the immediate neighborhood of the extremal points they are ellipsoidal. Any (closed) constant-energy surface close to an energy minimum encloses (in momentum space) a region where the energy is smaller than its value on the surface ($\nabla_p \epsilon$ directed out of the region), while any closed surface close to an energy maximum encloses a region where the energy is greater than its value on the surface ($\nabla_p \epsilon$ is directed into the region).

Since $\epsilon(\mathbf{p})$ is a periodic function, the surfaces described above will be repeated periodically throughout the reciprocal lattice. Between these surfaces, which are topologically simple, there must occur more complex ones--self-intersecting and open surfaces. We call open surfaces those which pass continuously through the whole reciprocal lattice. Thus Fig. 1 shows the energy surfaces in two dimensions given by the equation*

$$\varepsilon = A_1 \cos k_x a_x + A_2 \cos k_y a_y.$$

It will be seen that if $A_1 = A_2$, a single open surface exists (Fig. 1*a*), but that if $A_1 \neq A_2$, there exists a whole family of them (Fig. 1*b*).

In the real three-dimensional case, a great variety of open surfaces may arise, which may be simply or multiply connected (some examples of open surfaces are shown in Figs. 2-5).

The energy levels of a solid, the structure of which we have described above, are filled by elec-

---

* The corresponding equation in three dimensions gives the dependence of energy on momentum according to the tight-binding approximation[5].

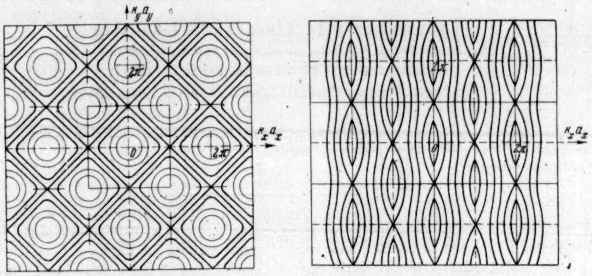

a *b*

FIG. 1

trons in a way which is determined (at absolute zero) by the number of electrons per atom and by the disposition of the zones (i.e., whether or not they overlap). In what follows, we shall be interested only in the zones which are only partly filled (clearly, such zones always exist in a metal[4]). In the general case, there will be several such zones, so that the limiting Fermi surface, $\epsilon(\mathbf{p}) = \zeta$, will in general consist of several separate surfaces, each repeated periodically because of the periodicity of the function $\epsilon(\mathbf{p})$.

Consider now the motion of a conduction electron in a constant and uniform magnetic field **H** directed along the *z* axis ($H_x = H_y = 0$; $H_z = H$). We shall use the classical equations of motion, i.e., we neglect quantization of motion in the magnetic field. For magnetic fields satisfying $\mu H \ll \zeta$

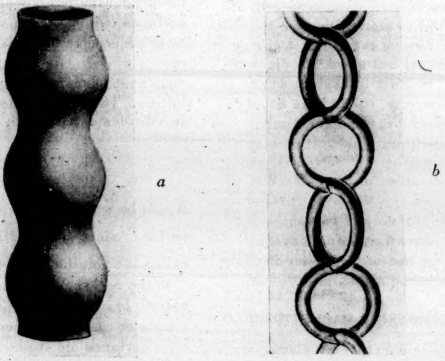

a *b*

FIG. 2

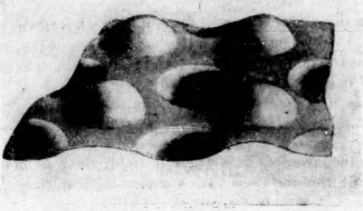

FIG. 3

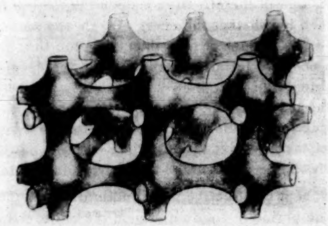

FIG. 4

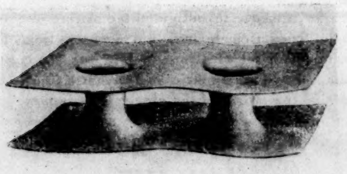

FIG. 5

(which is perfectly well satisfied for all attainable fields), this is clearly permissible if we are not interested in the small quantum oscillations[6] superposed on the monotonic rise of resistivity and Hall field with magnetic field*.

When moving in a magnetic field H, the conduction electrons conserve their energy ϵ and p_z, the component of the momentum p along the z axis. Thus the trajectory of the electrons in momentum space is given by the curve

$$\varepsilon(\mathbf{p}) = \text{const}; \quad p_z = \text{const}. \qquad (1)$$

The character of the motion along the trajectory in momentum space depends essentially on whether the curve (1) is closed, i.e., breaks up into a number of closed curves each lying within a single cell of the reciprocal lattice**, or open, i.e., running continuously through the whole reciprocal lattice.

For closed energy surfaces, every trajectory in a magnetic field is a closed curve. For open energy surfaces, both open and closed trajectories may occur. [Suppose, for instance, that the constant-energy surface is an "undulating cylinder" (Fig. 2*a*); then if the magnetic field is perpendicular to the axis of the cylinder, the trajectory is open, but for all other field directions it is closed.] In investigating the properties of conduction electrons in a magnetic field, it is convenient to classify open surfaces as follows:

1) Surfaces which contain open orbits only for unique directions of the magnetic field (or for none at all);

2) Those for which there is a one-dimensional infinity (two-dimensional angle) of directions of magnetic field leading to open trajectories;

3) Those for which there is a two-dimensional infinity (solid angle) of directions of magnetic field leading to open trajectories.

The simplest example of the first class of surface is that shown in Fig. 2*b*; of the second class, the

---

* More exactly, in order for the classical equations of motion, and in particular, the concept of a trajectory in phase space, to be valid, two conditions must be satisfied:

$$\lambda = \hbar / p_0 \ll r = cp_0 / eH, \quad a \ll r;$$

where a is the lattice constant. It is easy to see that the first condition is identical with that given above (assuming $\epsilon_0 = p_0^2 / 2m_0$), and the second condition is then evidently satisfied, since $\hbar / p_0 \approx n^{1/3}$, where n is the density of electrons, of the order of, or less than, one electron per atom (i.e., $\hbar/p_0 \geq a$.).

** Note that if the (x, y) plane does not coincide with one of the crystallographic planes, these closed curves will not all be identical.

"undulating cylinder"(Fig. 2*a*; the two-dimensional angle is here 2π); of the third class, the "undulating plane" (Fig. 3; the solid angle is here 4π, excluding only the direction perpendicular to the "plane"). A variety of multiply-connected surfaces can occur, all of which can be classified in this way. It should be noted that for surfaces of more complicated topology (as illustrated in Figs. 4 and 5) open trajectories are only encountered extremely rarely.

In the present work we shall examine in more detail the properties of conduction electrons in a magnetic field in those cases where the basic role (see below) is played by closed trajectories. The investigation of other cases involving more complicated topologies of the energy surfaces will be the subject of a separate communication.

The position of an electron on the curve (1) is determined by the time of rotation t, reckoned from some (arbitrary) point on the trajectory. From the equations of motion

$$d\mathbf{p}/dt = (e/c)[\mathbf{vH}]; \quad \mathbf{v} = \nabla_{\mathbf{p}}\varepsilon \qquad (2)$$

we obtain, noting that $\mathbf{v}_\perp$ (with components v_x and v_y) is normal to curve (1),

$$dl/dt = -(eH/c)v_\perp; \quad v_\perp = \sqrt{v_x^2 + v_y^2}.$$

Here dl is the element arc of the curve (1), taken in the direction of motion along the trajectory in momentum space. Integrating the above equation, we obtain

$$t = -(c/eH)\int dl/v_\perp. \qquad (3)$$

If the curve (1) is closed, then the period of rotation around the curve is

$$T = -\frac{c}{eH}\oint\frac{dl}{v_\perp} = -\frac{c}{eH}\frac{\partial S}{\partial \varepsilon} \qquad (4)$$

Here $S = S(\epsilon, p_z)$ is the area of the plane p_z = constant intersected by the surface $\epsilon(\mathbf{p})$ = constant. The last equation is easily obtained, noticing ing that

$$S = \iint dp_x\,dp_y = \int d\varepsilon \oint dl/v_\perp.$$

It is natural to call the quantity $m^* = (1/2\pi) \times \partial S/\partial\epsilon$ the effective mass of the electron in a magnetic field. For free electrons,

$$\varepsilon = p^2/2m_0, \quad S = \pi p_\perp^2 = \pi(2m_0\varepsilon - p_z^2),$$

so that $\partial S/\partial\epsilon = 2\pi m_0$. We note that $m^* = m^*(\epsilon, p_z)$ is a function of ϵ and p_z--quantities which are conserved in a magnetic field. The usual definition of the effective mass tensor--

$$(1/m)_{ik} = \partial^2\varepsilon/\partial p_i\,\partial p_k$$

is inconvenient in a magnetic field, since on this definition the mass varies around the trajectory. The connection between period and effective mass,

$$T = -2\pi c m^*/eH \qquad (5)$$

is the same as for free electrons.

The sign of the effective mass $m^*(\epsilon, p_z)$ is determined by whether the energy inside the surface $\epsilon(\mathbf{p}) = \epsilon$ is greater or less than ϵ. In the first case m^* is positive for all values of p_z; in the second case, negative.

If the curve (1) is self-intersecting, it is not possible to establish such a simple criterion for the sign of the effective mass.

It should be emphasized that for open trajectories the concept of effective mass, naturally connected with the period of rotation around the orbit, cannot be introduced.

2. KINETIC EQUATION FOR CONDUCTION ELECTRON IN A MAGNETIC FIELD

So far, we have investigated the motion of a single conduction electron in a magnetic field. We now consider the electron gas in a metal in constant and uniform electric and magnetic fields. To describe the states of the electrons it is now natural to use as variables ϵ, p_z and the dimensionless quantity

$$\tau = t/T_0 = (1/2\pi m_0)\int dl/v_\perp,$$

specifying the position of the electron along the trajectory in momentum space (cf. Eq. (3)]. Here

$$T_0 = -2\pi c m_0/eH, \qquad (5a)$$

where m_0 is a characteristic mass introduced only for convenience; since in the final formulas m_0 disappears, we need not specify it more precisely.

The kinetic equation for the distribution function $f = f(\epsilon, p_z, \tau)$ in the variables chosen has the form:

$$\frac{\partial f}{\partial \tau}\dot{\tau} + \frac{\partial f}{\partial p_z}\dot{p}_z + \frac{\partial f}{\partial \varepsilon}\dot{\varepsilon} + \left(\frac{\partial f}{\partial t}\right)_{\text{cT}} = 0. \qquad (6)$$

We consider the stationary case; the values of $\dot{\tau}$, $\dot{p}_z$ and $\dot{\epsilon}$ are obtained from the equations of motion

$$d\mathbf{p}/dt = (e/c)[\mathbf{vH}] + e\mathbf{E}, \qquad (7)$$

where **E** is the electric field strength. $(\partial f/\partial t)_{\text{coll}} \equiv t_0^{-1} W\{f\}$ is the collision integral, the form of which will not concern us except in Sec. 6; t_0 is a characteristic relaxation time. Using Eqs. (2) and (7), we find

$$\dot{\varepsilon} = e\mathbf{vE}; \quad \dot{p}_z = eE_z;$$

$$\dot{\tau} = \frac{1}{T_0}\left(1 - \frac{c}{v_\perp^2 H}[\mathbf{v}_\perp \mathbf{E}]_z\right). \qquad (8)$$

In what follows we shall, as is customary, assume that the energy acquired by an electron between collisions is not only very small compared with the Fermi energy ζ, but that it is also small compared with $k\theta$ (θ = temperature of the electron gas). This permits linearization of the kinetic equation with respect to the ekectric field E. Thus we suppose that

$$f = f_0 - et_0\psi_i E_i, \quad f_0 = [e^{(\varepsilon-\zeta)/k\theta} + 1]^{-1}, \qquad (9)$$

where f_0 is the equilibrium Fermi function. For ψ_i we easily get a linear equation, on neglecting terms quadratic in the electric field,

$$\partial\psi_i/\partial\tau + \gamma_0\hat{W}\{\psi_i\} = \gamma_0 f_0'(\varepsilon)v_i. \qquad (10)$$

Here $\gamma_0 = H_0/H$, where H_0 is the magnetic field for which the period of the Larmor precession T_0 is equal to the relaxation time t_0 [cf. (5a)]. The role of boundary condition for Eq. (10) is played for closed orbits by the periodicity condition (with period T/T_0) on the function ψ_i, and for open trajectories by the requirement that ψ_i shall remain finite.

Averaging Eq. (10) over τ, we obtain

$$\overline{\hat{W}\{\psi_i\}} = f_0'(\varepsilon)\overline{v}_i. \qquad (11)$$

The bar denotes an average with respect to the "time" τ;

$$\overline{u} = \frac{T_0}{T}\int_0^{T/T_0} u\,d\tau.$$

In the case of open curves the average must be taken in the limit as $T \to \infty$.

For the closed curves (1)

$$\overline{v_\alpha} = 0, \quad (\alpha = x, y). \qquad (12)$$

Indeed, the dependence of **v** on τ *in the linearized equation* is given by the equations of motion (2):

$$v_x = -\frac{1}{2\pi m_0}\frac{\partial p_y}{\partial \tau}; \quad v_y = \frac{1}{2\pi m_0}\frac{\partial p_x}{\partial \tau}. \qquad (13)$$

The averaging of the derivatives with respect to τ for closed trajectories leads naturally to the result (12). The mean value of the z-component of velocity v_z is always different from zero, because in the direction of the magnetic field the motion is unbounded.

As remarked above, a detailed study of the various types of open trajectory will be published separately. To show that a change in the topology of the energy surfaces leads to new results, we consider briefly here the simplest case*, in which the curves (1) are sections of the "undulating cylinder" by the planes p_z = constant. Suppose the magnetic field to be perpendicular to the cylinder axis. Choosing the x direction to be along the cylinder axis, we find, on averaging (13),

$$\overline{v_x} = 0; \quad \overline{v_y} \neq 0; \quad \overline{v_z} \neq 0. \qquad (14)$$

In the case of arbitrary open curves, $\overline{\mathbf{v}}_\alpha \neq 0$.

3. SOLUTIONS OF THE KINETIC EQUATIONS. STRONG MAGNETIC FIELD

In what follows we shall be interested in magnetic fields large compared with H_0, i.e., $\gamma_0 \ll 1$. We look for a solution of Eq. (10), satisfying condition (11), in the form of a power series in γ_0:

$$\psi_i = \sum_{k=0}^{\infty}\gamma_0^k\psi_i^{(k)}. \qquad (15)$$

---

* The major problem in treating surfaces of the second and third type (cf. Sec. 1) is to determine the variation of physically interesting quantities with field direction. In the present communication this problem is not solved.

Substituting (15) in (10), we obtain a set of equations for the functions $\psi_i^{(k)}$:

$$\frac{\partial\psi_i^{(0)}}{\partial\tau} = 0; \quad \frac{\partial\psi_i^{(1)}}{\partial\tau} + \hat{W}\{\psi_i^{(0)}\} = f_0'(\varepsilon)v_i;$$

$$\frac{\partial\psi_i^{(k)}}{\partial\tau} + \hat{W}\{\psi_i^{(k-1)}\} = 0; \quad (k = 2, 3, \ldots). \tag{16}$$

From these,

$$\psi_i^{(k)} = C_i^{(k)} - \tilde{\psi}_i^{(k)}; \quad \tilde{\psi}_i^{(0)} = 0; \tag{17}$$

$$\tilde{\psi}_i^{(1)} = \int_0^\tau \{\hat{W}(C_i^{(0)}) - f_0'(\varepsilon)v_i\}\,d\tau;$$

$$\tilde{\psi}_i^{(k)} = \int_0^\tau \hat{W}\{\psi_i^{(k-1)}\}\,d\tau \quad (k = 2, 3, \ldots).$$

Here the $C_i^{(k)}$ are functions only of ϵ and p_z, found from Eq. (11):

$$\hat{W}_0(C_i^{(0)}) = f_0'(\varepsilon)\bar{v}_i; \tag{18}$$

$$\hat{W}_0(C_i^{(k)}) = \overline{\hat{W}(\tilde{\psi}_i^{(k)})} \quad (k = 1, 2, \ldots);$$

$$\hat{W}_0 = \frac{T_0}{T}\int_0^{T/T_0}\int_0^{T/T_0}\hat{W}(\varepsilon, p_z, \tau; \varepsilon', p_z', \tau')\,d\tau\,d\tau'.$$

The expressions (17) and (18) enable us in principle to calculate the functions $\psi_i^{(k)}$. For explicit calculations, it is necessary to know the form of the operator $\hat{W}$. However, many important results (on the variation of conductivity, Hall field, etc. with H in strong magnetic fields) can be obtained without explicit calculation. We shall see that it is possible to deduce the asymptotic behavior of the experimentally measurable quantities simply from a knowledge of the topology of the constant-energy surfaces in the neighborhood of the limiting Fermi energy ζ.

Two cases may be distinguished (noting that because of the factor $f_0'(\epsilon)$ on the right-hand side of Eq. (10), only energies close to the Fermi energy are important]:

1) In the interval $\delta\epsilon \sim k\theta$ where the Fermi function is changing, there are no open trajectories for the field direction considered;

2) In the interval $\delta\epsilon \sim k\theta$ where the Fermi function is changing, open trajectories exist (in particular, the trajectories on the Fermi surface itself are open)*.

In the first case, we may use the fact that in the whole of the relevant energy interval, $\bar{v}_\alpha = 0$ ($\alpha = x, y$). We then have $C_\alpha^{(0)} = 0$** so that [cf (17) and (13)]:

$$\psi_x = \gamma_0(-p_y f_0'/2\pi m_0 + C_x^{(1)}) + \gamma_0^2\psi_x^{(2)} + \ldots, \tag{19}$$
$$\psi_y = \gamma_0(p_x f_0'/2\pi m_0 + C_y^{(1)}) + \gamma_0^2\psi_y^{(2)} + \ldots;$$
$$\psi_z = C_z^{(0)} + \gamma_0\psi_z^{(1)} + \ldots$$

The important result emerges that ψ_α and ψ_z have different asymptotic behaviors in high fields, i.e., for γ_0 tending to zero.

In the second case (where open trajectories exist in the interval $\delta\epsilon \sim k\theta$) zero-order terms appear in the expansion for all ψ_i:

$$\psi_i = C_i^{(0)} + \gamma_0\psi_i^{(1)} + \ldots \tag{20}$$

For the particular case of a magnetic field perpendicular to the axis of the "undulating cylinder", we obtain from (14) and (18):

$$\psi_x = \gamma_0(-p_y f_0'/2\pi m_0 + C_x^{(1)}) + \gamma_0^2\psi_x^{(2)} + \ldots; \tag{21}$$
$$\psi_{y,z} = C_{y,z}^{(0)} + \gamma_0\psi_{y,z}^{(1)} + \ldots$$

4. THE CONDUCTIVITY TENSOR

To construct the conductivity tensor we use the expression for the current density:

$$j_i = \frac{2e}{h^3}\int v_i f\,(d\mathbf{p}). \tag{22}$$

Here the integral should be understood in the following sense:

$$\int \ldots (d\mathbf{p}) = \lim_{G\to\infty}\frac{1}{G}\int_{(GV_0)} \ldots (d\mathbf{p}), \tag{22'}$$

where G is the number of cells in the reciprocal lattice and V_0 the volume of one cell of the reciprocal lattice.

In the case where only closed trajectories are present, the range of integration in (22′) must be chosen so that each orbit lies wholly within it. In particular, if these trajectories belong only to closed surfaces (more exactly, if only such trajectories are of importance), the integration over all p-space can be reduced to a sum of integrations over separate cells of the reciprocal lattice (summed over the different zones), where in each integral (i.e., in each zone) the cell must be chosen so that the whole closed surface lies within it.

---

* Various cases can then be distinguished, as was discussed above.

** The first of Eqs. (18) has in this case only the trivial solution $C_\alpha^{(0)} = 0$. This may be easily deduced from the fact that otherwise all the remaining equations for the $C_\alpha^{(k)}$ would have no solution.

Substituting for f in terms of the functions ψ_i and comparing the expression obtained with Ohm's law $j_i = \sigma_{ik}E_k$, we obtain

$$\sigma_{ik} = -2e^2 t_0 h^{-3} \int v_i \psi_k \, (d\mathbf{p}). \tag{23}$$

We note that $\sigma_{ik}(\mathrm{H}) = \sigma_{ki}(-\mathrm{H})$ in virtue of the principle of symmetry of kinetic coefficients (Ref. 7, Sec. 118). These relations are easily obtained by making direct use of the kinetic equations for the function f and the Hermitian property of the collision operator.

Substituting the value of ψ_k from (19) into (23), we obtain in the *first case* (no open trajectories in the interval where the Fermi function is changing) a conductivity tensor of the form:

$$\sigma_{ik}(\mathrm{H}) = \begin{pmatrix} \gamma_0^2 a_{xx} & \gamma_0 a_{xy} & \gamma_0 a_{xz} \\ \gamma_0 a_{yx} & \gamma_0^2 a_{yy} & \gamma_0 a_{yz} \\ \gamma_0 a_{zx} & \gamma_0 a_{zy} & a_{zz} \end{pmatrix}. \tag{24}$$

The expansion of the matrix elements a_{ik} in powers of γ_0 in general begins with the zero order term. It should be noted that in special cases some terms may be zero from symmetry requirements (for instance, $a_{xz} = a_{yz} = a_{zx} = a_{zy} = 0$ in the isotropic case)*.

All the matrix elements a_{ik} are functionals of $C_i^{(k)}$ and consequently depend on the collision integral (cf. below, Sec. 5). An exception is $a_{xy}^{(0)}\ (= -a_{yx}^{(0)})$ -- the zero-order term in the expansion of a_{xy} in powers of γ_0. Indeed, from (23) and (19),

$$a_{xy}^{(0)} = -\frac{2e^2 t_0}{h^3} \int v_x \left(\frac{p_x}{2\pi m_0} + C_y^{(0)} \right) f_0'(\varepsilon)\,(d\mathbf{p}).$$

changing the variables ϵ, p_z and τ, and noting that the Jacobian of the transformation is

$$\partial(p_x, p_y, p_z) / \partial(\varepsilon, \tau, p_z) = 2\pi m_0,$$

that $v_x = -(1/2\pi m_0)\,\partial p_y / \partial\tau$, and that $C_y^{(0)}$ is independent of τ [cf. (17)], we obtain

$$a_{xy}^{(0)} = -\frac{e^2 t_0}{\pi m_0 h^3} \int f_0'(\varepsilon) \frac{\partial p_y}{\partial\tau} p_x \, dp_z \, d\tau \, d\varepsilon$$

$$= -\frac{e^2 t_0}{\pi m_0 h^3} \int f_0'(\varepsilon)\, d\varepsilon \int dp_z \oint p_x \, dp_y.$$

The inner integral $\oint p_x dp_y = \pm S(\epsilon, p_z)$, where $S(\epsilon, p_z)$ is the area of the plane p_z = constant intersected by the surface $\epsilon(\mathbf{p}) = \epsilon$, and the sign is determined by the sense of rotation around the orbit, i.e., by the sign of the effective mass m^* (cf. Sec. 1). Since $\sigma_{xy} = \gamma_0 a_{xy}$, we have asymptotically in large fields:

$$\sigma_{xy} = -\frac{ec}{H}\frac{2}{h^3} \left\{ \int \frac{\partial f_0}{\partial\varepsilon} d\varepsilon \times \left[\int S_1(\varepsilon, p_z)\, dp_z - \int S_2(\varepsilon, p_z)\, dp_z \right] \right\}.$$

Here the first integral is taken over those parts of the zone where $m^* > 0$, and the second over those parts where $m^* < 0$.

If we put $-f_0'(\epsilon) = \delta(\epsilon - \zeta)$, we get

$$\sigma_{xy} = \frac{ec}{H}\frac{2}{h^3} \left\{ \int S_1(\zeta, p_z)\, dp_z - \int S_2(\zeta, p_z)\, dp_z \right\}. \tag{25}$$

Thus finally, *if the closed trajectories under consideration are situated on closed surfaces*, we obtain

$$\sigma_{xy} = (2ec / Hh^3)(V_1(\zeta) - V_2(\zeta)).$$

Here $V_1(\zeta)$ is the volume enclosed by the surfaces $\epsilon(\mathbf{p}) = \zeta$, within which the energy is less than ζ (i.e., $m^* > 0$), and $V_2(\zeta)$ the volume enclosed by the surfaces $\epsilon(\mathbf{p}) = \zeta$, within which the energy is greater than ζ (i.e., $m^* < 0$). Noting that states with energy less than ζ are occupied by electrons, we obtain

$$\sigma_{xy} = ec\,(n_1 - n_2) / H. \tag{26}$$

Here n_1 is the number of states occupied by electrons with positive effective mass, and n_2 the number of unoccupied states with negative effective mass. It is natural to call n_1 the number of "electrons", and n_2 the number of "holes".

---

* The first terms in the expansion of σ_{xx} and σ_{yy} in powers of γ_0 vanish because of the particular form of $\psi_x^{(1)}$ and $\psi_y^{(1)}$ in (19) [cf. below, calculation of $a_{yx}^{(0)}$].

It should be emphasized that it is only possible to introduce these concepts if in the energy interval $\delta\epsilon$ there exist only closed, nonintersecting energy surfaces. Thus, if in the interval $\delta\epsilon$ there exist only closed surfaces, the asymptotic value of σ_{xy} is given by Eq. (26). In this case we note that σ_{xy} does not depend on the direction of the magnetic field. If, however, the closed trajectories have arisen as sections of open surfaces, then the transition from (25) to (26) cannot be made. In this case σ_{xy} is as before proportional to $1/H$, but is now strongly dependent on the direction of the magnetic field.

The case $n_1 = n_2$ needs special consideration (here, of course, we are still considering closed energy surfaces). In this case $a^{(0)}_{xy} = 0$, i.e., generally speaking*,

$$\sigma_{xy} \sim \gamma_0^2 = H_0^2 / H^2. \tag{27}$$

It should be noted that equality of the numbers of electrons and "holes" is not something exceptional; all metals with an even number of electrons possess conduction electrons only because the energy bands in the metal overlap. It is natural that the number of vacant states (number of "holes") in the lower zone should be equal to the number of occupied states (number of electrons in the upper zone [cf. Fig. 6). We recall that it is only possible to speak of "holes" and "electrons" when the empty and occupied states correspond to closed energy surfaces. This will always be the case if the overlap of energy zones is not too great (Fig. 6). Strictly speaking, exact compensation ($n_1 = n_2$), leading to the result (27), is possible only at the absolute zero. Thermal excitation will cause the removal of electrons from deeper states in the zone, not equivalent to closed surfaces and therefore not contributing to the "number of holes". Thus, although the number of electrons in the upper zone is equal to the number of vacant states in the lower zone, the equation $n_1 - n_2 = 0$ is violated in this case. Evidently,

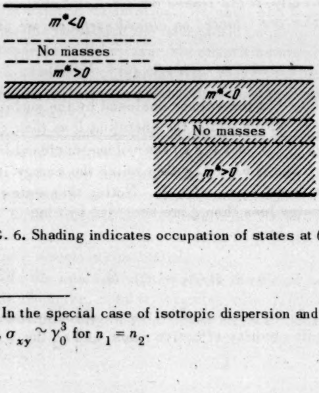

FIG. 6. Shading indicates occupation of states at $\theta = 0$.

$$n_1 - n_2 \sim ne^{-\Delta\varepsilon/k\theta}, \tag{28}$$

where n is the number of electrons in the zone and $\Delta\epsilon$ is the energy gap between the Fermi surface and the nearest open surface.

Thus, if there exist no open orbits in the interval $\delta\epsilon$, all σ_{ik} (except σ_{zz}) ten to zero as H tends to infinity ($H \gg H_0$); but the nature of the asymptotic approach to zero is different for the different coefficients [cf. Eq. (24)].

This statement is valid only at the absolute zero of temperature ($\theta = 0$). At finite temperatures, i.e., if $f_0'(\epsilon) \neq -\delta(\epsilon - \zeta)$, we cannot in general put $\bar{v}_\propto = 0$ everywhere, since among all trajectories there may be open ones. This leads to the appearance of zero-order terms in the expansion of all the σ_{ik} with respect to γ_0. However, owing to the factor $f_0'(\epsilon)$, the zero-order terms $\psi_i^{(0)}$ are of order $\exp(-\Delta\epsilon_1/k\theta)$, where $\Delta\propto_1$ is a quantity of the order of the energy gap from the Fermi surface to the nearest surface containing open trajectories. The appearance of zero-order terms in the expansion of ψ_i leads to the appearance of zero-order terms in the expansion with respect to γ_0 of all the matrix elements σ_{ik}. However, in all the elements σ_{ik} (except σ_{zz}) these terms are neglibly small up to fields of order $H_0 \exp(\Delta\epsilon_1/k\theta)$, which are at present unattainable*.

---

* In the special case of isotropic dispersion and $\hat{W} \equiv 1$, $\sigma_{xy} \sim \gamma_0^3$ for $n_1 = n_2$.

* Moreover, the quantization of orbits in a magnetic field[6] must be taken into account at a much earlier stage.

In the second case (when open trajectories do exist in the interval $\delta\epsilon \sim k\theta$) all $\psi_i^{(0)}$ are different from zero (20). In consequence of this, all the matrix elements σ_{ik} tend to saturation for $H >> H_0$. Moreover, all the σ_{ik} now depend on temperature even at low temperatures, where normally (in the absence of a magnetic field) the kinetic coefficients depend only feebly on temperature.

When the energy surfaces are of the second or third type (cf. Sec. 1), an extremely strong anisotropy should be observed in the dependence of σ_{ik} on magnetic field. In fact, as the direction of the magnetic field approaches that in which there exist open normal sections, the size of the tensor components σ_{ik} changes considerably [because of the change in character of the solutions of (16)]. For instance, in the simplest case of the "undulating cylinder" (see above), as long as the magnetic field H is not perpendicular to the cylinder axis, the asymptotic dependence of σ_{ik} on magnetic field is given by (24), while if H is perpendicular to the axis,

$$\sigma_{ik}(\mathbf{H}) = \begin{pmatrix} \gamma_0^2 a'_{xx} & \gamma_0 a'_{xy} & \gamma_0 a_{xz} \\ \gamma_0 a'_{yx} & a'_{yy} & a'_{yz} \\ \gamma_0 a'_{zx} & a'_{zy} & a'_{zz} \end{pmatrix} \qquad (29)$$

[cf. (23) and (21)]. As before, expansion of the matrix elements a'_{ik} in powers of γ_0 begins with the zero-order term.

Thus, an experimental determination of the asymptotic behavior of σ_{ik} in strong magnetic fields for various orientations in principle makes possible a clarification of the topology of the constant-energy surfaces in the region of the Fermi energy.

It should be noted that the usual experimental arrangement, in which the electric field is measured for only one current direction, does not permit a determination of the dependence of all σ_{ik} on magnetic field. It is essential to compare the results of measurements for three noncoplanar directions of current flow. There ate at present no experimental results which can be used for this purpose.

5. FOURIER METHOD

In cases where only electrons moving along closed trajectories are important (no open trajectories in the interval $\delta\epsilon \sim k\theta$), the Fourier method can be used to analyze the solution of Eq. (10). For convenience, the position of the electron in its orbit in momentum space will be specified in this section by the phase φ, varying from 0 to 2π:

$$\varphi = 2\pi\frac{t}{T} = 2\pi\int\frac{dl}{v_\perp}\Big/\oint\frac{dl}{v_\perp} \qquad (30)$$

[cf. (3) and (4)].

Expressing Eq. (10) in terms of the new variable φ, we obtain

$$(\partial\psi/\partial\varphi) + \gamma\hat{W}\{\psi\} = \gamma f_0'(\varepsilon)\,\mathbf{v}. \qquad (31)$$

Here $\gamma = (T/2\pi T_0)\gamma_0 = T/2\pi t_0$ and is a function of ϵ and p_z in distinction to the constant γ_0 introduced in Sec. 2. We now expand **v** and ψ in Fourier series:

$$\mathbf{v}(\varepsilon, p_z, \varphi) = \sum_{k=-\infty}^{\infty} \mathbf{v}_k(\varepsilon, p_z)\,e^{ik\varphi}, \qquad (32)$$

$$\psi(\varepsilon, p_z, \varphi) = \sum_{k=-\infty}^{\infty} \psi_k(\varepsilon, p_z)\,e^{ik\varphi}.$$

Expressed in Fourier components, Eq. (31) becomes:

$$ik\psi_k + \gamma\hat{W}_{kk'}\psi_{k'} = \gamma f_0'(\varepsilon)\,\mathbf{v}_k; \qquad (33)$$

here $\hat{W}_{kk'}$ is the Fourier component of the operator $\hat{W}$ and is an operator with respect to the variables ϵ and p_z; summation over doubly occurring indices is understood. Note that the equations of motion (2) (connecting the quantities **p** and **v** entering into the linearized equations), when applied to the Fourier components of **p** and **v** assume the form

$$ik\,\mathbf{p}_k = m^*[\mathbf{v}_k\,\mathbf{n}]; \quad \mathbf{H} = H\mathbf{n}. \qquad (34)$$

The vector ψ can be represented as follows:

$$\psi = [\mathbf{n}\boldsymbol{\varphi}] + \theta\,\mathbf{n}; \quad \boldsymbol{\varphi} = [\psi\mathbf{n}]; \quad \theta = (\psi\mathbf{n}). \qquad (35)$$

From (33), (34) and (35) we have

$$ik\,\boldsymbol{\varphi}_k + \gamma\hat{W}_{kk'}\boldsymbol{\varphi}_{k'} = ik\gamma f_0'(\varepsilon)\,\mathbf{p}_k/m^*; \qquad (36)$$
$$ik\theta_k + \gamma\hat{W}_{kk'}\theta_{k'} = \gamma f_0'(\varepsilon)\,v_k^z.$$

In expanding φ_k and θ_k in powers of γ it is convenient first to eliminate φ_0 and θ_0. Substituting $k = 0$ in Eqs. (36), we have

$$\boldsymbol{\varphi}_0 = -\hat{W}_{00}^{-1}\hat{W}_{0k'}\boldsymbol{\varphi}_{k'}; \tag{37}$$

$$\theta_0 = \hat{W}_{00}^{-1}\{f_0'(\varepsilon)v_0^z - \hat{W}_{0k'}\theta_{k'}\} \qquad (k' \neq 0).$$

from which

$$\begin{aligned} \boldsymbol{\varphi}_k - \gamma\hat{L}_{kk'}\boldsymbol{\varphi}_{k'} &= \gamma f_0'(\varepsilon)\mathbf{p}_k/m^*, \\ \theta_k - \gamma\hat{L}_{kk'}\theta_{k'} &= \gamma h_k. \end{aligned} \qquad (k, k' \neq 0) \tag{38}$$

Here

$$\hat{L}_{kk'} = \frac{i}{k}\{\hat{W}_{kk'} - \hat{W}_{k0}\hat{W}_{00}^{-1}\hat{W}_{0k'}\},$$

$$h_k = -\frac{i}{k}\{f_0'(\varepsilon)v_k^z - \hat{W}_{k0}\hat{W}_{00}^{-1}f_0'(\varepsilon)v_0^z\}. \tag{39}$$

The solution of Eq. (38) may be expressed as follows:

$$\boldsymbol{\varphi}_k = (1-\gamma\hat{L})_{kk'}^{-1}\gamma f_0'(\varepsilon)\frac{\mathbf{p}_{k'}}{m^*}$$

$$= \gamma f_0'\frac{\mathbf{p}_k}{m^*} + \gamma\hat{L}_{kk'}\gamma f_0'\frac{\mathbf{p}_{k'}}{m^*} + \ldots,$$

$$\theta_k = (1-\gamma\hat{L})_{kk'}^{-1}\gamma h_{k'} = \gamma h_k + \gamma\hat{L}_{kk'}\gamma h_{k'} + \ldots \tag{40}$$

From this and (37) it can be seen that the expansion of φ_k and θ_k in powers of γ begins with the first power ($\sim 1/H$). An exception is θ_0, for which the expansion begins with the term of zero order

$$\theta_0 = \hat{W}_{00}^{-1}f_0'(\varepsilon)v_0^z - \hat{W}_{0k'}\gamma h_{k'} + \ldots \tag{41}$$

The same results might, of course, have been obtained by the method of successive approximations, starting from Eqs. (16) and (18).

We note that the linear term in the expression for φ_k does not depend on the collision integral [cf. Eq. (21)]. Using Eqs. (22), (9) and (35), we find

$$\mathbf{j} = -\frac{2e^2}{h^3}\int\{(\boldsymbol{\varphi}[\mathbf{En}]) + \theta(\mathbf{nE})\}\mathbf{v}(d\mathbf{p})$$

from which

$$\sigma_{\alpha\beta} = -\frac{2e^2t_0}{h^3}\int v_\alpha[\mathbf{n}\boldsymbol{\varphi}]_\beta(d\mathbf{p}); \tag{42}$$

$$\sigma_{iz} = -\frac{2e^2t_0}{h^3}\int\theta v_i(d\mathbf{p}).$$

($\alpha, \beta = x, y$). We recall that $\sigma_{ik}(\mathrm{H}) = \sigma_{ik}(-\mathrm{H})$.

Substituting the Fourier expansions of φ and θ in these formulas, we obtain

$$\sigma_{\alpha\beta} = -\frac{2e^2t_0}{h^3}\sum_{k=-\infty}^{\infty}\int v_{-k}^\alpha[\mathbf{n}\boldsymbol{\varphi}_k]^\beta(d\mathbf{p});$$

$$\sigma_{iz} = -\frac{2e^2t_0}{h^3}\sum_{k=-\infty}^{\infty}\int v_k^i\theta_k(d\mathbf{p}),$$

or, since $\mathbf{v}$, φ and θ are real quantities and $v_0^\alpha = 0$,

$$\sigma_{\alpha\beta} = -\frac{4e^2t_0}{h^3}\mathrm{Re}\sum_{k=1}^{\infty}\int v_{-k}^\alpha[\mathbf{n}\boldsymbol{\varphi}_k]^\beta(d\mathbf{p});$$

$$\sigma_{iz} = -\frac{2e^2t_0}{h^3}\left\{\int v_0^i\theta_0(d\mathbf{p}) + 2\mathrm{Re}\sum_{k=1}^{\infty}\int v_{-k}^i\theta_k(d\mathbf{p})\right\}.$$

Using the expressions (40 and (31), and the equations of motion (34), we obtain the components of the conductivity matrix in powers of the reciprocal of the magnetic field:

$$\sigma_{xx} = -\frac{4c^2}{h^3H^2}\sum_{k=1}^{\infty}$$

$$\times\int p_{-k}^y(\hat{\mathscr{L}}_{kk'} - \hat{\mathscr{L}}_{k0}\hat{\mathscr{L}}_{00}^{-1}\hat{L}_{0k'})p_{k'}^y f_0'(\varepsilon)(d\mathbf{p}) + \ldots;$$

$$\sigma_{yy} = -\frac{4c^2}{h^3H^2}\sum_{k=1}^{\infty}$$

$$\times\int p_{-k}^x(\hat{\mathscr{L}}_{kk'} - \hat{\mathscr{L}}_{k0}\hat{\mathscr{L}}_{00}^{-1}\hat{L}_{0k'})p_{k'}^x f_0'(\varepsilon)(d\mathbf{p}) + \ldots;$$

$$\sigma_{xy} = (n_1 - n_2)ec/H + \ldots;$$

$$\sigma_{zz} = -\frac{2e^2}{h^3}\int v_0^z\hat{\mathscr{L}}_{00}^{-1}f_0'(\varepsilon)v_0^z(d\mathbf{p}) + \ldots;$$

$$\sigma_{xz} = \frac{4ec}{h^3H}\mathrm{Re}\sum_{k=1}^{\infty}$$

$$\times\int p_{-k}^y\{f_0'(\varepsilon)v_k^z - \hat{\mathscr{L}}_{k0}\hat{\mathscr{L}}_{00}^{-1}f_0'(\varepsilon)v_0^z\}(d\mathbf{p}) + \ldots;$$

$$\sigma_{yz} = -\frac{4ec}{h^3H}\mathrm{Re}\sum_{k=1}^{\infty}$$

$$\times\int p_{-k}^x\{f_0'(\varepsilon)v_k^z - \hat{\mathscr{L}}_{k0}\hat{\mathscr{L}}_{00}^{-1}f_0'(\varepsilon)v_0^z\}(d\mathbf{p}) + \ldots$$

($\mathfrak{L} = t_0\hat{W}$ is the collision integral). From these expressions it is simple to derive expressions for the matrix elements a_{ik}, but the explicit form of these will not be required in what follows.

The solutions of Eqs. (33) are particularly simple in cases where a time of relaxation exists, i.e., when*

$$\hat{\mathscr{L}} \equiv 1/t_0 \quad (\hat{\mathscr{L}}_{kk'} \equiv (1/t_0)\,\delta_{kk'}),$$

$$\psi_k = \gamma f_0'(\varepsilon)\,\mathbf{v}_k/(\gamma + ik). \tag{43}$$

We then have

$$\psi = \gamma f_0'(\varepsilon) \sum_{k=-\infty}^{\infty} \frac{\mathbf{v}_k e^{ik\varphi}}{ik+\gamma}, \tag{44}$$

$$\sigma^{xx'}(\mathbf{H}) = -\frac{2e^2t_0}{h^3} \sum_{k=-\infty}^{\infty} \int \frac{v^x_{-k} v^{x'}_k}{ik+\gamma} \gamma f_0'(\varepsilon)\,(d\,\mathbf{p}), \tag{45}$$

or

$$\sigma^{xx'}(\mathbf{H}) = -\frac{2e^2t_0}{h^3}\Big\{\int \overline{v^x}\,\overline{v^{x'}} f_0'(\varepsilon)\,(d\,\mathbf{p}) + 2\,\mathrm{Re}$$

$$\sum_{k=1}^{\infty} \int \frac{(v_k^x)^{*} v_k^{x'}}{ik+\gamma} \gamma f_0'(\varepsilon)\,(d\,\mathbf{p})\Big\}. \tag{46}$$

In the case of a quadratic isotropic dispersion law, only one term remains in the sum, and we easily obtain the well-known formulas:

$$\sigma_{xx} = \sigma_{yy} = \sigma/(1+\Omega_0^2 t_0^2); \qquad \sigma_{zz} = \sigma; \tag{47}$$

$$\sigma_{xy} = -\sigma_{yx} = \sigma\Omega_0 t_0/(1+\Omega_0^2 t_0^2); \qquad \sigma_{xz} = \sigma_{yz} = 0$$

(where σ is the conductivity of the metal in the absence of a magnetic field, and $\Omega_0 = 2\pi/T_0$ is the frequency of Larmor precession). It should be noted that such a dependence of the conductivity tensor on the magnetic field is obtained in all cases where an isotropic dispersion law is under consideration (independent of the detailed form of the collision integral). This is connected with the fact that in all such cases the action of the collision operator on a function of the form $\chi_i(\epsilon)v_i$ reduces to a multiplication of the latter by a quantity depending on energy but not on angle[4]. This leads to the identical vanishing of all ψ_k except ψ_0 and $\psi_{\pm 1}$. This can be seen from Eq. (41), if we notice that in the isotropic case $V_k = 0$ ($k = \pm 2, \pm 3, \ldots$), and we obtain Eq. (47).

6. ARBITRARY MAGNETIC FIELD ($\gamma \sim 1$)

The Fourier method is applicable only if the trajectories in momentum space are closed. If they are open, the expressions obtained in Sec. 5 have no meaning.

In the present section compact formulas are obtained for the conductivity in a magnetic field for those cases where the collision integral may be written in the form $(f - f_0)/t_0$ (i.e., $\hat{W} \equiv 1$). In such a case Eq. (10) becomes a differential equation instead of an integro-differential equation*:

$$\partial\psi_i/\partial\tau + \gamma_0\psi_i = \gamma_0 f_0'(\varepsilon)\,v_i.$$

The solution of this equation, satisfying (11), has the form

$$\psi_i = \gamma_0 \int_0^\infty e^{-\gamma_0\tau'} v_i(\tau - \tau')\,d\tau' f_0'(\varepsilon). \tag{48}$$

Substituting this expression for ψ_i into formula (23) for σ_{ik}, changing the order of integration and averaging, we obtain

$$\sigma_{ik} = -\frac{2e^2t_0}{h^3}\int \varphi_{ik}(\varepsilon, p_z) f_0'(\varepsilon)\,(d\mathbf{p}), \tag{49}$$

$$\varphi_{ik}(\varepsilon, p_z) = \gamma_0 \int_0^\infty e^{-\gamma_0\xi}\,\overline{v_i(\tau)\,v_k(\tau+\xi)}\,d\xi.$$

These expressions are convenient for investigating explicit laws of dispersion.

7. RESISTIVITY AND HALL FIELD

For the investigation of galvanomagnetic phenomena, it is usual to let a current of a given magnitude flow through the crystal in a given direction, and to measure the components of electric field in three noncoplanar directions (as far as possible, three orthogonal directions; cf, for example, Ref. 3). What is then studied is the resistivity tensor in a magnetic field.

$$\rho_{ik}(\mathbf{H}) = \sigma_{ik}^{-1}(\mathbf{H}).$$

Using the expressions obtained earlier for the asymptotic behavior of $\sigma_{ik}(\mathrm{H})$, it is easy to find the asymptotic behavior in high magnetic fields ($H \gg H_0$) of the resistivity tensor $\rho_{ik}(\mathrm{H})$.

---

* t_0 may here depend on ϵ and p_z.

* We revert now to the notation of Secs. 1-4.

1) *When only closed trajectories are important.*
a) According to (24),

$$\rho_{ik}(\mathbf{H}) = \begin{pmatrix} b_{xx} & \gamma_0^{-1} b_{xy} & b_{xz} \\ \gamma_0^{-1} b_{yx} & b_{yy} & b_{yz} \\ b_{zx} & b_{zy} & b_{zz} \end{pmatrix}. \qquad (50)$$

The expansion of the matrix elements b_{ik} in powers of γ_0 begins with the zero-order terms, which are determined by the zero-order terms of the matrix a_{ik} as follows:

$$b_{xx} = (a_{yy} a_{zz} + a_{yz}^2) / a_{zz} a_{xy}^2; \quad b_{xy} = -b_{yx} = 1 / a_{yx};$$
$$b_{xz} = -b_{zx} = a_{zy} / a_{zz} a_{xy}; \quad b_{yy} = (a_{xx} a_{zz} + a_{xz}^2) / a_{zz} a_{xy}^2);$$
$$b_{yz} = -b_{zy} = a_{zx} / a_{zz} a_{yx}; \quad b_{zz} = 1 / a_{zz}.$$

Thus if in the interval $\delta\epsilon$ there are only closed surfaces, then ρ'_{xx}, $\rho_{yy} \sim (n_1 - n_2)^{-2}$, and

$$\rho_{xy} / H = 1 / (n_1 - n_2) ec + \ldots \qquad (51)$$

If, however, the closed trajectories are formed by sections of open surfaces (cf. Sec. 4), then

$$\rho_{xy} / H = h^3 / 2 \{\int S_1(\zeta, p_z) dp_z - \int S_2(\zeta, p_z) dp_z\} \qquad (52)$$

and depends markedly on the direction of the magnetic fields.

Generally in experimental work the current j is perpendicular to the magnetic field. Let us take the x axis parallel as to the direction of current. Then the resistivity ρ (the ratio of electric field strength parallel to the current to the current density) is ρ_{xx}*, and ρ_{xy}/H coincides with the Hall "constant" $R = E_y / Hj$. Thus, in this case the resistivity tends to a saturation value, and ρ depends markedly on the direction of magnetic field independently of whether the closed trajectories arise as sections of closed surfaces or not.

The asymptotic behavior of the Hall "constant" is different in these two cases. If the surfaces are closed, then from (51) R is a constant determining the difference between electrons and "holes". If, however, the surfaces are open (though the sections are closed), then R is a complicated function of angle [cf. (52)]. Thus a study of the Hall field in large magnetic fields is particularly important in studying the topology of the Fermi surface.

We should note the following fact: Generally, by Hall field we mean the electric field, prependicular to the current, arising when a current passes through the metal in a magnetic field and changing sign when the magnetic field changes sign, i.e., with our choice of coordinates,

$$E_{\mathrm{Hall}} = {}^1/_2 [E_y(\mathbf{H}) - E_y(-\mathbf{H})]. \qquad (53)$$

On such a definition, the even powers of H naturally vanish. We should note that in the case considered the leading term in the asymptotic behavior of $E_y(\mathbf{H})$ contains the first (odd) power of magnetic field.

b) $n_1 = n_2$. In this case, as has been pointed out, $\sigma_{xy} \sim H_0^2 / H^2$. Consequently,

$$\rho_{\alpha\beta} \sim H^2 / H_0^2; \quad \rho_{\alpha z} \sim H / H_0;$$

$$\rho_{zz} \sim \mathrm{const} \quad (\alpha, \beta = x, y)$$

From this we see that in this case the resistivity grows quadratically with magnetic field. The significant difference of this case, moreover, lies in the presence of quadratic terms (in magnetic field) in the expression for $E_y(\mathbf{H})$, i.e.,

$$E_y(\mathbf{H}) = (AH^2 + BH) j,$$

where A and B are constants depending on the explicit form of the collision integral and the dispersion law. Because of this the Hall field (53) in the present case does not characterize the leading term in the asymptotic behavior of the electric field perpendicular to the current. Note that A is connected with the anisotropy of the crystal. In the isotropic case $A = 0$[*].

---

* For arbitrary current direction (n_i), $\rho = \rho_{ik} n_i n_k$.

This discussion shows that the experimentally well-known existence of a group of metals (Be, Zn, Cd, Mg, Ga, Sn, Pb, C, Bi, Sb, As, Mo, W, Ba) with anomalous group of resistance follows from the most general considerations of the modern theory of metals. Previously these results have been obtained only under extremely special assumptions[8].

The linear growth of resistivity with magnetic field observed by Kapitza[2] in many metals corresponds to a transition from a quadratic dependence in small fields to a quadratic dependence with a different coefficient in high fields. The same conclusion was reached by Borovik[3], from analysis of the data in the literature and also from experimental observation of both the quadratic dependencies and the transition region between them ,which approximates well to a linear dependence.

The influence of temperature, i.e., the effect of the exponentially small terms (of order $\exp(-\Delta\epsilon/k\theta)$--cf. (28)] leads to a satuartion of all components of the resistivity tensor. However, this saturation is reached only in extremely high fields, or order $H \sim H_0 \exp(\Delta\epsilon/k\theta)$.

2) *When open orbits do exist in the range* $\delta\epsilon \sim k\theta$.

Generally speaking, in this case all the matrix elements ρ_{ik} tend to stauration, which naturally leads to saturation of the resistivity. The Hall "constant", however, decreases quadratically with increasing magnetic field. However, the symmetry of the open surface may substantially change these results. For instance, in the special case of the "undulating cylinder" (with magnetic field perpendicular to cylinder axis), according to (29) the matrix ρ_{ik} has the form

$$\rho_{ik}(\mathbf{H}) = \begin{pmatrix} \gamma_0^{-2} b'_{xx} & \gamma_0^{-1} b'_{xy} & \gamma_0^{-1} b'_{xz} \\ \gamma_0^{-1} b'_{yx} & b'_{yy} & b'_{yz} \\ \gamma_0^{-1} b'_{zx} & b'_{zy} & b'_{zz} \end{pmatrix}.$$

The elements of the matrix b'_{ik} are determined by the values of the elements a'_{ik}. It should be remembered that in the present case the x axis is along the axis of the cylinder.

Thus, if the current flows in the (yz) plane, the resistivity tends to saturation; in other cases it grows quadratically.

The Hall field always grows linearly with magnetic field. The Hall "constant" has no simple physical meaning.

At the present time, apparently, there are still no experimental data on the asymptotic behavior of the tensor ρ_{ik} in high fields which can be used to draw conclusions about the topology of the Fermi surface.

In conclusion, the authors would like to thank L. D. Landau and E. S. Borovik for helpful discussions.

---

[*] Note that in the presence of two overlapping zones with quadratically anisotropic dispersion laws ($n_1 = n_2 = n$) and with proportional mobility tensors ($u_{ik}^{(2)} = k u_{ik}^{(1)}$)

$$\rho = \frac{\sigma_2 \cos^2\alpha + \sigma_1 \sin^2\alpha}{\sigma_1\sigma_2}\left(1 + \frac{H_2}{H_0^2}\right);$$

$$R = \frac{E_{\text{Hall}}}{jH} = -\frac{1}{nec}\frac{1-k}{1+k},$$

$$E_y^{(S)} = \frac{E_y(\mathbf{H}) + E_y(-\mathbf{H})}{2j}$$

$$= \frac{\sin\alpha\cos\alpha\,(\sigma_2 - \sigma_1)}{\sigma_1\sigma_2}\left(1 + \frac{H^2}{H_0^2}\right).$$

Here $H_0 = c/e\sqrt{u_1^{(1)} u_2^{(2)}}$; $\sigma_{1,2}$ are the principal values of the conductivity tensor $\sigma_{ik} = ne^2 u_{ik}(1+k)$. The magnetic field is chosen to lie along one of the principal axes (the third), the current is perpendicular to the magnetic field and α is the angle between the axis l and the current.

[1] Lifshitz, Azbel' and Kaganov, J. Exptl. Theoret. Phys. (U.S.S.R.) 30, 220 (1956); Soviet Phys. JETP 3, 143 (1956).

[2] P. L. Kapitza, Proc. Roy. Soc. (London) 125A, 292 (1929).

[3] E. Justi, *Leitfähigkeit und Leitungsmechanismus fester stoffe*, Göttingen, 1948; E. S. Borovik, J. Exptl. Theoret. Phys. (U.S.S.R.) 23, 83, 91 (1952).

[4] R. Peierls, *Electron Theory of Metals*, IIL, 1947 (Russian translation).

[5] F. Bloch, Z. Physik 52, 555 (1928).

[6] Lazarev, Nakhimovich and Parfenova, J. Exptl. Theoret. Phys. (U.S.S.R.) 9, 1169 (1939); I. M. Lifshitz, J. Exptl.

Theoret. Phys. (U.S.S.R.) 30, 814 (1956); Soviet Phys. JETP 3, 774 (1956).

[7] L. D. Landau and E. M. Lifshitz, *Statistical Physics*, GITTL, 1951.

[8] D. Blochinzev and L. Nordheim, Z. Physik 84, 168 (1953); T. Kontorova and Ia. Frenkel, J. Exptl. Theoret. Phys. (U.S.S.R.) 5, 405 (1935); B. Davydov and I. Pomeranchuk, J. Exptl. Theoret. Phys. (U.S.S.R.) 9, 1295 (1935); E. Sondheimer and A. Wilson, Proc. Roy. Soc. (London) 190A, 435 (1949); M. Kohler, Ann. d. Physik 6, 186 (1949); G. Zilberman, J. Exptl. Theoret. Phys. (U.S.S.R.) 29, 762 (1955); Soviet Phys. JETP 2, 650 (1956).

Translated by D. Shoenberg and R. G. Chambers
10

SOVIET PHYSICS JETP VOLUME 4, NUMBER 1 FEBRUARY, 1957

Structure of the Intermediate State of Superconductors

B. M. BALASHOVA AND IU. V. SHARVIN
Institute for Physical Problems, Academy of Sciences, USSR

(Submitted to JETP editor, March 13, 1956)
J. Exptl. Theoret. Phys. (U.S.S.R.) 31, 40-44 (July, 1956)

The structure of the intermediate state was studied by application of fine ferromagnetic powder to the surface of a tin specimen. Two-dimensional pictures of structures of various types were obtained for various contents of normal phase in the specimen. The influence of a number of other factors (method of transition, temperature, specimen size and others) on the character of the picture was also studied.

INTRODUCTION

As is well known, a superconductor in the intermediate state is broken up into regions or "domains" of superconducting and normal phases (s– and n– phases). The magnetic field is concentrated almost entirely in the n– domains. Thus the field outside the specimen and very close to its surface is also nonuniform. The dimensions of the s– and n–domains in thermodynamic equilibrium must be determined by two basic factors which act in opposing directions. The field energy close to the specimen will be reduced by reduction of the field inhomogeniety and from this point of view it is energetically favorable to increase the degree of disperseness of the state. On the other hand the presence of a positive surface tension at the phase boundaries tends to increase the dimensions of the domains.

Agreement between experimental and theoretical investigation of the geometry of the intermediate state would therefore permit the development of a method of finding the magnitude of the surface tension from observation of the equilibrium dimensions of the structure. A knowledge of this quantity and its dependence on various factors (temperature, crystallographic orientation of the phase boundary and others) would be very useful for the development of the theory of superconductivity.

This problem however is a long way from being solved. Mathematical difficulties prevent consideration in a general form of the problem of the shape of the phase boundaries. Landau succeeded, however, in giving exact calculation of the shapes and sizes of the domains under certain simplifying conditions. In one calculation nearly plane parellel s– and n– layers were considered,[1] while in another[2] a model was considered in which the n– layers repeacedly branched as they approached the external surface so that the structure was homogeneous or "mixed" at the surface. Subsequent work by other authors[3,4,5,6] is based on the methods used by Landau. In particular it was shown[4] that a model with layers branching a limited number of times and coming out to the surface without formation of the mixed phase (i.e., in a certain sense a combination of the models of Refs. 1 and 2) is energetically more favorable than the original methods. In one way or another all the formulas proposed for connecting the surface tension with the dimensions of the domains, have been obtained only under various simplifying assumptions, still requiring experimental verification, about the shapes of the domains.

The experiments of Shal'nikov, Meshkovskii and Tumanov[7-11] on the pattern of the field distribution in a gap between two tin hemispheres by the methods of a bismuth micro-probe and ferromagnetic powder have shown that the real structures of the intermediate state have not a regular or simple form and are not reproducible for various modes of transition to the given point in the intermediade state (for various procedures of changing the field and temperature). The $s-$ and $n-$ domains in these experiments have a range of sizes down to very small sizes. From other considerations Meshkovskii deduced the existence of a "fine structure" within the $n-$ layers observed by him (which were of width of order 1 mm and predominantly radial in direction), i.e., the existence of a large number of fine unresolved inclusions of $s-$ phase. The size of the domains was not determined in these experiments both because of the irregularity of the patterns and because of insufficient resolving power of the methods used. It should be noted that in spite of the irregularity of the general pattern of distribution of the domains, an averaged characteristic of the state such as the relative content of normal phase in the specimen (denoted in what follows by η) is practically a single valued function of H and T (at least for pure macroscopic spherical specimens of "soft" superconductors, such as tin). It was also shown[12] that the average domain size in a monocrystalline tin specimen is well reproducible for different modes of transition to the given point in the intermediate state.

In the present work, we investigated the topography of the $s-$ and $n-$ domains at the surface of tin specimens for various values of η . Our main aim was to sort out which qualitative features of the real structure were associated with an equilibrium and stable character, having in mind a possible comparison of the results with the above-mentioned theoretical studies, where only the case of thermodynamic equilibrium was considered.

METHOD OF OBSERVATION

The form of the $n-$ domains was investigated by depositing a fine ferromagnetic powder on the surface of the specimen. Nickel powder, consisting of rounded particles of average size about 1 μ was deposited by sprinkling on the open surface during the actual experiment. In order to do this a glass tube B was introduced into the cap of the liquid helium Dewar (Fig. 1), and connected to it was a coarse-pored filter F into which some well dried nickel powder was sprinkled.

The experiment was carried out as follows. The specimen A was brought into the desired point of the intermediate state by suitable variation of field and temperature and then by means of the pump H helium was blown through the filter F ; some of the smallest particles of the powder were then carried by the current of helium into the Dewar and on to the surface of A . Observation and photography of the patterns produced was carried out through the telescope T . In order that boiling of the helium should not disturb the photography, the pressure in the Dewar was increased during the time of exposure. After exposure, the powder could be removed from the surface by means of the brush K, and the experiment could then be repeated. Before each experiment the specimen was heated above the transition temperature. The powder clung rather firmly to the specimen surface and this made it possible to photograph patterns even after the specimen was taken out of the apparatus.

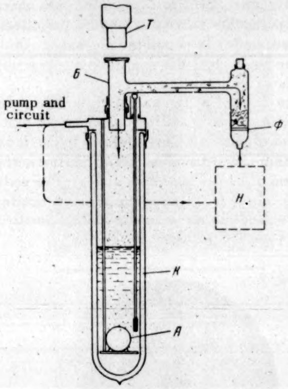

FIG. 1. Scheme of apparatus.

The resolving power of the method was checked by means of a special model prepared from alternating layers of copper and lead of various thicknesses in the range from 1 to 0.05 mm, and put into the apparatus in place of the specimen. The pattern obtained at 4.2 ° K in a field of 100 Oe reproduced the structure of the model very well.

For studying the distribution of domains in the gap between two hemispheres we used a method of Shal'nikov[9,11]. Nickel powder was introduced into the gap before the experiment and during the experiment it redistributed itself when the specimen was shaken, being drawn into the regions of maximum field.

RESULTS

The structure of the intermediate state observed in our experiments proved to be very complicated and varied, and it is possible here only to describe the most clear-cut qualitative characteristics of these structures.

Figures 2 to 4 show the patterns obtained on the surface of a monocrystalline tin sphere of diameter 30 mm and of purity 99.998% for $\eta = 0.15$. It can be seen that the *n*-domains issue from the surface in the form of narrow wrinkled strips. For still smaller η, slose to 0, the *n*-domains are scattered over the surface in the form of separate small regions of similar wrinkled strips.

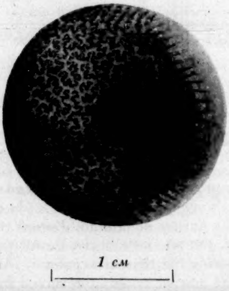

FIG. 2. General view of sphere of diameter 30 mm for $\eta = 0.15$, $T = 2.85^\circ$ K, Transition $n \rightarrow s$. H = const.

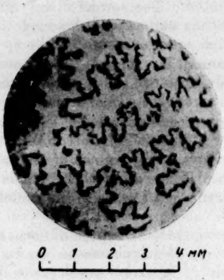

FIG. 3. Part of Fig. 2, greatly enlarged.

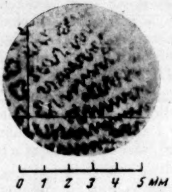

FIG. 4. Part of the surface of a sphere of diameter 30 mm close to a pole; photographed through the telescope; $\eta = 0.15$, $T = 2.85^\circ$ K, Transition $s \rightarrow n$, T = const.

With increase of η the wrinkled *n*-domains cover an even larger fraction of the specimen surface and their form gradually changes in such a way that completely closed little islands of *s*-phase are formed between them (Fig. 5). The type of structure for η close to 1 is shown in Fig. 6. No fine structure in the *n*-phase surrounding the rounded islands of *s*-phase visible in the picture is observed, and does not apparently exist. An indirect proof of this comes from a rough estimate of the relative area occupied by the *n*-phase in the photograph, and this agrees within an accuracy of 10% with the value of η determined from the diagram of state.

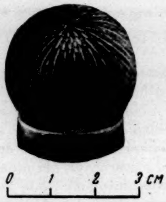

FIG. 5. General view of sphere of diameter 30 mm for $\eta = 0.72$, $T = 2.85^\circ$ K, Transition $s \rightarrow n$, T = const.

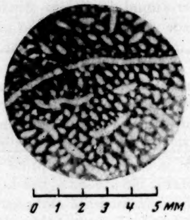

FIG. 6. Part of the surface of a sphere of diameter 30 mm close to a pole, photographed through the telescope; $\eta = 0.8$, $T = 2.85^\circ$ K, Transition $n \to s$, H=const.

FIG. 7. Pattern in a gap of width 0.3 mm between hemispheres of diameter 40 mm. $\eta = 0.145$, $T = 2.36^\circ$ K, Transition $n \to s$, T = const.

These qualitative characteristics (wrinkling of the n-domains for small η and "island-like" s-domains for η approaching 1) were observed whatever the mode of transition to the intermediate state, on monocrystalline specimens with electropolished or etched surfaces and on polycrystalline specimens with mechanically polished surfaces. In the latter case, however, the domains were somewhat more markedly wrinkled for small η, while for $\eta \sim 1$ they were somewhat less rounded than for the monocrystalline specimens.

We also varied the size and shape of the specimens. We investigated tin spheres of diameter 40, 30 and 12.6 mm diameter, and tin toruses and cylinders of diameters from 10 to 4 mm in transverse fields. Experiments were also made with a lead sphere of 40 mm. The specimen temperature was varied from 2.2 to 3.4° K.

In all these experiments the above-mentioned features were observed, and this supports the view that these features are characteristic of the equilibrium structure of the intermediate state.

In order to study the distribution of domains inside a superconductor we made experiments in the gap between two monocrystalline tin hemispheres of diameter 40 mm and of purity 99.9%. Gaps of width 0.3 and 0.1 mm gave no new qualitative results as compared with the external surface, both for large and small η (Fig. 7).

There is every reason for supposing that the wrinkled structure of the domains observed at the surface for small η is not preserved in the interior of the specimen, but that the domains tend to thicken, thus reducing the total surface area of the boundaries between s- and n-phases and consequently, also reducing the free energy. Thus the n-layer must have the form schematically illustrated in Fig. 8. In this connection a gap of 0.1 mm for a sphere of diameter 40 mm must be considered as insufficiently narrow for properly showing the character of the distribution within the specimen, i.e., the question of the critical gap width raised in Refs. 2 and 7 is once again relevant. In one experiment with a very narrow gap (0.05 mm) we did succeed in getting a pattern of nonwrinkled, comparatively broad layers (not sufficiently perfect, however, for photographic reproduction), and this apparently confirms the hypothesis proposed. The reason for the occurrence of wrinkling of domains at the surface, must presumably be analogous to the reason for the branching of the layers as they approach the surface in the model[4]. In both cases the disperseness of the structure grows towards the surface, and the field close to the surface becomes more uniform, which is favorable because of the accompanying reduction of the free energy of the state.

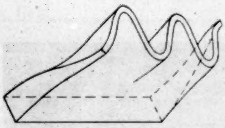

FIG. 8. Proposed form of an n-layer for small η.

The patterns obtained for various modes of transition to the given point of the intermediate state have besides the above-mentioned common features also certain marked differences. We have tried the following modes of transition: (a) cooling in a constant field ($n \rightarrow s$, H = const), (b) increase of field at constant temperature ($s \rightarrow n$, T = const); and (c) reduction of field at constant temperature ($n \rightarrow s$, T= const).

The influence of the mode of transition shows itself appreciably only in the general disposition and form of the coarser details of the structure (regions of fine structure as a whole and large s-domains), which for transition of type (b) were disposed in meridional directions over the whole surface right up to the "magnetic poles" (see Figs. 4 and 5). An analogous pattern, i.e., radial disposition of the domains, was observed in the gap (see Fig. 7). For the cylinders (and toruses) in transverse fields the coarse details of the structure were arranged perpendicular to the cylinder axis. For transitions of types (a) and (c), no such oriented distribution of the domains was observed (see, for instance, Figs. 2, 3 and 6).

It may be supposed that this difference is connected with the fact that in one case the transition starts from the completely superconducting state and in the other from the normal state. The general picture is apparently determined by the kinetics of the transition and the conditions of growth of the s- and n-domains. It is possible that the character of the patterns is influenced by the orienting action of the currents induced in the specimen at the moment of transition*. The clarification of the influences of these factors demands, however, a more detailed investigation.

Over a small part of the surface of the sphere close to its "magnetic equator" (in the lower part of the photographs of the sphere in Figs. 2 and 5) the pattern has a character different from that over the remaining larger part of the surface. Here the n-domains, independently of the mode of transition, always have the form of relatively broad unwrinkled strips of a meridional direction. Similar observations were made on the toruses and cylinders. Apparently this form of the layers at the equator is a peculiarity characteristic of the equilibrium state and connected with the smallness of the angle between the surface of the specimen and the magnetic field at these points. As was shown by Dzialoshinskii[6] for layer-like structures of the type of Ref. 1, in the case of a plate at a small angle to the field, the planes of the layers must be perpendicular to the external surface. For a sphere this condition is evidently satisfied by a meridional disposition of the layers. The thickness of the layers must grow at small angles, since in this case the inhomogeneity of the external field, connected with the existence of layers must also diminish (for plates or cylinders parallel to the field, the inhomogeneity evidently disappears altogether). Thus in this case the factor leading to wrinkling of the layers is weakened.

CONCLUSION

From our observations the conclusion can be drawn that the real structure of the intermediate state is considerably more complicated and varied than that of the theoretical models constructed up to now. This comes about not only because the structures achieved in practice are insufficiently completely equilibrium ones, but mainly because the equilibrium structures with least free energy are really highly complicated and varied in type for various forms of specimen and various η.

The theoretical calculation of the structure for all values of η would seem to be a very difficult problem as is the problem of quantitative treatment of the experimental results in the general case. The case of a specimen whose surface makes a small angle with the field, and the cases $\eta \rightarrow 1$ and $\eta \rightarrow 0$ are relatively much simpler and more suitable for quantitative investigation.

Undoubtedly other possibilities also exist for investigating the intermediate state apart from the direct observation of the shapes and sizes of the s- and n-domains (see, in particular, Refs. 13, 14 and 15). It should be noted, however, that in these cases also, an exact quantitative interpretation of the results requires a knowledge of the geometry of the structure of the intermediate state.

---

* We compared the patterns obtained on a torus and on the same specimen after transformation into a "horseshoe" after cutting a gap in it. In the second case, with other conditions remaining the same, the pattern seemed less ordered.

We express our sincere gratitude to A. I. Shal'nikov for advice and discussion of results, to E. A. Sharova for participation in some of the experiments and to S. A. Iakovlev for help in the work.

---

[1] L. D. Landau, J. Exptl. Theoret. Phys. (U.S.S.R.) 7, 371 (1937).

[2] L. D. Landau, J. Exptl. Theoret. Phys. (U.S.S.R.) 13, 377 (1943).

[3] E. R. Andrew, Proc. Roy. Soc. (London) 194A, 98 (1948).

[4] E. M. Lifshitz and Iu. V. Sharvin, Dokl. Akad. Nauk SSSR 79, 783 (1951).

[5] C. G. Huper, Phil. Mag. 42, 961 (1951).

[6] I. E. Dzialoshinskii, Dokl. Akad. Nauk SSSR 105, 244 (1955).

[7] A. I. Shal'nikov, J. Exptl. Theoret. Phys. (U.S.S.R.) 16, 757 (1946).

[8] A. G. Meshkovskii and A. I. Shal'nikov, J. Exptl. Theoret. Phys. (U.S.S.R.) 17, 851 (1947).

[9] A. G. Meshkovskii and A. I. Shal'nikov, Izv. Akad. Nauk SSSR, Ser. Fiz. 11, 39 (1947).

[10] A. G. Meshkovskii, J. Exptl. Theoret. Phys. (U.S.S.R.) 19, 54 (1949).

[11] A. I. Shal'nikov and K. A. Tumanov, Collection dedicated to the 70th birthday of A. F. Ioffe, Academy of Sciences Press, p. 303, 1950.

[12] Iu. V. Sharvin and B. M. Balashova, J. Exptl. Theoret. Phys. (U.S.S.R.) 23, 222 (1952).

[13] T. E. Faber, Proc. Roy. Soc. (London) 223A, 174 (1954).

[14] M. Désirant and D. Shoenberg, Proc. Roy. Soc. (London) 194A, 63 (1948).

[15] E. R. Andrew and J. M. Lock, Proc. Phys. Soc. (London) 63A, 13 (1950).

Translated by D. Schoenberg
7

SOVIET PHYSICS JETP VOLUME 4, NUMBER 1 FEBRUARY, 1957

π^+ – Meson Energy Spectrum for $pp \to np\pi^+$ Reaction at 556 and 657 MEV

M. G. MESCHERIAKOV, V. P. ZRELOV, B. S. NEGANOV, I. K. VZOROV AND A. F. SHABUDIN
Institute for Nuclear Problems, Academy of Sciences, USSR

(Submitted to JETP editor April 7, 1956)
J. Exptl. Theoret. Phys. (U.S.S.R.) 31, 45-54 (July, 1956)

The π^+ spectrum for the reaction $pp \to np\pi^+$ was studied at bombarding energies of 556 and 657 mev. By magnetic analysis at an angle of 24° to the proton beam. The ratio of the differential cross section at 45° (measured in the center-of-mass system) for the two energies proved to be $(d\sigma^*/d\omega^*)_{657} : (d\sigma^*/d\omega^*)_{556} = 2.2 : 1$. For both bombardment energies, approximately 80% of the available energy is spent in the formation of the π^+ – meson in a single elementary act. A comparison of the measured spectrum with the energy distribution corresponding to the statistical weights of the final states computed under the assumption that the meson is formed directly indicated that in the low energy part of the spectrum the matrix element associated with the initial and final state for the reaction varies linearly with meson momentum and has approximately the same value at identical momenta for both bombarding energies.

1. INTRODUCTION

ALL the present experimental results dealing with p-on-p collisions indicate that the basic inelastic process in the energy range of 560 – 660 mev is the production of π^+ – mesons by the reaction $pp \to np\pi^+$.

The total cross section for this reaction can be obtained from the total pp interaction cross section at 560 and 660 mev[1], $(34.0 \pm 0.5) \times 10^{-27}$ cm^2 and $(41.4 \pm 0.6) \times 10^{-27}$ cm^2, respectively, by subtracting the total cross sections for elastic scattering[2], $pp \to d\pi^+$ reaction[3] and $pp \to pp\pi^0$ reaction[4]. The results of this subtraction are listed in the Table together with the total cross sections of the listed processes. It appears that the total cross section for $pp \to np\pi^+$ is somewhat higher at 660 mev, a consequence of the omission of the contribution due to the formation of two π – mesons in a single pp collision. The $pp \to np\pi^+$ reaction, for which the final state is specified by the interaction of two nucleons and a nucleon and π^+ – meson, should be characterized by an energy spectrum for both mesons and nucleons. The existing data on the spectrum of mesons produced in p-on-p collisions are known only for bombarding energies of 340 mev[5], 380 mev[6] and 440 mev[7]. The data (see cited references) were obtained by passing the mesons through a filter and identifying the remaining mesons in a nuclear emulsion through $\pi^+ \to \mu^+$ decay. This method is applicable only for low energies and can give only approximate information about the form of the meson spectrum. In addition, considerable time must be spent in gathering necessary statistical material.

TABLE

Process	Total cross section in units of 10^{-25} cm^2	
	560 mev	660 mev
$pp \to pp$	25.2±0,8	24.7±1.0
$pp \to np\pi^+$	5.0±1,0	10.2±1.2
$pp \to d\pi^+$	2.6±0,2	3.1±0.2
$pp \to pp\pi^\circ$	1.2±0,3	3.4±0.4

In the present study, the π^+ – meson spectrum for proton energies of 556 and 657 mev has been studied by means of a magnetic analyzer. The same method was used to study the parallel problem of the secondary proton spectrum produced in the reactions $pp \to np\pi^+$ and $pp \to pp\pi^0$. The results of this experiment are presented in another paper (see following article).

2. EXPERIMENTAL PROCEDURE

The location of the magnetic spectrometer and concrete shield relative to the proton beam of the 6 – meter synchrocyclotron (of the Institute for Nuclear Problems of the Academy of Sciences, USSR) is indicated in Fig. 1. The proton beam was brought out by perturbing the radial motion of the

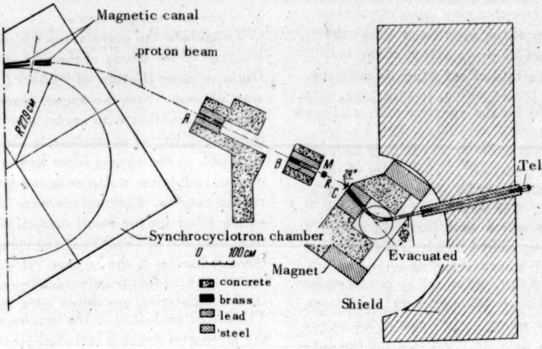

FIG. 1. Experimental layout.

accelerated protons in their final orbit by means of a local nonhomogeneous magnetic field of the synchrocyclotron[8]. At the target location the proton flux was about 2×10^9 protons/cm^2 sec. The mean proton energy proved to be 660 mev[9] and was measured by using the Cerenkov radiation of the beam. The mean dispersion in the primary beam was not greater than ± 5 mev.

An electromagnet with a circular pole piece 100 cm in diameter was used in the spectrometer. The maximum attainable magnetic field for an air gap of 10 cm was 19,000 oersteds. In order to compute the trajectory of a particle in the spectrometer one must include the leakage of the field. The field was held constant to 0.2% by means of an electron stabilizer. The field strength was measured to an accuracy of 0.2% by an instrument which utilized the proton nuclear resonance method.

The mesons which emerge at an angle of 24° to the proton beam pass in a vacuum through a slitted wedge-shaped collimator *C* and have an angular spread of ±1° in the magnetic field. The angle of deflection in the field was selected so that the particles were focused in a horizontal plane at the detector which was located behind a thick (3.6 meter) steel-concrete cyclotron shield. For an angular deflection of 62.5°, the radius of curvature for the average trajectory was 96.5 cm. A telescope, composed of three scintillation counters, served as the detector of the particles emerging from the spectrometer. For the range of energies studied the detector efficiency was independent of energy and was close to 100%. The second crystal of the telescope with a cross section 2.5 cm × 2.5 cm acted as the exit slit for the spectrometer. The particles leaving the spectrometer were identified by their momentum and range. Thus, slow protons with the same momentum as $\pi-$mesons are separated from the latter by means of a 2 cm thick copper filter inserted in front of the third counter in the telescope.

The proton beam falls on a hydrogen target *R* after passing through the collimators *A* and *B* and the monitor *M* which is a thin-walled ionization chamber filled with helium. In the first series of measurements the target was made of a glass dewar (with an overall wall thickness of 0.5 grams/cm^2) filled with liquid hydrogen. The effect of the liquid state was studied by utilizing the difference in measurements obtained with the dewar filled with liquid and then with gaseous hydrogen. In these measurements the background level which is produced by the scattered radiation from the synchrocyclotron amounted to about 10% for the low energy portion of the spectrum and decreased to 1% as the meson energy approached 300 mev. The mean proton energy at the center of the hydrogen target in measurements with the maximum attainable proton energy was equal to 657 mev. To reduce this mean energy to 556 mev a carbon filter, 42.7 grams/cm^2 thick, was inserted in collimator *A*.

The use of a collimator to define the meson beam for the spectrometer may introduce distortions into the form of the spectrum through the scattering and slowing-down action of the collimator walls. Since this effect depends upon the dimensions of the target which, in this case, acts as the entrance slit for the spectrometer, a second series of measurements were made with a polyethylene target 5 mm wide by 25 mm high having a thickness of 1.0 gram/cm^2. The effect of the carbon was subtracted out by measurements on a pure carbon target. The two series of measurements gave results which were identical within the errors of measurement (±5%). This fact, together with the agreement of the measured and calculated width of the line which is produced by π^+ – mesons from the reaction $pp \to d\pi^+$, indicates the absence of any gross distortions of the meson spectrum. Further definite proof that the spectrometer with the slitted collimator preserves, in all cases, the correct form of the meson distribution was demonstrated by experiments which measured the form of the diffracted proton peak produced by scattering in carbon. In these experiments it was found that the constant disturbance produced by protons being scattered and slowed down in the walls of the entrance collimator amounted to no more than 2% of the peak signal produced by the diffraction scattered protons.

These difficulties can be avoided for sufficiently high meson energies if the discrimination of the meson beam is performed upon its entrance into the spectrometer by a system of high speed counters in coincidence with the detector which then registers the mesons which pass through the spectrometer. At the present, such a method is in use in our laboratory and was used in the measurement of the π^+ – meson spectrum.

Corrections which allow for the presence of an admixture of μ^+ – mesons and positrons in the π^+ – meson beam as well as for the absorption and decay of the π^+ – mesons during flight must be applied to the measurements. The contamination of μ^+ – meson and positrons in the emergent beam was determined by measuring the absorption of particles in a copper filter. For these measurements a fourth counter, 10 cm in diameter, with a liquid scintillator was put in coincidence with the telescope which consisted of three counters (diphenyl acetylene scintillator) with dimensions 3 × 3, 2.5 × 2.5 and 4.5 × 4.5 cm. In front of the fourth counter copper filters were inserted. The spectrum was not measured below 60 mev because of the difficulty in determining the admixture of μ^+ – mesons and positrons.

To include the corrections which are necessary because of the decay of the π^+ – meson during flight, a mean lifetime of $(2.54 \pm 0.11) \times 10^{-8}$ sec[10] was adopted. With the known cross sections for π^+ – meson interaction with nuclei one can determine the probability of absorption in the first two scintillators, in the copper filter and in the liquid hydrogen and dewar walls or in the polyethylene and carbon targets. Corrections were also introduced which allow for the small distortion in the spectrum because of changes in the meson energy through losses in the targets. Distortions produced by accidental coincidences and miscounts in the registering apparatus were negligibly small. The errors indicated in the graphs which represent the measured spectra included all uncertainties introduced with the corrections enumerated above in addition to the statistical errors of measurement.

In practice, the relative momentum spectrum of the mesons was determined by changing the strength of the magnetic field. Calibration of the spectrometer was accomplished by the location of the peak of the line from the $pp \to d\pi^+$ reaction. In the measurements with a bombarding energy of 657 mev, the spectrometer resolving power was about 3.5% for mesons with an energy of 300 mev. In this case the most essential factors which produce an increase in the half-width of the peak are: a) nonmonochromatic primary proton energy; b) finite dispersion of the spectrometer; c) angular spread of the mesons, selection by the collimator and, in a much smaller degree, multiple scattering in the target; d) energy spread of the protons and mesons because of the finite target thickness. The total energy spread of the mesons amounted to about ±5 mev.

3. EXPERIMENTAL RESULTS

Measurements at 657 mev. The resultant π^+ spectrum for equal energy intervals is represented in Fig. 2 and shows a distinct peak near 304 mev, produced by mesons from the $pp \to d\pi^+$ reaction. The half-width of the peak (width at half maximum) is about 10 mev, which agrees with the calculated value. The continuous spectrum produced by the $pp \to np\pi^+$ reaction borders the peak quite closely. If one considers the kinematics of the reactions $pp \to d\pi^+$ and $pp \to np\pi^+$ one can show that for the conditions of this experiment the upper boundary of the continuous π^+ spectrum should lie 2.9 mev below the peak. The resolving power of the spectrometer was not sufficient to see this separation.

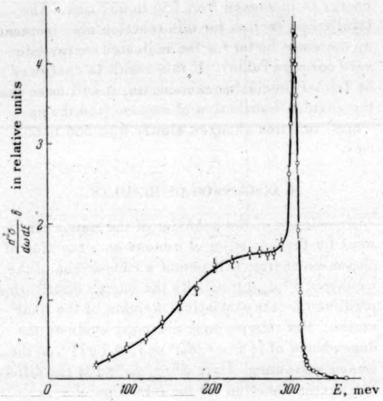

FIG. 2. The energy spectrum of π^+ – mesons for the reaction $pp \to np\pi^+$ at an angle of 24° in the laboratory system. Bombarding energy is 657 mev.

From the form of the continuous spectrum one can definitely conclude that at 657 mev there appears, together with a strong dispersion in meson energy, a clearly indicated tendency for the emission of mesons with energies near the upper limit. The average meson energy for the continuous spectrum is 220 mev.

The value of the differential cross section $d\sigma/d\omega(pp \to np\pi^+)$ for the formation of mesons with energies greater than 60 mev at an angle of 24° can be determined from the ratio of the area under the continuous spectrum to the area under the peak and the known cross section for the reaction $pp \to d\pi^+$ [3]. In this fashion it was found that $d\sigma/d\omega(pp \to np\pi^+)_{24^\circ} \simeq 4.7 \times 10^{-27}$ cm²/steradian with $d\sigma/d\omega(pp \to d\pi^+)_{24^\circ} = 0.95 \pm 0.05 \times 10^{-27}$ cm²/steradian. It is clear that such an evaluation of the magnitude of $d\sigma/d\omega(pp \to np\pi^+)_{24^\circ}$ is very approximate in view of the uncertain structure of the line on the low energy side.

The invariant expression $(1/p)\,d^2\sigma/d\omega dE$, where p is the π – meson momentum in the system of coordinates in which $d^2\sigma/d\omega dE$ is measured, was used to transform the measured meson spectrum into the center-of-mass system. As is seen from Fig. 3, the spectrum obtained at an angle of 24° to the beam in the laboratory system corresponds to the spectrum for angles from 60° to 43° in the center-of-mass system. The limits of the continuous spectrum fall at 15 and 148 mev. The average meson energy for this spectrum is 110 mev whereas the energy available from the collision of the protons amounts to 305 mev. Consequently, in the formation of a π^+ – meson in a single elementary act, 83% of the available energy is spent on the average. About 90% of the mesons are emitted with energies from 50 to 148 mev within the angles 43° to 48°. Hence, in the first approximation one can assume that the measured spectrum represents, basically, the energy distribution of mesons emitted at an angle of 45° in the center-of-mass system. The corresponding differential cross section $d\sigma^*/d\omega^*(pp \to np\pi^+)_{45^\circ}$ is about 1.4×10^{-27} cm²/steradian.

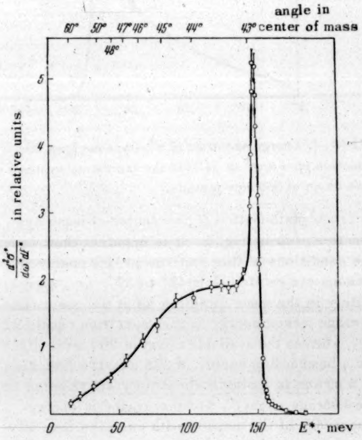

FIG. 3. The energy spectrum of π^+ – mesons in the center-of-mass system from the reaction $pp \to np\pi^+$ at 657 mev.

Measurements at 556 mev. The measured spectrum is given in Fig. 4. The peak, which corresponds to mesons from the reaction $pp \to d\pi^+$, falls at 227 mev. Because of the energy dispersion in the proton beam after passing through a filter 42.7 grams/cm^2 thick, the peak is more washed out than in the preceding measurements. As is evident the continuous π^+ spectrum is distorted in the high energy range. The average meson energy is 165 mev. The estimated differential cross section $d\sigma/d\omega(pp \rightarrow np\pi^+)_{24^\circ}$ is 1.5×10^{-27} cm^2/steradian, whereas $d\sigma/d\omega(pp \rightarrow d\pi^+)_{24^\circ} = (0.7 \pm 0.07) \times 10^{-27}$ cm^2/steradian.

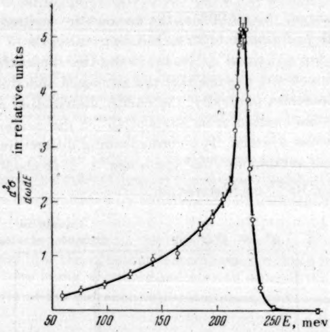

FIG. 4. Energy spectrum of π^+ – mesons from the reaction $pp \rightarrow np\pi^+$ at 24° (in the laboratory system) to the beam of 556 mev protons.

The transformation to the center-of-mass system is shown in Fig. 5. It is apparent that, under the conditions of this experiment, the observed mesons are emitted from 42° to 57°, i.e., approximately in the same direction as at 657 mev. The average meson energy in this spectrum equals 82 mev, whereas the available energy is 260 mev. Hence, for a bombarding energy of 556 mev the formation of a meson in a single elementary act requires on the average about 85 % of the available energy. About 90% of the mesons with energies from 40 mev to the upper limit of 112 mev are emitted within 47° to 42°. This permits one to consider the measured spectrum as approximately representing the energy spectrum of mesons emitted at 45°. Evaluation of the absolute differential cross section indicates that $d\sigma^*/d\omega^*, pp \rightarrow \pi^+)_{45^\circ} \simeq 0.6 \times 10^{-27}$ cm^2/steradian.

Comparison of the values of $d\sigma^*/d\omega^*(pp \rightarrow np\pi^+)$ obtained in this experiment indicates a factor 2.2 increase in the cross section when the energy is increased from 556 to 657 mev. The total cross section for this reaction also increases by the same factor for the indicated energy interval (compare Table). If this result is confirmed by further precise measurements, it will mean that the angular distribution of mesons from the $pp \rightarrow np\pi^+$ reaction changes slowly from 556 to 657 mev.

4. DISCUSSION OF RESULTS

Knowledge of the behavior of the matrix element for the formation of mesons as a function of meson momentum will permit a comparison of the measured π^+ spectrum with the energy distribution predicted by the statistical weights of the final states. For this purpose one must evaluate the dependence of $[(d^2\sigma^*/d\omega^* dq)/\rho_\epsilon(q)]^{1/2}$ on the meson momentum. Here $d^2\sigma^*/d\omega^* dq$ is the differential cross section for the formation of π^+ – meson in the center-of-mass system; $\rho_\epsilon(q)$ is the density of final states under the condition that the meson is emitted with a momentum between q and $q + dq$, where ϵ is the total energy of the two colliding nucleons. For the assumption that the formation of the meson occurs directly, without the participation of any intermediate state, the density of final states is given by (compare M. I. Podgoretskii and I. L. Rozental'[11])

$$\rho_\varepsilon(q) \sim \frac{B^{1/2}}{(A^2 - q^2)^2} \left\{\left(1 - \frac{4A^2}{A^2 - q^2}\right)\right.$$

$$\left. \times\ B + 6A^2[A^2 - (q^2 + 2M^2)]\right\} q^2,$$

where $A = \epsilon - \sqrt{q^2 + \mu^2}$, $B = (q^2 + 2M^2 - A^2)^2 - 4M^4$, $\epsilon = \sqrt{2M(E + 2M)}$, E is the kinetic energy of the incident proton and M and μ are the rest energies of the nucleon and π – meson ($c = 1$).

The transformation from the energy representation to momentum representation was performed with the use of the relation

$$d^2\sigma^* / d\omega^* \, dq = \beta^* \, d^2\sigma^* / d\omega^* \, dE^*,$$

where β^* is the velocity of the π – meson in the center-of-mass system. If absolute values from the independent measurements at 556 and 657 mev bombardment energies, which were determined by us with an accuracy of 20% are used for $d^2\sigma^*/d\omega^* dE^*$ then the values derived for $[(d^2\sigma^*/$

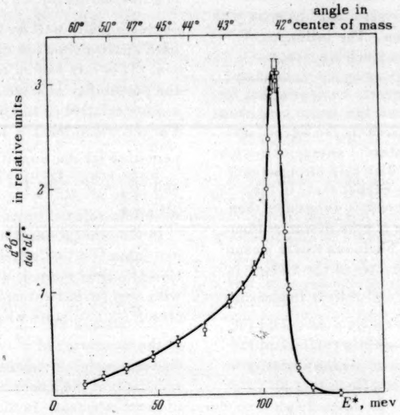

FIG. 5. Energy spectrum in the center-of-mass of π^+-mesons from the reaction $pp \to np\pi^+$ at 556 mev bombarding energy.

$d\omega^* dq)/\rho_\epsilon(q)]^{1/2}$ should represent the actual relation between the values of the matrix element for the indicated energies.

Figure 6 represents the results of the calculations. It is necessary to note two most essential characteristics of the results: a) the obtained values for $[(d^2\sigma^*/d\omega^* dq)/\rho_\epsilon(q)]^{1/2}$ are found to be approximately identical for the same value of q within the region of momentum overlap and b) the low energy part of the π^+ spectrum does not follow the statistical distribution. As is evident, the matrix element varies like a linear function of the momentum in the range from 60 to 160 mev/c for both 556 and 657 mev energies. For the latter bombardment energy the linear behavior for the matrix element continues up to 200 mev/c. The behavior at higher momenta was impossible to study because of the inability of accurately separating the spectrum at the upper limit into line and continuum. The resultant information regarding the dependence of the matrix element on the momentum would have been more reliable if spectra were obtained at other angles in the laboratory system.

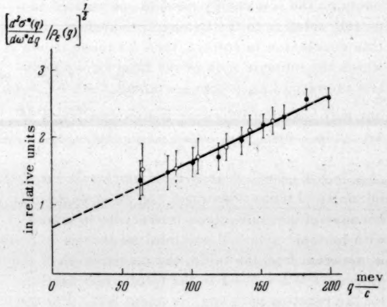

FIG. 6. Dependence of $[(d^2\sigma^*(q)/d\omega^* dq)/\rho_\epsilon(q)]^{1/2}$ on meson momentum in the center-of-mass system. O – $E_p = 556$ mev, O – $E_p = 657$ mev.

The more rapid increase of the number of π^+-mesons with momentum in comparison to the statistical distribution can be explained by two factors: a) the emission of mesons in states with non-zero orbital momentum; b) the presence of an interaction between the nucleons in their final states which leads to the emission of mesons with predominantly high energies. The influence of this last factor will be that much weaker, the larger the energy carried away by the secondary proton or neutron. It can easily be shown that for the range of the meson momentum under consideration, 60 mev or more is shared by the secondary nucleons, principally as internal energy of motion of a two-nucleon system. With this circumstance in mind it is reasonable to expect that, in the region of low energies where $\bar{\lambda}/q$ is greater than the characteristic distance R (the distance from the center of the colliding nucleons where meson formation occurs), the character of the change in $[(d^2\sigma^*/d\omega^* dq)/\rho_\epsilon(q)]^{1/2}$ will reflect fundamentally the dependence of the matrix element on the meson momentum. In Rosenfeld's review[7] of the experimental data dealing with meson formation in nucleon-nucleon collision one finds that $R \leq \frac{1}{2}\bar{\lambda}/\mu c$*. To the degree to which $\bar{\lambda}/q \gg \frac{1}{2}\bar{\lambda}/\mu c$ is almost fulfilled for the entire analyzed π^+ spectral region, the linear dependence of the matrix element on the meson momentum will approximately mean that at the given bombarding energies the low energy mesons are emitted in a p-state relative to the two-nucleon system. If this conclusion is correct, then for those cases in which the isotopic spin of the final $(n-p)$ system is unity (i.e., processes where $T=1 \rightarrow T=1$) one may have the following transitions ${}^3P_0 \rightarrow {}^3P_1$, ${}^3P_1 \rightarrow {}^3P_0$, ${}^3P_1 \rightarrow {}^3P_1$, ${}^3P_1 \rightarrow {}^3P_2$, ${}^3P_2 \rightarrow {}^3P_1$, ${}^3P_2 \rightarrow {}^3P_2$, ${}^3F_2 \rightarrow {}^3P_1$, ${}^3F_2 \rightarrow {}^3P_2$, ${}^3F_3 \rightarrow {}^3P_2$. The intensity of these transitions can be strengthened because of meson-nucleon interaction in states with isotopic spin 3/2 and total momentum 3/2. As is apparent from the table, the contribution of the process $T=1 \rightarrow T=1$ to the total cross section for the reaction $pp \rightarrow np\pi^+$ is about 30%. For the case of $T=1 \rightarrow T=0$, the emission of a π-meson in the p-state is possible by transitions such as ${}^1D_2 \rightarrow {}^3S_1$, ${}^1S_0 \rightarrow {}^3S_1$, ${}^3P_0 \rightarrow {}^1P_1$, ${}^3P_1 \rightarrow {}^1P_1$, ${}^3P_2 \rightarrow {}^1P_1$, ${}^3F_2 \rightarrow {}^1P_1$.

We note that the linear dependence of $[(d^2\sigma^*/d\omega^* dq)/\rho_\epsilon(q)]^{1/2}$ on q which is represented equally well by the experimental points of both spectra does not extrapolate through the origin. This fact can be explained if one allows for the possibility of some emission of mesons in the s-state relative to the final two-nucleon system[13]. For the transition $T=1 \rightarrow T=1$, the s-state is permitted for the transitions ${}^3P_0 \rightarrow {}^1S_0$, ${}^1S_0 \rightarrow {}^3P_0$, and ${}^1D_2 \rightarrow {}^3P_2$; for $T=1 \rightarrow T=0$, ${}^3P_1 \rightarrow {}^3S_1$ is allowed.

In the present experiment sufficient energy was available (particularly at 657 mev) for the excitation of one of the colliding protons into the state with angular momentum 3/2 and isotopic spin 3/2 (the $P_{3/2,3/2}$ state whose existence is indicated in the scattering of π^+-mesons by nucleons). Consequently, (in another attempt to explain the peculiarity of the measured spectrum), the formation of the π^+-meson in the $pp \rightarrow np\pi^+$ reaction as occurring through the intermediate excited $P_{3/2,3/2}$ state of a nucleon can be considered*. Such a model for the formation of mesons in nucleon-nucleon collisions, which had been proposed earlier by a number of authors[14-17], was used by Iappa[18] to calculate the form of the π^+ energy spectrum for the present energies. In these calculations it was assumed that: a) the formation and decay of the $P_{3/2,3/2}$ state occur independent of one another; b) the probability of exciting the $P_{3/2,3/2}$ state is given by the dispersion formula with parameters obtained from π^+-meson-proton scattering[19]; c) the scattering of the colliding particles was isotropic in the center-of-mass system, as was also the decay of the excited nucleon. It was found that the calculated spectra were similar in form to the experimental. The mean calculated energy was 112 mev for the 657 mev case, whereas the experimental value was 110 mev. The corresponding value at 556 mev was 76 mev in comparison to the observed 82 mev.

---

* This quantity also represents the radius of the region of meson-nucleon interaction[12].

* In experiments with the Birmingham proton accelerator, an angular correlation was found between the protons and the π^+-mesons for the $pp \rightarrow np\pi^+$ reaction at 650 mev (L. Riddiford, personal communication). This fact may indicate that the formation of π^+-mesons in the $pp \rightarrow np\pi^+$ reaction occurs at least partly through the intermediate state.

The above comparison indicates that the assumption of the existence of an intermediate $P_{3/2,3/2}$ state for the reaction $pp \to np\pi^+$ does not contradict the experimental results. However, the obtained agreement is hardly to be overrated in view of the rough initial assumptions and, as may be seen from the calculations, the slight difference in the form of the π^+ spectra obtained with this model (with the intermediate $P_{3/2,3/2}$ state) and with the model using the direct formation of a meson in the *p*-state. It is clear that, in order to resolve the question of the relative roles of the processes considered above in the $pp \to np\pi^+$ reaction, one needs more rigorous inclusion of the intermediate $P_{3/2,3/2}$ state in the theory of inelastic nucleon-nucleon collisions as well as further careful experimental studies of such collisions.

The authors are grateful to Iu. A. Iappa and L.M. Soroko for discussion of the results.

---

[1] Dzhelepov, Moskalev and Medved', Dokl. Akad. Nauk SSSR **104**, 380 (1955).

[2] N. P. Bogachev, Dokl. Akad. Nauk SSSR **108**, No. 5 (1956).

[3] M. G. Meshcheriakov, and B. S. Neganov, Dokl. Akad. Nauk SSSR **100**, 677 (1955).

[4] A. A. Tiapkin and Iu. D. Prokoshkin, Report (Otchet), Institute for Nuclear Problems, Academy of Sciences, USSR (1955).

[5] Cartwright, Richman, Whitehead and Wilcox, Phys. Rev. **91**, 677 (1953); V. Peterson, Phys. Rev. **79**, 407 (1950); Peterson, Iloff and Sherman, Phys. Rev. **84**, 372 (1951).

[6] Block, Passman and Havens, Phys. Rev. **88**, 1239 (1952).

[7] A. Rosenfeld, Phys. Rev. **96**, 138 (1954).

[8] Dmitrievskii, Danilov, Denisov, Zaplitin, Katyshev, Kropin and Chestnoi, *Instrumentation and Experimental Technique* (in press).

[9] V. P. Zrelov, Report (Otchet), Institute for Nuclear Problems, Academy of Sciences, USSR (1954).

[10] Jakobson, Schulz and Steinberger, Phys. Rev. **81**, 894 (1951).

[11] M. I. Podgoretskii and I. L. Rozental', J. Exptl. Theoret. Phys. (U.S.S.R.) **27**, 129 (1954).

[12] J. Orear, Phys. Rev. **100**, 288 (1955).

[13] J. W. Mather and E. A. Martinelli, Phys. Rev. **92**, 780 (1953).

[14] F. Belinfanti, Phys. Rev. **92**, 145 (1953).

[15] D. Peaslee, Phys. Rev. **94**, 1085 (1954).

[16] R. Gatto, Nuovo Cimento **1**, 159 (1955).

[17] C. Belen'kii and A. Nikishov, J. Exptl. Theoret. Phys. (U.S.S.R.) **28**, 744 (1955); Soviet Phys. JETP **1**, 593 (1955).

[18] Iu. A. Iappa, Report (Otchet), Institute for Nuclear Problems, Academy of Sciences, USSR (1955).

[19] M. Gell-Mann and K. Watson, Ann. Rev. Nucl. Sci. **4**, 219 (1954).

Translated by A. Skumanich
8

SOVIET PHYSICS JETP VOLUME 4, NUMBER 1 FEBRUARY, 1957

Variational Principles in Hydrodynamics

V. I. SKOBELKIN
Moscow State University

(Submitted to JETP editor May 30, 1955)
J. Exptl. Theoret. Phys. (U.S.S.R.) **31**, 317-323 (August, 1956)

New variational principles are formulated, characterized by a special variation subject to auxiliary constants. This makes possible the solution of boundary problems of hydrodynamics by direct methods.

SEVERAL attempts have been made recently to formulate a general variational principle for hydrodynamics.

Bateman[1] established a variational principle for isentropic gas flows. Lin and Rubinov[2] generalized Bateman's principle to plane isoenergetic flow. In the work of Ito[3], Bateman's principle was further generalized and applied to the construction of a quantum hydrodynamics and the study of the flow of liquid He II, which had been treated earlier by Landau[4] and London[5].

In these papers, the variational functional contained several field parameters which were varied independently (density, velocity, pressure and other parameters in Refs. 1 and 3; density and stream function in Ref. 2). However, such a set of parameters is not minimal, and as we shall show later, in the general case of three-dimensional flow, two quantities determining the flow are sufficient.

1. THE PRINCIPLE OF LEAST STREAMING POTENTIAL[6]

Let ψ, ϑ be parameters defining a particular stream line of the hydrodynamic field. ψ and ϑ remain constant along this line. The surfaces ψ = const and ϑ = const are surfaces of flow. At each point of the stream line ψ, ϑ we set up an orthogonal axis system $\overline{x}_i$ so that one axis, say $\overline{x}_1$, is along (ψ, ϑ). To each such axis system we associate an energy-momentum tensor T_{ik} in the particular coordinate system determined by the axes. We denote the component T_{11} of the energy-momentum tensor with respect to such a system by T_{ss}, so that $T_{11} = T_{ss}$. We define the field in terms of the quantities $\psi(x_i)$, $\vartheta(x_i)$, satisfying the relations:

$$\rho V_1 = \frac{D(\psi,\vartheta)}{D(x_2, x_3)}; \quad \rho V_2 = \frac{D(\psi,\vartheta)}{D(x_3, x_1)}; \quad \rho V_3 = \frac{D(\psi,\vartheta)}{D(x_1, x_2)}. \tag{1}$$

With this choice of the defining quantities, the equation of continuity is satisfied identically both for actual as well as the varied field. For a plane flow, the defining quantity is ψ, where

$$\rho V_1 = \partial\psi/\partial x_2; \quad \rho V_2 = -\partial\psi/\partial x_1. \tag{2}$$

Relation (2) follows from (1) if we set $\vartheta = x_3$, which characterizes plane-parallel fields. The function ψ in (2) is the stream function, and physically speaking determines the flux of matter through a stream tube. The difference $\psi_1 - \psi_2$ gives the flux of liquid through the region bounded by the stream lines ψ_1 and ψ_2. The pair of functions (ψ, ϑ) should be regarded as the generalized stream functions for three-dimensional flow. In this case the product $(\psi_1 - \psi_2)(\vartheta_1 - \vartheta_2)$ gives the value of the flux of material through the region bounded by the flow surfaces ψ_1, ψ_2 and ϑ_1, ϑ_2.

Let σ be the surface which bounds a certain closed volume Ω of the field which contains no strong or weak discontinuities, and on which the distribution of ψ and ϑ is known, i.e., we know the distribution of the matter flux through σ. We shall also assume that the distribution of the total mechanical energy per unit mass of liquid, $E(\psi, \vartheta)$, is known on the surface of σ. For the actual field along the stream line (ψ,) within Ω, we can write the equation of change of mechanical energy in the form:

$$\int \frac{\partial T_{sk}}{\partial x_k} dS = \frac{V^2}{2} + \int \frac{dP}{\rho} + R(\rho, \psi, \vartheta) = E(\psi, \vartheta), \tag{3}$$

where R is the work of the frictional forces per unit mass of liquid. The quantity R is that part of the mechanical energy which is converted into heat. We demand that Eq. (3) be satisfied for the varied as well as the actual field.

In addition, the law of conservation of energy (first law of thermodynamics) should be satisfied for both the real and the varied field:

$$dQ = dU + Pd(1/\rho), \tag{4}$$

where Q is the heat and U the internal energy per unit mass of material, expressed in mechanical units. Under the conditions (3) and (4), the Lagrangian is $L = T_{ss}$, and the integral

$$I = \int_{\Omega} T_{ss} d\omega \tag{5}$$

is an extremum for the actually established field. The integral (5) represents the work of the total flux of momentum of the directed motion of the gas molecules and is called the stream potential. The condition for an extremal of I gives equations of the form:

$$\frac{\partial T_{ss}}{\partial \psi} - \frac{\partial}{\partial x_i \partial} \frac{\partial T_{ss}}{(\partial \psi / \partial x_i)} = 0; \quad \frac{\partial T_{ss}}{\partial \vartheta} - \frac{\partial}{\partial x_i \partial} \frac{\partial T_{ss}}{(\partial \vartheta / \partial x_i)} = 0. \tag{6}$$

The equations (6) give the components of the vorticity which lie along the normals to the flow surfaces $\psi = \text{const}$ and $\vartheta = \text{const}$. Without loss of generality, we shall give the proof of the principle of minimum streaming potential formulated above, for the case of plane flow of an ideal gas which is barotropic with respect to a given particle. In this case

$$L = T_{ss} = P + \rho V^2; \quad R = 0;$$

$$\rho V_x = \partial \psi / \partial y; \quad \rho V_y = -\partial \psi / \partial x.$$

We introduce the geometrical characteristic of the flux

$$\Theta = (\partial \psi / \partial x)^2 + (\partial \psi / \partial y)^2 = \rho^2 V^2.$$

Then P, defined by the first law of thermodynamics, can be regarded as a function of ρ and ψ, and ρ as a function of Θ and ψ. We have

$$I = \int_{\Omega} \left[P(\rho, \psi) + \frac{\Theta}{\rho} \right] d\omega.$$

In general we can find ρ from Eq. (3) as a function of Θ and ψ. Regarding $\rho = \rho(\Theta, \psi)$ as the result of elimination of Eq. (3), we write the equation determining ψ from the condition for minimum I:

$$\frac{\partial}{\partial x} \left\{ \left[\left(\frac{\partial P}{\partial \rho} - \frac{\Theta}{\rho^2} \right) \frac{\partial \rho}{\partial \Theta} + \frac{1}{\rho} \right] 2 \frac{\partial \psi}{\partial x} \right\} + \frac{\partial}{\partial y} \left\{ \left[\left(\frac{\partial P}{\partial \rho} - \frac{\Theta}{\rho^2} \right) \frac{\partial \rho}{\partial \Theta} + \frac{1}{\rho} \right] 2 \frac{\partial \psi}{\partial y} \right\} = 0. \tag{7}$$

Differentiating (3) with respect to Θ for $\psi = \text{const}$, i.e., along a stream line:

$$-1/2\rho = (\partial P / \partial \rho - \Theta / \rho^2) \partial \rho / \partial \Theta. \tag{8}$$

Again differentiating (3) with respect to ψ for $\Theta = \text{const}$:

$$\rho E'(\psi) = -\frac{\Theta}{\rho^2} \frac{\partial \rho}{\partial \psi} + \rho \frac{\partial}{\partial \psi} \int \frac{dP(\rho, \psi)}{\rho} + \frac{\partial P}{\partial \rho} \frac{\partial \rho}{\partial \psi}. \tag{9}$$

Substituting (8) and (9) in (7) we get

$$\text{curl } \mathbf{V} = \frac{\partial P(\rho, \psi)}{\partial \psi} - \rho \frac{\partial}{\partial \psi} \int \frac{\partial P(\rho, \psi)}{\rho} + \rho E'(\psi). \tag{10}$$

Equation (10) gives the expression for the vorticity in a plane flow, and is equivalent to the field equation $\partial T_{2k} \partial x_k = 0$.

If the variation of ψ upon a certain surface σ is arbitrary, then from the equation $\delta I = 0$ we get (10) and the natural boundary condition $\mathbf{V} = V \cdot \mathbf{n}$, where $\mathbf{n}$ is the normal to the surface σ.

For adiabatic flow, for which $P = C^k(\psi) \rho^k$, Eq. (10) becomes

$$\text{curl } \mathbf{V} = -\rho \left(\frac{dE}{d\psi} - \frac{k}{k-1} P^{(k-1)/k} \frac{dC}{d\psi} \right). \tag{11}$$

If E and C do not depend on ψ and ϑ, then $L = L \times (\Omega)$, where

$$\Theta = \left(\frac{D(\psi, \vartheta)}{D(x_2 x_3)} \right)^2 + \left(\frac{D(\psi, \vartheta)}{D(x_3 x_1)} \right)^2 + \left(\frac{D(\psi, \vartheta)}{D(x_1 x_2)} \right)^2$$

is the geometrical characteristic of the flux for the case of three-dimensional flow. The equation $\delta \int L d\omega$ leads to the condition of irrotational flow, $\text{curl } \mathbf{V} = 0$.

2. RELATIVISTIC GENERALIZATION OF THE PRINCIPLE OF LEAST STREAMING POTENTIAL FOR A STATIONARY FIELD

In relativistic hydrodynamics[7], the energy-momentum tensor of an ideal gas is

$$T_{ik} = (P + \rho c^2)\, u_i u_k + P\delta_{ik}, \tag{12}$$

where u_i is the four-velocity of the flow of the gas. In this case

$$L = T_{ss} = \beta^2 (P + \rho c^2) V^2 + P. \tag{13}$$

The equation of continuity has the form:

$$\operatorname{div} n \frac{\mathbf{V}}{c} \beta = 0; \quad \beta = \frac{1}{1 - V^2/c^2}, \tag{14}$$

where n is the density of the gas in the reference frame in which the particular element of the gas is at rest. As before, we set

$$nu_x = n \frac{V_x}{c} \beta = \frac{D(\psi, \vartheta)}{D(y, z)}; \tag{15}$$

$$nu_y = n \frac{V_y}{c} \beta = \frac{D(\psi, \vartheta)}{D(z, x)};$$

$$nu_z = n \frac{V_z}{c} \beta = \frac{D(\psi, \vartheta)}{D(x, y)}.$$

Under the conditions (15), the equation (14) is satisfied identically. The first law of thermodynamics has the form[7]:

$$P d(1/n) + d(\rho c^2/n) = 0. \tag{16}$$

For an ideal gas, the energy integral along a stream line takes the form:

$$\int \frac{\partial T_{\bar{s}k}}{\partial \bar{x}_k} d\bar{s} = \beta^2 \frac{V^2}{2} + \int \beta^2 \frac{dP}{P + \rho c^2} = E(\psi, \vartheta). \tag{17}$$

In relativistic hydrodynamics, the adiabatic flow of an ideal gas possesses vorticity, except in the case of one-dimensional flow. We shall assume that E = const, $P = P(n)$, $\rho = \rho(n)$, and limit ourselves to the case of plane flow. Then

$$L = [P/c^2 + \rho]\, \Theta n^{-2} + P.$$

In classical hydrodynamics the condition for minimum I would lead in this case to vanishing vorticity: curl V = 0. In relativistic hydrodynamics, because of the relativistic change of mass, the minimum I occurs for a vorticity different from zero. To simplify the computations, we shall actually carry out the calculation for the limiting case when V is close to c. Then $\rho \to \alpha n^k$, where k is the relativistic component of an adiabat and is equal to 4/3, $P = 1/3\, \alpha k^2 n^k$. Substituting these values in L, we get

$$I = \int \left(\alpha k n^{k-2} \Theta + \frac{\alpha}{3} c^2 n^k \right) dx\, dy. \tag{18}$$

The Euler equation for (18) is:

$$\frac{\partial}{\partial x} \left\{ \left[\alpha k n^{k-2} + \left(\alpha k (k-2) n^{k-3} \Theta + \frac{k \alpha c^2}{3} n^{k-1} \right) \frac{dn}{d\Theta} \right] 2 \frac{\partial \psi}{\partial x} \right\} + \frac{\partial}{\partial y} \left\{ \left[\alpha k n^{k-2} + \left(\alpha k (k-2) n^{k-3} \Theta + \frac{k \alpha c^2}{3} n^{k-1} \right) \frac{dn}{d\Theta} \right] 2 \frac{d\psi}{\partial y} \right\} = 0. \tag{19}$$

We differentiate (17) with respect to Θ and determine $dn/d\Theta$:

$$dn/d\Theta = n/2\, (\Theta - {}^1/_3\, \beta^2 n^2).$$

Substituting this value of $dn/d\Theta$ in (19), we find after simple transformations,

$$\alpha k n^{k-1} \beta \operatorname{curl} \mathbf{V} + k(k-1)\, \alpha n^{k-3} \nabla\psi \nabla n = 0, \tag{20}$$

from which, if we assume that curl V = 0, it follows that $\nabla\psi \cdot \nabla n = 0$, but this is possible only for the case of one-dimensional flow. From (20) we obtain, in particular, the expression for the vorticity in the limiting case:

$$\operatorname{curl} \mathbf{V} = (1/3nc)\, (\mathbf{V} \nabla n). \tag{21}$$

3. NONSTATIONARY FIELD. THE PRINCIPLE OF LEAST ACTION

We introduce three "stream functions" ψ, ϑ, σ in four-dimensional space-time, and define the four-velocity u_i by the following formulas:

$$nu_1 = D(\psi, \vartheta, \sigma)/D(x_2 x_3 x_4); \tag{22}$$

$$nu_3 = D(\psi, \vartheta, \sigma)/D(x_4 x_1 x_2);$$

$$nu_2 = D(\psi, \vartheta, \sigma)/D(x_3 x_4 x_1);$$

$$nu_4 = D(\psi, \vartheta, \sigma)/D(x_1 x_2 x_3).$$

Under these conditions the continuity equation

$$(\partial/\partial x_i)\, (nu_i) = 0 \tag{23}$$

is satisfied identically. As before, the geometrical characteristic of the flux is

$$\Theta = \sum \left(\frac{D(\psi, \vartheta, \sigma)}{D(x_k x_r x_l)} \right)^2 ,$$

where the density n is related to Θ by the equation

$$\Theta = -n^2. \tag{24}$$

In the four-dimensional space, the "streamworld line" is defined by a triple of numbers $(\psi, \vartheta, \sigma)$ constant along the whole "streamworld line". The physical meaning of the streamfunction is that the product $d\psi d\vartheta d\sigma$ determines the "flux" of liquid through the region bounded by the stream hypersurfaces ψ, $\psi + d\psi$, ϑ, $\vartheta + d\vartheta$; σ, $\sigma + d\sigma$, or the flux through the region ψ, $\psi + d\psi$; ϑ, $\vartheta + d\vartheta$ of three-dimensional space during the time interval dt. For fixed t, the line $(\psi, \vartheta) = \text{const}$ is the field line $\bar{s}$ tangent to the velocity vector **V** in three-dimensional space.

To construct the Lagrangian L we construct at any given time, at each point of the actual stream line $\bar{s}$, an orthogonal set of four axes $\bar{x}_i$ so that one of the real axes, say $\bar{x}_1$, is always directed along the stream line $\bar{s}$. To each such axis system we associate an energy-momentum tensor T_{ik}, defined in the system of coordinates determined by the particular axes. We denote the tensor component T_{11} for such an axis system by $T_{\bar{s}\bar{s}}$, so that $T_{11} \equiv T_{\bar{s}\bar{s}}$. Then $L \equiv T_{\bar{s}\bar{s}}$. For an ideal gas,

$$L = T_{\bar{s}\bar{s}} = P + \left(\frac{P}{c^2} + \rho \right) u_s^2 . \tag{25}$$

The integral of the energy along the stream line $\bar{s}$ has the form:

$$\int \frac{\partial T_{\bar{s}k}}{\partial \bar{x}_k} \, d\bar{s} = E(\bar{s}, t). \tag{26}$$

The relation (26) can be regarded as the generalized Hamilton-Jacobi equation for the field. In particular, for $c \to \infty$, Eq. (26) goes over into the classical equation:

$$\int \frac{\partial V}{\partial t} \, d\bar{s} + \frac{V^2}{2} + \int \frac{dP}{\rho} = E(\bar{s}, t). \tag{27}$$

Again we write the first law of thermodynamics:

$$Pd(1/n) + dU = TdH, \tag{28}$$

where U is the internal energy of the gas, and H is the entropy of the gas per molecule. If $U = v\rho c^2$, where $v = 1/n$ is the volume per molecule, then as is shown in relativistic hydrodynamics[7], $H = \text{const}$ and (28) takes the form $Pd(1/n) + dU = 0$. The variational principle for the hydrodynamic field when the conditions (24), (26) and (28) are satisfied consists in the statement that the integral

$$S = \int T_{\bar{s}\bar{s}} \left(\psi, \vartheta, \sigma, \frac{\partial \psi}{\partial x_i}, \frac{\partial \vartheta}{\partial x_i}, \frac{\partial \sigma}{\partial x_i} \right) d\Omega \tag{29}$$

has a stationary value for the actual field. The quantities defining the field are ψ, ϑ, and σ, which are related by (24).

For $c \to \infty$,

$$L = P + \rho V^2, \quad \rho V_x = D(\psi, \vartheta, \sigma)/D(y, z, t);$$

$$\rho V_y = D(\psi, \vartheta, \sigma)/D(z, t, x);$$

$$\rho V_z = D(\psi, \vartheta, \sigma)/D(t, x, y);$$

$$n = \rho = D(\psi, \vartheta, \sigma)/D(x, y, z);$$

$$dQ = TdH = dU + Pd(1/\rho).$$

In this case the integral $S = \int_{t_1}^{t_2} dt \int_{\omega} (P + \rho V^2) \, d\omega$ takes on a stationary value for the actual field. The quantity S has, for a nonstationary field, the dimensions of action, so that the principle thus established for a non-stationary field in relativistic hydrodynamics may be regarded as a principle of least action.

4. THE EXISTENCE OF A STRONG MINIMUM FOR THE STREAMING POTENTIAL

We shall prove the existence of a strong minimum for the actual subsonic, adiabatic flow of a gas. To simplify the computations we shall, without loss of generality, limit ourselves to considering plane flow of the gas. Let ψ be the solution, subject to the given boundary conditions, of the equation

$$\delta \int L dx dy = \delta \int F(\Theta) \, dx dy = 0, \tag{30}$$

where $L = F(\Theta)$ is the Lagrangian for the hydrodynamic field of an ideal gas, and Θ has the same meaning as earlier.

The stream function ψ gives a strong minimum for the functional $I = \int L d\omega$. In proving this, we shall make use of the theory of the Weierstrass function in the calculus of variations[8]. For the construction of the Weierstrass function, it is sufficient to satisfy the following two conditions:

1) Every solution of (30) satisfies the self-adjoint Butler equation

$$\frac{\partial L}{\partial \psi} - \frac{\partial}{\partial x} \frac{\partial L}{\partial (\partial \psi / \partial x)} - \frac{\partial}{\partial y} \frac{\partial L}{\partial (\partial \psi / \partial y)} = 0; \tag{31}$$

2) If ψ is a solution of (31), then there exists at least one system φ of Lagrange surfaces which covers the extremal surface ψ, which depends on a single parameter ξ, and for which the Jacobi condition

$$P = \partial\varphi/\partial x = \partial\psi/\partial x = p; \quad Q = \partial\varphi/\partial y = \partial\psi/\partial y = q.$$

is satisfied on the extremal surface.

Conditions 1) and 2) are sufficient for the construction of a field consisting of Lagrange surfaces covering the surface-extremals ψ, which guarantees the possibility of constructing the Weierstrass function of the variational problem. Conditions 1) and 2) are satisfied for the continuous hydrodynamic field of an ideal gas. In particular, we can take $\psi + \xi$ for φ. The Figure shows the dependence of $L = F(\Theta)$*. The branch *1* which is concave upwards corresponds to subsonic flow, the curve *2* which is concave downwards, to supersonic flow of the gas. At the turning point Θ_{cr} the critical condition is reached where the flow velocity is equal to the local sound velocity.

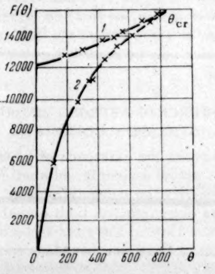

Corresponding to the Lagrangian L, we construct the phase surface

$$Z = L = F(\Theta) = F(p^2 + q^2) = Z(p, q) \quad (32)$$

in the space $p = \partial\psi/\partial x$, $q = \partial\psi/\partial y$. Let the aggregate of three numbers $\bar{p}$, $\bar{q}$, $\bar{L} = z(\bar{p}, \bar{q})$ represent a point of phase surface. The equation of the tangent plane at the point $(\bar{p}, \bar{q}, \bar{L})$ of the surface Z has the form:

$$Z = \bar{L} + (\partial\bar{L}/\partial\bar{p})(p - \bar{p}) + (\partial\bar{L}/\partial\bar{q})(q - \bar{q}), \quad (33)$$

where Z, P, q are running coordinates in the plane. We denote by $G(p, q, \bar{p}, \bar{q})$ the difference in the values of Z on the surface (32) and on the tangent plane (33) to the point $\bar{L}$, $\bar{p}$, $\bar{q}$, taken for the same point (p, q), and call it the deviation of the surface (32) from the plane (33) at that point. If this difference is positive, the deviation is positive, Thus

$$G(p, q, \bar{p}, \bar{q}) = L(p, q) - L(\bar{p}, \bar{q}) - \frac{\partial\bar{L}}{\partial\bar{p}}(\bar{p} - p) - \frac{\partial\bar{L}}{\partial\bar{q}}(q - \bar{q}). \quad (34)$$

Expression (34) coincides exactly with the Weierstrass function[8] of the variational problem which provides a sufficient condition for the existence of a strong minimum. If $G \geq 0$ everywhere within the domain of definition of $\bar{L}$, the solution of Eq. (30) guarantees a strong minimum for the functional I. From the Figure we see that the phase surface $Z = L(p, q)$ for subsonic flow is a convex surface, and $G \geq 0$. For supersonic flow the phase surface has a saddle at every point. In this case the actual field ψ_0 produces a minimax of I. If $I(\psi_0) = I_0$ then it is easily shown that ψ_0 gives a strong minimum, equal to I_0, for the functional $I^* = \frac{1}{2} I_0(I_0/I + I/I_0)$. Therefore, the actual field ψ_0, determined from the equation $\delta I = 0$, satisfies the equation $\delta I^* = 0$. In this way the minimax property of the streaming potential for supersonic flow is eliminated, and one can apply the direct method of Ritz to it just as for the streaming potential of subsonic flow. For subsonic, adiabatic gas flows, the Weierstrass function is essentially positive and goes to zero if, and only if, $p \equiv \bar{p}$, $q \equiv \bar{q}$. From this we get the uniqueness theorem: there cannot exist two solutions satisfying the same conditions for ψ on the boundary surfaces of the region of the flow.

---

* The curve was drawn for the initial conditions $P_0 = 1$ atm, $\rho_0 = 0.125$ kgm-sec^2/m^4, $k = c_p / c_v = 1.41$, $V_0 = a_0 / 2$, where a_0 is the sound velocity.

[1] H. Bateman, Proc. Roy. Soc. (London) 125A, 598 (1929).

[2] C. C. Lin and S. I. Rubinov, J. Math. Phys. 27, 105 (1948).

[3] Hirosi Ito, Progr. Theor. Phys. 9, 117 (1953).

[4] L. Landau, J. Phys. USSR 5, 71 (1941).

[5] F. London, Rev. Mod. Phys. 17, 310 (1945).

[6] V. I. Skobelkin, Report No. 84, NIVI MEP (1950).

[7] L. Landau and I. Lifshitz, *Classical Theory of Fields*, Addison-Wesley, 1951.

[8] N. M. Glunter, *Course in the Calculus of Variations*, GTTI, 1941.

Translated by M. Hamermesh
53

SOVIET PHYSICS JETP VOLUME 4, NUMBER 1 FEBRUARY, 1957

The Dynamical Magnetic Moment of the Deuteron

A. M. KOROLEV
Institute of Physics, Academy of Sciences, Ukrainian SSR

(Submitted to JETP editor March 18, 1955)
J. Exptl. Theoret. Phys. (U.S.S.R.) 31, 211-217 (August, 1956)

The dynamical magnetic moment of the deuteron is considered on the basis of the pseudoscalar meson theory with the pseudoscalar type of coupling, in the fifth order of perturbation theory. Exchange currents in the deuteron make an essential contribution to the dynamical magnetic moment.

INTRODUCTION

THE well-known experimental result that the constant magnetic moment of the deuteron differs from the sum of the magnetic moments of the neutron and proton is commonly explained phenomenonologically by the existence of a tensor interaction between nucleons. Because of this the ground state of the deuteron consists of an *S*-state with an admixture of a *D*-wave, which on one hand leads to the existence of the quadrupole moment of the deuteron, and on the other to the nonadditivity of the magnetic moments in the deuteron[1].

Although such an interpretation is not in qualitative contradiction with experiment, it still does not correspond exactly to the effect, since it does not take into account the existence of meson exchange currents in the deuteron, which are shown by experiment to have an essential effect on the electromagnetic properties of the deuteron, particularly on radiative effects in the neighborhood of the energy threshold for production of π-mesons.

Unfortunately there is at present no consistent phenomenological theory of exchange currents. Of the attempts in this direction most deserving of attention, mention must be made of the work of Sachs[2], and a paper of Villars[3] is devoted to the meson-field treatment of this effect.

An essential difficulty in the treatment of the magnetic moment of the deuteron on the basis of the meson theory of nuclear forces arises from the circumstance that within the framework of this theory the relativistic problem of two nucleons is at the present time unsolved, and the magnetic moments of the separate nucleons are explained only qualitatively by the theory with weak interaction between the nucleon and meson fields, so that any theoretical investigations in this subject are as yet only of a qualitative nature. Nevertheless, it can turn out that the perturbation theory to a certain extent gives a correct indication of the general tendencies in the behavior of the two-nucleon system in interaction with high-energy γ-ray quanta.

The present paper is devoted to a consideration of the dynamical magnetic moment of the deuteron on the basis of the pseudoscalar meson theory with the pseudoscalar type of coupling. In interaction with the meson field of the vacuum the nucleons making up the deuteron can emit and then absorb virtual mesons, so that the real nucleon can be thought of as surrounded by a certain stationary cloud. If the charged meson clouds of the neutron and proton overlap, exchange meson currents arise, flowing from one nucleon to the other. The interaction of the meson field surrounding the deuteron with the electromagnetic field can be interpreted as a supplementary direct electromagnetic interaction of the deuteron itself.

In the expression obtained for this supplementary interaction one can single out the terms that represent the energy of a certain additional magnetic moment in the electromagnetic field. The size of this magnetic moment will depend on the frequency of the electromagnetic field. Thus the energy of the supplementary electromagnetic interaction will have the form

$$(e\hbar/2Mc)\,(\sigma_{\mu\nu}F_{\nu\mu})\,[\mu_c + f(k)],$$

where $F_{\nu\mu}$ is the electromagnetic field tensor, $\sigma_{\mu\nu}$ is the spin operator, μ_c is the static magnetic moment of the deuteron, and $f(k)$ is a certain function of k that goes to zero for $k \to 0$. The quantity in square brackets represents the dynamical magnetic moment of the deuteron.

We shall consider the supplementary interaction of the deuteron with the electromagnetic field, including effects of exchange currents, on the basis of the symmetric pseudoscalar meson theory with pseudoscalar coupling, by the use of the relativistically invariant method of Feynman and Dyson[4,5].

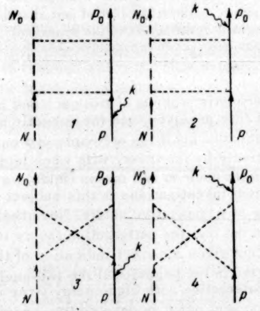

FIG. 1

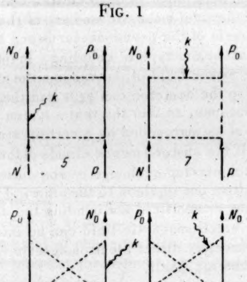

FIG. 2

In the case of the bound state we cannot apply directly the relativistically invariant method, which has been systematically developed only for the free states of two nucleons. Therefore, following the method of Brueckner[6], we develop the space factor of the initial state wave function into a Fourier integral, and in finding the matrix element we operate with one component of the expression, which, we may suppose, describes a "quasi-free state", and afterwards carry out the integration over the entire momentum space. The use of this method leads to the possibility of writing the matrix element for a radiative transition in the simple form

$$H_{if} = \Psi_d(0)M_{if}(0); \tag{1}$$

M_{if} is the matrix element, which is constructed by the method given in Refs. 4 and 5, and in which the momentum in the initial state is taken equal to zero*.

Figures 1 — 3 show the Feynman diagrams relating to the process under consideration.

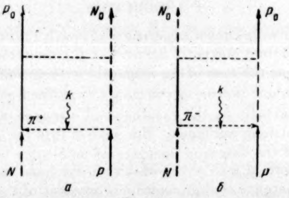

FIG. 3

In the expressions obtained for the supplementary interaction energy of the deuteron with the electromagnetic field we single out the terms having the form $i\gamma_\mu\gamma_\nu k_\mu A_\nu \mu(k)$ in the momentum representation (γ_ν are the Dirac matrices, A_ν the vector potential of the electromagnetic field, and k_μ the energy-momentum vector of the γ-quantum). In the

---

* The form of the expression (1) is due to the circumstance that in the absorption of a short-wavelength γ-quantum by the deuteron the nucleons in the deuteron must be separated only by small distances of the order

$$\lambda \sim h/p_0 \sim (\hbar/Mc)\,(Mc^2/2E_k)^{1/2}.$$

This means that we must take the wave function of the deuteron for some effective value of r, smaller than λ, but since $\Psi_d(r)$ is weakly dependent on r at small distances $r \leq h/Mc$, we may take $r_{\text{eff}} \sim 0$[6,8].

coordinate representation this term has the form $(\sigma_{\mu\nu}F_{\nu\mu})\mu(k)$, i.e., it represents the energy of the magnetic moment of the system in the electromagnetic field[7].

It can be shown that in the case in which the nucleons exchange an odd number of mesons the magnetic terms add up to zero. We first consider the case of the exchange of one meson. This corresponds to a process of third order in perturbation theory (exchange meson currents), and of the fifth order (the effect of the meson cloud surrounding the deuteron)[8].

In this case the terms in the magnetic interaction energy will have the form

$$\gamma_5'\gamma_5''\hat{k}'\hat{A}'\mu_1(k) + \gamma_5'\gamma_5''\hat{k}''\hat{A}''\mu_2(k). \tag{2}$$

The primes ′ and ″ indicate whether the Dirac matrices γ_5 and γ_μ refer to the first or the second particle.

If we denote the matrix-vectors for the initial and final states of the proton and neutron by $\hat{P}$, $\hat{N}$ and $\hat{P}_0$, $\hat{N}_0$, respectively, then on the basis of the Dirac equation we can write:

$$(\hat{P} - M)\,u(P) = 0; \quad (\hat{N} - M)\,u(N) = 0; \tag{3}$$

$$\bar{u}(P_0)(\hat{P}_0 - M) = 0; \quad \bar{u}(N_0)\,(\hat{N}_0 - M) = 0.$$

Moreover, the four-dimensional matrix-vectors satisfy the following relations

$$\hat{a}\hat{b} + \hat{b}\hat{a} = 2\,(ab), \tag{4}$$

$$(ab) = a_4b_4 - a_1b_1 - a_2b_2 - a_3b_3, \tag{5}$$

$$\gamma_5\hat{a} = -\hat{a}\gamma_5. \tag{6}$$

Thereupon, taking into account the law of conservation of energy in the initial and final states of the system, $k = P_0 + N_0 - P - N$, the transversality condition for free γ-quanta, which gives $(AP) = (AN) = (Ak) = 0$, and the relations (1), (3) and (4), we find that the matrix element of the operator (2) becomes zero. In the case of interchange of $(2n + 1)$ mesons by the nucleons, we can use Eq. (6) to bring all of the matrices γ_5 together, and since $\gamma_5^2 = -1$, the expression for the magnetic interaction energy again takes the form (2), and consequently is equal to zero.

This result is due to the specific form of meson theory used (pseudoscalar meson theory with pseudoscalar and pseudovector couplings). For other types of coupling these magnetic terms can be different from zero. When the nucleons exchange an even number of mesons the magnetic moment does not reduce to zero, and thus we begin our consideration with the next, the fifth, order of perturbation theory (case of exchange of two mesons). In the approximation in question all diagrams can be divided into two types: diagrams relating to the internal motion of the nucleons, and exchange nucleon and meson currents.

INTERNAL MOTION OF THE NUCLEONS

To the first type belong the diagrams (cf. Fig. 1) describing the absorption of the γ-quantum by a nucleon. Diagrams *1* and *2* relate to the case in which the emission and absorption of the first meson precede the emission and absorption of the second meson (nonintersecting meson lines). Diagrams *3* and *4* represent the case of intersecting meson lines, when the meson first emitted by a nucleon is absorbed after the emission and subsequent absorption of the second meson.

The exchange of the two mesons brings about a change of the internal motion of the nucleons in such a way that to the ground *S*-state of the deuteron there are also added states with other orbital angular momenta. When all approximations of the perturbation theory are taken into account, this should in principle give the experimentally observed combination of the *S*- and *D*-waves in the ground state of the deuteron.

To obtain the matrix elements corresponding to diagrams *1-4*, we choose a coordinate system connected to the center-of-mass of the system deuteron + γ-quantum. Then, according to Eq. (1), the initial four-vector momenta of the proton and neutron are equal to each other and have the components $P_4 = M$, $P = -k/2$, and the final momenta N_0 and P_0 of neutron and proton have the components $P_{04} = N_{04} = E_0$, $\overline{N_0} = -\overline{P_0}$.

If the second meson emitted is absorbed before the first (intersecting meson lines of diagrams *3* and *4*), then there also exist two possibilities of realization of the process in question: absorption of the γ-quantum by the proton before and after the exchange of the two mesons between the two nuclei (matrix elements M_3 and M_4).

For the symmetric meson theory of nuclear forces there are four matrix elements corresponding to diagrams *1* and *2*, differing from each other in that the exchange between the two nucleons is made by two charged mesons, two neutral mesons, or one charged and one neutral meson. These matrix elements either are equal to M_1 (or M_2), or else they differ from M_1 (or M_2) by the interchange of the indices of the particles. The same can be said with regard to diagrams 3 and 4, for each of which there exist three matrix elements.

The calculation of the integrals occurring in the matrix elements M_1 to M_4 is rather cumbersome. But if we restrict ourselves just to terms of order k^2/M^2, the result can be obtained in analytical form. Taking into account all matrix elements characterizing the internal motion of the nucleons, and using the method of parametric integration[4], we obtain the following expression for the radiative transition matrix element M_n characterizing the internal motion of the nucleons in the deuteron*.

$$M_n = -\frac{eg^4}{4\pi}<\frac{\hat{k}''\hat{A}''}{M^4}[F_1-(\gamma'_\mu\gamma''_\mu)\,G_1]> + \frac{eg^4}{4\pi}<\frac{(\hat{k}'\hat{A}'+\hat{k}''\hat{A}'')}{M^4}[F_2-(\gamma'_\mu\gamma''_\mu)G_2]>$$
$$-\frac{eg^4}{4\pi}<\frac{(^1/_2\hat{k}'A'+\hat{k}''\hat{A}'')}{M^4}[F_4^- - G_4^-(\gamma'_\mu\gamma''_\mu)]> + \frac{eg^4}{4\pi}\Big\{<\frac{\hat{k}'\hat{A}'}{M^4}[F_3^+ - G_3^+(\gamma'_\mu\gamma''_\mu)]>$$
$$+<\frac{\hat{k}''\hat{A}''}{2M^4}[F_3^- - G_3^-(\gamma'_\mu\gamma''_\mu)]>\Big\}, \tag{7}$$

where

$$F_1 = \left\{\frac{Mk+\mu^2}{M^2+2Mk}\left(\ln\frac{\mu^2}{M^2}+1\right)+\sqrt{\frac{k^2-\mu^2}{4M^2}}\ln\frac{[2(M^2+Mk)+M\sqrt{k^2-\mu^2}][2k+\sqrt{k^2-\mu^2}]}{[2(M^2+Mk)-M\sqrt{k^2-\mu^2}][2k-\sqrt{k^2-\mu^2}]}\right.$$
$$+\frac{Mk}{(M^2+Mk)}+\frac{Mk-2\mu^2}{2M^2}\ln\frac{k}{2M}-2\sqrt{\frac{k^2-4\mu^2}{M^2}}\,\mathrm{arctg}\,2\sqrt{\frac{M^2}{k^2-\mu^2}}$$
$$\left.+\sqrt{\frac{k}{M}}\,\mathrm{arctg}\,4\sqrt{\frac{M}{k}}\right\}\frac{M^2}{(Fk)};$$

$$G_1 = \left[\frac{Mk}{2(M^2+Mk)}+\frac{Mk-2\mu^2}{4M^2}\ln\frac{k}{2M}-\sqrt{\frac{|k^2-4\mu^2|}{M^2}}\,\mathrm{arctg}\,2\sqrt{\frac{M^2}{k^2-\mu^2}}\right.$$
$$\left.+\sqrt{\frac{k}{M}}\,\mathrm{arctg}\,4\sqrt{\frac{M}{k}}\right]\frac{M}{(P_0k)};$$

$$F_2^- = \left[1-\ln\frac{2M}{\mu}+\frac{\mu}{M}\,\mathrm{arctg}\,\frac{M}{\mu}-\frac{5}{24}\ln 2\right]\frac{M^2}{(P_0k)};$$

$$G_2^- = \left[\frac{\mu}{M}\,\mathrm{arctg}\frac{M}{\mu}+1-\ln\frac{2M}{\mu}\right]\frac{M^2}{(P_0k)};$$

$$F_3^+ = \left\{\left[\frac{2(M^2-(P_0k))}{M^2-3(P_0k)}+\frac{6}{5}\frac{(P_0k)}{M^4}\ln\frac{k}{M}+\frac{2}{3}\frac{(P_0k)}{M^2}\right.\right.$$
$$\left.+\frac{4}{3}\frac{(P_0k)}{M^2-3(P_0k)}\frac{M^2}{\lambda}T(k)\right\}\frac{M^2}{(Pk)};$$

$$G_3^+ = \left\{\frac{(P_0k)M}{(M^2-3(P_0k))k}\ln\frac{M}{k}+\frac{\lambda M}{(M^2-3(P_0k))k}T(k)+\frac{2}{9}\right\}\frac{M^2}{2(Pk)};$$

$$F_4^- = \frac{M^2+\beta^2}{2(M^2-2\beta^2)}\left\{\frac{(M^2-2\beta^2)}{2(M^2-\beta^2)}+\frac{9}{4}\frac{\beta^2M^2}{(M^2-\beta^2)^2}+\frac{2\beta^2}{d}\frac{(M^2-\beta^2)}{(M^2+\beta^2)}\ln\frac{2\beta^2-d}{2\beta^2+d}\right.$$
$$\left.+\frac{2M^2-5\beta^2}{M^2}\ln\frac{M}{\mu}\right\}\frac{M^2}{(P_0k)};$$

$$G_4^- = \left\{\frac{\mu}{M}\,\mathrm{arctg}\,\frac{M}{\mu}-\frac{\beta^2}{6M^2}\right\}\frac{M^2}{(P_0k)};$$

$$T(k) = \left[\mathrm{arctg}\,\frac{2(M^2-2(P_0k))}{\lambda}-\mathrm{arctg}\,\frac{2(P_0k)}{\lambda}\right];$$

$$\lambda = \sqrt{4M^2\beta^2-9(P_0k)^2};\quad d = 2\sqrt{M^2\mu^2-\beta^4};\quad \beta = (Mk-\mathbf{P}_0\mathbf{k});$$
$$(P_0k) = (E_0+P_0\cos\theta)\,k.$$

---

* In the expression (7) terms in the electric interaction $\sim(AP_0)$ are not included, since an estimate showed them to be small.

In Eq. (7), F_i^+, G_i^+ differ from F_i^-, G_i^- by the interchange of P_0 and N_0 in the scalar products (P_0k) and (N_0k) on which these functions depend; in other words, they differ by the sign of the spatial momentum of the nucleon.

NUCLEON AND MESON EXCHANGE CURRENTS IN THE DEUTERON

Diagrams *5-8* describe the absorption of the γ-quantum by the deuteron by nucleon (diagrmas *5* and *6*) and meson (diagrams *7* and *8*) exchange currents in the deuteron, which arise in the exchange between the nucleons of two mesons, of which at least one must be charged.

We have calculated the anomalous dynamic magnetic moment due to meson exchange currents in the deuteron (non-intersecting meson lines) when the second meson emitted by the nucleon absorbs the γ-quantum in the intermediate state. There exist, however, still other matrix elements that characterize the absorption of γ-quanta by meson exchange currents, but do not contribute to the effect. These are the matrix elements that are due to the absorption of the γ-quantum by the first meson exchanged, and also to the matrix elements corresponding to the diagrams with intersecting meson lines. To this case there correspond two matrix elements: a) with the second meson neutral (cf. Fig. 3), and b) with the secon meson charged. Then the absorption of the γ-quantum occurs in case a) by a π^+, and in case b) by a π^- meson, for the given direction of motion of the mesons from the final state neutron to the proton. Thus we have for these matrix elements $M_a = M_b$ [$P = N$ on the basis of (1)], and their sum is zero.

Similarly it can be shown that matrix elements of the type M_8 make a small contribution to the effect, and we neglect them. The matrix element for the electromagnetic transition arising from the existence of nucleon and meson exchange currents finally takes the form:

$$\begin{aligned} M_0 = &- eg^4/4\pi M^4 < (\hat{k}'\hat{A}' + \hat{k}''\hat{A}'')\,[(F_5 - {}^1/_2 F_7) - (\gamma'_\mu\gamma''_\mu)\,G_5] > \\ &+ \frac{eg^4}{4\pi M^4} < \hat{k}'\hat{A}'\,(F_6^- - (\gamma'_\mu\gamma''_\mu)G_6^-) > + \frac{eg^4}{2\pi M^4} < \hat{k}''\hat{A}''\,(F_6^+ - (\gamma'_\mu\gamma''_\mu)\,G_6^+) >, \quad (8) \end{aligned}$$

$$F_5 = -\frac{1}{8}\left[\frac{E_0^2}{E_0^2 - P_0^2\cos^2\theta} + 1\right]; \quad G_5 = -\frac{2}{5}\left[\frac{\mu^2}{7M^2} + \frac{k}{29\,M} - \frac{E_0 k}{72M^2}\right]; \qquad (8a)$$

$$\begin{aligned} F_6^+ = \Big\{ &\frac{M}{\mu}\left(\frac{3}{4} - \frac{\beta^2}{M^2} + \frac{10\,\mathbf{P}_0\mathbf{k}}{M^2}\right)\operatorname{arctg}\frac{M}{\mu} - \left(2 + \frac{10\,\mathbf{P}_0\mathbf{k}}{M^2} + \frac{\beta^2}{M^2}\right)\ln\frac{M}{\mu} \\ &- \left(\frac{3}{4} + \frac{10\,\mathbf{P}_0\mathbf{k}}{M^2}\right)\ln 2 + \frac{3}{8} + \left[\frac{3}{4}\sqrt{\frac{\beta^2 + 4\mu^2}{4\beta^2}} + \frac{\sqrt{\beta^4 + 4\mu^2\beta^2}}{M^2}\right. \\ &\left. + \left(\frac{3}{2}\frac{k}{M} - \frac{5}{8}\frac{(P_0k)}{M^2}\right)\frac{M^2}{\sqrt{\beta^4 + 4\mu^2\beta^2}}\right]\ln\frac{\beta^2 + \sqrt{\beta^4 + 4\beta^2\mu^2}}{\beta^2 - \sqrt{\beta^4 + 4\beta^2\mu^2}}\Big\}; \end{aligned}$$

$$G_6 = \left\{\left(1 + \frac{4}{3}\frac{\beta^2}{M^2}\right)\frac{M}{\mu}\operatorname{arctg}\frac{M}{\mu} - \left(1 + \frac{\beta^2}{4M^2}\right)\ln\frac{2M}{\mu} - \frac{3}{4}\frac{\beta^2}{M^2}\ln 2\right\};$$

$$\begin{aligned} F_7 = \Big\{ &\frac{(M^2 + \beta^2)\ln 4}{M^2 - 2(N_0k)} + \frac{3\pi}{8}\frac{(N_0k)}{M^2} + \frac{M^2}{2(M^2 - (N_0k))} - \frac{M^2 + 2(N_0k)}{M^2 - 2(N_0k)}\ln\frac{M^2}{(N_0k)} \\ &- \frac{M}{\beta}\left[\ln\frac{(2M^2 - \beta^2 - 2M\beta)\,|\,\beta^2 - 2M\beta\,|}{(2M^2 - \beta^2 + 2M\beta)\,|\,\beta^2 + 2M\beta\,|}\right] + \frac{(M^2 + \beta^2)}{4\,(M^2 - 2\,(N_0k))}\frac{M}{\sqrt{(N_0k)}} \\ &\times \ln\frac{|2M^2 + \beta^2 - 2M\sqrt{(N_0k)}\,|\,\beta^2 + 2M\sqrt{(N_0k)}\,|}{|2M^2 + \beta^2 + 2M\sqrt{(N_0k)}\,|\,\beta^2 - 2M\sqrt{(N_0k)}\,|} - \frac{1}{4}\ln\frac{M}{\mu} \\ &- \frac{c_0M^3}{(N_0k)^{3/2}}\ln\frac{M - \sqrt{(N_0k)}}{M + \sqrt{(N_0k)}} + \frac{(P_0k)}{2(N_0k)}\left[9c_1 + \frac{3}{2}\ln\frac{M}{\mu} + \frac{M^2 + 2\beta^2}{2M\beta}\ln\frac{M}{\mu}\right]\ln\frac{M - \beta}{M + \beta} \\ &+ \frac{4c_1M}{\sqrt{(N_0k)}}\ln\frac{M - \sqrt{(N_0k)}}{M + \sqrt{(N_0k)}}\Big\}; \; c_0 = 0.93; \; c_1 = 0.65. \end{aligned}$$

It must be noted that the functions F_i appear in the matrix elements M_n and M_0 in an unsymmetrical way, so that the angular dependence for the radiative transitions must have an asymmetry in the direction of small angles (when $\cos\theta \sim 1$).

THE DYNAMICAL MAGNETIC MOMENT OF THE DEUTERON

The additional interaction energy of the deuteron with the electromagnetic field, which appears because of the existence of nucleon and meson exchange currents in the deuteron and the change of the internal motion of the nucleons owing to them, can be written by (1), (7) and (8) in the following form:

$$H_{if} = \frac{eg^4}{4\pi}\frac{\Psi_d(0)}{M^4}\{<\hat{k}'\hat{A}'(\mathfrak{F}' - (\gamma'_\mu\gamma''_\mu)\mathfrak{G}')>_{if} \quad (9)$$

$$+ <\hat{k}''\hat{A}''(\mathfrak{F}'' - (\gamma'_\mu\gamma''_\mu)\mathfrak{G}'')>_{if}$$

$$+ <(\hat{k}'\hat{A}' + \hat{k}''\hat{A}'')(\mathfrak{F} - (\gamma'_\mu\gamma''_\mu)\mathfrak{G})>_{if}\}.$$

Here the new functions $\mathfrak{F}$ and $\mathfrak{G}$ are connected with the old functions F_i and G_i [cf. Eqs. (7a) and (8)] in the following way:

$$\mathfrak{F}' = \left(F_3^+ + F_6^- + \frac{1}{2}F_4^-\right); \quad (9a)$$

$$\mathfrak{F}'' = \left(2F_6^+ + \frac{1}{2}F_3^- - F_1\right);$$

$$\mathfrak{F} = \left(F_2^- - F_4^- - F_5 + \frac{1}{2}F_7\right);$$

$$\mathfrak{G}' = \left(G_3^+ + G_6^- + \frac{1}{2}G_4^-\right);$$

$$\mathfrak{G}'' = \left(2G_6^+ + \frac{1}{2}G_3^- - G_1\right);$$

$$\mathfrak{G} = (G_2^- - G_4^- - G_5).$$

Let us consider the form of the operators appearing in Eq. (9) in the x-representation. Since by the law of conservation of energy and momentum

$$k_\mu = P_{0\mu} + N_{0\mu} - P_\mu - N_\mu = \Delta P_\mu \rightarrow i\partial/\partial x_\nu,$$

we can write the operator $\hat{k}\hat{A}$ in the following form:

$$\hat{k}\hat{A} = \gamma_\mu\gamma_\nu k_\mu A_\nu = \sigma_{\mu\nu}\mathfrak{F}_{\nu\mu},$$

where $\sigma_{\mu\nu} = (i/2)(\gamma_\mu\gamma_\nu - \gamma_\nu\gamma_\mu)$ is the four-dimensional spin vector and $\mathfrak{F}_{\mu\nu}$ is the electromagnetic field tensor. If we introduce the total spin of the system, $S_{\mu\nu} = (\sigma'_{\mu\nu} + \sigma''_{\mu\nu})$, Eq. (9) takes the form:

$$H_{if} = (eh/2Mc)(g^2/hc)^2\Psi_d(0)/2\pi M^3 \quad (10)$$

$$<\{(\sigma'_{\mu\nu}\mathfrak{F}_{\nu\mu})(\mathfrak{F}' - (\gamma'_\mu\gamma''_\mu)\mathfrak{G})$$

$$+ (\sigma''_{\mu\nu}\mathfrak{F}_{\nu\mu})(\mathfrak{F}'' - (\gamma'_\mu\gamma''_\mu)\mathfrak{G}'')$$

$$+ (S_{\mu\nu}\mathfrak{F}_{\nu\mu})(\mathfrak{F} - (\gamma'_\mu\gamma''_\mu)\mathfrak{G})\}>_{if}.$$

Now H_{if} has the form of the energy of the dynamical magnetic moment in the electromagnetic field.

By means of the expression just obtained one can consider various radiative processes for the system neutron-proton, for example, the photodisintegration of the deuteron, the production of γ-quanta in collisions of high-energy neutrons with protons, and the Compton effect with the deuteron.

Let us consider as an illustration the photodisintegration of the deuteron. In the Pauli approximation, H_{if} takes the form

$$H_{if} = -\left(\frac{eh}{2Mc}\right)\left(\frac{g^2}{\hbar c}\right)^2\frac{\Psi_d(0)}{2\pi M^3c^3} \quad (11)$$

$$\times <\{(\mathbf{SH})\left[F + \frac{F' + F''}{2}\right.$$

$$\left. - \left(1 + \frac{k}{Mc^2}\right)\left(\mathfrak{G} + \frac{\mathfrak{G}' + \mathfrak{G}''}{2}\right)\right]$$

$$+ (\mathbf{CH})\left[\frac{\mathfrak{F}' - \mathfrak{F}''}{2} - \left(1 + \frac{k}{Mc^2}\right)\left(\frac{\mathfrak{G}' - \mathfrak{G}''}{2}\right)\right]>_{if},$$

$$\mathbf{S} = (\sigma' + \sigma''), \quad \mathbf{C} = \sigma'_1 - \sigma''_2,$$

The first term in Eq. (11) describes the triplet-triplet transitions, and the second, the triplet-singlet transitions. For the triplet-triplet transitions the differential cross section for the photodisintegration of the deuteron can be written in the following form:

$$d\sigma_\Phi = \frac{\pi^2}{32}\left(\frac{e^2}{\hbar c}\right)\left(\frac{g^2}{\hbar c}\right)^4\frac{\Psi_d^2(0)}{M^3c^3}\left(\frac{k}{Mc^2}\right)^{3/2}D^2(k)\,d\Omega, \quad (12)$$

$$D(k) = \left(\mathfrak{F} + \frac{\mathfrak{F}' + \mathfrak{F}''}{2}\right)$$

$$-\left(1 + \frac{k}{Mc^2}\right)\left(\mathfrak{G} + \frac{\mathfrak{G}' + \mathfrak{G}''}{2}\right).$$

The function $D(k)$ increases slowly with the energy of the absorbed γ-ray.

With increasing γ-ray energy the effective cross section for the photodisintegration of the deuteron, Eq. (12), increases as $k^{3/2}$. The angular distribution of the photonucleons is isotropic in the range of energies in which the magnitude of the spatial momentum of the nucleon can be neglected in comparison with Mc, and the anisotropy increases with increase of the energy of the absorbed γ-quantum. Such a picture agrees qualitatively with the experimental data[9-11].

In conclusion, the writer regards it as his pleasant duty to express his gratitude to M. A. Markov for suggesting this problem and for valuable discussions.

[1] W. Rarita and J. Schwinger, Phys. Rev. 59, 436 (1941).

[2] R. G. Sachs, Phys. Rev. 74, 433 (1948).

[3] F. Villars, Phys. Rev. 86, 476 (1952).

[4] *The Newest Development in Quantum Electrodynamics* (collection of papers), IIL (Foreign Lit. Press), 1954, pp. 138, 161, 205.

[5] *The Displacement of Levels of Atomic Electrons* (collection of papers), IIL (Foreign Lit. Press), 1950,

[6] K. Brueckner, Phys. Rev. 82, 598 (1951).

[7] K. M. Case, Phys. Rev. 76, 1 (1949).

[8] A. M. Korolev, Dissertation, Physical Institute, Academy of Sciences, USSR, Moscow, 1952.

[9] S. Kikuchi, Phys. Rev. 85, 753, 1062 (1952).

[10] R. Littauer and J. Keck, Phys. Rev. 86, 1051 (1952).

[11] W. S. Gilbert and J. Rosengren, Phys. Rev. 88, 901 (1952).

Translated by W. H. Furry
41

SOVIET PHYSICS JETP VOLUME 4, NUMBER 1 FEBRUARY, 1957

The Production of Charged Mesons by the Bombardment of Beryllium and Carbon with 660 MEV Protons

M. G. MESHCHERIAKOV, I. K. VZOROV, V. P. ZRELOV, B. S. NEGANOV AND A. F. SHABUDIN
Institute for Nuclear Problems, Academy of Sciences, USSR

(Submitted to JETP editor April 7, 1956)
J. Exptl. Theoret. Phys. (U.S.S.R.) 31, 55-62 (July, 1956)

The energy spectra of positive and negative pions released in $p + \mathrm{Be}$ and $p + \mathrm{C}$ collisions was measured with a magnetic spectrometer at an angle 24° to a 660 mev proton beam. The π^+–meson spectrum has a clearly defined maximum at an energy of about 210 mev in the laboratory system, whereas the spectrum for the π^-–mesons varied only slightly over a range from 60 to 250 mev. The probability of positive pion formation when protons collide with protons bound in Be and C nuclei was discovered to be at least three times less than where protons act on free protons. The maximum of the π^+–meson spectrum in the center-of-mass coordinate system is situated near 100 mev. The ratio of positive to negative pion emission was determined for Be and C over the whole spectral range. The ratio of total emission of positive to negative pions for these two elements is equal, respectively, to 5.3 ±0.6 and 7.0 ±0.8.

1. INTRODUCTION

THE present article is devoted to research on the energy spectra of positive and negative pions released during the bombardment of beryllium and carbon with protons whose energy was sufficient to excite one of the colliding nucleons to the state with an angular momentum of 3/2 and an isotopic spin of 3/2 (i.e., a $P_{3/2,3/2}$ state). The proton energy was not so high that the process of forming two pions in a single collision occurred to any appreciable degree.

2. THE EXPERIMENTAL PROCEDURE

A magnetic spectrometer was used to obtain the energy distributions of the pions. Those pions which are emitted at an angle 24° to the proton beam pass through the spectrometer and are recorded with a telescope of three scintillation counters. Information on the proton beam and magnetic spectrometer was presented in a previous paper[1]. The method for determining the contamination of the pion beam by μ–mesons and electrons upon exit from the spectrometer was described in the same paper. The influence of pion absorption in the target, as well as in the crystals and filters, was evaluated in the light of current data on total cross sections of pion-nucleus interaction[2-5]. For the beryllium and carbon targets, with thicknesses selected so that the energy loss suffered by the 660 mev protons was 3.7 mev in both, this correction varied from 3% at the bottom of the spectrum to 6.6% at 200 mev and then dropped again to 3.5% at 420 mev. In calculating the correction for pion disintegration in flight, the lifetime of π^+- and π^--mesons was taken to be $(2.54 \pm 0.11) \times 10^{-8}$ sec[6,7].

3. THE ENERGY SPECTRA OF THE PIONS

Figures 1 and 2 show the energy distributions of the π^+- and π^-–mesons in the laboratory system as obtained for beryllium and carbon. The errors indicated in the measured points allow for statistical errors of measurement and for all uncertainties in the evaluation of the corrections for negative pion disintegration in flight and for determining the contamination by μ–mesons and electrons. The spectra were normalized to the value of the area under the peak belonging to the π^+–mesons from the $pp \to d\pi^+$ reaction[8].

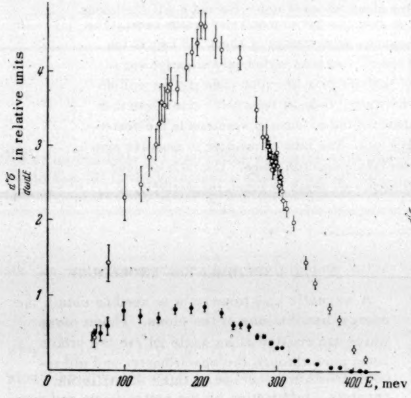

FIG. 1. Energy distributions of pions from Be at an angle of 24° in the laboratory system. O represents π^+-mesons and ●, π^- – mesons.

The basic properties of the measured spectra are the following:

a) At the upper part of the spectra the number of π^-–mesons becomes zero for lower energies than for the π^+–mesons;

b) For both elements the average energy of π^+-mesons is equal to about 215 mev, and the average energy of π^- – mesons is about 180 mev;

c) Both π^+ – meson spectra have a clearly defined maximum at an energy of about 210 mev, whereas the number of π^- – mesons in the spectra of both elements shows only slight variation over a range from 60 to 250 mev. One should not rule out the possibility that the negative pion spectra has a slight indentation in the region of 100-130 mev;

d) In the π^+ – meson spectra there is a certain distortion in the smooth variation in the number of mesons with energy in the interval from 140-200 mev, i.e., for those energies where the cross section of π^+ – meson-proton interaction attains its maximum value. This circumstance is cause for assuming that the reason for the distortion of the smooth variation in the spectrum in the indicated region is the interaction of the π^+ – meson with the nucleons in the original nuclei.

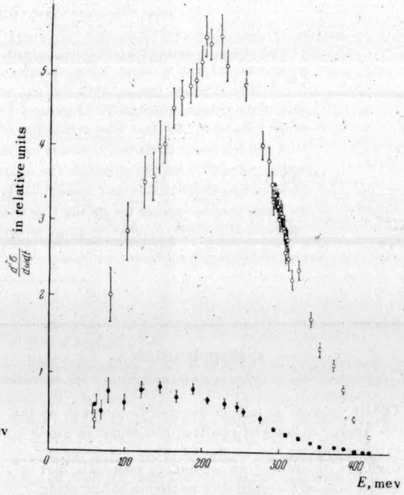

FIG. 2. Energy distributions of pions from C at an angle of 24° in the laboratory system. O represents π^+ – mesons and ●, π^- – mesons.

Special attention was given to measurements of the π^+– meson spectra in the 300 mev region, where a peak can be observed for π^+– mesons from the $pp \to d\pi^+$ reaction. If this peak should be discovered in the present experiments, this might mean that the protons within Be and C nuclei spend an appreciable time at the surface of the nuclei, i.e., outside the region of strong interaction with other nucleons. In this case the protons must exhibit a small dispersion in momentum. As may be seen from Figs. 1 and 2, the results obtained give no indication of the existence of observable deviations from the monotonic decrease in the number of π^+– mesons throughout the studied energy range other than deviations within the limits allowed for by experimental error.

4. COMPARISON OF PION YIELDS FROM FREE AND BOUND PROTONS

The values of positive and negative pion yields for an angle of 24° were determined by integrating the spectra over energy. Shown below are the yields per target nucleus and the total yield of positive pions from the $pp \to np\pi^+$ and $pp \to d\pi^+$ reactions measured under the same conditions and taken as unity.

Element	Y^+	Y^-
H	1.0	–
Be	1.4	0.26
C	1.7	0.24

Because of charge independence the total cross sections $\sigma(pn \to nn\pi^+)$ and $\sigma(np \to pp\pi^-)$ must be identical, and the π^+– meson yield at an angle θ in the first reaction must be equal in the center-of-mass system to the π^-– meson yield at the angle $(180° - \theta)$ for the second reaction. For an energy of about 660 mev we have $\sigma(pp \to d\pi^+) = (3.1 \pm 0.2) \times 10^{-27}$ cm^2 [8], $\sigma(pp \to np\pi^+) = (10.2 \pm 1.2) \times 10^{-27}$ cm^2 [1], $\sigma(pp \to pp\pi^0) = (3.4 \pm 0.4) \times 10^{-27}$ cm^2 [9] and $\sigma(pn \to pn\pi^0) = (7.8 \pm 1.6) \times 10^{-27}$ cm^2 [10]. From the relation

$$\tfrac{1}{2}[\sigma(pp \to d\pi^+) + \sigma(pp \to np\pi^+)]$$

$$= \sigma(pp \to pp\pi^0) + \sigma(pn \to pn\pi^0) - \sigma(pn \to nn\pi^+)$$

it follows that $\sigma(pn \to nnn^+) = \sigma(np \to pp\pi^-) = (4.6 \pm 1.8) \times 10^{-27}$ cm^2. This estimate is compatible with the Y^+/Y^- ratio obtained for the 24° angle. Bearing all this in mind, we cannot be too far wrong in assuming that in the studied energy region positive pion formation inside a nucleus occurs mostly in $(p - p)$-collisions. If the values for Y^+ obtained for Be and C refer to a single proton in a target nucleus, then it turns out that the probability of π^+-meson formation in $(p - p)$-collisions inside the nucleus is at least three times less than the probability of π^+– meson formation where the protons are free.

This large reduction in the probability of π^+– meson formation in collisions with bound protons is caused to a certain degree my meson absorption in the original nuclei, and also by the slowing-down and scattering of impinging protons in the nuclear matter. The effect of these processes is such that the nucleons situated on the surface of the nucleus participate principally in meson formation. The presence of nuclear bonds in the nuclear matter may also prove to be one of the additional reasons for the reduction in the probability of meson formation inside the nucleus, even at high energies.

5. ANALYSIS OF THE PION ENERGY SPECTRA

On the assumption that pion formation in compound nuclei occurs through the interaction of an impinging proton with one of the bound nucleons and that pion scattering in the original nuclei is insignificant, the spectra obtained were transformed to the center-of-mass system of the two nucleons. In this system the kinetic energy of the two nucleons is equal to 305 mev when one of them has an energy of 660 mev in the laboratory system. The values of $d^2\sigma^*/d\omega^* dE^*$ in the center-of-mass system were found by calculating the invariant expression $(1/p)d^2\sigma/d\omega dE$, where p is the momentum of the pion. Figures 3 and 4 show the spectra obtained in this way for positive and negative pions, with the angles at which the pions of a given energy were emitted*. It is apparent that the angular interval 48° to 42° corresponds to the energy interval 50-200 mev. For both elements the average total energy of a π^+– meson proved equal to 242 mev, which comes close to the value found under similar circumstances for free $(p - p)$-collisions[1]; the average total energy of π^-– mesons in both cases is equal to 225 mev. These figures indicate that in

---

* These values for the angles are approximate, since motion of the nucleons in the nucleus was disregarded in the calculations.

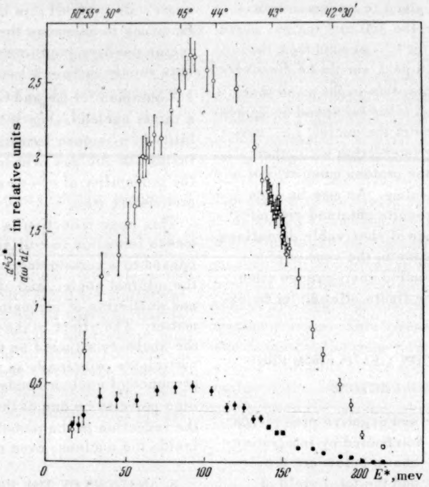

FIG. 3. Energy spectra in the center-of-mass system for Be. O represents π^+–mesons and ●, π^-–mesons.

a single act of pion formation an average of about 75% of the energy available in the center-of-mass system is expended.

Both π^+–meson spectra disclose a maximum near 100 mev. If the recoil energy of the nucleon and the rest energy of the meson are added to this most probable value of the π^+–meson energy, then the most probable value of the total energy released in the elementary act of positive pion formation will be equal to about 260 mev. The value obtained for the total energy is only slightly less than the resonance energy of the excited $P_{3/2,3/2}$ state.

It is of considerable interest to compare the π^+–meson spectra obtained in these experiments with spectra measured at far greater energies. According to Yuan and Lindenbaum[11] the maximum for the π^+–meson spectrum formed by the action of 2300 mev protons on beryllium and measured at an angle of 32° to the primary beam is close to 130 mev. It is also known that for the π^+– and π^-–meson spectrum from the $np \rightarrow np\pi^+\pi^-$ reaction at an energy of 1720 mev, the average energy is 112 mev and 120 mev, respectively[12].

The cited facts are evidence that with the increase in energy from 660 to 2300 mev, the maximum in the π^+–meson spectrum changes its position only slightly, remaining always close to the resonance energy of the $P_{3/2,3/2}$ state. On this basis it may be assumed that throughout the entire energy interval investigated the main effect is due to the same specific mechanism of pion formation. This mechanism may be taken to consist of a transition in the energy region of 600-1000 mev of one, or where the energy is greater, of both the colliding nucleons to an excited state, from which the nucleons, acting almost like free particles, return to their ground state by emitting pions. A similar supposition was used by Fowler, Shutt et al.[12] to explain the predominant formation of two pions in one elementary act and the angular correlations of particles in the reaction $np \rightarrow np\pi^+\pi^-$ at 1720 mev.

The question of the reasons for the striking difference in the forms of the spectra of positive and negative pions deserves to be treated separately. Let us assume that nucleonic collisions inside nuclei possess the same properties as collisions

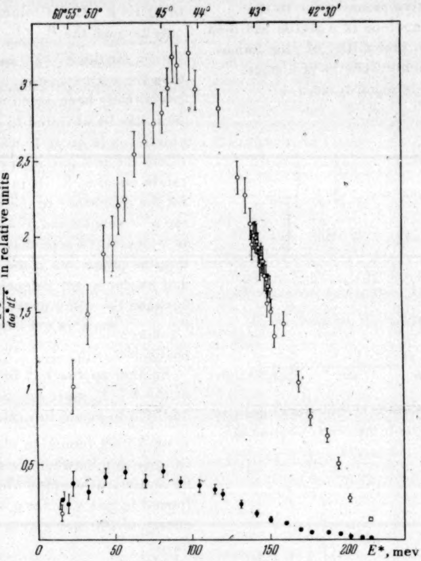

FIG. 4. Energy spectra in the center-of-mass system for C. O represents π^+–mesons and ●, π^-–mesons.

of free nucleons with regard to the nature of particle interaction in the final nucleonic system, conservation of the isotopic spin and the predominant emission of mesons in the *p*-state. Now the mentioned difference in the spectra of positive and negative pions may be qualitatively explained, if it is borne in mind that for the $pp \to np\pi^+$ and the $pn \to pp\pi^-$ reaction, there is a difference in the relative contribution of the transitions to the final *P* and *S* states of the two-nucleon system and and that the form of the pion spectrum is sensitive to nucleon interaction in the final state. It is for this reason that transitions to *P* states, where nucleons interact weakly, should lead to a softer spectrum than transitions to ${}^1S_0$ and ${}^3S_1$ states, which are characterized by strong nucleon interaction.

6. THE π^+/π^- RATIO

The dependence of the ratio of positive and negative pion yields on energy was determined from the measured values of $d^2\sigma^*/d\omega^* dE^*$. As can be seen from Figs. 5 and 6, for both elements at energy $E \simeq 15$ mev, $\pi^+/\pi^- \leq 1$. In the region from 160-180 mev the π^+/π^- ratio attains its maximum value of 14 ± 1.9 for Be and 17.7 ± 3.2 for C. For these same elements the ratio of integral yields of positive to negative pions is equal to 5.3 ± 0.6 and 7.0 ± 0.8, respectively. According to Sidorov[13], the ratio of integral yields of positive to negative pions for $p + C$ collisions at an energy of 660 mev is 5.0 ± 0.7 at a 90° angle in the laboratory system. The large increase in the yield of positive pions over that of negative pions is due to the fact that the impinging nucleon is a proton and also to the comparatively low probability of pion formation when the two-nucleon system is in a state where the isotopic spin is equal to zero.

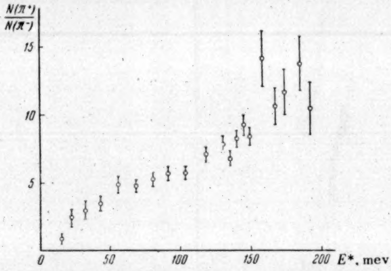

FIG. 5. The energy dependence of the ratio of positive to negative pion yields for Be in the center-of-mass system.

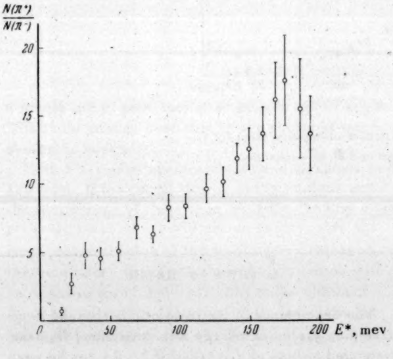

FIG. 6. The energy dependence of the ratio of positive to negative pion yields for C in the center-of-mass system.

A theoretical attempt has been made[14] to predict the magnitude of the Y^+/Y^- ratio on the assumption that the inelastic collision of the nucleons occurs through two independent stages: excitation of one or both of the nucleons and then decay by emission of a pion. For this case, when the energy is sufficient to excite only one nucleon, the Y^+/Y^- ratio should be equal to 9 for p + Be collisions and to 11 for p + C collisions, if pion formation occurs only through the $P_{3/2,3/2}$ state. These predicted values for the Y^+/Y^- ratio are noticeably greater than the corresponding experimental values. As has already been noted elsewhere[14], this discrepancy may be obviated to some extent if due consideration is given to meson formation in a state where the isotopic spin of the meson-nucleon system is equal to ½. It is also necessary to account for the difference in the angular distributions of the π^+–mesons and π^-–mesons. Furthermore, it is essential to note that the original assumption that the processes of the excitation of a nucleon and its decay are independent raises doubts simply because the width of the energy level of the $P_{3/2,3/2}$ state is not much less than the excitation energy[15].

Another approach[16] in evaluating the magnitude of the Y^+/Y^- ratio has been to assume that, in addition to meson formation through the $P_{3/2,3/2}$ state, direct formation also occurs, and that the relationship between these processes is determined by statistical weights alone. Calculations performed in this way for p + Be collisions at an energy of 100 mev give a value of 5 for the Y^+/Y^- ratio.

7. CONCLUSIONS

These experiments established the following facts regarding the formation of charged pions by the action of 660 mev protons on beryllium and carbon nuclei:

1. The probability of π^+–meson formation by a proton in a target nucleus is decreased by more than three in comparison with the probability of formation in free $(p-p)$-collisions.

2. The spectra of positive and negative pions differ in form and average pion energy. The relative softness and diffuseness of the π^-–meson spectra are cause to assume that there is a weak interaction among nucleons in part of the final state of the $pn \rightarrow pp\pi^-$ reaction.

3. On the average about 75% of the available energy is expended on charged pion formation in an elementary act during nucleon-nucleon interaction.

4. Perhaps the least expected fact of all was that in these experiments the maximum of the π^+–meson spectrum was discovered in the same energy region where it was observed by experiments with the Brookhaven proton accelerator at bombardment energies of 1720 and 2300 mev. This result lends

direct support to the conclusion that both single positive pion formation in nucleon-nucleon collisions at an energy of 660 mev and pair formation of pions at energies of 1720 and 2300 mev are essentially due to strong meson-nucleon interaction in the intermediate $P_{3/2,3/2}$ state.

5. The ratio of yields of positive and negative pions increases with energy up to 160-180 mev in the center-of-mass system. The ratio of integral yeilds of positive and negative pions is noticeably lower than the values predicted by theory based on the assumption that formation and decay in the intermediate $P_{3/2,3/2}$ state are independent.

---

[1] Meshcheriakov, Zrelov, Neganov, Vzorov and Shabudin, J. Exptl. Theoret. Phys. (U.S.S.R.) 31, 45 (1956).

[2] Chedester, Isaacs, Sachs and Steinberger, Phys. Rev. 82, 958 (1951).

[3] D. H. Stork, Phys. Rev. 93, 868 (1954).

[4] J. O. Kessler and L. M. Lederman, Phys. Rev. 94, 689 (1954).

[5] Ignatenko, Mukhin, Ozerov and Pontecorvo, Dokl. Akad. Nauk SSSR 103, 395 (1955).

[6] Jakobson, Schulz and Steinberger, Phys. Rev. 81, 894 (1951).

[7] Durbin, Loar and Havens, Phys. Rev. 88, 179 (1952).

[8] M. G. Meshcheriakov and B. S. Neganov, Dokl. Akad. Nauk SSSR 100, 677 (1955).

[9] A. A. Tiapkin and Iu. D. Prokoshkin, Record (Otchet), Institute for Nuclear Problems, Academy of Sciences, USSR (1955).

[10] Tiapkin, Kozodaev and Prokoshkin, Dokl. Akad. Nauk SSSR 100, 689 (1955).

[11] L. C. L. Yuan and S. J. Lindenbaum, Phys. Rev. 93, 1431 (1954).

[12] Fowler, Shutt, Thorndike and Whittemore, Phys. Rev. 95, 1026 (1954).

[13] V. M. Sidorov, J. Exptl. Theoret. Phys. (U.S.S.R.) 28, 727 (1955); Soviet Phys. JETP 1, 600 (1955).

[14] D. C. Peaslee, Phys. Rev. 94, 1085; 95, 1580 (1954).

[15] B. d'Espagnat and J. Prentki, Nuovo Cimento 1, 1223 (1955).

[16] A. I. Nikishov, J. Exptl. Theoret. Phys. (U.S.S.R.) 29, 246 (1955); Soviet Phys. JETP 2, 161 (1956).

Translated by A. Skumanich
9

SOVIET PHYSICS JETP VOLUME 4, NUMBER 1 FEBRUARY, 1957

Solution of the Fundamental Diffusion Equation for Cosmic Ray Particles Emitted by a Constant Energy Concentrated Pulsed Source

IU. A. POPOV
Moscow State University

(Submitted to JETP editor March 19, 1955)
J. Exptl. Theoret. Phys. (U.S.S.R.) 31, 80-85 (July, 1956)

The fundamental diffusion equation deduced by Terletskii[1] for cosmic ray protons emitted in magnetized interstellar space during a short period of time by a concentrated source of given energy is solved. It is shown that consideration of the particles which remain after collision of cosmic ray protons with protons of the interstellar gas leads to a power spectrum similar to that observed experimentally, if the source is assumed to be a supernova which appeared in the center of the galaxy over 10^8 years ago.

THE distribution function of cosmic ray protons in interstellar space $f(\mathbf{r}, E, t)$ can be found from the diffusion equation for cosmic ray particles.[2-4] In full form, with account taken of particles that remain after the collision of cosmic ray protons with the protons of an interstellar gas, this equation was found in Ref. 1 :

$$\frac{\partial f(E)}{\partial t} + \frac{f(E)}{T} - D\Delta_r f(E) + \frac{\partial}{\partial E}[\alpha E f(E)] - \frac{\partial^2}{\partial E^2}[\alpha E f(E)] - \frac{1}{T}\left[\frac{1}{a_1} f\left(\frac{E}{a_1}\right) + \frac{1}{a_2} f\left(\frac{E}{a_2}\right)\right] = Q, \qquad (1)$$

where Δ_r is the Laplace operator, α is a coefficient characterizing the mean increase of energy per unit time ($d\bar{E}/dt = \alpha\bar{E}$), T is the mean lifetime of a particle up to its collision with an atom of interstellar gas, Q is the density of sources of particles, D is the amount of energy of the first particle that insures meson formation in a collision with motionless particles, a_1 and a_2 are the amounts of energy possessed by the two particles after collision ($a_0 + a_1 + a_2 = 1$).

To find the particle spectrum, definite assumptions must be made on the particle sources. We assume that the primary cosmic ray protons arise in outbursts of nova and supernova[5-7], are first accelerated in the expanding envelopes of the stars, and then are ejected into the interstellar medium. Acceleration in the envelopes of the stars is controlled by the action of the statistical mechanism of Fermi.[8] In this case, there do not arise the usual difficulties, associated with the fact that this mechanism begins to operate only for energies which exceed the threshold energy determined by ionization losses to the surrounding medium. Actually, for envelopes expanding at $\alpha = 10^{-9}$/sec (see Ref. 9), the threshold energy for protons is negligibly small and does not exceed the initial kinetic energy associated with particles in the explosion of a star.

Further acceleration to the limiting energies occurs upon multiple collisions with the turbulent pulsations of the interstellar gas,[4] i. e., by the Fermi mechanism.

It is evident that acceleration in the envelope of the star is possible up to a certain limiting energy E which is determined by the condition that the radius of curvature r of the trajectory of the particle in a magnetic field H of the envelope corresponding to the energy E ought to be many times smaller than the radius of the envelope ρ. The diffusion path length of the particles, $L = [\sqrt{6Dt}\,]^{1/2}$, where t is the acceleration time, ought also not to exceed ρ, i.e., the condition

$$\rho \gg r = E/300H, \quad \rho \gg L = \sqrt{6Dt}. \tag{2}$$

ought to be satisfied.

On the other hand, the energy E and the time t are connected in approximate fashion:

$$E \approx e^{\alpha t}. \tag{3}$$

Because of (2) and (3), the particle can be found within the limits of the envelope only during a finite time t_0

According to Refs. 9, 10, taking

$$\rho \approx 10^{19}\ \text{cm}, \quad H \approx 10^{-4}\ \text{oe},$$

$$D \approx 10^{24}\ \text{cm}^2/\text{sec}, \quad \alpha \approx 10^{-9}\ \text{sec}^{-1},$$

we estimate [from (2) and (3)] the acceleration time of the particle in the envelope of the star up to the threshold energy to be $t_0 \sim 10^{10}$ sec or $\sim$ 300 years.

Thus, we can assume that, at time $t_0 \sim 300$ years after eruption of the star, particles are generated from the resulting envelope and are accelerated in the medium to the energy E_0 ($E_0 \approx 10^{10}$ ev). Particles with such an energy can accelerate in interstellar space. Therefore we can represent the sources which generate particles in interstellar space in the form

$$Q = Q_0\,\delta(t - t_0)\,\delta(\mathbf{r} - \mathbf{r}_0)\,\delta(E - E_0); \tag{4}$$

Q_0 = strength of source.

The further process of acceleration of the particle in interstellar space is described by Eq. (1) with Q from (4). For the solution of this equation we multiply both sides by E and carry out the following change of variables:

$$E = e^x, \quad u = Ef(E)$$

After substitution Eq. (1) is simplified:

$$\begin{aligned} \frac{\partial u}{\partial t} - D\Delta_r u - \alpha\frac{\partial^2 u}{\partial x^2} + \frac{1}{T}[u(x) & \\ - u(x + \Delta_1) - u(x + \Delta_2)] & \\ = Q_0\delta(\mathbf{r} - \mathbf{r}_0)\,\delta(x - x_0)\,\delta(t - t_0); & \\ \Delta_1 = \ln(1/a_1), \quad \Delta_2 = \ln(1/a_2). & \end{aligned} \tag{5}$$

We look for a solution in the form of a Fourier integral

$$u(\mathbf{r}, x, t) = \frac{1}{2\pi}\int_{-\infty}^{\infty} e^{i\mu x} F(\mu, \mathbf{r}, t)\,d\mu \tag{6}$$

and obtain for F the equation

$$\begin{aligned} \frac{\partial F}{\partial t} - D\Delta_r F + \alpha\mu^2 F + \frac{F}{T}(1 - e^{i\mu\Delta_1} - e^{i\mu\Delta_2}) & \\ = Q_0 e^{-i\mu x_0}\,\delta(\mathbf{r} - \mathbf{r}_0)\,\delta(t - t_0). & \end{aligned} \tag{7}$$

We set

$$F(\mathbf{r}, \mu, t) = \Phi_0(\mu, t)\, X(\mathbf{r}, \mu, t), \tag{8}$$

$$\Phi_0(\mu, t) = \exp\left\{-t\left[\alpha\mu^2 + \frac{1}{T}\left(1 - e^{i\mu\Delta_1} - e^{i\mu\Delta_2}\right)\right]\right\}.$$

Substituting (8) in (7), we get for X the inhomogeneous diffusion equation, the solution of which has the form

$$X = \frac{Q_0 e^{-i\mu x_0}}{8\pi^{3/2}\Phi_0(t_0)} \tag{9}$$

$$\times \exp\left\{-\frac{(\mathbf{r}-\mathbf{r}_0)^2}{4D(t-t_0)}\right\}\frac{1}{[D(t-t_0)]^{3/2}}.$$

Thus, the solution of Eq. (5) has the form

$$u(\mu, \mathbf{r}, t) = \frac{\dot{Q}_0}{16\pi^{3/2}}\frac{\exp\{(\mathbf{r}-\mathbf{r}_0)^2/4D(t-t_0)\}}{[D(t-t_0)]^{3/2}} \tag{10}$$

$$\times \exp\left\{-\frac{t-t_0}{T}\right\} I,$$

where

$$I = \int_{-\infty}^{\infty} \exp\left\{i\mu(x-x_0)\right. \tag{11}$$

$$\left.-\alpha\mu^2(t-t_0) + \frac{t-t_0}{T}\left[e^{i\mu\Delta_1} + e^{i\mu\Delta_2}\right]\right\} d\mu.$$

Now everything is reduced to the calculation of the integral (11). Introducing the notation

$$x - x_0 = \ln\frac{E}{E_0} = \varkappa,$$

$$\frac{t-t_0}{T} = \beta', \quad \alpha' = \alpha(t-t_0),$$

$$f(\mu) = i\mu - \frac{\alpha'}{\varkappa}\mu^2 + \frac{\beta'}{\varkappa}\left(e^{i\mu\Delta_1} + e^{i\mu\Delta_2}\right),$$

we write the integral in the form

$$I = \int_{-\infty}^{\infty} e^{\varkappa f(\mu)}\, d\mu$$

and compute its value by the method of steepest descents, assuming that $\varkappa$ is a large parameter.

For the computation we must find the line of steepest descent

$$\operatorname{Im} f(\mu) = s - \frac{2\alpha'}{\varkappa}s\sigma + \frac{\beta'}{\varkappa}e^{-\Delta_1\sigma}\sin(\Delta_1 s) \tag{12}$$

$$+ \frac{\beta'}{\varkappa}e^{-\Delta_2\sigma}\sin(\Delta_2 s) = \text{const}$$

and the saddle point, which is determined from the equation

$$\left.\frac{\partial f}{\partial\mu}\right|_{\mu=\mu_0} = i\left[1 + 2\frac{\alpha'}{\varkappa}z + \frac{\Delta_1\beta'}{\varkappa}e^{\Delta_1 z} + \frac{\Delta_2\beta'}{\varkappa}e^{\Delta_2 z}\right] = 0, \tag{13}$$

where $z = i\mu_0$. It is then easy to show that saddle point $\mu_0 = -iz = i\sigma_0$ lies on the imaginary axis in the upper half plane:

$$s - \frac{2\alpha'}{\varkappa}s\sigma + \frac{\beta'}{\varkappa}e^{-\Delta_1\sigma}\sin(\Delta_1 s) \tag{14}$$

$$+ \frac{\beta'}{\varkappa}e^{-\Delta_2\sigma}\sin(\Delta_2 s) = 0,$$

where $\mu = s + i\sigma$. We now specify the contour determined by this equation. We show that σ is an even function of s. Denoting the left side of Eq. (14) by $F(s, \sigma(s))$, we have

$$F(s, \sigma(-s)) = F(-s', \sigma(s'))$$

$$= F(-s, \sigma(s)) = 0.$$

It then follows that $\sigma(s) = \sigma(-s)$ and the line of steepest descent is symmetrical relative to the imaginary axis.

We write Eq. (14) in the form

$$\frac{\varkappa}{\beta'}\left(1 - \frac{2\alpha'}{\varkappa}\sigma\right)e^{\Delta_2\sigma} \tag{15}$$

$$+ e^{(\Delta_2-\Delta_1)\sigma}\frac{\sin(\Delta_1 s)}{s} + \frac{\sin(\Delta_2 s)}{s} = 0$$

and construct a nomogram for the graphical investigation of this equation.

We erect vertical axes Y_1 and Y_2 on the plane, perpendicular to the X axis and a certain curve Y, the coordinates of a point of which we shall denote as (x_3, y_3). We connect the points with the coordinates y_1 and y_2 on the axes Y_1 and Y_2 by a straight line and find the point of intersection of this line with the curve Y (Fig. 1).

We then have the relation

$$-y_1 + \frac{y_3}{x_3} + y_2\left(1 - \frac{1}{x_3}\right) = 0. \tag{16}$$

Equation (16) coincides with Eq. (15) if

$$y_2 = \sin(\Delta_1 s)/s,$$

$$-y_1 = \sin(\Delta_2 s)/s, \quad 1/x_3 = 1 - e^{(\Delta_2-\Delta_1)\sigma},$$

$$\frac{y_3}{x_3} = \frac{\varkappa}{\beta'}\left(1 - \frac{2\alpha'}{\varkappa}\sigma\right)e^{\Delta_2\sigma}.$$

With increase in s, the points y_1 and y_2 undergo damped oscillations about the points $y_1 = y_2 = 0$. The point x_3, y_3 has a damped oscillation about the point y_3 σ_0) = 0, which corresponds to $\sigma_0 = \varkappa / 2\alpha'$. Therefore the contour of integration has the form shown in Fig. 2.

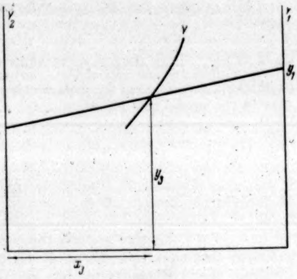

FIG. 1

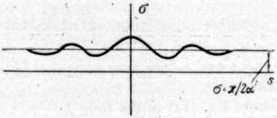

FIG. 2

The rest of the problem reduces to the integration over the contour C. Since $\operatorname{Im} f(\mu) = 0$ on C, then

$$I = \int_C \exp\{\varkappa \operatorname{Re} f(\mu)\}\, d\mu \tag{17}$$

$$= \int_C \exp\Big\{\varkappa\Big[-\sigma - \frac{\alpha'}{\varkappa} s^2 + \frac{\alpha'}{\varkappa}\sigma^2$$

$$+ \frac{\beta'}{\varkappa}\cos(\Delta_1 s)\, e^{-\Delta_1\sigma} + \frac{\beta'}{\varkappa}\cos(\Delta_2 s)\, e^{-\Delta_2\sigma}\Big]\Big\} d(s + i\sigma).$$

The integral over $d\sigma$ vanishes.

The principal contribution to the integral comes from the cutting off of the contour of integration which runs to the saddle point.

We have

$$I = \exp\{-\varkappa\sigma_0 + \alpha'\sigma_0^2\} \int_{-\varepsilon}^{\varepsilon} \exp\{-\alpha' s^2$$

$$+ \beta' \cos(\Delta_1 s)\, e^{-\Delta_1\sigma_0} + \beta' \cos(\Delta_2 s)\, e^{-\Delta_2\sigma_0}\}\, ds.$$

Setting $\epsilon = (\alpha')^{-2/5}$, expanding the integrand in a series in s and limiting ourselves to the first 3 terms of the expansion, we get

$$I = \exp\Big\{-\varkappa\sigma_0 + \alpha'\sigma_0^2 + \frac{\beta'}{e^{\Delta_1\sigma_0}} + \frac{\beta'}{e^{\Delta_2\sigma_0}}\Big\}$$

$$\times \sqrt{\pi\Big/\Big(\alpha' + \frac{\Delta_1^2\beta'}{2e^{\Delta_1\sigma_0}} + \frac{\Delta_2^2\beta'}{2e^{\Delta_2\sigma_0}}\Big)}\,[1 + O(\alpha'^{-1/5})].$$

Thus, the desired fundamental solution of Eq. (1) is

$$f(\mathbf{r}, x, t) = \frac{Q_0}{16\pi^2 D^{3/2} (t - t_0)^2} \tag{18}$$

$$\times \exp\Big\{-\sigma_0(x - x_0) - x - \frac{(\mathbf{r} - \mathbf{r}_0)^2}{4D(t - t_0)}$$

$$+ \frac{t - t_0}{T}(-1 + e^{-\Delta_1\sigma_0} + e^{-\Delta_2\sigma_0} + \alpha\sigma_0^2 T)\Big\}$$

$$\times \Big[\alpha + \frac{\Delta_1^2}{2T} e^{-\Delta_1\sigma_0} + \frac{\Delta_2^2}{2T} e^{-\Delta_2\sigma_0}\Big]^{-1/2}$$

Hence it follows that

$$f(\mathbf{r}, E, t) = E^{-\gamma}\varphi(\mathbf{r}, t), \tag{19}$$

where $\gamma \approx 1 + \sigma_0$ and $\varphi(\mathbf{r}, t)$ does not depend on E. Consequently, the exponent γ of the power spectrum of the primary component of the cosmic rays is determined by the quantity $\sigma_0 = -z$ which is a root of the transcendental Eq. (13).

The exponent γ satisfies the equation

$$1 - \frac{2\alpha'}{\varkappa}(\gamma - 1)$$

$$+ \frac{\Delta_1\beta'}{\varkappa} e^{-\Delta_1(\gamma-1)} + \frac{\Delta_2\beta'}{\varkappa} e^{-\Delta_2(\gamma-1)} = 0.$$

Recalling the definitions of α', β, $\varkappa$, and assuming that for our galaxy the factor $\alpha T = 0.6$ (see Refs. 7,8), we obtain

$$\frac{0,6}{\alpha(t - t_0)} \ln\frac{E}{E_0} \tag{20}$$

$$= 1.2(\gamma - 1) - \Delta_1 e^{-\Delta_1(\gamma-1)} - \Delta_2 e^{-\Delta_2(\gamma-1)}.$$

In the collision of two protons of high energy, one of the colliding protons carries away the principal amount of energy, and the energy of the second is less than 1/5 the initial energy of the colliding particles.* The estimates

---

*Private communication of N. L. Grigorov; see also Ref. 11.

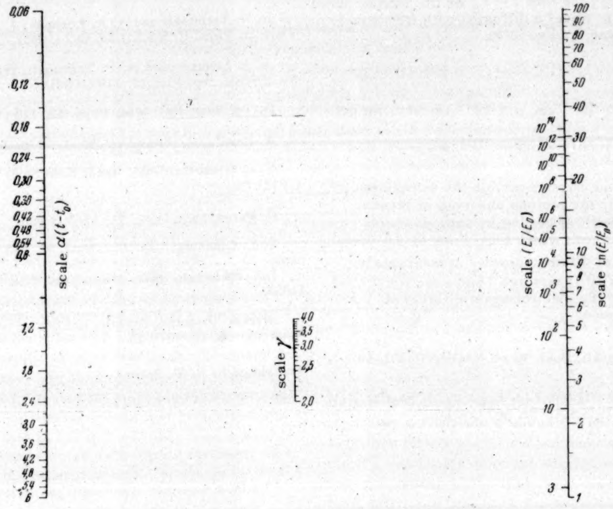

FIG. 3

$$a_1 = 0.1; \quad a_2 = 0.6; \quad \Delta_1 = 2.3 \text{ and } \Delta_2 = 0.5.$$

then follow.

A nomogram is shown in Fig. 3 for the solution of Eq. (20). It is evident from the nomogram that for $0.4 \leqq \alpha' \leqq 6$ and $3 \leqq E / E_0 \leqq 10^{10}$, the exponent is confined to the range $2 \leqq \gamma \leqq 3$.

In particular, in accord with the experimental data, for an initial energy of $E_0 = 5 \times 10^8$ ev, which is approximately equal to the energy of the protons, we obtain for the energy $E \sim 10^9 - 10^{10}$ ev in the case of $\alpha' = 0.6$, $\gamma = 2.2$.

It follows from the nomogram that α' must be greater than 0.6 in order to determine the spectrum in the range of very high energies.

For example,

$$\text{for } E \sim 5 \cdot 10^{11}\,\text{eV} \;\; \gamma = 2.5 \;\; \text{for } \alpha' = 2.75; \tag{21}$$

$$\text{for } E \sim 10^{15}\,\text{eV} \;\; \gamma = 3 \;\; \text{for } \alpha' = 4.$$

This means that the high energy primary particles are long-lived particles $[\,(t - t_0) > T\,]$ which experience a large number of collisions with the turbulent pulsations of the interstellar material and are accelerated to high energies, or are particles with areal increase in energy per unit time above the average increase, corresponding to $\alpha\ T = 0.6$.

It then follows that the source of particles which reach the earth with comparatively low energies ($E \sim 10^{10}$ ev) and consequently, which are accelerated in interstellar space for a comparatively short time must be Nova and Supernova which erupted about T years ago. The source of particles that are accelerated to the highest energies ($E \sim 10^{15} - 10^{16}$ ev), and which consequently remain in the interstellar fields a far longer time, must be stars that erupted $(1 - 10)\,T$ years ago.

Thus the spectrum is formed by particles which arise at different times as the result of the explosion of many stars, in which the protons of each of the explosions contribute to the power spectrum of the energy. Therefore it is quite apparent that the fundamental solution ought to be integrated over the variables $\mathbf{r}_0, t_0$ and E_0 of the separate explosions.

From the estimates (21) of the time $(t - t_0)$ it follows that the sources of the primary cosmic ray particles are located in the center of the galaxy at a distance of $r \sim 10^{23}$ cm from the earth.

Actually, taking the time $t - t_0$ as the time required for particles to travel a diffusion path from source to earth, we get, by Eq. (21):

$$(t - t_0) \sim (1 \div 10)\, T \sim (1 \div 10) \cdot 10^{16} \text{ sec}$$

and setting $l \sim 10^{19}$ cm, $v \sim 10^{10}$ cm/sec, we get

$$r \sim \sqrt{lv\,(t - t_0)} \sim 10^{23} \text{ cm.}$$

This analysis makes possible the assumption that the cosmic ray protons observed at present arose as the result of very many explosions of Nova and Supernova which took place at the center of the galaxy at different times (approximately $4 \times 10^8 - 3 \times 10^9$ years ago) and were then accelerated by the electromagnetic fields of interstellar space.

---

[1] Ia. P. Terletskii, Dokl. Akad. Nauk SSSR **101**, 59 (1955).

[2] Ia. P. Terletskii and A. A. Logunov, J. Exptl. Theoret. Phys. (U.S.S.R.) **21**, 567 (1951).

[3] Ia. P. Terletskii and A. A. Logunov, J. Exptl. Theoret. Phys. (U.S.S.R.) **23**, 682 (1952).

[4] A. A. Logunov and Ia. P. Terletskii, Izv. Akad. Nauk SSSR, Ser. Fiz. **17**, 119 (1953).

[5] D. Ter Haar, Rev. Mod. Phys. **22**, 119 (1950).

[6] A. Unsold, Z. Astrophys. **29**, 176 (1949).

[7] V. L. Ginzburg, Dokl. Akad. Nauk SSSR **92**, 1133 (1953).

[8] E. Fermi, Phys. Rev. **75**, 1169 (1949).

[9] V. L. Ginzburg, Usp. Fiz. Nauk **51**, 343 (1953).

[10] I. S. Shklovskii, Dokl. Akad. Nauk SSSR **41**, 475 (1953).

[11] Brikker, Grigorov, Rybkina and Savin, Dokl. Akad. Nauk SSR **86**, 1089 (1952).

Translated by R. T. Beyer
11

SOVIET PHYSICS JETP VOLUME 4, NUMBER 1 FEBRUARY, 1957

The Application of Non-Self-Adjoint Operators to Scattering Theory

M. S. LIVSHITS
Odessa Hydro-Meteorological Institute

(Submitted to JETP editor April 25, 1955)
J. Exptl. Theoret. Phys. (U.S.S.R.) 31, 121-131 (January, 1956)

It is proved that for any given scattering matrix there exists a non-self-adjoint operator defining the energy of the compound nucleus in a simple triangular representation. The relation between the decay of the compound nucleus and its spectrum is investigated.

IN recent years a large number of purely mathematical investigations have appeared[1-8], dealing with the spectral theory of a wide class of non-self-adjoint operators. In the general theory of scattering there appears the idea of a compound or intermediate nucleus, which is formed during the course of various nuclear reactions. The main property of the compound nucleus is to possess complex energy levels or quasi-stationary states, and in mathematical language this means that the energy operator is not self-adjoint. The spectral decomposition of a non-self-adjoint operator, discovered by the present author[5], proceeds by means of the so-called characteristic matrix-function which defines the operator to within a unitary equivalence-class. The present paper establishes the existence of a close connection between the scattering matrix[9-16] of a compound nucleus and the characteristic matrix-function of its energy-operator. This makes it possible to construct the energy operator of a compound nucleus when the scattering matrix is given. In addition, some new properties of the scattering matrix are discovered. The energy operator is put into a triangular representation in which the equation of motion and the decay of the compound nucleus can be studied and related to the character of its spectrum (discrete or continuous, etc.).

Previous knowledge of the mathematical papers quoted above is not required for understanding the present work.

1. THE ENERGY OPERATOR OF A COMPOUND NUCLEUS

To explain the essence of our method we consider the simple case of a purely elastic scattering reaction described by $a + X \to C \to X + a$. Here a is the incident particle, x the target nucleus and C the compound nucleus. There is only one channel[16], and there are no external fields.

The wave function $u(r)$ $(0 < r < \infty)$ of this system can be represented as a vector with two components $\varphi(r)$ and $\psi(r)$ defined by

$$\varphi(r) = \begin{cases} a_0 (e^{-iKr} - S(W) e^{iKr}) & r > R, \\ 0 & r < R, \end{cases} \tag{1}$$

$$\psi(r) = \begin{cases} 0 & r > R, \\ \sum_{j=0}^{n} c_j \psi_j(r) & r < R \quad (n \leqslant \infty). \end{cases} \tag{2}$$

Here K is the wave number, and $W = h^2K^2/2\mu$. The $\psi_j(r)$ are a complete orthonormal set of wave-functions for the compound nucleus in the interval $(0, R)$, the C_j are constant coefficients, and R is the channel radius[16]. The Hamiltonian* may accordingly be written as a 2×2 matrix

$$\begin{Vmatrix} T & \Gamma \\ \Gamma^* & A \end{Vmatrix}$$

where $T = -(h^2/2\mu)(d^2/dr^2)$ is the Hamiltonian in the center-of-mass system in the absence of interactions. A is an operator acting on the wave-functions $\psi(r)$ $(r < R)$ inside the compound nucleus, and the operators Γ and Γ^* describe the probabilities for decay and formation of the compound nucleus.

The function $\varphi(r)$ may also be written

$$\varphi(r) = \text{const}\,(e^{-iK(r-R)} - S_0(W) e^{iK(r-R)}) \quad (r > R), \tag{3}$$

where $S_0(W) = e^{2iKR} S(W)$ describes the resonance scattering associated with the formation of the compound nucleus. We call the function $S_0(W)$ the reduced (one-dimensional) scattering matrix. Introducing the functions

---

* Here we used the method of Bethe[15] with some minor alterations.

$$\varphi_1(r) = \sin K(r - R),$$

$$\varphi_2(r) = \cos K(r - R) \quad (r > R),$$

[$\varphi_1(r) = \varphi_2(r) = 0$ for $r < R$], we may represent $\varphi(r)$ in the form

$$\varphi(r) = a\varphi_1(r) + b[\varphi_2(r) + i\varphi_1(r)]. \tag{4}$$

The function $\varphi(r)$ has a discontinuity at R of magnitude $b = \varphi(R+0) - \varphi(R-0)$.

Consider the wave-equation

$$\left\| \begin{matrix} T & \Gamma \\ \Gamma^* & A \end{matrix} \right\| \begin{pmatrix} \varphi(r) \\ \psi(r) \end{pmatrix} = W \begin{pmatrix} \varphi(r) \\ \psi(r) \end{pmatrix},$$

which separates into the two equations

$$T\varphi + \Gamma\psi = W\varphi, \tag{5}$$

$$\Gamma^*\varphi + A\psi = W\psi. \tag{6}$$

Equations (4) and (5) imply*

$$\begin{aligned}(\Gamma\psi, \varphi_1) &= \int_0^\infty \varphi_1(r)\left(W + \frac{h^2}{2\mu}\frac{d^2}{dr^2}\right)\varphi(r)\,dr \\ &= \int_{R-\varepsilon}^{R+\varepsilon} \frac{h^2}{2\mu} b\delta'(r-R)\varphi_1(r)\,dr \\ &= (h^2/2\mu)\varphi_1'(R) = -(h^2/2\mu)bK.\end{aligned} \tag{7}$$

Next, Eqs. (2) and (7) give

$$b = -\frac{2\mu}{h^2K}\sum_{j=1}^{n} c_j\gamma_j \quad (\gamma_j = (\Gamma\psi_j, \varphi_1)). \tag{8}$$

In the same way we can prove that $(\Gamma\psi_j, \varphi_2) = 0$. Hence we deduce from Eqs. (6) and (4)

$$a\Gamma^*\varphi_1 + b\Gamma^*\varphi_2 + ib\Gamma^*\varphi_1 + A\psi = W\psi. \tag{9}$$

Multiplying Eqs. (2) and (9) by $\psi_k(r)$ and integrating, we find

$$\begin{aligned}a(\Gamma^*\varphi_1, \psi_k) &+ b(\Gamma^*\varphi_2, \psi_k) \\ &+ ib(\Gamma^*\varphi_1, \psi_k) + (A\psi, \psi_k) = Wc_k.\end{aligned} \tag{10}$$

Since

$$(\Gamma^*\varphi_1, \psi_k) = (\varphi_1, \Gamma\psi_k) = \gamma_k^* \quad (k = 1, 2, \ldots, n),$$

$$(\Gamma^*\varphi_2, \psi_k) = (\varphi_2, \Gamma\psi_k) = 0,$$

equations (8) and (10) lead to

$$a\gamma_k^* - i\frac{2\mu}{h^2K}\sum_{j=1}^{n} c_j\gamma_i\gamma_k^* + \sum_{j=1}^{n} A_{jk}c_j = Wc_k, \tag{11}$$

with $A_{jk} = (A\psi_j, \psi_k)$.

Let f be the vector with components $c_1, c_2, \ldots, c_n$, and let the operators A, B, H, H^* be defined by

$$[Af]_k = \sum_{j=1}^{n} A_{jk}c_j; \tag{12}$$

$$[Bf]_k = \sum_{j=1}^{n} c_j\beta_j^*\beta_k \quad (\beta_j = \sqrt{2\mu/h^2K}\,\gamma_j^*),$$

$$H = A + iB, \quad H^* = A - iB,$$

where $[Af]_k$, $[Bf]_k$ $(k = 1, 2, \ldots, n)$ are the components of the vectors Af, Bf. Equation (11) can then be written in the form

$$H^*f - Wf = g_0, \tag{13}$$

$$g_0 = -a\sqrt{h^2K/2\mu}\,\{\beta_k\}_{k=1}^{n}.$$

If $a = 0$, there is no incident wave, and the equation $H^*f = Wf$ defines the complex-levels and quasi-stationary states of the decaying compound nucleus. The equation of motion of the compound nucleus is

$$ihdf/dt = H^*f. \tag{14}$$

2. THE SCATTERING MATRIX

We now calculate the scattering matrix. If e is the vector $e = \{\sqrt{2}\beta_k\}_{k=1}^{n}$, Eq. (12) gives*

$$-i(H - H^*)f = 2\sum_{j=1}^{n} c_i\beta_j^*\beta_k = (f, e)e. \tag{15}$$

Equations (4) and (8) imply

$$\varphi(r) = \frac{a}{2i}(e^{iK(r-R)} - e)^{-iK(r-R)} - \sqrt{\frac{2\mu}{h^2K}}\frac{(f, e)}{\sqrt{2}}e^{iK(r-R)}, \tag{16}$$

---

* The symbol

$$(u, v) = \int_0^\infty v^*(r)\,u(r)\,dr$$

represents a scalar product. The function $b\delta'(r-R)$ arises from double differentiation of the simple discontinuity.

* Here $(f, e) = \Sigma_{j=1}^{n} e_j^* c_j = \sqrt{2}\,\Sigma_{j=1}^{n} c_j\beta_j^*$ is the scalar product.

while Eq. (13) gives

$$f = (H^* - WI)^{-1} g_0 \tag{17}$$

$$= -\frac{a}{\sqrt{2}} \sqrt{\frac{\hbar^2 K}{2\mu}}\, (H^* - WI)^{-1} e.$$

Thus the function $\varphi(r)$ becomes

$$\varphi(r) = \frac{a}{2i}\left(e^{iK(r-R)} - e^{-iK(r-R)}\right) \tag{18}$$

$$+ \frac{a}{2}\left((H^* - WI)^{-1} e, e\right) e^{iK(r-R)}$$

$$= -\frac{a}{2i}\{e^{-iK(r-R)}$$

$$- [1 + i\left((H^* - WI)^{-1} e, e\right)]\, e^{iK(r-R)}\}.$$

Comparing this with Eq. (3), we obtain the following expression for the one-dimensional scattering matrix

$$S_0(W) = 1 + i\left((H^* - WI)^{-1} e, e\right), \tag{19}$$

$$S(W) = e^{-2iKR} S_0(W). \tag{20}$$

The cross section for resonance scattering[16] is

$$\sigma_{\text{res}} = \pi\lambda^2 |1 - S_0(W)|^2 \tag{21}$$

$$= \pi\lambda^2 |\left((H^* - WI)^{-1} e, e\right)|^2.$$

It is clear from Eq. (15) than an arbitrary vector f is either annihilated by the operator $-i(H - H^*)$ or is transformed into a vector parallel** to e. In addition, we have the inequality

$$(-i(H - H^*) f, f) = |(f, e)|^2 \geqslant 0. \tag{22}$$

The function $S_0(W)$, related to the operator H by Eq. (19), is called the characteristic function of H. It was studied in a number of papers[1,2,5,7] on the theory of non-self-adjoint operators. We quote without proof some of the main results of the theory.

1. The function $S_0(W)$ determines H to within a unitary equivalence-class. Thus the scattering matrix completely determines* (in the quantum mechanical sense) the motion of the intermediate nucleus C. Later we shall show how, given $S_0(W)$, H or H^* can be constructed in their simplest representation, which is one in which they become triangular matrices.
2. $S_0(W)$ is an analytic function of W.
3. The identity

$$1 - |S_0(W)|^2 \tag{23}$$

$$= \frac{W - W^*}{i}(R_W e, R_W e) \quad (\operatorname{Im} W \neq 0),$$

holds, implying that

$$1 - |S_0(W)|^2 > 0, \quad (\operatorname{Im} W > 0). \tag{24}$$

Here R_W denotes the operator $(H^* - WI)^{-1}$.

4. The eigenvalues $W_k = E_k + \tfrac{1}{2} i\,\Gamma_k$ $(k = 1, 2, \ldots)$ of H lie in the upper half-plane and are roots of the equation $S_0(W) = 0$.
5. The continuous spectrum of H (if it exists) lies on the real W-axis. A real value of W belongs to the continuous spectrum if $1 - |S_0(W + i0)|^2 > 0$. Intervals in which $1 - |S_0(W + i0)|^2 = 0$ contain no continuous spectrum. If $1 - |S_0(W + i0)|^2 > 0$ with $W > 0$, then there exist alternative reaction channels which have not been considered. Equation (14) implies

$$\frac{d|f|^2}{dt} = \frac{d(f, f)}{dt} = \left(\frac{df}{dt}, f\right) + \left(f, \frac{df}{dt}\right)$$

$$= -\frac{i}{h}(H^* f, f) + \frac{i}{h}(f, H^* f)$$

$$= -\frac{1}{h}\left(\frac{1}{i}(H - H^*) f, f\right).$$

From Eq. (22) we have

$$d|f|^2/dt = -h^{-1}|(f, e)|^2 \leqslant 0, \tag{25}$$

and therefore the total decay probability (for one particle and per unit time) is

---

** The departure of the operator H from Hermiticity (the rank of non-Hermiticity) is characterized in this case by a single vector e, because there exists only one reaction channel. In Ref. 5, operators with arbitrary rank of non-Hermiticity are considered. The rank of non-Hermitcity is equal to the number of channels.

* This result is important in connection with the S-matrix theory of Heisenberg (see Ref. 17). In Ref. 5, the results (1-5) are proved under the assumption that e is independent of W.

$$P = h^{-1}(e, e) = \frac{2}{h} \sum_{j=1}^{n} |\beta_j|^2. \tag{26}$$

This quantity can be calculated directly from $S_0(W)$. In fact, Eq. (19) implies*

$$\begin{aligned} S_0(W) &= 1 + iW((H^* W^{-1} - I)^{-1} e, e) \\ &\doteq 1 - iW^{-1}[(e, e) + W^{-1}(H^* e, e) + \ldots], \end{aligned}$$

from which it follows that

$$P = \frac{1}{h} \lim_{W \to \infty} W\,|1 - S_0(W)| \tag{27}$$

$$= \frac{1}{hi} \operatorname*{residue}_{W \to \infty} S_0(W).$$

Next we derive a formula for the population q of compound nuclei existing per unit volume during a sustained scattering process. Comparing the well-known expansion[18] of a plane wave e^{iKz} into spherical harmonics with Eq. (4), we obtain

$$|a| = 1/K. \tag{28}$$

The state of the compound nucleus is defined by the vector $f = R_W g_0$ according to Eq. (13). Hence, q becomes

$$q = |f|^2 = (h^2/2\mu K)(R_W e, R_W e),$$

which by Eq. (23) may be written

$$q = (h^2/2\mu K) \lim_{y \to \infty} (1 - |S_0(W + iy)|^2/2y).$$

Hence the formula for q

$$q = -\frac{W}{K^3}\left[\frac{\partial}{\partial y}|S_0(W + iy)|\right]_{y=0}. \tag{29}$$

3. A FINITE NUMBER OF COMPLEX LEVELS. TRIANGULAR MODEL.

We shall find the energy-operator H^* of the compound nucleus, in the case when this operator possesses a finite number of eigenvalues $W_k^* = E_k - \frac{1}{2} i \Gamma_k$ ($k = 1, 2, \ldots$). According to the results 4 and 5 above, the reduced scattering matrix $S_0(W)$ is of the form

$$S_0(W) = \prod_{k=1}^{n} \frac{W - W_k}{W - W_k^*} \tag{30}$$

$$= \prod_{k=1}^{n} \frac{W - E_k - (i/2)\Gamma_k}{W - E_k + (i/2)\Gamma_k}.$$

By choosing a particular orthonormal basis $\psi_k(r)$ ($k = 1, 2, \ldots, n$) for the wave-functions of the compound nucleus, we can reduce the operator H^* to triangular form. Thus

$$d_k = \sum_{j=1}^{n} (H^*)_{kj} c_j \quad ((H^*)_{kj} = 0,\ j > k). \tag{31}$$

The elements $(H^*)_{kk}$ on the principal diagonal* coincide with the eigenvalues $(H^*)_{kk} = W_k^*$. We now derive the remaining elements $(H^*)_{kj}$ $(j < k)$. We observe that the operator $g = -i(H - H^*)f$ is defined by the equations

$$\begin{aligned} d_1 &= \Gamma_1 c_1 + \frac{1}{i} H_{12} c_2 + \ldots + \frac{1}{i} H_{1n} c_n, \\ d_2 &= -\frac{1}{i} H_{12}^* c_1 + \Gamma_2 c_2 + \ldots + \frac{1}{i} H_{2n} c_n, \\ &\cdots\cdots\cdots\cdots\cdots\cdots \\ d_n &= -\frac{1}{i} H_{1n}^* c_1 - \frac{1}{i} H_{2n}^* c_2 - \ldots + \Gamma_n c_n. \end{aligned} \tag{32}$$

Comparing Eqs. (32) with (15), we obtain

$$2|\beta_k|^2 = \Gamma_k, \quad H_{jk} = 2i\beta_j\beta_k^* \quad (j < k).$$

Hence

$$H_{jk} = i\sqrt{\Gamma_j \Gamma_k} \exp\{i(\varphi_j - \varphi_k)\} \quad (\varphi_j = \arg \beta_j).$$

Replacing the functions $\psi_k(r)$ by $\psi_k(r)\exp\{i\varphi_k\}$, we have

$$(H^*)_{kj} = H_{jk}^* = -i\sqrt{\Gamma_j \Gamma_k}.$$

Thus the operator $g = H^* f$ takes the form

$$d_k = \left(E_k - \frac{i}{2}\Gamma_k\right) c_k \tag{33}$$

$$- i \sum_{j=1}^{k-1} \sqrt{\Gamma_k \Gamma_j}\, c_j \quad (k = 1, 2, \ldots n).$$

The operator (33) is uniquely determined by the roots of the function $S_0(W)$. In the simplest case of a single root, the system (33) reduces to one equation $d_1 = (E_1 - \frac{1}{2} i \Gamma_1) c_1$,

$$S_0(W) = \frac{W - E_1 - (i/2)\Gamma_1}{W - E_1 + (i/2)\Gamma_1},$$

and the cross section becomes

$$\sigma_{\mathrm{Res}} = \pi\lambda^2 \left| 1 - \frac{W - E_1 - (i/2)\Gamma_1}{W - E_1 + (i/2)\Gamma_1} \right|^2$$

$$= \pi\lambda^2 \frac{\Gamma_1}{(W - E_1)^2 + \Gamma_1^2/4}$$

---

* It is assumed that the spectrum of H does not extend to infinity.

* See Ref. 19 for the reduction of finite matrices to triangular form.

(Breit-Wigner). The motion of the compound nucleus is given by

$$ihdc_1/dt = (E_1 - {}^1/_2 i\Gamma_1)c_1,$$

so that

$$c_1(t) = c_1(0)e^{-itE_1/h}e^{-(\Gamma_1/2h)t}$$

and Γ_1/h is the decay probability. For an arbitrary number of levels, the decay probability becomes by Eq. (27)

$$P = \frac{1}{h}\lim_{W\to\infty} W\left|1 - \sum_{k=1}^{n}\frac{W - W_k}{W - W_k^*}\right| \tag{34}$$

$$= \frac{1}{h}\sum_{k=1}^{n}|W_k^* - W_k| = \frac{1}{h}\sum_{k=1}^{n}\Gamma_k.$$

The total decay probability is equal to the sum of the probabilities for the individual levels, as one would expect.

4. CONTINUOUS SPECTRUM OF THE COMPOUND NUCLEUS. TRIANGULAR MODEL

Suppose that the number of complex levels $W_k^{(n)} = E_k^{(n)} + \frac{1}{2}i\Gamma_k^{(n)}$ $(k = 1, 2, \ldots, n)$ increases indefinitely, and that in the limit as $n \to \infty$ the numbers $E_k^{(n)}$ fill a certain interval $a \leq E \leq b$ continuously. If the decay probability P of the compound nucleus is held fixed, then by Eq. (34) the $\Gamma_k^{(n)}$ must tend to zero as $n \to \infty$. Introducing the step-function

$$p_n(E) = \Gamma_k^{(n)}/E_{k+1}^{(n)} - E_k^{(n)} \quad (E_k^{(n)} \leqslant E < E_{k+1}^{(n)};$$
$$E_1^{(n)} = a,\quad E_{n+1}^{(n)} = b)$$

and using Eqs. (34) and (30), we obtain

$$P = h^{-1}\sum_{k=1}^{n} p_n(E_k^{(n)})(E_{k+1}^{(n)} - E_k^{(n)}),$$

$$S_0^{(n)}(W) = \prod_{k=1}^{n}\left[1 - i\frac{p_n(E_k^{(n)})(E_{k+1}^{(n)} - E_k^{(n)})}{W - E_k^{(n)} + \frac{i}{2}\Gamma_k^{(n)}}\right].$$

Since $E_{k+1}^{(n)} - E_k^{(n)} \to 0$ and $\Gamma_k^{(n)} \to 0$ as $n \to \infty$, we have

$$1 - i\frac{p_n(E_k^{(n)})(E_{k+1}^{(n)} - E_k^{(n)})}{W - E_k^{(n)} + \frac{i}{2}\Gamma_k^{(n)}}$$

$$\approx \exp\left\{-i\frac{p_n(E_k^{(n)})(E_{k+1}^{(n)} - E_k^{(n)})}{W - E_k^{(n)}}\right\},$$

from which it follows that as $n \to \infty$ the function $S_0^{(n)}(W)$ tends to the limit

$$S_0(W) = \exp\left\{-i\int_a^b\frac{p(E)\,dE}{W - E}\right\}. \tag{35}$$

The total decay probability is

$$P = \frac{1}{h}p(E)\,dE, \tag{36}$$

and the probability for decay $P(E, E + dE)$ belonging to the interval $(E, E + dE)$ is given by

$$P(E, E + dE) = h^{-1}p(E)\,dE. \tag{37}$$

If the compound nucleus has both a continuous and a discrete (complex) spectrum, the reduced scattering matrix has the form

$$S_0(W) \tag{38}$$
$$= \prod_{k=1}^{n}\frac{W - E_k - (i/2)\Gamma_k}{W - E_k + (i/2)\Gamma_k}\exp\left\{-i\int_a^b\frac{p(E)\,dE}{W - E}\right\}.$$

It is interesting that the density $h^{-1}p(E)$ of decay probability can be found directly from the function $S_0(W)$. Taking the logarithm, we find

$$\ln|S_0(W)| = \ln\left|\prod_{k=1}^{n}\frac{W - W_k}{W - W_k^*}\right|$$
$$+ \operatorname{Im}\int_a^b\frac{p(E)\,dE}{W - E} \quad (\operatorname{Im} W \neq 0),$$

and the Stieltjes inversion formula[20] then gives

$$h^{-1}p(E) = -(1/h\pi)\ln|S_0(E - i0)|. \tag{39}$$

Next we determine the operator H^* in the case of a pure continuous spectrum, passing to the limit in the equations

$$d_k^{(n)} = (E_k^{(n)} - \frac{i}{2}\Gamma_k^{(n)})c_k^{(n)} - i\sum_{j=1}^{k-1}c_j^{(n)}\sqrt{\Gamma_j^{(n)}\Gamma_k^{(n)}}.$$

We define the step-functions

$$f_n(E) = c_k^{(n)},\quad p_n(E) = \Gamma_k^{(n)}/E_{k+1}^{(n)} - E_k^{(n)}$$
$$\left(E_k^{(n)} \leqslant E < E_{k+1}^{(n)},\quad E_{k+1}^{(n)} - E_k^{(n)} = \frac{b - a}{n}\right)$$

and obtain in the limit as $n \to \infty$ the following representation for the operator $g = H^*f$,

$$g(E) = Ef(E) \tag{40}$$
$$- i\int_a^E f(\xi)\sqrt{p(\xi)p(E)}\,d\xi \quad (a \leqslant E \leqslant b).$$

The corresponding equation of motion* is

$$ih\frac{\partial f(E,t)}{\partial t} = Ef(E,t) - i\int_a^E f(\xi,t)\sqrt{p(\xi)\,p(E)}\,d\xi. \qquad (41)$$

In this case also the equation of motion is determined uniquely by $S_0(W)$.

5. DECAY OF THE COMPOUND NUCLEUS IN THE CASE OF A CONTINUOUS SPECTRUM

If $f(E,t)$ satisfies Eq. (41) and $g(E,t)$ satisfies the adjoint equation

$$ih\frac{dg}{dt} = Eg(E,t) + i\int_E^b g(\xi,t)\sqrt{p(\xi)\,p(E)}\,d\xi, \qquad (42)$$

the scalar product (f, g) is constant in time. Explicitly,

$$\frac{d(f,g)}{dt} = \left(\frac{df}{dt}, g\right) + \left(f, \frac{dg}{dt}\right) = \frac{1}{ih}(H^{*}f, g) - \frac{1}{ih}(f, Hg) = 0.$$

It follows that

$$|f|^2_\infty \geqslant |(f_0, g_0)|^2/|g|^2_\infty \qquad (43)$$

holds, where

$$|f|^2_\infty = \lim_{t\to\infty}\int_a^b |f(E,t)|^2 dE,$$

$$|g|^2_\infty = \lim_{t\to\infty}\int_a^b |g(E,t)|^2\, dE,$$

$$f_0 = f(E, 0), \quad g_0 = g(E, 0).$$

We shall show that the initial state $f_0 = f(E, 0)$ can decay incompletely**:

$$\lim_{t\to\infty}\int_a^b |f(E,t)|^2 dE > 0.$$

This means that after all decaying waves are removed there remains a certain population of nuclei which do not decay into the channel which is under consideration. Such a phenomenon obviously cannot occur when there exist only complex levels.

A solution of Eq. (42), or of

$$ih\frac{dg}{dt} = Hg \quad \left(Hg = Eg(E) + i\int_E^b g(\xi)\sqrt{p(\xi)\,p(E)}\,d\xi\right) \qquad (44)$$

can be obtained from the formula

$$g(E,t) = -\frac{1}{2\pi i}\int_\gamma e^{-i\lambda t/h}(H - \lambda I)^{-1} g_0\, d\lambda, \qquad (45)$$

where γ is a contour enclosing the spectrum $a \leq E \leq b$ of H. It is easy to verify Eq. (45). Putting $g_0 = e$ and using Eqs. (45) and (19), we have

$$(g, e) = -\frac{1}{2\pi i}\int_\gamma e^{-i\lambda t/h}((H - \lambda I)^{-1}e, e)\, d\lambda = \frac{1}{2\pi}\int_\gamma e^{-i\lambda t/h}(S_0^{*}(\lambda^{*}) - 1)\, d\lambda.$$

When the contour γ is contracted onto the interval $a \leq E \leq b$, this becomes

$$(g, e) = \frac{1}{2\pi}\int_a^b e^{-iEt/h}[S_0^{*}(E + i0) - S_0^{*}(E - i0)]\, dE. \qquad (46)$$

Equation (25) when applied to the operator H becomes $d|g|^2/dt = h^{-1}|(g, e)|^2$, and therefore

$$|g|^2_\infty = |g_0|^2 + \frac{1}{h}\int_0^\infty |(g,e)|^2 dt = |g_0|^2 + \frac{1}{4\pi^2 h}\int_0^\infty \left|\int_a^b e^{-\frac{iEt}{h}}[S_0^{*}(E + i0) - S_0^{*}(E - i0)]\, dE\right|^2 dt \leqslant |g_0|^2 + \frac{1}{2\pi}\int_a^b |S_0(E - i0)|^2 dE. \qquad (47)$$

The initial state f_0 is given by Eq. (13),

$$f_0 = -\frac{1}{K}\sqrt{\frac{h^2 K}{2\mu}}(H^{*} - WI)^{-1}e,$$

and the scalar product is given by

---

[*] Similar equations can be derived (see Ref. 5) for any number of reaction channels.

[**] We give later a quantitative estimate of this limit.

$$|(f_0, g_0)|^2 = \frac{h^2}{2\mu K}|((H^* - WI)^{-1}e, e)|^2 \tag{48}$$

$$= \frac{h^2}{2\mu K}|1 - S_0(W)|^2.$$

From Eqs. (47), (48) and (43) we derive the inequality

$$|f|_\infty^2 \geqslant W|1 - S_0(W)|^2 / K^3 \Big[hP + \frac{1}{2\pi}\int_a^b |S_0(E + i0) - S_0(E - i0)|^2\, dE\Big], \tag{49}$$

where, by virtue of the Stieltjes inversion formula,

$$|S_0(E + i0) - S_0(E - i0)| = e^{\pi p(E)} - e^{-\pi p(E)}. \tag{50}$$

6. A DEGENERATE REAL LEVEL

Returning to the case of a finite number of complex levels, we may take in particular $W_1^{(n)} = W_2^{(n)} = \ldots = W_n^{(n)} = E_0 + \frac{1}{2} i\Gamma_0^{(n)}$, and derive

$$S_0^{(n)}(W) = \left(\frac{W - W_1^{(n)}}{W - W_1^{*(n)}}\right)^n = \left(1 - \frac{i\Gamma_0^{(n)}}{W - E_0 + (i/2)\Gamma_0^{(n)}}\right)^n. \tag{51}$$

The corresponding operator $g = H^*f$ becomes

$$d_k^{(n)} = \left(E_0 + \frac{i}{2}\Gamma_0^{(n)}\right)c_k^{(n)} - i\sum_{j=1}^{k-1} c_j^{(n)}\Gamma_0^{(n)}, \tag{52}$$

and the decay probability is $P = (n/h)\Gamma_0^{(n)}$. We fix P and let $n \to \infty$. Since $\Gamma_0^{(n)} = hP/n \to 0$, we have $W_k^{(n)} \to E_0$. Equation (51) gives the following expression for the one-dimensional scattering matrix in the case of a degenerate real level

$$S_0(W) = \exp\{-ihP/W - E_0\}. \tag{53}$$

We define step-functions $f_n(x)$ $(0 \le x \le hP)$ by $f_n(x) = c_k^{(0)}$ $((k-1)hP/n \le x \le khP/n)$, $(k = 1, 2, \ldots, n)$, and then pass to the limit in Eq. (52). The energy operator corresponding to a single infinitely degenerate real level E_0 is thus

$$H^*f = E_0 f(x) - i\int_0^x f(\xi)\, d\xi \quad (0 \leqslant x \leqslant hP). \tag{54}$$

The equation of motion is

$$ih\frac{\partial f(x, t)}{\partial t} = E_0 f(x, t) - i\int_0^x f(\xi, t)\, d\xi. \tag{55}$$

Using Eq. (45), it is easy to obtain the solution $f(x, t)$ of Eq. (55) corresponding to the initial condition $f(x, 0) = f_0(x)$:

$$f(x, t) = e^{-iE_0 t/h}\Big[f_0(x) - \sqrt{\frac{t}{h}}\int_0^x f_0(\xi)\frac{J_1(2\sqrt{t(x - \xi)/h})}{\sqrt{x - \xi}}\, d\xi\Big], \tag{56}$$

where $J_1(\lambda)$ is a Bessel function.

7. EFFECT OF AN EXTERNAL FIELD ON THE COMPOUND NUCLEUS SCATTERING MATRIX

In Secs. 1-6 we obtained the general properties of the amplitude of the elastic scattering process $a + X \to C \to X + a$ (a is the incident particle and X the target), assuming that the scattering is caused by the formation of the compound nucleus and by an impenetrable-sphere interaction. The effect of a spherically symmetrical potential can be included by the following simple argument. We suppose that for $r > R_c$ the interaction between a and X is described by a potential $V(r)$, while for $r < R_c$ the compound nucleus C is formed and can be described by a non-self-adjoint operator. Here r is the distance between a and X, and R_c is the radius of C. The radial function $U_l(r)$ $(r > R_c)$ corresponding to angular momentum l satisfies the equation

$$\frac{h^2}{2\mu}\frac{d^2U_l}{dr^2} + \Big[W - \frac{h^2}{2\mu}\frac{l(l+1)}{r^2} - V(r)\Big]U_l(r) = 0. \tag{57}$$

Let $E_l(r)$ be the solution of Eq. (57) satisfying the initial conditions $E_l(R_c) = 1$, $E_l'(R_c) = iK$. Then

$$U_l(r) = \text{const}\,\{E_l^*(r) - S_l^{(C)}(W)E_l(r)\}. \tag{58}$$

Since at $r = R_c$ we have

$$E_l(r) = e^{iK(r - R_C)},\ E_l'(r) = [e^{iK(r - R_C)}]',$$

the function $S_l^{(c)}(W)$ may be regarded as the amplitude of pure resonance scattering caused by the formation of the compound nucleus C in the absence of a potential. On the other hand, as $r \to \infty$ we have the asymptotic relation

$$U_l(r) \approx \text{const}\,\{e^{-i(Kr - l\pi/2)} - S_l(W)\,e^{i(Kr - l\pi/2)}\}, \tag{59}$$

where $S_l(W)$ is the total ampiitude, including the effects both of the compound nucleus and of the potential. In the case of a short-range potential $[V(r) \equiv 0 \text{ for } r > R]$ the function $U_l(r)$ can also be presented in the form

$$U_l(r) = \text{const}\,\{U_l^{(-)}(r) - S_l(W)\,U_l^{(+)}(r)\} \quad (r > R), \tag{60}$$

where $U_l^{(+)}(r)$ and $U_l^{(-)}(r)$ are the solutions of Eq. (57) which are asymptotically of the forms $U_l^{(+)}(r) \approx e^{i(Kr - l\pi/2)}$, $U_l^{(-)}(r) \approx e^{-i(Kr - l\pi/2)}$. Comparing the values of $U_l(R)$ and $dU_l/dr|_{r=R}$ obtained from Eqs. (58) and (60), we find

$$S_l(W) = a_l S_l^{(C)}(W) - b_l/(b_l^* S_l^{(C)}(W) - a_l^*),$$

with

$$a_l = \frac{dE_l}{dr} U_l^{(-)} - E_l \frac{dU_l^{(-)}}{dr}\bigg|_{r=R},$$

$$b_l = \frac{dE_l^*}{dr} U_l^{(-)} - E_l^* \frac{dU_l^{(-)}}{dr}\bigg|_{r=R}.$$

In this way the scattering amplitude with an external potential appears as a fractional linear transformation of the amplitude $S_l^{(c)}(W)$, and the coefficients a_l, a_l^*, b_l, b_l^* can be computed if the potential $V(r)$ is given. If the compound nucleus C has the complex energy-levels $W_j^{(l)}$, then by Eq. (30) the amplitude $S_l^{(c)}(W)$ is

$$S_l^{(C)}(W) = \prod_{j=1}^{n} \frac{W - E_j^{(l)} - (i/2)\,\Gamma_j^{(l)}}{W - E_j^{(l)} + (i/2)\,\Gamma_j^{(l)}}.$$

Recently, various attempts have been made to unify the idea of a compound nucleus with the theory of nuclear shells[21], so it is interesting to consider the case in which the compound nucleus C possesses in a certain energy interval a large number of almost equally spaced levels $W_j = W_0 + jD + i\Gamma/2$ ($j = 1, 2, \ldots, n$), where D is the mean level spacing and Γ the mean width. In this case

$$S_l^{(C)} = \prod_{j=1}^{n} \frac{1 - \left(W - W_0 - \frac{i}{2}\Gamma\right)/jD}{1 - \left(W - W_0 + \frac{i}{2}\Gamma\right)/jD}.$$

If $\Gamma/D \ll 1$, we have approximately

$$S_l^{(C)} = \frac{\sin\pi\left(W - W_0 - \frac{i}{2}\Gamma\right)/D}{\sin\pi\left(W - W_0 + \frac{i}{2}\Gamma\right)/D}.$$

In conclusion, I express my thanks to M. M. Al'perin for valuable discussions while this work was in progress.

---

[1] M. S. Livshits, Mat. Sbornik **19**, 239 (1946).

[2] V. P. Potapov, Dokl. Akad. Nauk SSSR **72**, 849 (1950).

[3] M. V. Keldysh, Dokl. Akad. Nauk SSSR **77**, 11 (1951).

[4] I. M. Gel'fand, Usp. Mat. Nauk **7**, Part 6, 183 (1952).

[5] M. S. Livshits, Mat. Sbornik **34**, 145 (1954).

[6] M. A. Naimark, Dokl. Akad. Nauk SSSR **98**, 727 (1954).

[7] M. S. Brodskii, Dokl. Akad. Nauk SSSR **97**, 761 (1954).

[8] B. R. Mukminov, Dokl. Akad. Nauk SSSR **99**, 499 (1954).

[9] E. P. Wigner and L. Eisenbud, Phys. Rev. **72**, 29 (1947).

[10] T. D. Newton, Canad. J. Phys. **30**, 53 (1952).

[11] E. P. Wigner, Phys. Rev. **70**, 606 (1946).

[12] T. Teichmann and E. P. Wigner, Phys. Rev. **87**, 123 (1952).

[13] H. Feshbach and V. P. Weisskopf, Phys. Rev. **76**, 1550 (1949).

[14] R. G. Thomas, Phys. Rev. **97**, 224 (1955).

[15] H. A. Bethe, Rev. Mod. Phys. **9**, 69 (1937).

[16] J. M. Blatt and V. F. Weisskopf, *Theoretical Nuclear Physics* (Wiley, New York), 1952.

[17] W. Heisenberg, Z. Physik **120**, 513 (1943); **120**, 673 (1943).

[18] L. Landau and E. Livshits, *Quantum Mechanics*, Part 1, (GTTI, Moscow), 1948.

[19] A. I. Mal'tsev, *Fundamentals of Linear Algebra* (GTTI, Moscow), 1948.

[20] V. I. Smirnov, *Course of Higher Mathematics 5* (GTTI, Moscow), 1947.

[21] Feshbach, Porter and Weisskopf, Phys. Rev. **96**, 448 (1954).

Translated by F. J. Dyson
15

SOVIET PHYSICS JETP VOLUME 4, NUMBER 1 FEBRUARY, 1957

Interaction of Nitrogen Nucleus with Nuclei in an Emulsion

D. M. PARFANOVICH, N. V. RABIN AND A. M. SEMCHINOVA

(Submitted to JETP editor March 28, 1956)
J. Exptl. Theoret. Phys. (U.S.S.R.) 31, 188-193 (August, 1956)

The results of an experimental investigation of the interaction between nitrogen nuclei, accelerated to an energy of 100 mev, and nuclei in an emulsion are presented. The range-energy relation for nitrogen nuclei in the emulsion is determined. The angular and energy distributions for protons and α – particles produced in the reactions are examined. The experimental results reveal a number of interesting features in the emission of charged pasticles which characterizes the interaction of the nitrogen nuclei with the nuclei of the emulsion.

NUCLEAR reactions involving nuclei heavier than α – particles have received little attention until recently. This situation is a result of the technical difficulties associated with the acceleration of heavy ions to high energies and the desire to deal with as simple an interaction as possible, the latter suggesting the use of elementary particles as bombarding particles. However, study of the interaction of more complicated nuclei should yield valuable data on nuclear deformation, the structure of the nuclear surface, nucleon exchange, and so on[1].

In the small amount of work which has been carried out in this field several interesting features of this type of reaction have been observed. In the bombardment of aluminum by nitrogen nuclei and carbon nuclei[2,3] with energies of 50-80 mev, a considerably greater number of charged particles was produced than had been predicted by the analysis based on evaporation of nucleons from a compound nucleus. In spite of the fact that the bombarding nuclei were comparatively slow--3 to 5 mev per nucleon--the authors assumed that a "stripping" reaction was possible. On the other hand, in Ref. 4, a study was made of the excitation function for reactions occuring in bombardment Mg^{25} by protons and C^{12} by nitrogen nuclei. The excitation functions were similar: this finding indicates that both reactions proceed via the same compound nucleus, Al^{26}.

In the work cited above a radiochemical method was employed; this method does not permit detailed observation of the interaction. A more comprehensive picture of the interaction can be obtained through the use of photographic emulsions, since in these it is possible to determine the identity as well as the energy and angular distribution of all charged particles produced in the reaction.

Below are described the experimental results obtained in a study of the interaction of nitrogen nuclei with nuclei in an emulsion.

The emulsions were bombarded by nitrogen nuclei accelerated in a 150 cm cyclotron. The acceleration of the nitrogen nuclei to high energies was accomplished as follows: The cyclotron was adjusted to accelerate sextuply-charged nitrogen ions ($e/m = 6/14$); it is also possible for doubly-charged ions to be accelerated under these conditions. The ion source was of the usual type and yielded singly- and doubly-charged nitrogen ions. The doubly-charged ions, having been accelerated to an energy of 4-5 mev, subsequently lost four more electrons to atoms of the residual gas in the cyclotron chamber. These ions were then accelerated as sextuply-charged nitrogen ions acquiring thereby an energy of 120-130 mev. A similar acceleration mechanism has been described by Walker[5].

However, since the electron-loss process can occur anywhere in the volume of the cyclotron chamber, the energy spectrum for nitrogen ions in the last orbit (70 cm) ranges from 0 to 130 mev. Furthermore, the beam is comprised of ions of different charge. To obtain monochromatic ions in the emulsion, the beam was extracted from the cyclotron chamber and passed through an analyzing magnet. In front of the analyzer there was an aluminum foil 2μ thick in which the nitrogen ions were completely stripped of electrons. By varying the magnetic field in the analyzer it was possible to obtain nitrogen nuclei with energies up to 130 mev. The analyzer resolution was about 3 mev.

In order to investigate the interaction of nitrogen nuclei with the nuclei of the emulsion at any energy, the range-energy relation for nitrogen nuclei in the emulsion must be known. This relation was determined with the magnetic analyzer. It was found, after a careful check, that the magnetic field in the analyzer was a linear function of the current in the winding. Thus, by measuring, at a given value of the analyzer current, the deflection of deuterons of known energy, it is possible to determine the energy of the nitrogen nuclei from the relation

$$E_N = \left(\frac{Z_N}{Z_d}\right)^2 \frac{M_d}{M_N} \left(\frac{i_N}{i_d}\right)^2 E_d ,$$

where Z is the charge, M is the mass and i is the current in the analyzer winding. The emulsions were exposed to nitrogen nuclei of various energies and the range measured with a microscope. The results obtained are shown in Fig. 1.

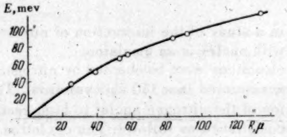

FIG. 1. The range-energy relation for nitrogen nuclei in an emulsion.

The range-energy relation in an emulsion for nitrogen nuclei with energies from 4 to 30 mev has been measured by Zucker and his collaborators[6]. In the region ~30 mev the results of the present work are in agreement with those of Zucker.

In the experiments an Ilford E-1 plate was bombarded by nitrogen nuclei with an energy of 115 mev. 25 cm^2 of the emulsion was scanned and 198 events were found in which an interaction took place with the emission of charged particles. Because of the complicated constitution of the emulsion it is impossible to determine exactly with which element the nitrogen nucleus interacts. It was possible, however, to distinguish cases in which the nitrogen nucleus interacted with "light" nuclei--carbon, oxygen and "heavy" nuclei--bromine and silver. The nitrogen nucleus, having an energy of several tens of mev, has a large momentum; hence, the constituent nuclei has a considerable range. Estimates indicate that for collisions of the nitrogen nuclei with silver or bromine nuclei the range of the constituent nuclei is 2-5 μ and in collisions with "light" nuclei erect this range is 10-15 μ. It should be noted that in each case it was necessary to take into account the momentum imparted to the residual nucleus by the emitted particles. If there is a preliminary emission of several particles the range of the "light" residual nucleus can be reduced to 5-8 μ. Hence, the cases in which the range of the residual nucleus was of the order 5-8 μ were attributed to interactions with carbon or oxygen nuclei.

Out of 198 cases 70 were assigned to interactions with "heavy" nuclei and 128 with "light" nuclei.

Knowing the initial energy of the nitrogen nucleus, by measuring the length of track from the beginning to the "star" it is possible to determine the energy at the point of interaction.

Using photographic plates it is possible to distinguish between tracks of protons, particles and heavier fragments but it is not possible to identify these heavier fragments.

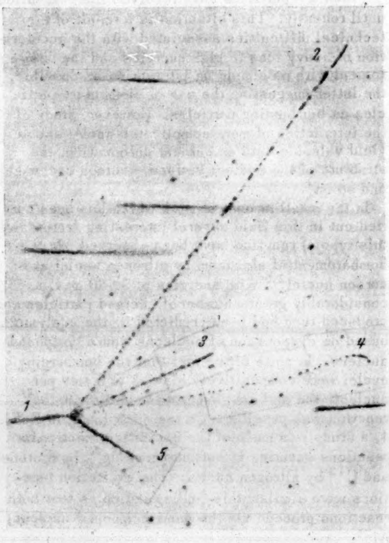

FIG. 2. Photograph of an interaction between a nitrogen nucleus and a "light" nucleus. The following tracks are visible: *1* – incoming nitrogen nucleus, *2*, *3* – α–particles, *4* – proton and *5* – recoil nucleus.

In Fig. 2 is presented a photograph of a star which shows the emission of two α – particles and

TABLE

Reaction	Number of events	
	Nitrogen on carbon, oxygen	Nitrogen on bromine, silver
N; p	2	7
N; $2p$	5	5
N; α	6	14
N; α, fragment . .	4	1
N; α. p	8	10
N; α, p, fragment.	3	1
N; α, $2p$	2	0
N; 2α	9	11
N; 2α, fragment .	2	0
N; 2α, p	12	11
N; 2α, p, fragment	2	1
N; 3α	6	7
N; 3α, p	4	1
N; 4α	1	0

a proton. In the Table are listed stars with different numbers of emitted charged particles (interactions with "light" and "heavy" nuclei are shown spearately). In this Table are included all reactions induced by nitrogen nuclei with energies from 30 to 110 mev. The number of interactions of nitrogen nuclei with carbon and oxygen is normalized to the number of interactions with bromine and silver (70).

All charged particles produced in the reactions are listed; the recoil nuclei are omitted.

The considerable preponderance of α – particles merits attention. On the average, in all stars the α – particles are found to be twice as numerous as protons both for "light" and "heavy" target nuclei. In the interaction of nitrogen nuclei with carbon and oxygen, in 25 percent of the cases emission of fragments heavier than α – particles was observed. Out of 70 cases of interaction of nitrogen nucleus with bromine and silver only 3 cases of fragment omission were observed.

In Figs. 3 and 4 are shown the angular and energy distributions for α – particles in the center-of-mass system. In converting to the center-of-mass system, the mass of the target nucleus was taken to be an average between that of carbon and oxygen (14) and bromine and silver (94). Because of the small amount of data it is not possible to determine accurately the angular and energy distributions for the α – particles at different nitrogen energies. In Figs. 3 and 4 are shown the distributions as summed over all cases in which the incident nitrogen nuclei had an energy from 70 to 110 mev.

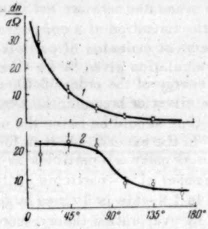

FIG. 3. Angular distribution for α – particles in the center-of-mass system. The interactions are between a nitrogen nucleus and *1* – Br, Ag nuclei; *2* – C, O nuclei.

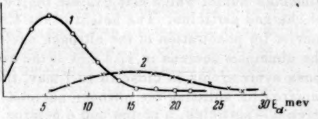

FIG. 4. Energy distribution for α – particles in the center-of-mass system. The interactions are between a nitrogen nucleus and *1* – C, O nuclei; *2* – Br, Ag nuclei.

The α – particle angular distribution is characterized by a noticeable directional effect in the forward direction, particularly in the case of "heavy" target nuclei . In the energy spectra, attention is directed to the considerable number of low-energy α – particles, having energies below the Coulomb barrier for a nitrogen nucleus. Within the limits of experimental error, the proton angular distribution for "light" nuclei, presented in Fig. 5, is isotropic. The number of proton-emission cases in the "heavy" nuclei was not large enough to permit plotting of the angular distribution. However, the proton distribution is approximately isotropic. Out of 31 protons, 17 were emitted in the forward direction and 14 in the backward direction.

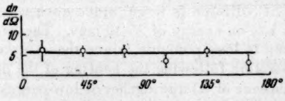

FIG. 5. Proton angular distribution in the center-of-mass system in the interaction of a nitrogen nucleus with C, O nuclei.

The results presented here are not in accord with the notion of the formation of a compound nucleus with the subsequent emission of particles. According to a calculation given by Le Couteur[7], at an excitation energy of the order 50-100 mev in nuclei such as silver or bromine, the number of evaporated protons should be twice the number of α – particles. In the experiment, it is found that there are twice as many α – particles as protons. The average number of α – particles emitted per disintegration is 1.3--this is 3 times larger than that predicted by evaporation theory; moreover, the α – particles are emitted chiefly in the forward direction while the angular distribution predicted by evaporation theory is isotropic.

In Ref. 2 there has been presented a qualitative picture of the interaction between nitrogen and aluminum nuclei which may explain the large number of charged particles. The height of the Coulomb barrier for penetration of the nitrogen nucleus into the aluminum nucleus is 17.4 mev in the center-of-mass system; this is close to 19.7 mev, the energy required for splitting the nitrogen nucleus into three α – particles, a proton and a neutron. Thus, in its approach to the aluminum nucleus, the nitrogen may be split into separate particles, some of which penetrate the aluminum nucleus and some of which are scattered by the Coulomb field. In this case, conditions are most favorable for the penetration of the neutron, since it sees no potential barrier. The next most favored is the α – particle since its energy is 4 times larger than the proton energy, although the barrier it sees is only 2 times larger; the proton will have the highest probability for being scattered. The angular distribution for all particles should be characterized by a predominance in the forward direction.

The isotropic proton angular distribution observed in the experiment is not in agreement with this hypothesis.

It may also be assumed that the nitrogen nucleus undergoes disintegration into individual particles only after penetration into the target nucleus. If the α – particles are maintained as individual objects, the probability of their being emitted at the moment of collision is large, since each α – particle has an energy of 25-30 mev. The emission of protons is less probable, since these are emitted by evaporation following the heating of the nucleus. The existence of a large number of low-energy α – particles would seem to indicate that a considerable deformation of the nucleus occurs during the time of collision; this deformation causes a reduction in the potential barrier.

It would be of interest to study the interaction of carbon nuclei or oxygen nculei, consisting of α – particles only, with nuclei in an emulsion. If the picture given in Ref. 2 is correct, a considerably smaller number of protons should be observed. On the other hand, if the hypothesis presented here, is valid, the number of protons should not vary to any great extent. If a more complete picture of the interaction of nitrogen nuclei with nuclei in the emulsion is to be obtained we shall require a detailed explanation of the dependence of the angular and energy distributions for protons and α – particles on the energy of the incident nitrogen nucleus; the relation between the proton and α – particle angular distributions and energies also requires study.

In conclusion, we wish to express our gratitude to the cyclotron crew and particularly to Iu. M. Pustovoi for providing reliable cyclotron operation in the course of the work.

Note added in proof: The interaction of accelerated oxygen nuclei with nuclei in an emulsion has been studied in a recent experiment. The emulsion was bombarded by a monochromatic beam of oxygen nuclei accelerated to an energy of 110 mev. The results have been analyzed in the same way as in the nitrogen experiments.

The ratio between the number of α – particles and the number of protons, averaged over all reactions, has been found to be 2 ±0.5. Thus the probability for the emission of protons is virtually the same in reactions induced by nitrogen nuclei and oxygen nuclei. This would seem to corroborate the assumption that, in general, the reactions proceed via the formation of a conglomerate nucleus.

[1] Breit, Hull and Gluckstern, Phys. Rev. **87**, 74 (1952).

[2] Chackett, Fremlin and Walker, Phil. Mag. **45**, 173 (1954).

[3] Chackett, Chackett and Fremlin, Phil. Mag. **46**, 1 (1955).

[4] Cohen, Reynolds and Zucker, Phys. Rev. **96**, 1617 (1954).

[5] D. Walker and J. H. Fremlin, Nature **171**, 189 (1953).

[6] H. L. Reynolds and A. Zucker, Phys. Rev. **96**, 393 (1954).

[7] K. J. Le Couteur, Proc. Phys. Soc. **63A**, 259 (1950).

Translated by H. Lashinsky
38

SOVIET PHYSICS JETP VOLUME 4, NUMBER 1 FEBRUARY, 1957

Generalized Phase Analysis as a Corollary of the Unitary Property of the S-Matrix

IU. F. GOL'FAND
P. N. Lebedev Physical Institute, Academy of Sciences, USSR

(Submitted to JETP editor, April 26, 1955)
J. Exptl. Theoret. Phys. (U.S.S.R.) 31, 224-231 (August, 1956)

A method is given for the determination of the general form of the scattering amplitude, providing a generalization of the usual formulas of phase-shift analysis. An invariant operational technique is developed which simplifies the calculations connected with the expansion in terms of eigenfunctions of the total angular momentum.

INTRODUCTION

THE problem of phase-shift analysis is the determination of the general form of the scattering amplitude of particles of definite type. It is well known that in the simplest cases (spins 0 and ½) the scattering amplitude can be expressed in terms of the phases of the scattered partial waves. A phase analysis establishing only the general form of the scattering amplitude cannot determine the concrete values of the phases. The values of the phases are determined either by solution of the dynamical problem of the scattering or by means of analysis of experimental data. In spite of this, the general formula expressing the scattering amplitude or cross-section in terms of a number of independent parameters is extremely useful, since on one hand it facilitates the analysis of the experimental data, and on the other hand it reduces the dynamical problem of the scattering to the problem of determining the phases.

But in the more complicated cases (when the spin of the system exceeds ½) the simple formulas of phase analysis are no longer valid. For instance, for the scattering of a nucleon by a nucleon, instead of real phases one must introduce complex phases for the triplet states, and the amplitude for photoproduction of mesons is not expressible in terms of phases at all.

A second important point is the question of the foundation of the phase analysis. In the simplest cases the formulas of phase analysis have been obtained from a consideration of the asymptotic behavior of the solution of the Schrödinger equation. but for many important cases, in particular for the scattering of relativistic particles, the question of the existence of the corresponding Schrödinger equation cannot be regarded as settled. On the other hand it is obvious that the formulas of the phase analysis are applicable also in those cases in which a Schrödinger equation does not exist for the system under consideration.

In the present paper a method is proposed for obtaining the formulas of the phase analysis from an extremely general requirement, namely from the condition of the unitary character of the S-matrix. In the simplest cases this method leads to the well-known expressions for the scattering amplitude in terms of phases. In other cases the scattering amplitude is expressed in a more complicated fashion, but a general procedure is indicated for determining formulas expressing the scattering amplitude in terms of the minimum number of independent parameters.

An analogous program has been carried out in a number of papers devoted to the formal theory of nuclear reactions (cf., for example, Ref. 1). But in the general case the formulas there obtained have an extraordinarily cumbersome appearance because of the unfortunate choice of the eigenfunctions of the total angular momentum. Instead of the expansion in terms of eigenfunctions of the angular momentum, we develop in Sec. 2 a technique of invariant operators W. The expansion of the various operators encountered in the scattering theory in terms of the operators W generalizes to the case of spin different from zero the usual expansion in terms of Legendre polynomials for spin zero. The orthogonality conditions, Eq. (2.7), in a certain sense play the role of the addition theorem for Legendre polynomials, and this makes it possible to use the operators W for the separation of the angular variables. The use of the invariant operators W frees us from the necessity of a definite choice of a coordinate system and spares us the cumbersome calculations associated with spherical functions involving spin.

It must be remarked that the invariant operators W are determined for spin ½ in Ref. 2, and for the general case in Ref. 3, where some of their properties are investigated. Unlike the previous treatment[3] we do not use the apparatus of polarized solid harmonics in determining the operators W. Since the problem of the present paper did not involve the calculation of the quantities W in explicit form, we have not definitely specified the forms of the eigenfunctions of the angular momentum, but have only used their orthogonality relations. The explicit calculation of the quantities W in closed form can be carried through by means of the generalized spherical functions introduced by Gel'fand[4], which, in our opnion, should be included in the apparatus of theoretical physics along with the ordinary spherical functions.

The calculation of the quantities W and the consideration of the formulas of the generalized phase analysis will be the subject of another paper.

1. THE S-MATRIX AND THE SCATTERING AMPLITUDE

The scattering operator Ω, which transforms the incident wave into the sum of the incident and scattered waves, can be written in the form[5]

$$\Omega = I + \delta_+ (\varepsilon - \varepsilon') R \qquad (1.1)$$

where I is the identity operator, $\delta_+ (\epsilon) = \frac{1}{2}\delta(\epsilon) + 1/2\pi i \epsilon$, and the matrix R is a regular function of the energy. Since energy is conserved in the scattering, a description of the scattering requires only the value of R on the energy surface, i. e., those matrix elements of R for which the energies of the initial and final states are equal.

The operator

$$S = I + R, \qquad (1.2)$$

considered on the energy surface, is called the S-matrix. In the theory of scattering it is shown that the S-matrix is unitary.[5,6]

In what follows we shall consider only those scattering processes in which two colliding particles give two scattered particles, i. e., reactions of the type

$$a + b \rightarrow c + d \qquad (1.3)$$

We shall not, however, assume that c and d are particles of the same kind as a and b. In particular, they can have different masses, as for example, in photomesic reactions. When we speak of the complete set of states of the system, we shall have in mind noth all possible initial states and also all possible final states that can be formed as a result of the scattering. For example, for the reaction

$$\gamma + p \rightarrow \pi^+ + n$$

we shall consider the initial state $\gamma + p$ and the final state $\pi^+ + n$ as different states of one and the same system. We note that the definition of a complete set of states is of a somewhat conventional nature and depends on the degree of precision with which the given scattering process is treated. For example, in studying the scattering of π-mesons by nucleons, one may to a high degree of accuracy neglect the radiative capture of the π-meson. In this case the complete set of states of the system is the manifold of all possible states of the type "π-meson + nucleon." If, however, we do not neglect the radiative capture, then it is necessary to include in our consideration also states of the type "nucleon + γ-quantum." In this case four different processes —the scattering of the meson by the nucleon, the radiative capture of the meson by the nucleon and its inverse process, the photoproduction of a meson, and also the scattering of light by nucleons — are united in a single scattering process.

Accordingly, in considering any sort of scattering process, one must specify a system of states which can, to a certain approximation, be regarded as closed with respect to this scattering. Only in relation to a closed system of states can one speak of the unitary nature of the S-matrix. Indeed, if we confine ourselves to an unclosed system of states, the concept of the unitary property of the S-matrix loses its meaning. Thus, for example, one cannot speak of the unitary property of the S-matrix describing only the process of photoproduction of mesons.

Let us introduce dynamical variables defining the states of the system. It is convenient to consider the reaction (1.3) in the center-of-mass system, in which the total momentum vanishes

$$\mathbf{p} = \mathbf{p}_a + \mathbf{p}_b = \mathbf{p}_c + \mathbf{p}_d = 0. \qquad (1.4)$$

In what follows we shall assume that all quantities are referred to the center-of-mass system.

We shall describe a complete set of states by the variables ϵ, $\mathbf{n}$, σ, α, where ϵ is the total energy of the system, $\mathbf{n}$ is a unit vector directed along the momentum of one of the particles (in virtue of Eq. (1.4), apart from sign, $\mathbf{n}$ determines the direction of motion of both particles), σ is the total spin variable of the system, and α is the set of all other variables, which we shall not specify explicitly. In particular, the value of α

determines the types of particles in one or another state.

With a view to the application to the scattering of relativistic elementary particles, we shall suppose that the energy ϵ is connected with the momentum p of one particle [because of (1.4) the magnitude of p is the same for both particles) in the state α by the relation

$$\varepsilon = \varepsilon_\alpha(p) = \sqrt{p^2 + M_\alpha^2} + \sqrt{p^2 + \mu_\alpha^2}, \quad (1.5)$$

where M_α and μ_α are the masses of the particles in the state α (we use a system of units in which $\hbar = 1$, $c = 1$).

The matrix elements of the operator A will be denoted by symbols $(\epsilon\, \mathbf{n}\, \sigma\, \alpha \mid A \mid e'\mathbf{n}'\sigma'\alpha')$. If, however, the operator is considered on the energy surface, i.e., for $\epsilon = \epsilon'$, then we shall omit ϵ from the labels of the matrix elements. Thus an element of the S-matrix will be denoted by the symbol $(\mathbf{n}\,\sigma\,\alpha \mid S \mid \mathbf{n}'\sigma'\alpha')$, with the understanding that this quantity is a function of ϵ. The connection between the S-matrix and the scattering amplitude is given by the relations (1.1) and (1.2). In the coordinate representation these relations have the following form. If the incident plane wave is

$$\psi_0 = e^{i\mathbf{p}_0\mathbf{x}}\delta_{\sigma\sigma_0}\delta_{\alpha\alpha_0},$$

then at great distances the sum of the incident and scattered waves is equal to

$$\Omega\psi_0 = \exp\{i\mathbf{p}_0\mathbf{x}\}\,\delta_{\sigma\sigma_0}\delta_{\alpha\alpha_0} + \frac{\exp\{ip_\alpha r\}}{r}F; \quad (1.6)$$

$$F = \frac{2\pi}{ip_0}\sqrt{\frac{v_0}{v_\alpha}}\,(\mathbf{n}\sigma\alpha \mid R \mid \mathbf{n}_0\sigma_0\alpha_0),$$

where $\mathbf{p}_0 = p_0\mathbf{n}_0$ and $\mathbf{p}_\alpha = p_\alpha\,\mathbf{n}_\alpha$ are the momenta in the initial and final states, $\mathbf{x} = r\mathbf{n}$, and $v_\alpha = \partial\epsilon_\alpha / \partial p$ is the relative velocity. According to Eq. (1.5), the absolute values of the momenta are determined in terms of the total energy ϵ_0 by the relations

$$\varepsilon_{\alpha_0}(p_0) = \varepsilon_\alpha(p_\alpha) = \varepsilon_0.$$

The asymptotic expression (1.6) for the wave function is calculated in a well-known way. It is only necessary to keep in mind that the operators (1.1), (1.2) are taken to be in the ϵ-representation, and in the passage to the x-representation one must use plane waves, normalized to a δ-function of the total energy ϵ.

By means of Eq. (1.6) one can easily find the expression for the differential scattering cross-section

$$d\sigma/d\Omega = |F|^2 v_\alpha/v_0.$$

Substituting the value of F from Eq. (1.6), we obtain

$$d\sigma/d\Omega = (4\pi^2/p_0^2)\,|(\mathbf{n}\sigma\alpha \mid R \mid \mathbf{n}_0\sigma_0\alpha_0)|^2. \quad (1.7)$$

2. THE INVARIANT OPERATORS W AND THE EXPANSION OF THE S-MATRIX

If no external fields act on the system, then the total angular momentum $\mathbf{M}$ of the system (including spin) is conserved. In this case it is convenient to transform to a representation in which the quantities M^2 and M_z are diagonal. This representation will be called the angular momentum representation.

We construct a complete orthonormal system of eigenfunctions of M^2 and M_z : $Y_{jm}^r(\mathbf{n}, \sigma)$, where j,m are the values of the total angular momentum and of its projection, and for a given j the index r runs through as many values as there are distinct independent systems of states with the total angular momentum j. For example, for the system of two nucleons the total spin takes the values 0 and 1 , and corresponding to this the index r runs through four values: one for the single state of the system and three for the triplet.

The orthogonality condition for the functions Y_{jm}^r has the form

$$\sum_\sigma \int Y_{jm}^{r*}(\mathbf{n}\sigma)\,Y_{j'm'}^{r'}(\mathbf{n}\sigma)\,d\Omega = \delta_{jj'}\delta_{mm'}\delta_{rr'}; \quad (2.1)$$

$$\sum_{jmr} Y_{jm}^{r*}(\mathbf{n}\sigma)\,Y_{jm}^{r}(\mathbf{n}'\sigma') = \delta_{\mathbf{n}\mathbf{n}'}\delta_{\sigma\sigma'}.$$

Here $\delta_{\mathbf{n}\mathbf{n}'}$, the δ-function on the sphere, is defined by the equation

$$\int \delta_{\mathbf{n}\mathbf{n}'} f(\mathbf{n}')\,d\Omega' = f(\mathbf{n}).$$

The S-matrix can be expanded in terms of the system of functions Y_{jm}^r

$$(\mathbf{n}\sigma\alpha \mid S \mid \mathbf{n}'\sigma'\alpha') \quad (2.2)$$

$$= \sum_{jmr}\sum_{j'm'r'} (jmr\alpha \mid S \mid j'm'r'\alpha')\,Y_{jm}^r(n\sigma)\,Y_{j'm'}^{*r'}(\mathbf{n}'\sigma').$$

We now make use of the conservation of angular momentum and the absence of any favored direction in space, in consequence of which the

S-matrix in the angular momentum representation will have the form

$$(jmr\alpha \,|\, S \,|\, j'm'r'\alpha') = (r\alpha \,|\, S_j \,|\, r'\alpha')\,\delta_{jj'}\delta_{mm'}. \qquad (2.3)$$

Here S_j is a matrix with respect to the variables r, α, and depends on the value j of the total angular momentum, but not on the projection m. The relation (2.3) shows that in the angular momentum representation the S-matrix divides into diagonal blocks, S_j corresponding to the various values of j. In concrete cases the matrices S_j can be further broken down, by using, in addition to the conservation of angular momentum, other conservation laws as well – conservation of parity, of isotopic spin, etc. We note that the system of functions Y^r_{jm} with given jm and various values of r is determined apart from a unitary transformation. It is convenient to choose the functions Y^r_{jm} in such a way as to secure the most complete breaking up of the matrices S_j that is possible. For example, for systems consisting of two nucleons it is convenient to choose them that the singlet states are separated from the triplets, and then owing to the conservation of the total spin the matrix S_j breaks up into singlet and triplet parts.

When Eq. (2.3) is used, we can write Eq. (2.2) in the form

$$(\mathbf{n}\sigma\alpha \,|\, S \,|\, \mathbf{n}'\sigma'\alpha') = \sum_j \sum_{rr'} (r\alpha \,|\, S_j \,|\, r'\alpha')\, W^{rr'}_j(\mathbf{n}\sigma;\ \mathbf{n}'\sigma'), \qquad (2.4)$$

where

$$W^{rr'}_j(\mathbf{n}\sigma,\ \mathbf{n}'\sigma') = \sum_{m=-j}^{j} Y^r_{jm}(\mathbf{n}\sigma)\, Y^{r'*}_{jm}(\mathbf{n}'\sigma'). \qquad (2.5)$$

We indicate certain simple properties of the operators $W^{rr'}_j$ that follow directly from the definition (2.5) and the orthogonality condition (2.1):

Hermitian character

$$(W^{rr'}_j(\mathbf{n}\sigma;\ \mathbf{n}'\sigma'))^* = W^{r'r}_j(\mathbf{n}'\sigma';\ \mathbf{n}\sigma), \qquad (2.6)$$

orthogonality

$$\sum_{\sigma'} \int d\Omega'\, W^{rr_1}_j(\mathbf{n}\sigma;\ \mathbf{n}'\sigma')\, W^{r_1 r_0 *}_{j'}(\mathbf{n}'\sigma';\ \mathbf{n}_0 r_0) = \delta_{jj'}\delta_{r_1 r_1} W^{rr*}_j(\mathbf{n}\sigma;\ \mathbf{n}_0\sigma_0), \qquad (2.7)$$

completeness

$$\sum_{jr} W^{rr}_j(\mathbf{n}\sigma;\ \mathbf{n}'\sigma') = \delta_{\mathbf{n}\mathbf{n}'}\delta_{\sigma\sigma'}. \qquad (2.8)$$

In what follows we shall need the equation

$$\sum_{\sigma} W^{rr'}_j(\mathbf{n}\sigma;\ \mathbf{n}\sigma) = \frac{2j+1}{4\pi}\,\delta_{rr'}, \qquad (2.9)$$

which follows easily from the orthogonality conditions (2.1) if we note that as an invariant function of the single vector **n** the left-hand member of Eq. (2.9) must be a constant.

Taking into account the condition (2.8), we easily find for the operator $R = S - 1$ a representation analogous to Eq. (2.4)

$$(\mathbf{n}\sigma\alpha \,|\, R \,|\, \mathbf{n}'\sigma'\alpha') = \sum_j \sum_{rr'} (r\alpha \,|\, S_j - I_j \,|\, r'\alpha')\, W^{rr'}_j(\mathbf{n}\sigma;\ \mathbf{n}'\sigma'); \qquad (2.10)$$

where

$$(r\alpha \,|\, I_j \,|\, r'\alpha') = \delta_{rr'}\delta_{\alpha\alpha'}.$$

In general, representations of the type (2.4) exist for any operator invariant with respect to rotations. Such operators are characterized by the fact that in the angular momentum representation their matrices are diagonal with respect to the quantities jm and do not depend on m, i. e., are of a form analogous to Eq. (2.3). Therefore all of the considerations leading to the expression (2.4) hold for such operators. In the Appendix we shall make use of this remark to accomplish the separation of the angular variables.

Let us consider the form of the operators W^{rr}_j for the simplest cases. For spin 0, the index r takes one value, which can be omitted. The functions $Y_{jm}(\mathbf{n})$ are identical with the ordinary spherical functions $Y_{jm}(\theta, \varphi)$, where θ and φ are the polar angles of the vector **n**. By means of the addition theorem for the Legendre polynomials it is easy to establish the equation

$$W_j(\mathbf{n};\ \mathbf{n}') = \frac{2j+1}{4\pi} P_j(\mathbf{n}\mathbf{n}'), \qquad (2.11)$$

where $P_j(x)$ is the Legendre polynomial (unnormalized).

The case of spin ½, corresponding to the system π-meson + nucleon, is less trivial. As the functions Y^r_{jm} we take the spherical spinors. The index r takes two values ±, corresponding to the two different states with a fixed total angular momentum j, for which the quantity j is connected with the orbital angular momentum

l by the equations $j = l \pm \frac{1}{2}$. The operators W have the following form:

$$\begin{aligned} W_j^{++} &= \frac{1}{4\pi}[P'_{j+1/2}(\mathbf{nn}') - P'_{j-1/2}(\mathbf{nn}')(\sigma\mathbf{n})(\sigma\mathbf{n}')]; \\ W_j^{--} &= \frac{1}{4\pi}[-P'_{j-1/2}(\mathbf{nn}') + P'_{j+1/2}(\mathbf{nn}')(\sigma\mathbf{n})(\sigma\mathbf{n}')]; \\ W_j^{+-} &= \frac{1}{4\pi}[P'_{j-1/2}(\mathbf{nn}')(\sigma\mathbf{n}) - P'_{j+1/2}(\mathbf{nn}')(\sigma\mathbf{n}')]; \\ W_j^{-+} &= \frac{1}{4\pi}[-P'_{j+1/2}(\mathbf{nn}')(\sigma\mathbf{n}) + P'_{j-1/2}(\mathbf{nn}')(\sigma\mathbf{n}')]. \end{aligned} \tag{2.12}$$

In these equations $P_l'(x) = (d/dx)P_l(x)$, and σ are the Pauli spin matrices. The operators (2.12) are the same as the invariant polynomials defined in Ref. 2. For the system nucleon + photon the expressions for the operators W can be found in Ref. 3. We shall devote space here to the details of the determination of the explixit form of the operators W; we merely remark that in the general case the operators can be calculated in closed form by means of Gel'fand's generalized spherical functions.[4]

3. UNITARY PROPERTY OF THE S-MATRIX GENERALIZED PHASE ANALYSIS

We now consider the consequences that follow from the condition that the S-matrix be unitary.

From Equation (2.3) it can be seen that the diagonal blocks S_j must be unitary matrices. The condition that the matrices S_j be unitary imposes definite connections on their matrix elements, and thus reduces the number of essential parameters involved in the general expression (2.4) for the S-matrix. We assume that it is possible to carry out in a general form the further splitting up of the matrices S_j into diagonal blocks. These blocks will also be unitary matrices, which leads to a further reduction of the number of essential parameters in the S-matrix. We consider the extreme case of complete splitting-up.

In this case the condition that S_j be unitary leads to the relation

$$(r\alpha|S_j|r'\alpha') = \exp\{2i\delta_{jr\alpha}\}\,\delta_{rr'}\,\delta_{\alpha\alpha'}. \tag{3.1}$$

Here $\delta_{jr\alpha}$ are real numbers, and the factor 2 is placed in the exponent in order to obtain a more complete analogy with the equations of phase analysis. Substituting (3.1) into the general formula (2.4), we find that in this special case the S-matrix has the form

$$(\mathbf{n}\sigma\alpha|S|\mathbf{n}'\sigma'\sigma') = \delta_{\alpha\alpha'}\sum_{jr}\exp\{2i\delta_{jr\alpha}\}\,W_j^{rr}(\mathbf{n}\sigma;\mathbf{n}'\sigma'). \tag{3.2}$$

From Eq. (3.2) the various formulas of phase analysis follow as special cases. For the particle with spin zero, taking into account Eqs. (1.6), (2.10), and (2.11), we obtain the scattering amplitude F in the form

$$F = \frac{1}{2ip_0}\sum_j(2j+1)(e^{2i\delta_j}-1)P_j(\mathbf{nn}_0),$$

which agrees with the well-known formula of scattering theory.

For the system π-meson + nucleon a complete spiitting-up also takes place owing to the laws of conservation of parity and isotopic spin. The corresponding formulas of phase analysis can be found in Ref. 2.

It must be pointed out that a complete breaking-up of the matrices S_j on the basis of the general conservation laws alone is possible only in exceptional cases. More generally speaking, only a partial breaking-up can be achieved. In this case the simple formula (3.2) must be replaced by the general formula (2.4). If in Eq. (2.4) the maximum possible splitting-up of the matrices S_j has been carried out, then, using the unitary property, we can express the scattering amplitude of the partial waves in terms of a certain number of parameters. In the general case these parameters play precisely the same role as the scattering phases do in the simplest cases. Ordinarily the number of these parameters is not large, and we arrive in this way at a generalized phase analysis, the merit of which is that without the solution of the dynamical problem one obtains the general form of the scattering amplitude, containing the minimum number of arbitrary parameters.

The actual values of these parameters can be obtained from the solution of the dynamical problem or by means of the analysis of experimental data. But even without fixing the values of the parameters it often turns out to be possible to draw certain general conclusions about the character of the scattering, and in particular about the shape of the angular distribution.

In the general case the differential scattering cross-section is expressed by the formula (1.7).

We state the expression for the total cross-section for an unpolarized beam, which is obtained from Eq. (1.7) by integration over all final states and averaging over the spin of the initial state. Using Eqs. (2.6) – (2.10) and the unitary property of the matrices S_j, we find

$$\sigma = \frac{2\pi}{N_0 p_0^2}\sum_{jr}(2j+1)\left[-\mathrm{Re}\,(r\alpha_0\,|\,R_j\,|\,r\alpha_0)\right]. \quad (3.3)$$

Here N_0 is the number of orientations of the spin in the initial state. For a particle with spin zero, $R_j = e^{2i\delta_j} - 1$, and Eq. (3.3) goes over into the well-known expression of scattering theory

$$\sigma = \frac{4\pi}{p_0^2}\sum_j (2j+1)\sin^2\delta_j.$$

APPENDIX. SEPARATION OF ANGULAR VARIABLES

Using the equation of the stationary scattering problem as an example, we shall show how the separation of the angular variables can be carried out in the general case by means of the operators W.

The scattering amplitude R (not on the energy surface) defined in Eq. (1.1), satisfies the equation

$$\begin{aligned}
&-(1/2\pi i)\,(\varepsilon\mathbf{n}\sigma\,|\,R\,|\,\varepsilon_0\,\mathbf{n}_0\,\sigma_0) = (\varepsilon\mathbf{n}\sigma\,|\,V\,|\,\varepsilon_0\,\mathbf{n}_0\,\sigma_0) \\
&\quad + \sum_{\sigma'}\int d\varepsilon'\,d\Omega'\,(\varepsilon\mathbf{n}\sigma\,|\,V\,|\,\varepsilon'\,\mathbf{n}'\,\sigma') \\
&\quad \times\ \delta_+(\varepsilon'-\varepsilon_0)\,(\varepsilon'\,\mathbf{n}'\,\sigma'\,|\,R\,|\,\varepsilon_0\,\mathbf{n}_0\,\sigma_0).
\end{aligned} \quad (1)$$

We assume that the interaction Hamiltonian V is invariant with respect to rotations and consequently permits an expansion analogous to Eq. (2.4). It is obvious that in this case R also has such an expansion:

$$\begin{aligned}
&(\varepsilon\mathbf{n}\sigma\,|\,V\,|\,\varepsilon'\,\mathbf{n}'\,\sigma') \\
&\quad = \sum_j\sum_{rr'}(\varepsilon r\,|\,V_j\,|\,\varepsilon'\,r')\,W_j^{rr'}(\mathbf{n}\sigma;\,\mathbf{n}'\,\sigma'), \\
&(\varepsilon\mathbf{n}\sigma\,|\,R\,|\,\varepsilon'\,\mathbf{n}'\,\sigma') \\
&\quad = \sum_j\sum_{rr'}(\varepsilon r\,|\,R_j\,|\,\varepsilon'\,r')\,W_j^{rr'}(\mathbf{n}\sigma;\,\mathbf{n}'\,\sigma').
\end{aligned} \quad (2)$$

Substituting Eq. (2) into Eq. (1) and taking into account the orthogonality conditions (2.7), we obtain a system of integral equations in which the angular variables are eliminated.

$$\begin{aligned}
&-\frac{1}{2\pi i}\,(\varepsilon r\,|\,R_j\,|\,\varepsilon_0\,r_0) = (\varepsilon r\,|\,V_j\,|\,\varepsilon_0\,r_0) \quad (3) \\
&+\sum_{r'}\int d\varepsilon'\,(\varepsilon r\,|\,V_j\,|\,\varepsilon'\,r')\,\delta_+(\varepsilon'-\varepsilon_0)\,(\varepsilon' r'\,|\,R_j\,|\,\varepsilon_0\,r_0).
\end{aligned}$$

The system (3) takes the simplest form in the case of complete resolution of the matrices V_j, i.e., when we have the equation

$$(\varepsilon r\,|\,V_j\,|\,\varepsilon'\,r') = (\varepsilon\,|\,V_j\,|\,\varepsilon')\,\delta_{rr'}.$$

In this case the system of equations (3) breaks up into individual equations involving the quantities $(\epsilon r_0\,|\,R_j\,|\,\epsilon_0\,r_0)$.

---

[1] J. M. Blatt and L. C. Biedenharn, Rev. Mod. Phys. **24**, 258 (1952).

[2] Tamm, Gol'fand and Fainberg, J. Exptl. Theoret. Phys. (U.S.S.R.) **26**, 649 (1954).

[3] V. I. Ritus, J. Exptl. Theoret. Phys. (U.S.S.R.) **27**, 660 (1954).

[4] I. M. Gel'fand and Z. Ia. Shapiro, Usp. Mat. Nauk **7**, 3 (1952).

[5] W. Pauli, *Meson Theory of Nuclear Forces*, IIL (Foreign Lit. Press), 1947 (Russian translation).

[6] M. Gell-Mann and M. L. Goldberger, Phys. Rev. **91**, 398 (1953).

[7] P. A. M. Dirac, *The Principles of Quantum Mechanics*, Moscow-Leningrad, 1937 (Russian translation).

Translated by W. H. Furry
43

SOVIET PHYSICS JETP VOLUME 4, NUMBER 1 FEBRUARY, 1957

The Antiferromagnetism of Anhydrous Sulfates of Ni^{++}, Fe^{++}, Co^{++} and Cu^{++}

A. S. BOROVIK-ROMANOV, V. R. KARASIK AND N. M. KREINES
All-Union Scientific Research Institute of Physicotechnical and Radiotechnical Measurements

(Submitted to JETP editor January 25, 1956)
J. Exptl. Theoret. Phys. (U.S.S.R.) 31, 18-24 (July, 1956)

The temperature dependence of magnetic susceptibility has been studied in the temperature range 12 to 300° K, for the four anhydrous sulfates $NiSO_4$, $FeSO_4$, $CoSO_4$ and $CuSO_4$. For the first three sulfates, the susceptibility maximum characteristic of an antiferromagnetic transition was observed. It is hypothesized that in $CuSO_4$ at 35° K, half the Cu^{++} ions form an antiferromagnetic array. It is shown that the magnetic susceptibility of $NiSO_4$, below the Curie point, decreases with temperature according to a quadratic law.

1. INTRODUCTION

ANTIFERROMAGNETISM was first predicted theoretically by Landau[1] and was observed experimentally by Shubnikov and Trapeznikova[2] and by Shalyt[3] in the special case of a layered ordering in the compounds $FeCl_2$, $CoCl_2$ and $NiCl_2$. In the ensuing years a considerable number of chemical compounds of the iron group, showing characteristic ferromagnetic properties, were studied (see, for example, the review by Nagamiya, Yosida and Kubo[4]). The chief shortcoming of most of these studies was that the experimental data obtained in them were insufficient for establishing the temperature dependence of the magnetic susceptibility below the Curie point.

In the present study, the magnetic properties of anhydrous sulfates of nickel, iron, cobalt and copper were investigated. X-ray analysis[5] of these compounds shows that in them the shortest distance between magnetic ions is less than 5 A. This provided grounds for expecting antiferromagnetism to exist at liquid hydrogen temperatures. However, results obtained in 1924 by Jackson[6] on the magnetic susceptibility of $NiSO_4$, $FeSO_4$ and $CoSO_4$ at hydrogen and nitrogen temperatures were insufficient for drawing any conclusions in regard to an antiferromagnetic transition in these compounds.

2. APPARATUS AND SPECIMENS

The magnetic susceptibility was measured by the Faraday method, with apparatus developed earlier by Borovik-Romanov and Kreines[7]. This apparatus permitted continuous coverage of the broad temperature range from 12 to 300° K. The temperature was measured with a copper-constantan thermocouple, calibrated against a standard resistance thermometer[8]. The error of measurement at hydrogen temperatures was not over ±0.5° C; with increasing temperature it decreased to ±0.1°. The susceptibility measurement was made at several values of field intensity from 500 to 2500 Oe (oersteds). The error in the absolute determination of the susceptibility was not over ±5%, and in the relative determination less than ±2%. No correction was made for the diamagnetism of $SO_4^{=}$, since it amounted to less than 1%.

All the specimens of anhydrous sulfates that were studied were obtained by dehydration of the corresponding crystalline hydrates. The original products used were of "ch. d. a" make. An anhydrous sample of $NiSO_4$ was obtained by calcination of the heptahydrate at a temperature of about 500° C for two to three hours. Observations were also made on a sample dehydrated by melting of $NiSO_4 \cdot 7H_2O$ in ammonium sulfate and subsequent evaporation of the melt[9]. In both cases the sample was obtained in the form of a fine-grained yellow powder.

The anhydrous sample of $FeSO_4$ was made by heating the heptahydrate in a stream of pure dry hydrogen at about 300° C for four hours. A sample obtained in this way could contain up to 3% $Fe_2(SO_4)_3$. The anhydrous sample of $CoSO_4$ was obtained by heating $CoSO_4 \cdot 7H_2O$ for five hours at 500° C. The results presented below relate to this sample, which had the form of a pale violet powder. Another sample was also studied; it was obtained by evaporation of a solution of $CoSO_4 \cdot 7H_2O$ in concentrated sulfuric acid[10]. By this method fine violet crystals were obtained. Upon cooling, these crystals crumble into a powder and lose their bright color. The magnetic properties of this powder differ from the magnetic properties of $CoSO_4$ obtained by calcination. This is of course connected with the fact that crystals obtained by evaporation from a solution contain a certain amount of H_2SO_4.

The anhydrous $CuSO_4$ was obtained in the form of a white powder by heating of blue vitriol to 300° C with constant stirring over a period of two hours.

TABLE I

Author	$\chi_M \cdot 10^3$		
	$NiSO_4$	$FeSO_4$	$CoSO_4$
Jackson[6]	4.13	10.3	9.63
Present work	4.97	12.4	9.87

3. RESULTS OF THE MEASUREMENTS

The magnetic susceptibility of all four anhydrous sulfates was measured at temperatures from 13 to 300° K. Table I shows the values obtained by us for the molar magnetic susceptibility of the three sulfates $NiSO_4$, $FeSO_4$ and $CoSO_4$ at room temperature ($T = 290°$ K). The magnetic susceptibility of these sulfates was studied earlier by Jackson[6], whose data are also shown in Table I. The low values obtained by Jackson can be attributed to incomplete dehydration of the samples studied by him.

Figure 1 shows the temperature dependence of the molar magnetic susceptibility of the three sulfates. In all of them one observes the characteristic maximum of the susceptibility at Curie temperatures $T_C = 37°$ K for $NiSO_4$, 21° K for $FeSO_4$ and 15.5° K for $CoSO_4$. In Jackson's work, measurements were made only in baths of liquid hydrogen and liquid nitrogen; consequently, he was unable to detect these maxima. At temperatures appreciably higher than T_C, the Curie-Weiss law

$$\chi = C/(T + \Theta) \qquad (1)$$

is obeyed by all four sulfates, with the values of the constants C and Θ listed in Table II.

TABLE II

Compound	Range of validity of Curie-Weiss law T in °K	C_M	Θ
$NiSO_4$	45—300	1.83	82
$FeSO_4$	40—300	3.98	30.5
$CoSO_4$	95—300	3.37	47
$CuSO_4$	40—300	0.45	55

The results obtained for the anhydrous sample of $CuSO_4$ are shown in Fig. 2. The magnetic susceptibility of this compound was measured earlier in the Leiden laboratory, but likewise only in baths of liquid hydrogen and nitrogen. Those results, also, are shown in Fig. 2. The chief difference is observed at temperatures below 20° K, where, according to our measurements, the susceptibility noticeably increases, but according to the data of the Leiden laboratory it depends little on temperature. This is perhaps attributable to insufficient heat exchange between the bath and the specimen in the apparatus used in the Leiden laboratory. In agreement with the results of the Leiden laboratory, we observed a slight dependence of the susceptibility on the field at hydrogen temperatures. Upon change of the magnetic field from 1800 to 4500 Oe, the susceptibility decreased 10%. Note the abrupt break in the curve in the neighborhood of 35° K.

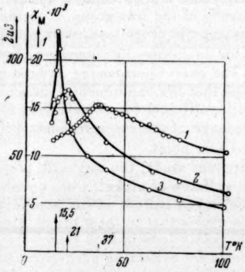

FIG. 1. Temperature dependence of the molar magnetic susceptibility χ_M of anhydrous sulfates: *1*, $NiSO_4$; 2, $FeSO_4$; *3*, $CoSO_4$. The values of T_C are shown by the arrows.

4. DISCUSSION OF RESULTS

Our results on the temperature dependence of the magnetic susceptibility of the first three sulfates show that they all undergo a transition to the antiferromagnetic state at T_C, corresponding to the susceptibility maximum. Hammel[5] carried out a detailed x-ray study (by the powder method) of all the anhydrous sulfates under consideration. He reached the conclusion that their structure is very nearly rhombic with four molecules in the unit cell. The lattice parameters obtained by Hammel are shown in Table III. We do not at

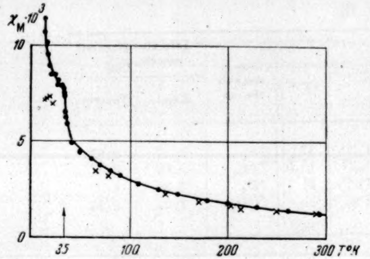

FIG. 2. Temperature dependence of the molar magnetic susceptibility χ_M of anhydrous $CuSO_4$. ×, results of the Leiden laboratory[11]; ●, data from the present work.

present have enough information to determine what the magnetic structure of the sulfates under investigation is in the antiferromagnetic state. This requires x-ray and magnetic studies of monocrystals. However, consideration of the extant data provides a basis for some preliminary conclusions. The lattice of magnetic ions in the anhydrous sulfates can be divided into four sublattices. The arrangement of nearest neighbors about the ions of each of these sublattices will be different. Consequently, the interactions between each pair of sublattices will likewise be different.

In a system of four sublattices it can happen that the interaction between one pair of sublattices differs appreciably from the interaction of another pair. Then, if the two sublattices of the first pair interact in a similar manner to those of the second pair, the ordering of magnetic ions in the first pair of sublattices will occur independently of, and earlier than, the onset of ordering of ions in the other pair. Our observed temperature dependence of the magnetic susceptibility of $CuSO_4$ can be explained by supposing that at $T_C = 35°$ K half the ions undergo a transition to an antiferromagnetic state. Then above this temperature, the magnetic susceptibility will obey the Curie-Weiss law. The quantity Θ will be proportional to the sum of all the interactions. Below the transition point, the susceptibility will be composed of two parts,

$$\chi = \chi_p + \chi_{af} \qquad (2)$$

The antiferromagnetic part χ_{af} can be described approximately by the formula

$$\chi_{af} = \frac{C}{6(T_C + \Theta)}\left[2 + \left(\frac{T}{T_C}\right)^2\right] \qquad (3)$$

The paramagnetic part χ_p can be described as before by the Curie-Weiss law (1), with constants $C' = C/2$ and $\Theta' < \Theta$.

In Fig. 3 our results for $CuSO_4$ are shown as a plot of $1/\chi$ against T. The dotted curve was calculated by formula (2), with the value of Θ' taken as 12°. We see that the outcome of the calculation is not inconsistent with the experimental results. For final confirmation of the proposed interpretation, investigations of the magnetic and thermal properties of $CuSO_4$ at helium temperatures are being undertaken.

Our hypothesis is also supported by experimental results of Stout[12] on the specific heat of $CuSO_4$. Stout observed on the specific heat curve the anomaly characteristic of a second-order phase transition, with a maximum at $T = 34.8°$ K. The experimental value of the entropy corresponding to this anomaly is 0.48 cal degree^{-1} mol^{-1}; this is appreciably less than the theoretical value, $R \ln 2 = 1.377$ cal degree^{-1} mol^{-1}, that should be obtained if all the ions went over to an antiferromagnetic state.

In the last column of Table III are given the values of the effective magnetic moments ($\mu_{eff} = \sqrt{3kC/N\beta^2}$) calculated from our experimental data, and the theoretical values [$\mu_{eff} = 2\sqrt{S(S+1)}$] calculated on the assumption of complete "quenching" of the orbital moment[13]. Comparison of these results shows that for quantitative explanation of the observed values of μ_{eff} in anhydrous slufates, we require a precise calculation of the splitting of the levels by the crystalline field. The crystalline fields have an especially pronounced effect on the magnetic properties of the Co^{++} ion.

In Fig. 4 are shown the results on sulfates of nickel, iron and cobalt, plotted with coordinates $1/\chi$ and T. We see that the experimental points for $NiSO_4$ and $FeSO_4$ deviate negligibly from the straight line corresponding to the Curie-Weiss law. The slight rise in the curve for $NiSO_4$ can be attributed to the effect of short-range order above the Curie point[14]. The results obtained for $FeSO_4$ must be regarded as only qualitative, because of the possible presence in the sample of decomposition products, formed during the calcination. In the case of $CoSO_4$ we observe below 100° K a very

TABLE III

Compound	Lattice parameters[8]				T_C in °K	Ground state of the ion	Effective magnetic moment, μ_{eff}	
	a	b	c	$a:b:c$			Exptl.	Theoret.
$NiSO_4$	4.62	6.51	8.49	0,71 : 1 : 1.30	37	$^3F_4$	3.82	2.83
$CoSO_4$	4.65	6.66	8.46	0.69 : 1 : 1.27	15.5	$^4F_{9/2}$	5.65	3.87
$FeSO_4$	4.82	6.81	8.67	0.71 : 1 : 1.27	21	$^5D_4$	5.20	4.90
$CuSO_4$	4.88	6.66	9.32	0.73 : 1 : 1.25	35	$^2D_{5/2}$	1.91	2.73

appreciable deviation of the experimental curve from the straight line that describes the results in the higher-temperature range. At the transition point, the susceptibility exceeds by almost a factor 2 the value extrapolated along the straight line. The anomalous behavior of the magnetic properties of cobalt is connected with a peculiarity of the splitting of the ground level of the ion by the crystalline field[15,16]. Whereas in the ions Ni^{++}, Fe^{++} and Cu^{++} the splitting of the orbital levels by the crystalline field results in a singlet ground state, in Co^{++} it results in a triplet. This causes a strong anisotropy of the magnetic properties of compounds containing the Co^{++} ion. Each level of the triplet possesses a fourfold spin degeneracy. This degeneracy is removed by spin-orbit interaction, and a Kramers six-doublet system is obtained. Abragam and Pryce[16] showed that the difference between the energies of the lower two doublets may be of the order of 100° K. The calculation of Abragam and Pryce relates to hydrated complex salts of cobalt. However, the pattern of the splitting should be essentially the same in an anhydrous sulfate. The temperature dependence that we have observed in the susceptibility is then easy to explain. At high temperatures, both the lower doublets are filled, and the susceptibility varies in accordance with the Curie-Weiss law. Below 100° K a preferential filling of the lower doublet begins, and this leads to an abrupt deviation from the Curie-Weiss law. At the same time the anisotropy of the magnetic properties should suddenly increase, so that at the Curie point $\chi_{\parallel}$ is several times larger than $\chi_{\perp}$. This causes a sudden decrease of susceptibility below T_C and accounts for the fact that as T approaches 0, the susceptibility approaches a value appreciably smaller than $(2/3) \times \chi(T_C)$.

For anhydrous $NiSO_4$, the Curie point is high enough to permit a conclusion to be drawn from our measurements regarding the law of temperature dependence of the magnetic susceptibility below the Curie point. In Fig. 5 the results of a measurement of the magnetic susceptibility of $NiSO_4$ are shown in coordinates χ and T^2. We see that almost up to the transition temperature itself, the law

$$\chi = a + b(T/T_C)^2, \tag{4}$$

is obeyed, where

$$a \approx 2/3\chi(T_C) \text{ and } b \approx 1/3\chi(T_C).$$

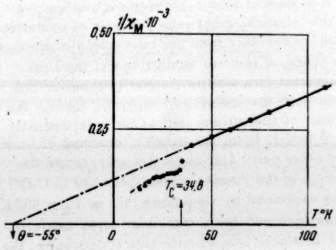

FIG. 3. Temperature dependence of the reciprocal of the molar magnetic susceptibility, $1/\chi_M$, of anhydrous $CuSO_4$. The dotted curve was drawn according to the formula (2).

This result is in agreement with deductions from the theory of spin waves[17,18].

5. CONCLUSIONS

The following basic conclusions can be drawn from this work:

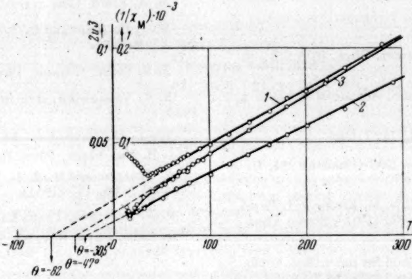

FIG. 4. Temperature dependence of the reciprocal of the molar magnetic susceptibility, $1/\chi_M$ of anhydrous $CuSO_4$. The dotted curve was drawn according to formula (2).

1. It has been shown that the three anhydrous sulfates $NiSo_4$, $FeSO_4$, and $CoSO_4$ undergo a transition to an antiferromagnetic state at temperatures 37, 21, and 15.5 ° K, respectively.

2. The curve of temperature variation of the magnetic susceptibility of $CuSO_4$ displays a sharp break at the temperature 35° K. This anomaly, as well as the general shape of the curve below 35° K, can be explained by supposing that below this temperature half the magnetic copper ions are ordered antiferromagnetically. The other half of the ions remain disordered and cause an increase of susceptibility.

3. The temperature dependence of the magnetic susceptibility of $CoSO_4$ at low temperatures deviates widely from the Curie-Weiss law in the paramagnetic range and displays an anomalously large decrease in the antiferromagnetic range. This is explained qualitatively by the splitting of the ground state of the Co^{++} ion by a crystalline field.

4. It has been shown that over the rather wide temperature interval 14 to 34° K, the magnetic susceptibility of $NiSO_4$ in the antiferromagnetic state varies with temperature according to a quadratic law.

In closing, the authors express their profound thanks to Prof. P. G. Strelkov for his constant interest in the work.

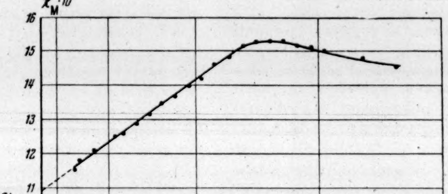

FIG. 5. Temperature dependence of the magnetic susceptibility of the anhydrous sulfate $NiSO_4$ below the Curie point.

---

[1] L. D. Landau, Physik. Z. Sowjetunion **4**, 675 (1933).

[2] O. N. Trapeznikova and L. V. Shubnikov, Physik. Z. Sowjetunion **7**, 66, 255 (1935).

[3] S. S. Shalyt, J. Exptl. Theoret. Phys. (U.S.S.R.) **8**. 518 (1938).

[4] Nagamiya, Yosida, and Kubo, Advances in Phys. **4**, 1 (1955).

[5] F. Hammel, Ann. Chim. **11**, 247 (1939).

[6] L. C. Jackson, Trans. Roy. Soc. (London) **224**, 1 (1924).

[7] A. S. Borovik-Romanov and N. M. Kreines, J. Exptl. Theoret. Phys. (U.S.S.R.) **29**, 790 (1955); Soviet Phys. JETP **2**, 657 (1956).

[8] Borovik-Romanov, Orlova, and Strelkov, *Establishment of the low-temperature scale between 90 and 10° K by means of the calibration chart of a set of standard platinum resistance thermometers*, Moscow, 1954.

[9] M. P. Klobb, Compt. rend. **114**, 836 (1892).

[10] M. A. Etard, Compt. rend. **87**, 602 (1878).

[11] W. J. De Haas and C. J. Gorter, Leid. Commun. No. 215a, 1931.

[12] J. W. Stout, J. Chem. Phys. **9**, 285 (L), (1941).

[13] S. V. Vonsovskii, *Recent research in magnetism*, 1953.

[14] Y.–Y. Li, Phys. Rev. **84**, 721 (1951).

[15] J. H. Van Vleck, Phys. Rev. **41**, 208 (1942).

[16] A. Abragam and M. H. L. Pryce, Proc. Roy. Soc. (London) **A206**, 173 (1951).

[17] P. W. Anderson, Phys. Rev. **79**, 350 and 705 (1950).

[18] R. Kubo, Phys. Rev. **87**, 568 (1952).

Translated by W. F. Brown, Jr.
3

SOVIET PHYSICS JETP VOLUME 4, NUMBER 1 FEBRUARY, 1957

Cascade Showers Produced by Electrons and Photons in Light and Heavy Elements

I. P. IVANENKO
Moscow State University

(Submitted to JETP editor April 18, 1955)
J. Exptl. Theoret. Phys. (U.S.S.R.) 31, 86-104 (July, 1956)

A regular method is given for plotting cascade curves from known moments. The cascade curves in light elements for primary electrons and photons with an energy E_0 are computed (E_0 is of the order of the critical energy for the given substance). A recursion formula is deduced which permits the calculation of all cascade curve moments with account of scattering, ionization losses and the dependence of the total photon absorption coefficient $\sigma(E)$ on energy for an arbitrary primary particle spectrum. Numerical calculations of the first two momenta of the electron distribution curve in lead were carried out for a primary photon spectrum of the form $1/E$. The cascade curves in lead were computed from the known moments $\overline{t}$ and $\overline{t^2}$. The results of the calculations are compared with experiment.

THE cascade theory of showers, developed in Ref. 1, describes with sufficient completeness the propagation of electron-photon high energy showers [when $\ln (E_0/\beta) > 1$] in light elements. The basic equations of the theory are usually solved by the method of functional transforms (the Laplace-Mellin transform in the energy E and the Laplace transform in the depth t)*. We employ this method because the asymptotic function (used in the theory) for the cross section of the processes of pair formation by photons and bremsstrahlung are homogeneous functions of the energy of the particles.

If the energy E_0 of the initial particle which starts the shower is not very great in comparison with the critical energy β for the given element, then we cannot obtain a solution of the basic equations by the method of functional transforms. The solution of the equations of cascade theory in analytic form in this energy region is of considerable mathematical difficulty. In the passage of electrons and photons through heavy elements, the formation of showers becomes very intense. We recall the difficulties which are encountered in the theory of showers for heavy elements: (1) the total photon absorption coefficient $\sigma(E)$ depends very strongly on the energy, σ changing from the value 0.773 for high energies to 0.24 at its minimum; (2) the scattering of the shower particles in heavy elements is very great.

A method was developed in Refs. 2 and 3 for the solution of the basic equations of cascade theory (integrated over the depth) in the variable σ, which permits us to obtain an expression for the "equilibrium" spectrum of electrons and photons and, using this spectrum to calculate successively, in principle, all the moments of the distribution function of the shower particles. The effect of scattering on the magnitude of the moments and the form of the curve for heavy elements was considered in Refs. 3 and 4. The treatment in Ref. 3 was highly approximate, since it was carried out without consideration of the ionization loss. A recursion formula was obtained in Ref. 4 which permits successive calculation of all the moments $\overline{t^n}$ of the distribution function, with consideration of scattering and ionization losses for an original spectrum of δ-shape. A recursion formula was obtained in Ref. 5 for the determination of the moments $\overline{t^n}$ without regard to scattering in the case of an arbitrary spectrum of the primary particles. The first two moments were calculated in lead for a spectrum of primary photons of the form $1/E$. The computed moments agree with experiment. However, inasmuch as scattering was not considered in this work, accuracy is lacking. For the solution of the fundamental equation of cascade theory, it is possible to approach the problem differently, i.e., to determine the function $N(E_0,0,t)$ (the number of particles with energy greater than zero at the depth t^n, created by an initial particle with energy E_0) along with its moments $\overline{t^n}(E_0, 0)$.

The purpose of the present work is the calculation, by the method of moments, of the cascade curves from primary electrons and photons of not very great energy E_0 in light and heavy elements.

---

* The depth t is measured in so-called "cascade" units.

In the first part of the work, explicit analytical expressions are derived for the first and second moments of cascade curves in light elements; the first three moments of cascade curves are calculated for light elements; these cascade curves are calculated by the use of available values of the moments. In the second section, a recursion formula is derived which permits successive calculation of all moments of the cascade curve with consideration of scattering and ionization losses for an arbitrary spectrum of the primary particles. This conclusion is a generalization of the results of Ref. 5, where a similar formula was obtained without taking scattering into account, and of Ref. 4, where a similar formula was obtained for a $\delta-$type spectrum with consideration of scattering. Numerical calculations are carried out for the first two moments of the electron distribution function in lead for a primary spectrum of the form $1/E$. According to the method developed in the first part of the work, the cascade curves are then computed for this same spectrum.

I. CASCADE SHOWERS IN LIGHT ELEMENTS

1. The basic equations of cascade theory have the form

$$L_1[P(E_0, E, t), \Gamma(E_0, E, t)] = \frac{\partial P(E_0, E, t)}{\partial t}; \quad (1)$$

$$L_2[P(E_0, E, t), \Gamma(E_0, E, t)] = \frac{\partial \Gamma(E_0, E, t)}{\partial t}.$$

Here $P(E_0, E, t)$ and $\Gamma(E_0, E, t)$ are distribution functions for electrons and photons at the depth t and energy E, L_1, L_2 are integro-differential operators (linear in P and Γ) which take into account pair formation by photons, bremsstrahlung and ionization losses for electrons. For small energies, the operators must also take the Compton effect into account[1]. The cascade curve--the total number of particles as a function of the depth--is determined by the relation

$$N(E_0, 0, t) = \int_0^{E_0} P(E_0, E, t)\, dE.$$

The moments of the cascade curves are determined by the expression

$$\overline{t^n}(E_0, 0) \quad (1a)$$

$$= \int_0^\infty N(E_0, 0, t)\, t^n\, dt \Big/ \int_0^\infty N(E_0, 0, t)\, dt.$$

A recursion formula was obtained in Ref. 3 which permits successive calculation of all moments of the cascade curve

$$\{\overline{t_P^n}(E_0, 0)\}^P \quad (2)$$

$$= \frac{n}{E_0} \int_0^{E_0} [P_P(E_0, E)\{\overline{t_P^{n-1}}(E, 0)\}^P$$

$$+ \Gamma_P(E_0, E)\{\overline{t_P^{n-1}}(E, 0)\}^\Gamma]\, E\, dE,$$

where the superscripts on P and Γ distinguish the moments of the electron distribution functions in a shower produced by an electron or a photon, respectively. $P_P(E_0, E)$ and $\Gamma_P(E_0, E)$ are the "equilibrium" spectra (integrated over the depth) of electrons and photons from the primary electron. Thus, in principle, the problem of the solution of the basic equations of the theory reduce to the finding of the equilibrium spectrum when one has recursion formulas of the type (2). An analytical expression for the equilibrium spectrum was first found by Tamm and Belen'kii[2] who solved approximately the basic equations of the theory, integrated over the depth. One can estimate the mathematical approximations used in this solution by the method of successive approximations developed in Ref. 6. The correction to the solution of Tamm and Belen'kii does not exceed 4.5%. The computation was carried out for $E_0/\beta = 2.29$; with increase in E_0, the correction diminishes.

The error introduced in the spectrum of Tamm and Belen'kii by the inaccuracy of the initial assumptions (in the equations, use was made of asymptotic relations for the cross section of processes of pair formation and bremsstrahlung which are strictly correct only for very high energies; the Compton effect was taken approximately into account; the yield of high energy electrons which is obtained in collisions of electrons of the shower with electrons of the medium was neglected) can be estimated only by comparison with the results of computations in which these simplifying assumptions were not made.

Rossi and Klapman[7], by integrating Eqs. (1), averaged over t, obtained $N_P(E_0, E)$ for a fixed value of E as a function of the primary energy E_0. The computation was carried out for air: $E = 10^7$ ev, $E_0 \geq 10^7$ ev; in the calculations, all processes were considered that take place in the substance as a result of radiation; exact formulas were obtained for the cross section. Pair creation, radiation in the field of the electrons and the effect of the density on the ionization loss were not considered. The spectrum of Tamm and Belen'kii did not differ by more than 4% from the spectrum computed by Rossi and Klapman.

Thus it can be said that for $E \geqq 10^7$ ev, in light elements, the approximate "equilibrium" spectrum differs from the exact by not more than 4%. We note that a mathematically exact solution of the equation (1), integrated over the depth, differs by 8.5% from the calculation of Rossi and Klapman. Consequently, the equilibrium spectrum of Tamm and Belen'kii is a better approximation to the actual case.

Richards and Nordheim[8], with the help of difficult computational methods, solved Eqs. (1) approximately (integrated over t). For $E/\beta < 1$, and also for $E/\beta > 1$, where the equation is applicable, the spectra of Tamm and Belen'kii and Richards and Nordheim coincide.

Carrying out calculations of the moments of the electron distribution function for the showers produced by photons of energy E_0, we get the following expressions

$$\{\bar{t}_P(E_0,\ 0)\}^{\Gamma} \tag{3}$$

$$= \frac{1}{f(0)}\int_0^{\varepsilon_0}\left(1+\frac{1}{\sigma(\varepsilon)}\right)\chi_2(\varepsilon_0,\varepsilon)\,d\varepsilon + \frac{1}{\sigma(\varepsilon_0)};$$

$$\{\bar{t}_P^2(E_0,\ 0)\}^{\Gamma} = \tau_{\Gamma_1}+\tau_{\Gamma_2}+\tau_{\Gamma_3}+\tau_{\Gamma_4}+\tau_{\Gamma_5}; \tag{4}$$

$$\tau_{\Gamma_1} = \frac{2}{[f(0)]^2}\int_0^{\varepsilon_0}\int_{\varepsilon_1}^{\varepsilon_0}\left(1+\frac{1}{\sigma(\varepsilon_1)}\right)$$

$$\times\left(1+\frac{1}{\sigma(\varepsilon_{11})}\right)\chi_2(\varepsilon_0,\varepsilon_1)\,\chi_2(\varepsilon_0,\varepsilon_{11})\,d\varepsilon_{11}\,d\varepsilon_1;$$

$$\tau_{\Gamma_2} = \frac{2}{f(0)}\int_0^{\varepsilon_0}\left(\frac{1}{\sigma(\varepsilon_0)}+\frac{1}{\sigma^2(\varepsilon_1)}+\frac{1}{\sigma(\varepsilon_0)\,\sigma(\varepsilon_1)}\right)\chi_2$$

$$\times(\varepsilon_0,\varepsilon_1)\,d\varepsilon_1 + \frac{2}{\sigma^2(\varepsilon_0)};$$

$$\tau_{\Gamma_3} = \frac{2}{[f(0)]^2}\int_0^{\varepsilon_0}\int_{\varepsilon_1}^{\varepsilon_0}\left(1+\frac{1}{\sigma(\varepsilon_1)}\right)\left(1+\frac{1}{\sigma(\varepsilon_{11})}\right)\chi_2(\varepsilon_0,\ \varepsilon_{11})$$

$$\times[\chi_1(\varepsilon_{11},\ \varepsilon_1)-\chi_2(\varepsilon_0,\ \varepsilon_1)]\,d\varepsilon_{11}\,d\varepsilon_1;$$

$$\tau_{\Gamma_4} = \frac{2}{[f(0)]^2}\int_0^{\varepsilon_0}\int_{\varepsilon_1}^{\varepsilon_0}\left(1+\frac{1}{\sigma(\varepsilon_1)}\right)\frac{1}{\sigma(\varepsilon_{11})}\chi_2$$

$$\times(\varepsilon_0,\varepsilon_{11})\,[\chi_2(\varepsilon_{11},\varepsilon_1)-\chi_1(\varepsilon_0,\varepsilon_1)]\,d\varepsilon_{11}\,d\varepsilon_1;$$

$$\tau_{\Gamma_5} = \frac{2}{[f(0)]^2}\int_0^{\varepsilon_0}\int_{\varepsilon_1}^{\varepsilon_0}\left(1+\frac{1}{\sigma(\varepsilon_1)}\right)$$

$$\times\frac{\partial\chi_1(\varepsilon_{11},\ \varepsilon_1)}{\partial\varepsilon_{11}}\varepsilon_{11}\,\chi_2(\varepsilon_0,\varepsilon_{11})\,d\varepsilon_{11}\,d\varepsilon_1,$$

where

$$\varepsilon_0 = f(0)\,E_0/\beta;\quad \varepsilon = f(0)\,E/\beta;$$

$$f(0) = 2.29;\ \sigma_0 = 0{,}773;$$

$$\chi_1(\varepsilon_0,\ \varepsilon) = \varepsilon e^{\varepsilon}\int_{\varepsilon}^{\varepsilon_0}\frac{e^{-x}}{x^2}\,dx;\ \chi_2(\varepsilon_0,\varepsilon)$$

$$= \chi_1(\varepsilon_0,\varepsilon) - \frac{\varepsilon}{\varepsilon_0^2}\left(1-e^{-(\varepsilon_0-\varepsilon)}\right).$$

Similar expressions for the moments of the electron distribution function in a shower produced by an electron of energy E_0 were obtained in Ref. 1. The integrals which enter into both these expressions are expressed by elementary functions, exponential integrals and rapidly converging series. Carrying out the appropriate steps, we get, in the case of the primary electron,

$$\{\bar{t}_P(E_0,0)\}^P = \frac{1+1/\sigma_0}{f(0)}\left\{\frac{1}{\varepsilon_0}-1-\frac{e^{-\varepsilon_0}}{\varepsilon_0}\right. \tag{5}$$

$$\left.+C+\ln\varepsilon_0-\mathrm{Ei}(-\varepsilon_0)\right\};$$

$$\tau_{P_4} = \frac{(2/\sigma_0)(1+1/\sigma_0)}{[f(0)]^2}\left\{-1{,}5\left(\frac{1}{\varepsilon_0}-\frac{e^{-\varepsilon_0}}{\varepsilon_0}-1\right)\right.$$

$$-0.5\left(\ln\varepsilon_0+C-\mathrm{Ei}(-\varepsilon_0)\right)$$

$$\left.-\int_0^{\varepsilon_0}e^{-x}\left(\frac{1}{2!2}+\frac{x}{3!3}+\ldots\right)dx\right\};$$

$$\tau_{P_2} = \frac{2}{f(0)\,\sigma_0^2}\left\{\frac{1}{\varepsilon_0}-1-\frac{e^{-\varepsilon_0}}{\varepsilon_0}\right.$$

$$\left.+C+\ln\varepsilon_0-\mathrm{Ei}(-\varepsilon_0)\right\},$$

$$\tau_{P_5} = \frac{2(1+1/\sigma_0)}{[f(0)]^2}\left\{2\left(\frac{1}{\varepsilon_0}-\frac{e^{-\varepsilon_0}}{\varepsilon_0}-1\right)\right. \tag{6}$$

$$\left.+\ln\varepsilon_0+C-\mathrm{Ei}(-\varepsilon_0)\right\},$$

$$\tau_{\Gamma_1}+\tau_{P_3} = \frac{2(1+1/\sigma_0)^2}{[f(0)]^2}(1+1/\sigma_0)^2$$

$$\left\{C\left(\frac{1}{\varepsilon_0}-\frac{e^{-\varepsilon_0}}{\varepsilon_0}-1+\ln\varepsilon_0+C-\mathrm{Ei}(-\varepsilon_0)\right)\right.$$

$$+(1-e^{-\varepsilon_0})\left(\frac{\ln^2\varepsilon_0}{2}+\frac{\ln\varepsilon_0}{\varepsilon_0}\right)$$

$$-\ln\varepsilon_0-0.5\int_0^{\varepsilon_0}\ln^2 x e^{-x}\,dx$$

$$+2\int_0^{\varepsilon_0}e^{-x}\left(\frac{1}{2!2}+\frac{x^2}{4!4}+\frac{x^4}{6!6}+\ldots\right)dx$$

$$+\int_0^{\varepsilon_0}e^{-x}\left[\frac{1}{2!}-\frac{x}{3!2}+\frac{x^2}{4!3}+\ldots\right]dx$$

$$\left.-\mathrm{Ei}(-\varepsilon_0)\int_0^{\varepsilon_0}\left(\frac{e^{-x}}{x^2}-\frac{1}{x^2}+\frac{1}{x}\right)dx\right\},$$

where $C = 0.5772$ is Euler's constant, $\mathrm{Ei}(-\epsilon) = -\int_{\epsilon}^{\infty} (e^{-x}/x)\,dx$.

In the case of a primary photon,

$$\{\overline{t}_P(E_0, 0)\}^{\Gamma} = \{\overline{t}_P(E_0, 0)\}^{P} + \frac{1 + 1/\sigma_0}{f(0)}\left(-0.5 + \frac{1}{\varepsilon_0} - \frac{1}{\varepsilon_0^2} + \frac{e^{-\varepsilon_0}}{\varepsilon_0^2}\right) + \frac{1}{\sigma_0}. \tag{7}$$

$$\begin{aligned}\{\overline{t_P^2}(E_0,0)\}^{\Gamma} &= \{\overline{t_P^2}(E_0, 0)\}^{P} \\ &+ \frac{2}{[f(0)]^2}\left[\left(1+\frac{1}{\sigma_0}\right)\left\{\left(1-\frac{1}{\sigma_0}\right)\left[0.5\left(C+\ln\varepsilon_0-\mathrm{Ei}(-\varepsilon_0)\right.\right.\right.\right. \\ &+ \left.\frac{1}{\varepsilon_0} - \frac{e^{-\varepsilon_0}}{\varepsilon_0} - 1\right) - 0.5\left(\frac{e^{-\varepsilon_0}}{\varepsilon_0^2} + \frac{1}{\varepsilon_0^2} - \frac{1}{\varepsilon_0} + 0.5\right)\Bigg] \\ &+ \left(\frac{1}{\sigma_0} - 1\right)\left[\frac{\varepsilon_0 - 1}{\varepsilon_0^2}\left(C + \ln\varepsilon_0 - \mathrm{Ei}(-\varepsilon_0)\right.\right. \\ &+ \left.\frac{1}{\varepsilon_0} - \frac{e^{-\varepsilon_0}}{\varepsilon_0} - 1\right) \\ &- \frac{e^{-\varepsilon_0}}{\varepsilon_0^2}\left(\frac{1}{\varepsilon_0} + e^{\varepsilon_0} - \frac{e^{\varepsilon_0}}{\varepsilon_0} - \mathrm{Ei}(\varepsilon_0) + \ln\varepsilon_0 + C\right)\Bigg] \\ &- \left[\frac{\varepsilon_0^2 - 2\varepsilon_0 + 2}{\varepsilon_0^2}\left(C + \ln\varepsilon_0 - \mathrm{Ei}(-\varepsilon_0)\right.\right. \\ &+ \left.\frac{1}{\varepsilon_0} - \frac{e^{-\varepsilon_0}}{\varepsilon_0} - 1\right) - \frac{e^{-\varepsilon_0}}{\varepsilon_0^2}\left(\varepsilon_0 - \frac{2}{\varepsilon_0} + \varepsilon_0 e^{\varepsilon_0} - 4e^{\varepsilon_0}\right. \\ &+ \left.\left. 2\left(\mathrm{Ei}(\varepsilon_0) - \ln\varepsilon_0 - C\right) + \frac{2e^{\varepsilon_0}}{\varepsilon_0} + 2\right)\right] \\ &+ \frac{1}{\sigma_0}\left[0.25 - 0.5\frac{\varepsilon_0 - 1}{\varepsilon_0^2}\right. \\ &- 0.5\frac{e^{-\varepsilon_0}}{\varepsilon_0^2} - \frac{1}{\varepsilon_0^2}\left(\mathrm{Ei}(-\varepsilon_0) - C - \ln\varepsilon_0 + \varepsilon_0\right) \\ &+ \left.\left.\frac{e^{-\varepsilon_0}}{\varepsilon_0^2}\left(e^{\varepsilon_0} - \mathrm{Ei}(\varepsilon_0) + \ln\varepsilon_0 + C - 1\right)\right]\right\} \\ &+ f(0)\left(1 + \frac{2}{\sigma_0}\right)\frac{1}{\sigma_0}\left(-0.5 + \frac{\varepsilon_0 - 1}{\varepsilon_0^2} + \frac{e^{-\varepsilon_0}}{\varepsilon_0^2}\right) \\ &+ \left.\frac{[f(0)]^2}{2}(\sigma_0 + 1)\tau_P + \frac{[f(0)]^2}{\sigma_0^2}\right],\end{aligned} \tag{8}$$

where $\mathrm{Ei}(\epsilon) = \int_{-\infty}^{\epsilon} (e^{x}/x)\,dx$.

The values of these moments are listed in Table I for values of ϵ_0 from 0.2 to 10. The third moment $\overline{t^3}$, which is in the form of unwieldy explicit formulas, was calculated by means of numerical integration.

For $E_0/\beta \gg 1$, Eqs. (5), (6) and (7) are written in the following form (with accuracy up to terms of order $1/\epsilon_0$):

$$\begin{aligned}\{\overline{t}_P(E_0, 0)\}^{P} &= \ln(E_0/\beta) + 0.41; \\ \{\overline{t}_P(E_0, 0)\}^{\Gamma} &= \ln(E_0/\beta) + 1{,}2; \\ \{\overline{t_P^2}(E_0, 0)\}^{P} - \{\overline{t}_P^2(E_0, 0)\}^{P} &= 1.76\ln(E_0/\beta) - 0.21; \\ \{\overline{t_P^2}(E_0, 0)\}^{\Gamma} - \{\overline{t}_P^2(E_0, 0)\}^{\Gamma} &= 1.76\ln(E_0/\beta) + 2.32.\end{aligned} \tag{9}$$

Values are given in Table II for these moments, for ϵ_0 from 15 to 2290. The values were computed from Eqs. (9) and from the formulas of Rossi and Greisen[10]:

$$\begin{aligned}\{\overline{t}_P(E_0, 0)\}^{P} &= 1{,}01\ln(E_0/\beta) + 0.4; \\ \{\overline{t}_P(E_0, 0)\}^{\Gamma} &= 1.01\ln(E_0/\beta) + 1.2; \\ \{\overline{t_P^2}(E_0, 0)\}^{P} - \{\overline{t}_P^2(E_0, 0)\}^{P} &= 1.61\ln(E_0/\beta) - 0.2; \\ \{\overline{t_P^2}(E_0, 0)\}^{\Gamma} - \{\overline{t}_P^2(E_0, 0)\}^{\Gamma} &= 1.61\ln(E_0/\beta) + 0.9.\end{aligned} \tag{10}$$

It is seen from Table II that the first and second moments, computed by Eqs. (9) and (10), differ from one another by not more than 1% over a wide energy range. Thus, the expression for the moments, according to Tamm and Belen'kii, does not differ markedly from the solution of the basic equation of cascade theory obtained by the method of Snyder. As shown in Ref. 1, Snyder's solution is the first term in the expansion of the total energy in powers of β/E_0. However, the method of Snyder permits us to find only the total number of particles as a function of the depth and does not give any possibility of calculating the energy spectrum of the particles.

2. For high energy showers, when $\ln(E_0/\beta) > 1$, we can determine the position of the maximum and the number of particles in the maximum of the cascade curve if the quantities $E_0/\beta, \overline{t}$ and $\overline{t^2}$ are known. For low energy showers, where $E_0/\beta \sim 1$, similar relations cannot be obtained, since the procedure employed in deriving the relations

$$t_{\max} \text{ and } N_{\max} \sim f(E_0/\beta, \overline{t}, \overline{t^2}),$$

TABLE I

ε_0	$\{\overline{t}_P\}^P$	$\{\overline{t}_P\}^\Gamma$	$\{\overline{t^2_P}\}^P$	$\{\overline{t^2_P}\}^\Gamma$	$\{\overline{t^3_P}\}^P$	$\{\overline{t^3_P}\}^\Gamma$
0.2	0.096	1.357	0.148	3.694		
0.4	0.188	1.421	0.301	3.899		
0.6	0.273	1,480	0,459	4.119		
0.8	0.353	1.536	0,619	4.375		
1.0	0.429	1.590	0.780	4,609	2.940	19.79
1.2	0.500	1.641	0,943	4.850		
1,4	0,568	1.691	1.107	5.083		
1,6	0.633	1.740	1,271	5.313		
1.8	0,694	1.785	1.434	5.540		
2.0	0,752	1,829	1,599	5.762	6.364	26.51
3.0	1.006	2.027	2.392	6,803	9.817	32.78
4,0	1.213	2,195	3,132	7.746	13.37	38.79
5.0	1.386	2.340	3.845	8.625	16.84	44.52
6.0	1,536	2,468	4.503	9.429	20.29	50.02
7.0	1.666	2.582	5,192	10,26	29.53	61.29
8.0	1.782	2.685	5.691	10.87	32.73	65.86
9.0	1.886	2.778	6.233	11.53	42.83	77.59
10.0	1,979	2,862	7.140	12.53	48.16	86.07

TABLE II

ε_0	$\{\overline{t}_P\}^P$		$\{\overline{t}_P\}^\Gamma$		$\{\overline{t^2_P}\}^P$		$\{\overline{t^2_P}\}^\Gamma$	
	according to Belen'kii	according to Rossi and Greisen	according to Belen'kii	according to Rossi and Greisen	according to Belen'kii	according to Rossi and Greisen	according to Belen'kii	according to Rossi and Greisen
15	2,290	2,298	3.080	3,098	8.343	8,108	13,40	13,52
20	2.577	2,589	3,367	3,389	10,24	9.992	15,74	15.87
25	2.800	2,814	3.590	3.614	11,84	11,56	17,66	17.81
30	2,983	2,999	3,773	3.799	13.22	12.94	19.32	19.47
40	3.270	3,289	4.060	4.089	15.52	15.22	22.06	22.22
63,6	3.734	3,757	4.524	4,557	19.58	19,27	26,84	27.02
229	5,015	5,051	5.805	5,851	33.04	32,73	42,64	42.55
2290	7,318	7,377	8,108	8,177	65.5	65.34	78,78	78.88

is equivalent to the method of steepest descents, usually employed in cascade theory. One can put the problem of the calculation of the cascade curve in terms of known moments $\overline{t^n}$; knowing all moments, we can, in principle, find the function itself. However, in practice, it is possible to find only the first 2-3 moments; therefore, one must find approximation formulas which describe the cascade curves with sufficient accuracy by means of the first 2-3 moments. In Ref. 1, the cascade curves are approximated for very high values of E_0 by a curve of the form

$$\exp(\alpha t^{1/2} - \gamma t). \tag{11}$$

The coefficients α and γ are so chosen that (11) gives the correct value of the area under the cascade curve (law of conservation of energy) and the first moment $\overline{t}$. For smaller E_0, we can look for the cascade curve in the form

$$\exp(\alpha t^{1/2} - \gamma t) + \chi e^{-\gamma t}. \tag{11′}$$

The coefficients α, γ, and χ are so chosen that (11′) gives correct results for the area under the curves $\overline{t}$ and $\overline{t^2}$. The cascade curves for lead were obtained in the work of Zatsepin[11] with the help of approximations similar to (11′).

The approximation used in Ref. 11 describes the cascade process satisfactorily for the case $\ln(E_0/\beta) > 1$ and $t > t_{\max}$. To determine the coefficients which enter into the approximating formula (11) we must solve a system of 3 transcendental equations, which greatly complicates the computation. We also note that in the method of Ref. 11 for constructing the curve from three moments, it is necessary to choose another form of the approximating dependence, which cannot be determined without detailed investigation. For the determination of the coefficients, we must solve a system of 4 transcendental equations.

We can suggest a regular method of constructing cascade curves, using a set of polynomials that are orthogonal in the interval $(0, \infty)$. We approximate the function $\varphi(x)$ by the sum of polynomials

$$\varphi(x) = A_0 + A_1 L_1^i(x) + A_2 L_2^i(x) + A_3 L_3^i(x) + \ldots \tag{12}$$

Here $L_n^i(x)$ are the Laguerre polynomials which are determined for real values of $i > -1$ by the equation[12]

$$L_n^i(x) = e^x \frac{x^{-i}}{n!} \frac{d^n}{dx^n} (e^{-x} x^{n+i}) \quad (i = 0, 1, 2, \ldots).$$

The general expression for the polynomial of n th order is given by

$$L_n^i(x) = \sum_{k=0}^{n} \frac{\Gamma(n+i+1)}{\Gamma(k+i+1)} \frac{(-x)^k}{k!\,(n-k)!}.$$

The Laguerre polynomials are orthogonal in the interval $(0, \infty)$ with weight $x^i e^{-x}$:

$$\int_0^\infty e^{-x} x^i L_m^i(x) L_n^i(x)\,dx = \begin{cases} 0 & \text{for} \quad m \neq n,\ i > -1 \\ \dfrac{\Gamma(n+i+1)}{n!} & \text{for} \quad m = n,\ i > -1 \end{cases}$$

$$n = 0, 1, 2, 3, \ldots$$

The approximate improves as the mean square error

$$M = \int_0^\infty e^{-x} x^i (A_0 + A_1 L_1^i(x) + A_2 L_2^i(x) + A_3 L_3^i(x) + \ldots - \varphi(x))^2\,dx$$

grows smaller. The coefficients A_n, determined from the condition of minimum mean square error, are equal to

$$A_n = \frac{n!}{\Gamma(n+i+1)} \int_0^\infty e^{-x} x^i \varphi(x) L_n^i(x)\,dx.$$

We replace x in Eq. (12) by γt, where γ is an arbitrary positive number, and multiply both parts by $(\gamma t)^i e^{-\gamma t}$; introducing the notation

$$(\gamma t)^i e^{-\gamma t} \varphi(\gamma t) = N(t), \tag{13}$$

we get

$$N(t) = (\gamma t)^i e^{-\gamma t} \sum_{n=0}^{\infty} A_n L_n^i(\gamma t). \tag{14}$$

The coefficients A_n in our case are equal to*

$$A_n = \frac{\gamma n!}{\Gamma(n+i+1)} \int_0^\infty N(t) L_n^i(\gamma t)\,dt. \tag{15}$$

3. We approximate the cascade curves from the primary photons with the help of the Laguerre polynomials $L_n^1(x)$

$$N(t) = \gamma t e^{-\gamma t} \sum_{n=0}^{k} A_n L_n^1(\gamma t). \tag{16}$$

Here

$$L_0^1(x) = 1; \quad L_1^1(x) = 2 - x; \quad L_2^1(x) = 3 - 3x + \frac{x^2}{2};$$

$$L_3^1(x) = 4 - 6x + 2x^2 - \frac{x^3}{6}.$$

In accordance with Eq. (15),

$$A_n = \frac{\gamma}{n+1} \int_0^\infty N(t) L_n^1(\gamma t)\,dt;$$

$$A_0 = \gamma \frac{E_0}{\beta}; \quad A_1 = \frac{\gamma}{2} \frac{E_0}{\beta} (2 - \gamma \{\overline{t_P}(E_0, 0)\}^\Gamma);$$

$$A_2 = \frac{\gamma}{3} \frac{E_0}{\beta} (3 - 3\gamma \{\overline{t_P}(E_0, 0)\}^\Gamma + \frac{\gamma^2}{2} \{\overline{t_P^2}(E_0, 0)\}^\Gamma), \text{ etc.}$$

The coefficient γ is taken to be equal to the overall absorption coefficient of the most penetrating part of the radiation--the photons. We recall that the cascade theory (see, for example, Ref. 1) makes it possible to calculate the dependence of the total number of particles in the shower on the depth t for particles of large energy $\ln(E_0/\beta) > 1$

---

* The coefficients A_n can be determined from the orthogonality condition of the Laguerre poylnomials. Multiplying Eq. (14) by $L_m^i(x)$ and integrating over x from 0 to ∞, we obtain expressions for the A_n that coincide with Eq. (15).

(in the work, formulas are obtained for the cascade curve from a primary electron). On the other hand, according to the approximation Eq. (16), we can compute the cascade curves from primary particles of high energy by making use of the first two moments ($k = 2$).

For a primary photon of high energy, it is easy to obtain the following exact formulas for the number of electrons:

$$\{N_P(E_0, 0, t)\}^\Gamma \tag{17}$$
$$= \frac{1}{2\pi i} \int_{\delta - i\infty}^{\delta + i\infty} H_1(s) D_1(s) \exp(\lambda_1(s) t + ys) \frac{ds}{s};$$

where

$$y = \ln \frac{E_0}{\beta}; \quad D_1(s) = \frac{2\sigma_0 [f(\lambda_1(s))]^s}{(\lambda_1(s) + \sigma_0) \Gamma(s-2)};$$
$$H_1(s) = \frac{\sigma_0 + \lambda_1(s)}{\lambda_1(s) - \lambda_2(s)}$$

(for the determination of the remaining terms, see Ref. 1). We compute the integral in Eq. (17) by the method of steepest descents with accuracy up to terms of $1/t^2$:

$$\{N_P(E_0, 0, t)\}^\Gamma \tag{18}$$
$$= \frac{H_1(s) D_1(s)}{s} e^{ys + \lambda_1(s) t} (2\pi \lambda_1''(s) t)^{-1/2} \left[1 + \frac{\alpha(s)}{t}\right],$$

where

$$\alpha(s) = -\frac{1}{2\lambda_1''(s)} \frac{d^2}{ds^2} \ln \frac{H_1(s) D_1(s)}{s}$$
$$+ \frac{1}{8} \frac{\lambda_1^{\mathrm{IV}}(s)}{[\lambda_1''(s)]^2} - \frac{5}{24} \frac{[\lambda_1'''(s)]^2}{[\lambda_1''(s)]^3}.$$

The parameter s is determined from the condition

$$t = -\frac{1}{\lambda_1'(s)} \left[y + \frac{d}{ds} \ln \frac{H_1(s) D_1(s)}{s}\right].$$

The values of the converging functions here are tabulated in Table III.

The cascade curves for $\epsilon_0 = 63.62$ are plotted in Fig. 1. Curve *1* is based on the exact Eq. (18), curve *2* on the approximate formula (16). The curves differ after the maximum by no more than 5%, before the maximum by no more than 15%*, but in this latter region, Eq. (18) has already ceased to be applicable [condition of the applicability of Eq. (18): $t > 1$].

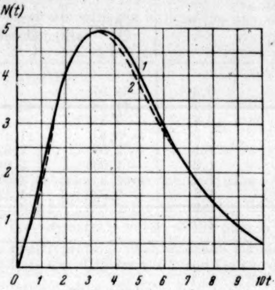

FIG. 1. Cascade curves from a primary photon of energy $\epsilon_0 = 63.62$. Curve *1* is drawn according to Eq. (18), curve *2*, according to Eq. (16).

The cascade curves from photons were also approximated with the help of a sum of Laguerre polynomials:

$$N(t) = e^{-\gamma t} \sum_{n=0}^{k} A_n L_n^0(\gamma t);$$

here

$$L_0^0(x) = 1; \quad L_1^0(x) = 1 - x;$$
$$L_2^0 = 1 - 2x + {}^1/{}_2 x^2, \text{ etc.}$$

According to Eq. (15),

$$A_n = \gamma \int_0^\infty N(t) L_n^0(\gamma t)\, dt; \tag{18'}$$

$$A_0 = \gamma \frac{E_0}{\beta}; \quad A_1 = \gamma \frac{E_0}{\beta} (1 - \gamma \{\overline{t_P}(E_0, 0)\}^\Gamma);$$

$$A_2 = \gamma \frac{E_0}{\beta} (1 - 2\gamma \{\overline{t_P}(E_0, 0)\}^\Gamma + \frac{\gamma^2}{2} \{\overline{t_P^2}(E_0, 0)\}^\Gamma).$$

For approximation by means of the polynomials, we require $N(t)|_{t=0} = 0$. For this, we must now insert the additional term

$$N(t) = e^{-\gamma t} \left(\sum_{n=0}^{k} A_n L_n^0(\gamma t) + C L_{k+1}^0(\gamma t)\right) \tag{19}$$

in the approximating formula. The constant C is determined by the condition

---

[*] We note that the curves differ by more than 15% at very small depths; there the curves change so rapidly that it is difficult to represent the difference in Fig. 1.

TABLE III

s	$\lambda_1^{III}(s)$	$\lambda_1^{IV}(s)$	$D_1(s)$	$\frac{d}{ds} \ln \frac{H_1(s) D_1(s)}{s}$	$\alpha(s)$
0.5	—38.07		1.173	—0.589	
0.7	—11.58	62.9	1.573	—0.475	—0.0924
0.8	— 7.31	33.45	1.79	—0.421	—0.1057
1.0	— 3.43	11.45	2.291	—0.390	—0.0791
1.1	— 2.50	7.62	2.58	—0.384	—0.0503
1.2	— 1.905	5.04	2.89	—0.381	—0.095
1.4	— 1.2	2.52	3.63	—0.391	—0.084
1.6	— 0.829	1.42	4.53	—0.403	—0.193
1.8	— 0.605		5.71	—0.408	
2.0			6.93	—0.417	

$$\{N_P(E_0, 0, t)\}_{t=0}^{\Gamma} = 0. \tag{19'}$$

The cascade curves calculated by Eqs. (16) and (19) for certain values of the primary energy ϵ_0 are drawn in Fig. 2. The curves *1* are drawn according to Eq. (16) for the first two moments ($k = 2$). The triangles denotes points of the curves established by Eq. (19) for $k = 2$ and for the same value of ϵ_0. The curves coincide within 10 percent. Such coincidence (in percent) exists over a wide range of energies ϵ_0, from 0.2 to ~ 100.

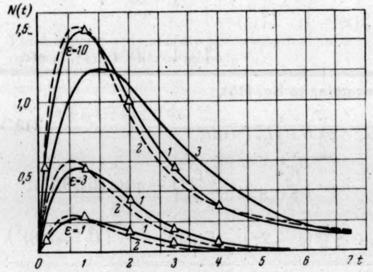

FIG. 2. Cascade curves from a primary photon of energy $\epsilon_0 = 1, 3, 10$. The curves are drawn: *1* – according to Eq. (16) for $k = 2$ [triangular points computed by Eq. (19)]; *2* – according to Eq. (16) for $k=3$; *3* – according to Eq. (16) for $k = 1$.

Thus the approximation by means of the polynomials $L_n^0(x)$ with the additional condition (19′) is completely equivalent to the approximation with the help of the polynomials $L_n^1(x)$ in the energy range from 0.2 to 100 and beyond.

Since we wish to obtain cascade curves for energies E_n^0 of the order of the critical energy β (for which the number of particles at the maximum is of the order of unity (in "cascade" units), and the maximum lies at the order of 1 t-unit in depth), it is particularly important that the approximating curve satisfy the limiting condition exactly, i.e., to obtain the greatest precision in the first t-units of the absorber. In this same Figure, the curves *2* are drawn: these are constructed from Eq. (16) with the use of the three first moments ($k = 2$). Curve *3* was constructed for $\epsilon_0 = 10$ by Eq. (16), using only the single first moment ($k = 1$). It differed from curves *1* and *2* by 30% and more. This demonstrates that the series (16) converges sufficiently rapidly. We recall that the curves corresponding to primary particles of high energy, constructed by Eq. (16) for $k = 2$ differ from the exact by no more than 5%. Taking these two circumstances into account, we can specify that only the three first terms of the series approximate the exact solution with error not exceeding 10%.

Figure 3 shows cascade curves which correspond to a primary photon for from 0.2 to 10, computed by Eq. (16) for $k = 2$. An experimental curve was obtained in carbon in Ref. 13 for a spectrum of primary photons of the form

$$1/E_{\text{where}}\ E < 330 \text{ Mev}, \tag{20}$$

$$\Phi_\gamma(E) = {}_{0 \text{where} E} > 330 \text{ Mev},$$

Averaging the curves (16) over the primary spectrum (20) we can compute the corresponding theoretical curve. The results of the calculation are given

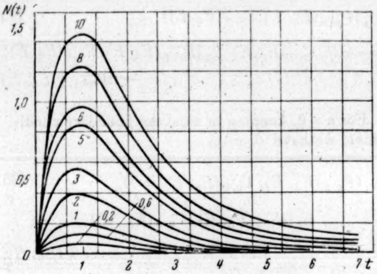

FIG. 3. Cascade curves from a primary photon for ϵ_0 from 0.2 to 10 (number on curve). Curves are constructed from Eq. (16) for $k = 2$.

in Fig. 4: *1* – experimental curve[13], *2* – theoretical curve (normalized for $t = 0.1$). Up to $t = 2$, the

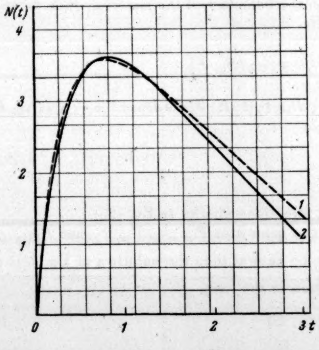

FIG. 4. *1* – experimental curve[13] obtained in graphite for a photon spectrum of the form $1/E$; *2* – obtained by averaging Eq. (16) over a photon spectrum $1/E$.

curves differ from one another by less than 5%; on the tail the difference reaches 20%, the latter because the coefficient γ was assumed to be equal to the asymptotic value of the absorption coefficient of the photons, $\gamma = 0.773$, since the σ of the photons in the energy interval considered is approximately 15% smaller, which leads to large increases in the capacity of the cascade. Making use of the values of the moments $\{\overline{t}_P\}^P$ and $\{\overline{t_P^2}\}^P$, we can compute the cascade curves from the primary electrons. We approximate the cascade curve from the primary electrons with the help of the sum of Laguerre polynomials

$$\{N_P(E_0, 0, t)\}^P \qquad (21)$$

$$= e^{-\gamma t}\left(\sum_{n=0}^{k} A_n L_n^0(\gamma t) + C L_{k+1}^0(\gamma t)\right).$$

We find the constant C from the condition $\{N_P(E_0, 0, t)\}^P_{t=0} = 1$, the constant γ we take equal to the asymptotic value of the photon absorption coefficient σ_0. The cascade curves constructed from Eq. (21) for $k = 2$ and for ϵ_0 running from 1 to 10 are shown in Fig. 5.

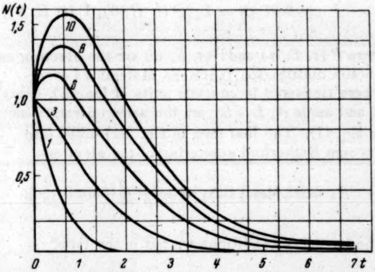

FIG. 5. Cascade curves from a primary electron for ϵ_0 from 1 to 10 (number on curve). The curves are drawn according to Eq. (21) for $k = 2$.

To verify the correctness of the cascade curves for small energies, the energy lost by the electron in radiation for the length of its mean free path was calculated by use of the data of Ref. 14. The electron of energy $\epsilon_0 = 1$ loses $\epsilon_{\text{rad}} \approx 0.3\epsilon_0$ in radiation, the electron with energy $\epsilon_0 = 3$ loses $\epsilon_{\text{rad}} \approx 0.54\epsilon_0$. The ratio of the area under the cascade curve from $t = 0$ to $t \approx E_0/\beta$ and $t \approx E_0/\beta$ to $t = \infty$ must be approximately equal to $(\epsilon_0 - \epsilon_{\text{rad}})/\epsilon_{\text{rad}}$. This ratio for curves computed from Eq. (21) for $\epsilon_0 = 1$ is 2 and for $\epsilon_0 = 3$, is equal to 1.

To estimate the accuracy of the formula, we computed the cascade curve from the primary electron with $\epsilon_0 = 229$ according to exact formulas of the theory (up to terms in $1/t^2$) and according to the approximation (21). The curves after the maximum differ from one another by no more than 5%. Thus, with the help of the method of moments developed above on the basis of "equilibrium" spectrum of Tamm and Belen'kii, one can compute the cascade curves from primary electrons and photons in light elements with errors not exceeding 10% in a broad range of depths and energies ϵ_0 from 0.2 to ~ 100.

2. CASCADE SHOWERS IN HEAVY ELEMENTS

1. We rewrite the basic equations of the cascade theory with account of scattering

$$\cos\vartheta\,\partial P/\partial t = L_1[P(t, E, \vartheta), \Gamma(t, E, \vartheta)] + (E_k^2/4E^2)\,\Delta_\vartheta P(t, E, \vartheta), \qquad (22)$$

$$\cos\vartheta\,\partial\Gamma/\partial t = L_2[P(t, E, \vartheta), \Gamma(t, E, \vartheta)]$$

Here $P(t, E, \vartheta)$ and $\Gamma(t, E, \vartheta)$ are the electron and photon distribution functions at depth t (everywhere measured in cascade units of length), energy E and angle ϑ, L_1, L_2 are the same operators as in Eq. (1). The last term in Eq. (22) takes into account Rutherford scattering of the electrons

$$E_k = 21 \text{ Mev}; \quad \Delta_\vartheta = \frac{1}{\sin\vartheta}\frac{\partial}{\partial\vartheta}\left(\sin\vartheta\frac{\partial}{\partial\vartheta}\right).$$

The boundary conditions we put in the form*

$$P(0, E, \vartheta) = 0; \qquad (23)$$

$$\Gamma(0, E, \vartheta) = \Phi(E_0, E)\,\delta(\vartheta),$$

where E_0 is the upper limit of the spectrum of primary photons. We neglect here the "inverse flow" of particles at $t = 0$. In Ref. 13, it was shown that the number of electrons going through the boundary of the material in the opposite direction is not large (of the order of 5% of the incident beam); therefore, neglect of the inverse flow is reasonable.

The moments of the distribution functions for the shower particles are determined by Eq. (1′). We multiply Eq. (22) by t^n and integrate over t from 0 to ∞, and over all solid angles

$$L_1[P_{n,0}(E_0, E), \Gamma_{n,0}(E_0, E)] = -nP_{n-1,1}(E_0, E), \quad L_2[P_{n,0}(E_0, E), \Gamma_{n,0}(E_0, E)] = -n\Gamma_{n-1,1}(E_0, E). \qquad (24)$$

For $n = 0$, keeping in mind the boundary conditions, we have

$$L_1[P_{0,0}(E_0, E), \Gamma_{0,0}(E_0, E)] = 0, \qquad (25)$$

$$L_2[P_{0,0}(E_0, E), \Gamma_{0,0}(E_0, E)] = -\Phi(E_0, E),$$

where

$$P_{n-i,k}(E_0, E) = \int_0^\infty\int_{(\omega)} P(t, E, \vartheta)\,t^{n-i}\cos^k\vartheta\,d\omega\,dt;$$

$$\Gamma_{n-i,k}(E_0, E) = \int_0^\infty\int_{(\omega)} \Gamma(t, E, \vartheta)\,t^{n-i}\cos^k\vartheta\,d\omega\,dt.$$

If an electron or a photon with energy E_0 is incident on the boundary of the material, then for the quantity

$$P_{(P,\Gamma),0,0}(E_0, E) = \int_0^\infty\int_{(\omega)} P_{(P,\Gamma)}(t, E, \vartheta)\,d\omega\,dt \text{ and } \Gamma_{(P,\Gamma),0,0}(E_0, E) = \int_0^\infty\int_{(\omega)} \Gamma_{(P,\Gamma)}(t, E, \vartheta)\,d\omega\,dt$$

we get equations similar to Eq. (25).

Let the quantities $P_{P,0,0}$, $\Gamma_{P,0,0}$ and $P_{\Gamma,0,0}$, $\Gamma_{\Gamma,0,0}$ be known; then the solution of Eq. (24) can be written in the form

$$P_{n,0}(E_0, E) = n\int_E^{E_0}\{P_{n-1,1}(E_0, E_1)\,P_{P,0,0}(E_1, E) + \Gamma_{n-1,1}(E_0, E_1)\,P_{\Gamma,0,0}(E_1, E)\}\,dE_1, \qquad (26)$$

$$\Gamma_{n,0}(E_0, E) = n\int_E^{E_0}\{P_{n-1,1}(E_0, E_1)\,\Gamma_{P,0,0}(E_1, E) + \Gamma_{n-1,1}(E_0, E_1)\,\Gamma_{\Gamma,0,0}(E_1, E)\}\,dE_1.$$

Integrating Eq. (26) over E from 0 to E_0, and replacing $P_{n-1,1}$ and $\Gamma_{n-1,1}$ by $P_{n-2,2}$ and $\Gamma_{n-2,2}$ we get

---

* Boundary conditions of the type (23) are not essentially different from the case of an arbitrary spectrum of primary particles.

$$\int_0^{E_0} P_{n,0}(E_0, E)\,dE \tag{27}$$

$$= n(n-1)\int_0^{E_0} [P_{n-2,2}(E_0, E')\,F^P_{1,\vartheta}(E') + \Gamma_{n-2,2}(E_0, E')\,F^\Gamma_{1,\vartheta}(E')]\,dE'.$$

Similarly,

$$\int_0^{E_0} \Gamma_{n,0}(E_0, E)\,dE \tag{27'}$$

$$= n(n-1)\int_0^{E_0} [P_{n-2,2}(E_0, E')\,\widetilde{F}^P_{1,\vartheta}(E') + \Gamma_{n-2,2}(E_0, E')\,\widetilde{F}^\Gamma_{1,\vartheta}(E')]\,dE'.$$

Here we introduce the notation

$$F^P_{1,\vartheta}(E) = \int_0^E dE' \int_0^{E'} dE''\,[P_{P,0,1}(E, E')\,P_{P,0,0}(E', E'') + \Gamma_{P,0,1}(E, E')\,P_{\Gamma,0,0}(E', E'')],$$

$$F^\Gamma_{1,\vartheta}(E) = \int_0^E dE' \int_0^{E'} dE''\,[P_{\Gamma,0,1}(E, E')\,P_{P,0,0}(E', E'') + \Gamma_{\Gamma,0,1}(E, E')\,P_{\Gamma,0,0}(E', E'')];$$

$$\widetilde{F}^P_{1,\vartheta}(E) = \int_0^E dE'' \int_0^{E'} dE''\,[P_{P,0,1}(E, E')\,\Gamma_{P,0,0}(E', E'') + \Gamma_{P,0,0}(E, E')\,\Gamma_{\Gamma,0,0}(E', E'')],$$

$$\widetilde{F}^\Gamma_{1,\vartheta}(E) = \int_0^E dE' \int_0^{E'} dE''\,[P_{\Gamma,0,1}(E, E')\,\Gamma_{P,0,0}(E', E'') + \Gamma_{\Gamma,0,1}(E, E')\,\Gamma_{\Gamma,0,0}(E', E'')]$$

and by definition,

$$F^P_{0,\vartheta}(E) = \int_0^E P_{P,0,0}(E, E')\,dE';$$

$$F^\Gamma_{0,\vartheta}(E) = \int_0^E P_{\Gamma,0,0}(E, E')\,dE';$$

$$\widetilde{F}^P_{0,\vartheta}(E) = \int_0^E \Gamma_{P,0,0}(E, E')\,dE';$$

$$\widetilde{F}^\Gamma_{0,\vartheta}(E) = \int_0^E \Gamma_{\Gamma,0,0}(E, E')\,dE'.$$

Consequently, substituting in Eq. (27) $P_{n-3,3}$, $\Gamma_{n-3,3}$ for $P_{n-2,2}$, $\Gamma_{n-2,2}$, etc., we get

$$\int_0^{E_0} P_{n,0}(E_0, E)\,dE = n!\int_0^{E_0} [P_{0,n}(E_0, E)\,F^P_{n-1,\vartheta}(E) + \Gamma_{0,n}(E_0, E)\,F^\Gamma_{n-1,\vartheta}(E)]\,dE, \tag{28}$$

$$\int_0^{E_0} \Gamma_{n,0}(E_0, E)\,dE = n!\int_0^{E_0} [P_{0,n}(E_0, E)\,\widetilde{F}^P_{n-1,\vartheta}(E) + \Gamma_{0,n}(E_0, E)\,\widetilde{F}^\Gamma_{n-1,\vartheta}(E)]\,dE.$$

The functions $F^P_{n,\vartheta}$ and $F^\Gamma_{n,\vartheta}$ are subject to the following recursion relations:

$$F^P_{n,\vartheta}(E) = \int_0^E [P_{P,0,n}(E, E_1)\,F^P_{n-1,\vartheta}(E_1) + \Gamma_{P,0,n}(E, E_1)\,F^\Gamma_{n-1,\vartheta}(E_1)]\,dE_1, \tag{29}$$

$$F^\Gamma_{n,\vartheta}(E) = \int_0^{E_0} [P_{\Gamma,0,n}(E, E_1)\,F^P_{n-1,\vartheta}(E_1) + \Gamma_{\Gamma,0,n}(E, E_1)\,F^\Gamma_{n-1,\vartheta}(E_1)]\,dE_1$$

and similarly for $\widetilde{F}^P_{n,\vartheta}$ and $\widetilde{F}^\Gamma_{n,\vartheta}$.

We multiply Eq. (22) by $\cos^n\vartheta$ and integrate over t from 0 to ∞ and over all solid angles for boundary conditions of the type (23). As a result, we get the following equation

$$L_1(P_{0,n}(E_0, E), \Gamma_{0,n}(E_0, E)] + \frac{E_k^2}{4E^2} \int\limits_{(\omega)} \Delta_\vartheta P_0(E_0, E) \cos^n \vartheta \, d\omega = 0, \tag{30}$$

$$L_2[P_{0,n}(E_0, E), \Gamma_{0,n}(E_0, E)] = -\Phi(E_0, E).$$

In the case of a primary electron with energy E_0, we get equations for the functions $P_{P,0,n}$ and $\Gamma_{P,0,n}$ that are similar to (30), except that on the right side of the equation, there is the term $-\delta(E_0 - E)$, while the right side of the second equation is equal to zero. In the case of a primary photon with energy E_0, the right side of the first equation is equal to zero, while the right side of the second equation is $-\delta(E_0 - E)$ (the equation pertaining to the functions $P_{\Gamma,0,n}$ and $\Gamma_{\Gamma,0,n}$.

Let the functions $P_{(P,\Gamma),0,0}$ and $\Gamma_{(P,\Gamma),0,0}$ be known; then we can write the solution to Eq. (30) in the following form:

$$P_{0,n}(E_0, E) = \int\limits_E^{E_0} \Phi(E_0, E') P_{\Gamma,0,n}(E', E) \, dE', \tag{31}$$

$$\Gamma_{0,n}(E_0, E) = \int\limits_E^{E_0} \Phi(E_0, E') \Gamma_{\Gamma,0,n}(E', E) \, dE'.$$

Substituting Eq. (31) in (38), changing the order of integration in E and E' and making use of Eq. (29), we get

$$\int\limits_0^{E_0} P_{n,0}(E_0, E) \, dE = n! \int\limits_0^{E_0} \Phi(E_0, E) F^{\Gamma}_{n,\vartheta}(E) \, dE \tag{32}$$

and similarly,

$$\int\limits_0^{E_0} \Gamma_{n,0}(E_0, E) \, dE = n! \int\limits_0^{E_0} \Phi(E_0, E) \tilde{F}^{\Gamma}_{n,\vartheta}(E) \, dE.$$

The functions $\tilde{F}^{P}_{n,\vartheta}$ and $\tilde{F}^{\Gamma}_{n,\vartheta}$ coincide with accuracy to a constant multiplier, with similar functions introduced in Ref. 4. With their help, the moments of cascade curves from primary electrons or from photons of energy E_0 can be determined. Consequently, the moments of the cascade curves for an arbitrary spectrum of primary particles can be expressed by the corresponding moment of the cascade curves from a primary electron or photon of energy E_0:

$$\{\overline{t_P^n}(E_0, 0)^{\Phi} = \int\limits_0^{E_0} \Phi_\gamma(E_0, E) \{\overline{t_P^n}(E, 0)\}^{\Gamma} \times \int\limits_0^{E} P_{\Gamma,0,0}(E, E') \, dE' dE \Bigg/ \int\limits_0^{E_0} P_{\Phi,0,0}(E_0, E) \, dE. \tag{33}$$

$$\{\overline{t_\Gamma^n}(E_0, 0)\}^{\Phi} = \int\limits_0^{E_0} \Phi_\gamma(E_0, E) \{\overline{t_\Gamma^n}(E, 0)\}^{\Gamma} \times \int\limits_0^{E} \Gamma_{\Gamma,0,0}(E, E') \, dE' dE \Bigg/ \int\limits_0^{E_0} \Gamma_{\Phi,0,0}(E_0, E) \, dE.$$

Equation (33) can be considerably simplified by use of the conservation law for electrons and protons. For electrons,

$$\int\limits_0^{E_0} P_{P,0,0}(E_0, E) \, dE = \int\limits_0^{E_0} P_{\Gamma,0,0}(E_0, E) \, dE = \frac{E_0}{\beta}. \tag{34}$$

These relations have a simple physical meaning: all the energy of the primary particle in the final total will be dissipated in ionization. It is shown that for photons also, if we consider $\sigma(E)$ as the variable quantity, similar relations are satisfied[5]:

$$\int\limits_{E'}^{E_0} \Gamma_{P,0,0}(E_0, E) \, dE = \int\limits_{E'}^{E_0} \Gamma_{\Gamma,0,0}(E_0, E) \, dE \approx \frac{E_0}{\beta_\Gamma}, \tag{34'}$$

where β_Γ are functions only of the lower limit. The equality (34′) is satisfied only for the condition $E_0 \gg E'$. Numerical calculations carried out in Ref. 5 for various values of E_0 in lead show that (34′) is satisfied to within 5% for $\epsilon_0 > 10 (\epsilon_0 \gg \epsilon')$. Making use of Eqs. (34) and (34′), we can rewrite Eq. (33) in the form

$$\{\overline{t_P^n}(E_0, 0)\}^{\Phi} = \int\limits_0^{E_0} \Phi_\gamma(E_0, E) E \{\overline{t_P^n}(E, 0)\}^{\Gamma} dE \Bigg/ \int\limits_0^{E_0} \Phi_\gamma(E_0, E) E \, dE, \tag{35}$$

$$\{\overline{t_\Gamma^n}(E_0, E_1)\}^{\Phi} = \int\limits_{E_1}^{E_0} \Phi_\gamma(E_0, E) E \{\overline{t_\Gamma^n}(E, 0)\}^{\Gamma} dE \Bigg/ \int\limits_{E_1}^{E_0} \Phi_\gamma(E_0, E) E \, dE.$$

Thus, if the functions $P_{(P,\Gamma),0,n}$; $\Gamma_{(P,\Gamma),0,n}$ are known, we can, by making use of Eq. (2), compute successively all the moments of the cascade curves from the primary electron or photon with energy E_0, and then, making use of Eq. (35) we can successively calculate all the moments of the cascade curve for an arbitrary spectrum of primary particles.

2. The zero moments for our problem are the functions $P_{(P,\Gamma),0,n}$ and $\Gamma_{(P,\Gamma),0,n}$. In Ref. 4, explicit expressions were found for the functions $P_{P,0,n}$ and $P_{P,0,n}$:

$$\{N_P(E,\vartheta)\}^P = \sum_{n=0}^{\infty} f_n^P(\varepsilon)\,P_n(\cos\vartheta); \tag{36}$$

$$f_n^P(\varepsilon) = \frac{2n+1}{4\pi q}\varepsilon_0 \frac{1}{\sqrt{\varepsilon^2+a_n^2}}\left[1-\frac{1}{1+a_n}\varphi(y)\right],$$

where $\varphi(y) = e^{-y}(y+1)\sqrt{y^2+1}$ [the remaining quantities are defined below in Eq. (39)].

Let a photon of energy E_0 be incident on a layer of the material. In the first interaction in the material, a photon can create an electron-positron pair with energy E' for the positron, with probability $W_P(E_0, E')$, or can create a Compton electron and remain a photon of high energy E' with probability $W_{\text{comp}}(E_0, E')$.

For calculation of the differential or integral "equilibrium spectrum", the first photon is equivalent to a secondary particle created by it in the primary act[6]. Consequently,

$$P_\Gamma(E_0, E, \vartheta) \tag{37}$$

$$= \frac{1}{\sigma(E_0)}\left[2\int_E^{E_0} W_P(E_0, E')\,P_P(E', E, \vartheta)\,dE' + \int_E^{E_0} W_{\text{comp}}(E_0, E')\,P_\Gamma(E', E, \vartheta)\,dE'\right],$$

$$\{N_P(E_0, E, \vartheta)\}^\Gamma$$

$$= \frac{1}{\sigma(E_0)}\left[2\int_E^{E_0} W_P(E_0, E')\,\{N_P(E', E, \vartheta)\}^P\,dE' + \int_E^{E_0} W_{\text{comp}}(E_0, E')\,\{N_P(E', E, \vartheta)\}^\Gamma\,dE'\right].$$

For higher energies (greater than 10^7 ev in lead) the probability W_{comp} is very small. Therefore, the second term in (37) can be neglected. Thus, Eq. (37) permits the calculation of P_P and $\{N_P\}^P$ from the known P_Γ and $\{N_P\}^\Gamma$. As shown in Ref. 7, the probability of pair formation, $W_P(E, E')$, can be represented in the form

$$W_P(E, E')\,dE' = \frac{\sigma(E)}{\sigma_0}\frac{dE'}{E}U\left(\frac{E'}{E}\right); \tag{38}$$

$$U\left(\frac{E'}{E}\right) = \left(\frac{E'}{E}\right)^2 + \left(1-\frac{E'}{E}\right)^2 + \left(\frac{E'}{E}\right)\left(1-\frac{E'}{E}\right)\left(\frac{2}{3}-2b\right);$$

$$1/b = 18\ln(191\,Z^{-1/3})$$

with a high degree of accuracy.

The function U is close to unity, and for small energies can be even more accurately replaced by one. Substituting Eqs. (38) and (36) in (37) and carrying out the integration, we get the following for $\{N_P(E,\vartheta)\}^\Gamma$:

$$\{N_P(\varepsilon,\vartheta)\}^\Gamma = \sum_{n=0}^{\infty} f_n^\Gamma(\varepsilon)\,P_n(\cos\vartheta); \tag{39}$$

$$f_n^\Gamma(\varepsilon) = \frac{2n+1}{4\pi q\sigma_0\varepsilon_0}(\varepsilon_0^2-\varepsilon^2)\left[1-\frac{1}{1+a_n}\varphi(y)\right](\varepsilon^2+a_n^2)^{-1/2},$$

where

$$y = \varepsilon/a_n; \quad \varepsilon = qE/\beta; \quad q = 2{,}29;$$

$$a_n = {}^1/_2\,\varepsilon_k\sqrt{n(n+1)/q}.$$

The greatest practical interest is presented by a cascade process which is created in lead by initial photon or electron distributions of the form $1/E$. Numerical calculations of $\{\overline{\tau}_P\}^\Phi$ and $\{\overline{t_P^2}\}$ are carried out exactly for the spectrum $1/E$. For this purpose, it is necessary to know the moments $\{\overline{\tau}_P\}^P$, $\{\overline{\tau}_p\}^\Gamma$ and $\{\overline{t_P^2}\}^\Gamma$ as functions of the upper limit. In accord with Eq. (2),

$$\{\overline{t}_P(E_0, 0)\}^P \tag{40}$$

$$= \frac{1}{q}\int_0^{\varepsilon_0}\left(1+\frac{1}{\sigma(\varepsilon)}\right)\frac{1}{\sqrt{\varepsilon^2+a_1^2}}\left[1-\frac{1}{1+a_1}\varphi\left(\frac{\varepsilon}{a_1}\right)\right]d\varepsilon;$$

$$\{\overline{t}_P(E_0, 0)\}^\Gamma = \frac{1}{q\sigma_0}\int_0^{\varepsilon_0}\left(1+\frac{1}{\sigma(\varepsilon)}\right)\frac{1}{\sqrt{\varepsilon^2+a_1^2}}$$

$$\times\left(1-\frac{\varepsilon^2}{\varepsilon_0^2}\right)\left[1-\frac{1}{1+a_1}\varphi\left(\frac{\varepsilon}{a_1}\right)\right]d\varepsilon+\frac{1}{\sigma(\varepsilon_0)};$$

$$\{\overline{t_P^2}(E_0, 0)\}^P$$

$$= \frac{8\pi}{3\varepsilon_0}\int_0^{\varepsilon_0}\left\{\left[-\frac{\partial f_0^P}{\partial\varepsilon}-\frac{2}{5}\frac{\partial f_2^F}{\partial\varepsilon}\right]\{\overline{t}_P(\varepsilon, 0)\}^P\varepsilon\right.$$

$$\left.+\left[f_0^P(\varepsilon)+\frac{2}{5}f_2^P(\varepsilon)\right]\frac{\{\overline{t}_P(\varepsilon, 0)\}^\Gamma}{\sigma(\varepsilon)}\right\}d\varepsilon;$$

$$\{\overline{t_P^2}(E_0, 0)\}^\Gamma$$

$$= \frac{8\pi}{3\varepsilon_0}\int_0^{\varepsilon_0}\left\{\left[-\frac{\partial f_0^\Gamma}{\partial\varepsilon}-\frac{2}{5}\frac{\partial f_2^\Gamma}{\partial\varepsilon}\right]\{\overline{t}_P(\varepsilon, 0)\}^P\varepsilon\right.$$

$$\left.+\left[f_0^\Gamma(\varepsilon)+\frac{2}{5}f_2^\Gamma(\varepsilon)\right]\frac{\{\overline{t}_P(\varepsilon, 0)\}^\Gamma}{\sigma(\varepsilon)}\right\}d\varepsilon$$

$$+\frac{2}{\sigma(\varepsilon_0)}\{\overline{t}_P(\varepsilon_0, 0)\}^\Gamma.$$

Inasmuch as the dependence of σ on ϵ for lead cannot be given analytically, $\{\overline{t}_P\}^{P,\Gamma}$ and $\{\overline{t_P^2}\}^{P,\Gamma}$ are found by means of numerical integration of Eq. (40). The quantity $\sigma(\epsilon)$ for different ϵ is obtained from Ref. 14. Further, with the help of Eq. (35), which, for a spectrum of the type (20), takes the form

$$\{\overline{t_P^n}(E_0, 0)\}^\Phi = \frac{1}{E_0}\int_0^{E_0}\{\overline{t_P^n}(E, 0)\}^\Gamma dE,$$

the quantities $\{\overline{t}_P(E_0, 0)\}^\Phi$ and $\{\overline{t_P^2}(E_0, 0)\}^\Phi$ are found by numerical integration. These same quantities are computed on the basis of experimental data[13]. Particles are measured experimentally with energy greater than a certain amount. In Ref. 13, the lower limit lay below 1 mev; therefore, the quantities $\{\overline{t}_P(E_0, E^0)\}^\Phi$ and $\{\overline{t_P^2}(E_0, E^0)\}^\Phi$ were computed, E^0 being taken = 0.5 mev. The results of the calculations for the spectrum (20) are

$\overline{t}_{\text{theoret}}$	$\overline{t}_{\text{exp}}$	$\overline{t^2}_{\text{theoret}}$	$\overline{t^2}_{\text{exp}}$
5.89 ± 0.12	5.9 ± 0.2	53.4 ± 2	55 ± 4

The mean value of $\overline{t}$ varies by 1.0%, of $\overline{t^2}$ by 4.0%; however, the difference lies with the errors of the experiment and the calculation. While the theoretical value of $\overline{t}$ for $\sigma = \sigma_0$, without consideration of scattering, is less than the experimental by 33%, for $\sigma = \sigma(\epsilon)$, it is larger than the experimental by about 10%. Making use of the method of construction of cascade curves developed in the first part of this work, we can obtain (for lead) not only the moments but also the cascade curves themselves. We approximate the cascade curves from the primary photon with energy E_0 with the aid of the Laguerre polynomials:

$$\{N_P(E_0, 0, t)\}^\Gamma = \gamma t e^{-\gamma t}\sum_{n=0}^{k} A_n L_n^1(\gamma t). \tag{41}$$

The coefficients A_n are determined by Eq. (15). The coefficient γ is taken to be equal to the minimum value of the absorption coefficient of the most penetrating portion of the radiation--for photons, $\gamma = 0.24$.

The cascade curves computed with Eq. (41) for $k = 2$ are averaged over the spectrum of primary photons of type (20). The results of the calculations are shown in Fig. 6: curve *1* is the experimental transmission curve for lead[13], curve *2* is the calculated curve. The values of curves *1* and *2* differ by less than 5%. Thus the cascade theory satisfactorily describes the development of showers in heavy elements.

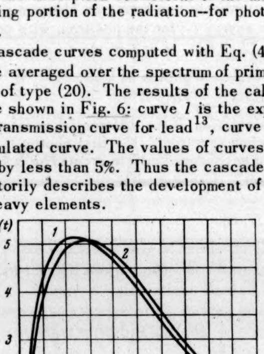

FIG. 6. *1* – experimental curve obtained in lead for a photon spectrum of the form $1/E$; *2* – obtained by averaging Eq. (41) over the photon spectrum of the form (20).

A series of papers by several authors have illuminated the problem under discussion. In Ref. 15, the fundamental equations of cascade theory are solved by a perturbation method. As a first approximation, the solution was used that had been obtained by Snyder[16], who used asymptotic expressions for the cross section of elementary processes. The correction to them was calculated by means of a more accurate approximation of the cross section due to Bethe and Heitler[17]. However, the results obtained by numerical methods are valid only for light elements (where the accurate cross sections of Bethe and Heitler differed only slightly from the asymptotic values) and for initial energies $\ln(E_0/\beta) > 1$. The method developed in Ref. 15 was not applied to heavy elements, where the cross sections of elementary processes change strongly with change of element. In Ref. 18, the basic equations of the theory were solved with approximate cross section of the absorption coefficients of photons and electrons. However, the resultant curves are not satisfactory, since the law of conservation of energy is not satisfied for them--the areas under the curves are approximately $0.6\,E_0/\beta$. Further, the energy spectra of electrons in the maximum shower in air and in lead differ distinctively from each other and from the equilibrium spectrum which was established incorrectly*.

In Ref. 19, an approximate formula was obtained for $N(E_0, E, t)$--the number of particles with energy greater than E at the depth t, created by primary particles with energy E_0:

$$N(E_0, E, t) \tag{42}$$

$$= \frac{e^{K_0}}{\sqrt{t+K_1}} \exp\left(-t + 2\sqrt{(t+K_1)(y+K_2)}\right);$$

$$K_n = K_{n0} + \frac{\varepsilon K_{n1}(Z)}{E+\beta}\,; \quad y = \ln\frac{E_0}{E+\bar{\varepsilon}}\,; \quad \bar{\varepsilon} = \frac{\beta}{2.3}\,,$$

$K_{n,t}$ are constants that depend only on the atomic number Z of the element. The curve computed from Eq. (42) differs (for air) by about 30% from the accurate curve of Snyder. The energy spectra at the maximum of the shower for air and lead differ markedly from the experimental values. At an arbitrary point of the shower they differ significantly for air from the spectra given by the usual cascade theory. All this does not permit us to assume Eq. (42) to be satisfactory for the description of the cascade process.

For individual cases, cascade curves were computed for lead in Ref. 20 by a method of random sampling on a special machine. Here electrons from photons with energies less than 10 mev and Rutherford scattering of charged particles were considered approximately.

In Ref. 5, the values of $\bar{t}$ and $\overline{t^2}$ were computed from an arbitrary spectrum of primary particles, but scattering of shower particles was not considered; the role of the latter is important at low energies. Moreover, there are errors in Ref. 5 for the formulas for

$$\{\bar{t}_P(E_0, E)\}^{P,\Gamma}; \{\overline{t_P^2}(E_0, E)\}^{P,\Gamma} \text{ and } \{\overline{t_P^n}(E_0, E^0)\}^{\Phi}.$$

In conclusion, I express my deep appreciation to S. Z. Belen'kii for his advice and help with the work.

[1] S. Z. Belen'kii, *Cascade processes in cosmic rays*, Gostekhizdat, 1948.

[2] I. Tamm and S. Belen'kii, J. Phys. USSR 1, 177 (1939).

[3] S. Z. Belen'kii, J. Exptl. Theoret. Phys. (U.S.S.R.) 19, 940 (1949).

[4] S. Z. Belen'kii and B. I. Maksimov, J. Exptl. Theoret. Phys. (U.S.S.R.) 22, 102 (1952).

[5] V. Ia. Fainberg, J. Exptl. Theoret. Phys. (U.S.S.R.) 22, 112 (1952).

[6] B. Rossi, *High energy particles*, Gostekhizdat, Moscow, 1955 (Russian translation).

[7] B. Rossi and S. Klapman, Phys. Rev. **61**, 414 (1942).

[8] J. A. Richards and L. W. Nordheim, Phys. Rev. **74**, 1106 (1948).

[9] L. Eyges, Phys. Rev. **74**, 1801 (1948).

[10] B. Rossi and K. Greisen, *The interaction of cosmic rays with matter*, IIL, 1948 (Russian translation).

[11] G. T. Zatsepin, Dokl. Akad. Nauk SSSR **63**, 243 (1948).

[12] N. Lebedev, *Special functions and their application*, 1953.

[13] Blocker, Kenney and Panofsky, Phys. Rev. **79**, 419 (1950).

---

* In cascade theory, it is shown that for arbitrary dependence of the absorption coefficient of photons on the energy spectrum of electrons at maximum must be close to the "equilibrium" spectrum[1].

[14] W. Heitler, *The quantum theory of radiation*, Oxford, 1953.

[15] I. B. Bernstein, Phys. Rev. **80**, 995 (1950).

[16] H. Snyder, Phys. Rev. **53**, 960 (1938).

[17] H. A. Bethe and W. Heitler, Proc. Roy. Soc. (London) **159A** (1937).

[18] N. Dellaporta and E. Clementel, Nuovo Cimento **3**, 235 (1946); **4**, 1 (1947); **5**, 78 (1948).

[19] W. Heisenberg, *Kosmische Strahlung*, Berlin, Springer, 1953.

[20] R. R. Wilson, Phys. Rev. **86**, 261 (1952).

Translated by R.T. Beyer
12

Letters to the Editor

Discrete Energy Losses of Electrons Reflected from a MoO_2 Surface

N. B. Gornyi

(Submitted to JETP editor July 24, 1955)
J. Exptl. Theoret. Phys. (U.S.S.R.) 31, 132-134
(July, 1956)

We have investigated by the method of electronic differentiation in a spherical capacitor circuit[1,2] the discrete energy losses of electrons reflected from a surface of molybdenum coated with MoO_2. The MoO_2 was obtained by heating molybdenum in air with an increased percentage of steam and at a temperature of 800° – 900°. Under these conditions the surface of molybdenum took on the copper-brown color characteristic of MoO_2.

The curves in Fig. 1 represent the energy distribution of the reflected electrons and were obtained at $t = 400°$ and with different energies of the incident electrons V_p. All these curves, except the peak of the elastically reflected electrons, have a series of clearly defined peaks. These peaks, corresponding to the discrete energy losses, are situated near all the curves with identical values for the losses $V_p - V_k$.

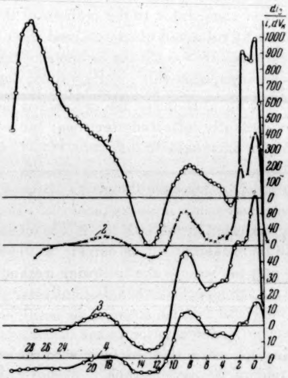

FIG. 1. The distribution curves of the electrons reflected according to (their) energies are obtained from the four values V_p: 1 – 30, 2 – 75, 3 – 150, 4 – 260 v. The maximum of curve 1 when $V_p - V_k = 27$ v is dependent on the true secondary electrons.

TABLE I

h	h	l	W(ev)	$V_p - V_k$(v)
1	0	0	1.6	1.8
0	0	1	4.8	4.5
1	0	1	6.4	6.4
1	1	1	8	8.4
2	2	1	17.6	18.5
0	0	2	19.3	

TABLE II

$n^2 = h^2 + k^2 + l^2$	W(ev)	$V_p - V_k$(v)
1	2.1	2
2	8.3	8.3
3	18.7	17.5

Taking the values $\pm 2\pi n/d$ for the oscillating vector determining the momentum transferred by the electrons of the crystal lattice (in conformance with the theory[3,4]) the discrete values of energies transferred to the incident electrons by the electrons of the crystal lattice can be expressed by the formula

$$W = (h^2 / 8m\pi^2)(2\pi n / d)^2, \qquad (1)$$

where h is Planck's constant, m the mass of the electron and n/d is determined by the corresponding interplane distances in the crystal lattices. For MoO_2, crystallized in a tetragonal lattice,

$$(n/d)^2 = (h^2 + k^2) / a^2 + l^2 / c^2,$$

where h, k and l are Miller indices and $a = 4.86$ A and $c = 2.79$ A are the lattice constants.

The energy losses according to (1) give only one value, $W = 19.3$ ev, which is close to the value of the losses obtained experimentally. The remaining peaks, corresponding to the smallest values of the losses, cannot be interpreted by this formula. However, if we take for the oscillating vector determining the momentum transmitted to

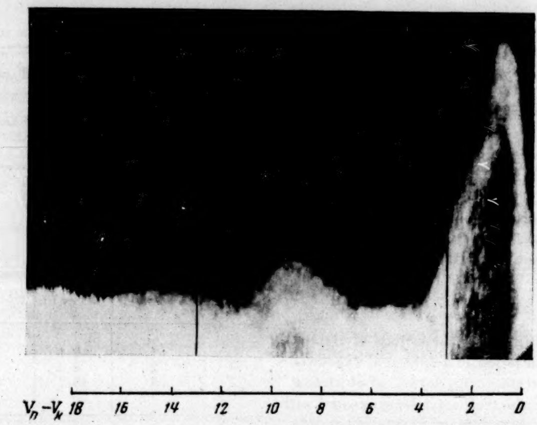

FIG. 2. Photograph obtained by the method described in the text when $V_p = 75$ v and when the exposure $t = 4$ min; in the figure only one-half of the photograph is presented, the second half, being symmetrical with the one presented, is cut off. The distance between the marks corresponds to 10 v.

the electron of the crystal lattice the values $\pm\pi n/d$, which corresponds to the Wulf-Bragg reflection of electron waves, then for the discrete energy losses we obtain the expression:

$$W = \frac{h^2}{8m\pi^2}\left(\frac{\pi n}{d}\right)^2, \tag{2}$$

which describes well all the peaks of discrete losses which we obtained.

In Table I are introduced the values of the losses of energies which were calculated according to (2) for the series of values h, k and l, and likewise the experimental values obtained by us for the discrete losses $V_p - V_k$. All the peaks in the experimental curves for which the values in Table I are introduced are well-defined except for the one when $V_p - V_k = 6.4$ v. From Table I it is seen that the values of the discrete losses $V_p - V_k$, which we obtained experimentally correspond well with the values W calculated according to (2).

Comparing the curves of Fig. 1, one can notice that with the increase of the energy of the incident electrons V_p the possibility of discrete losses of large energies increases, and with the decrease of V_p the possibility of discrete losses of small energies increases. Thus, the ordinate of the peak corresponding to $V_p - V_k = 1.8$v, when $V_p = 30$ v, is almost comparable to the ordinate of the peak of elastically reflected electrons, and when $V_p = 260$ v, it decreases to ~ 0.65; the ordinate of the peak which corresponds to $V_p - V_k = 8.4$ v, when $V_p = 30$ v, is equal to 0.2 of the ordinate of the peak of the elastically reflected electrons, and when $V_p = 260$ v it increases to 0.9 (see Fig. 1, curves *1* and *4*).

In order to decrease the errors introduced into the measurements in consequence of some arbitrary variation in the system, it is necessary to make the measurement as quickly as possible. For this purpose we use the following method, presenting the smoothly changing collector potential and the signal from the output of the amplifier of the electrical differentiation to the oscillograph and photograph while this picture is on the screen of the tube of the oscillograph[5]. Figure 2 is a photograph obtained by us by such a method from the investigated sample when $t = 400°$. Comparing Fig. 2 and curve *2* in Fig. 1, which were obtained with the same V_p's, one can note the following:

1) the peak of the elastically reflected electrons and the peak of the nonelastically reflected electrons when $V_p - V_k = 1.8$ v are resolved well on curve 2 of Fig. 1, and in the photograph in Fig. 2 these two peaks unite into one wide peak; 2) on the photograph there is a peak when $V_p - V_k \sim 13$ v which, in fact, corresponds to the minimum (see Fig. 1, curve 2). This is explained by the fact that the sign of the output of the amplifier, characterizing the derivative, is presented to the oscillograph in the form of a variable voltage, and, therefore, the sign of the derivative cannot be shown--the minima will be recorded in the form of peaks, just as the maxima.

Considering the investigation of nonelastically reflected electrons from cuprous oxide[6] when $V_p = 21.5$ v, there were discovered three alues of discrete losses from which it was possible to compare two with the values obtained by means of the formula (1), and the third value when $V_p - V_k \sim 2$ v was not explained. However, by means of the formula (2) there are obtained values of the discrete losses of energy which correspond well with all the experimental values of $V_p - V_k$ obtained by us (Table II).

For their great help and interest in the experiments, I express thanks to A. Myaniko and R. Reban.

---

[1] N. B. Gornyi, J. Exptl. Theoret. Phys. (U.S.S.R.) 27, 171 (1954).

[2] N. B. Gornyi and L. M. Rhakhovich, J. Exptl. Theoret. Phys. (U.S.S.R.) **26**, 454 (1954).

[3] A. Y. Viatskin, J. Exptl. Theoret. Phys. (U.S.S.R.) 20, 547 (1950).

[4] D. E. Wooldridge, Phys. Rev. **56**, 562 (1939).

[5] A. R. Shul'man and I. I. Farbshtein, Dokl. Akad. Nauk SSSR **104**, 56 (1955).

[6] N. B. Gornyi, J. Exptl. Theoret. Phys. (U.S.S.R.) 27, 649 (1954).

Translated by B. Abbott
16

K-Shell Gamma Ray Internal Conversion Coefficients

L. A. SLIV AND I. M. BANK
Leningrad Physical-Technical Institute,
Academy of Sciences, USSR

(Submitted to JETP editor, February 2, 1956)
J. Exptl. Theoret. Phys. (U.S.S.R.) **31**,
134-136 (July, 1956)

THE most complete of the tables of the K-shell gamma ray internal conversion coefficients * which we have at present (Rose's tables) were established without accounting for the influence of the finite dimensions of the nucleus and of the screening effect. Besides that, there are no data in them for small values of the energies.[1] Consequently, we undertook anew work on the establishment of tables of coefficients of internal conversion (c. i. c.) which would not possess the defects indicated.

Calculations were carried out for 16 elements from $Z = 25$ to $Z = 98$ and for 13 values of energy beginning with energies close to the threshold values and going to $k = 5$ (in units of mc^2). The values of the energies were chosen by such a method that later on it might be possible to interpolate with a sufficient degree of accuracy. In each point the c. i. c. were obtained for the first five electrical and the first five magnetic multipoles.

The relativistic wave functions of the electron were calculated from the potential which inside of the nucleus corresponds to a uniform distribution of the charge and outside of the nucleus has the following form:

$$V = -(\alpha Z/r)\varphi(r) - D + K.$$

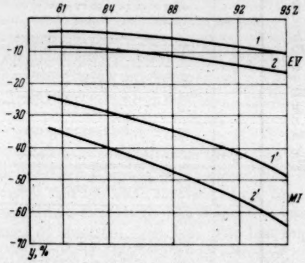

For the curves 1, 1′, $k = 0.5$, for the curves 2, 2′, $k = 5$.

TABLE 1

The *K*-shell coefficients of internal conversion for uranium (Z=92) (in parentheses are given the powers of ten by which one must multiply the appropriate number)

K	α_1	α_2	α_3	α_4	α_5	β_1	β_2	β_3	β_4	β_5
0,25	2,17 (—1)	2.04 (—1)	1.19 (—1)	5,81 (—2)	2,74 (—2)	8.85 (0)	3.90 (1)	4.89 (1)	3.10 (1)	1.48 (1)
0,30	1,43 (—1)	2.09 (—1)	2,88 (—1)	4.01 (—1)	5,79 (—1)	5,28 (0)	2.13 (1)	3,87 (1)	5,54 (1)	7.34 (1)
0.35	1,00 (—1)	1.79 (—1)	3.30 (—1)	6.29 (—1)	1,23 (0)	3,41 (0)	1.28 (1)	2.67 (1)	4.90 (1)	8.72 (1)
0,40	7,39 (—2)	1.47 (—1)	3.14 (—1)	6.89 (—1)	1,55 (0)	2,34 (0)	8.23 (0)	1,82 (1)	3.73 (1)	7.52 (1)
0,50	4,47 (—2)	1.01 (—1)	2.43 (—1)	5,94 (—1)	1.46 (0)	1.26 (0)	3.98 (0)	9.09 (0)	2.00 (1)	4.38 (1)
0,70	2.16 (—2)	5,39 (—2)	1.38 (—1)	3,42 (—1)	8,38 (—1)	4.95 (—1)	1.37 (0)	3.02 (0)	6,54 (0)	1.42 (1)
1.00	1,05 (—2)	2.78 (—2)	6,91 (—2)	1.61 (—1)	3,62 (—1)	1.88 (—1)	4.67 (—1)	9.45 (—1)	1,89 (0)	3.78 (0)
1,50	4.92 (—3)	1.34 (—2)	3.11 (—2)	6,49 (—2)	1,29 (—1)	6.38 (—2)	1.47 (—1)	2.68 (—1)	4,79 (—1)	8.50 (—1)
2.00	2,97 (—3)	8,11 (—3)	1,77 (—2)	3.43 (—2)	6,26 (—2)	2.98 (—2)	6.70 (—2)	1,16 (—1)	1.92 (—1)	3.14 (—1)
3.00	1.50 (—3)	3.98 (—3)	8,15 (—3)	1,44 (—2)	2,37 (—2)	1.02 (—2)	2.33 (—2)	3.79 (—2)	5,79 (—2)	8,61 (—2)
4,00	9,33 (—4)	2,39 (—3)	4,71 (—3)	7.92 (—3)	1,23 (—2)	4.72 (—3)	1,13 (—2)	1,80 (—2)	2,63 (—2)	3.72 (—2)
5,00	6.50 (—4)	1,61 (—3)	3.08 (—3)	5.02 (—3)	7,54 (—3)	2.58 (—3)	6.53 (—3)	1.03 (—2)	1,47 (—2)	2.01 (—2)

Here $\varphi(r)$ is the Thomas-Fermi-Dirac function which we obtained for different elements by the use of the tables of Ref. 2; D is the exchange correction; [3] K is the correction which is introduced for the functions of the free electrons, taking into account the change of potential as a result of the departure of the s-electron.

The potentials of the transition within the nucleus were determined from assumptions on the charge distribution in the volume and on the currents distribution on the surface of the nucleus. The radius of the nucleus is assumed to be equal to $1.2\,A^{1/3} \times 10^{-13}$ cm. As it was shown in Ref. 4, the making of all of the enumerated assumptions more precise can change the final result only by a small percentage. The determination of c. i. c. is made with an accuracy to within 0.5 %. However, the assumptions which are fundamental to the calculations decrease the accuracy of the tables by 2–3 %. All the calculations were carried out on a high-speed electronic calculating machine BESM of the Academy of Sciences. In Table 1 the c. i. c. are given for uranium ($Z = 92$).

The values of c. i. c. which we calculated are everywhere less than the values given by Rose. This is illustrated by Table 2 in which the per cent of decrease of the c. i. c. is shown in comparison with these data (assumed for 100 %). In so far as the calculation of the screening effect in this area gives an unknown correction (~ 1 %), the decrease of the c. i. c. obtained shows how great is the influence of the calculation of the final measurements of the nucleus.

In the Figure, there are introduced the curves of departure γ (in per cent) of the c. i. c. from Rose's data for the transitions *MI* and *EV* depending on Z. A similar dependence on Z takes place also for other multipoles. For $Z < 40$ the calculation of the final measurements of the nucleus does not play a practical role, but the influence of the screening effect grows.

For $Z = 25$ our results coincide with Rose's results (with consideration of the screening effect) with an exactness to within 2 %, everywhere exceeding them. That they exceed his results is the consequence of the fact that the exchange correction, which was not calculated in Rose's computations, was included by us in the potential V.

* The full tables of c. i. c. will be published shortly.

---

*For small energies the c. i. c. were determined only for four Z, with consideration of screening.

TABLE 2

The deviation (decrease) in % of the c. i .c. from the calculations of Rose ($Z=92$)

K	α_1	α_2	α_3	α_4	α_5	β_1	β_2	β_3	β_4	β_5
0,5	1	5.3	9,2	9.9	8.8	41.8	21.3	17,2	14,5	11
1	1,7	9,8	12.3	13	13,2	44.4	22,2	18	16	14.8
4	3,42	14	14.5	14.2	14	54.2	26,2	20,7	18,1	16,6
5	3,1	13	14,3	14.3	14.1	56.5	27.7	21.1	18.6	17.2

---

[1] K. Siegbahn, *Beta and Gamma-ray Spectroscopy*, (1955).

[2] M. Metropolis and J. R. Reitz, J. Chem. Phys. 19, 555 (1951).

[3] L' Brillouin, *L'Atom de Thomas, Fermi et la metode du champ "Self-Consistent "*, (1934). J. R. Reitz, Phys. Rev., 77, 10 (1950).

[4] L. A. Sliv, J. Exptl. Theoret. Phys. (U.S.S.R.) 21, 770 (1951).

B. Abbott
17

Selection Rules for Antiproton Annihilation Into π – Mesons

L. M. AFRIKIAN
The P. N. Lebedev Physical Institute,
Academy of Sciences, USSR
The Institute of Physics,
Academy of Sciences, Armenian SSR

(Submitted to JETP editor February 22, 1956)
J. Exptl. Theoret. Phys. (U.S.S.R.) 31, 136-137
(July, 1956)

IN a previously published article Amati and Vitale[1] have given selection rules for the annihilation of antiprotons into two and three π– mesons. However, following from general considerations which take into account the strong interaction of π– mesons with nucleons, and also on the basis of the already available experimental data[2], the greatest practical interest lies in the effects of the multiple meson annihilation of antiprotons. The present article is devoted to a possible generalization of the selection rules to an arbitrary number of π– mesons being produced, and also contains some remarks on the dependence which follows from these rules of the effective cross sections for annihilation on the velocity of the antiproton in the region of nonrelativistic energies. We shall restrict ourselves to a consideration of strict selection rules which are based on the requirement that the laws of conservation of the total angular momentum and of the space and charge parities be satisfied simultaneously.

We recall that the requirement indicated above leads to the fact that the annihilation of antiprotons in singlet states of the nucleon-antiproton system into two π– mesons is strictly forbidden. On the other hand, in triplet states of such a system, the effects

$$1)\ \tilde{p} + p \rightarrow \pi^- + \pi^+, \quad 2)\ \tilde{p} + n \rightarrow \pi^- + \pi^0$$

can occur only under the condition

$$L_i = 0 \rightarrow L_f = 1, \quad L_i = 2n \rightarrow L_f = 2n \pm 1, \qquad \text{(a)}$$

or

$$L_i = 1 \rightarrow L_f = 0, \quad L_i = 2n \pm 1 \rightarrow L_f = 2n \qquad \text{(b)}$$
$$(n = 1, 2, \ldots),$$

where L_i is the orbital angular momentum of the nucleon-antiproton system; L_f is the orbital angular momentum of the system of two π– mesons. Thus in the triplet nucleon-antiproton system annihilation into two π– mesons [effects (1) and (2)] may occur only under the condition

$$\Delta L = L_f - L_i = \pm 1.$$

A characteristic property of the selection rules for the annihilation into two neutral π – mesons

$$3)\ \tilde{p} + p \rightarrow \pi^0 + \pi^0$$

is the additional restriction on the states of the π– mesons being formed which comes from the requirement that the wave function of the final system should be symmetric with respect to interchanges of identical particles. The last requirement excludes the possibility of states of odd parity for a system of two π^0 – mesons and leads to the additional requirement [in comparison with (1) and (2)] that the transitions (a) be forbidden. Thus the only allowed transitions with formation of two π^0 – mesons for the system of proton-antiproton mutually annihilating each other are the transitions in the spin-triplet state for which

$$L_i = 1 \rightarrow L_f = 0, \quad L_i = 2n \pm 1 \rightarrow L_f = 2n.$$

Thus in the system of a proton and an antiproton being mutually annihilated into two π^0 – mesons the states with the lowest value of the orbital angular momentum are the states ${}^3P_0$ and ${}^3P_2$. This last circumstance makes the transition matrix element for the effect (3) in the region of small energies proportional to the momentum of the antiproton (q). In connection with this, the probability of effect (3) turns out to be proportional to the square of the momentum of the antiproton:

$$\omega_3 = A_3 q^2 / M^2.$$

while the cross section for the effect (3) in a nonrelativistic approximation becomes proportional to the velocity of the antiproton (in the observer's system):

$$\sigma_3 = \omega_3 / v_{\tilde{p}} = A'_3 v_{\tilde{p}} / c.$$

At the same time, the cross sections for the effects (1) and (2), which take place at low velocity in states with zero angular momentum (*S*-wave) have the usual form

$$\sigma_{1,2} = A_{1,2} c / v_{\tilde{p}}.$$

The effects of the annihilation of antiprotons into three π – mesons are not, generally speaking, subject to any strict selection rules. However, in the case of annihilation into three neutral π^0 – mesons

$$4) \quad \tilde{p} + p \rightarrow \pi^0 + \pi^0 + \pi^0$$

the requrement of the conservation of charge parity restricts the possible states of $\tilde{p} - p$ to singlet states with even orbital momentum and to triplet states with odd orbital momentum.

Now going over to the effects of the annihilation of antiprotons into an arbitrary number of π – mesons we shall point out that the following effects are strictly forbidden.

1. Annihilation into an even number of π – mesons in a singlet system with zero (total) orbital angular momentum is strictly forbidden. This selection rule is related to the incompatibility of the requirements of conservation of total angular momentum and of space parity. In view of the fact that in states with zero orbital angular momentum the parities of the initial and final states ($I_{\tilde{N}-N}$ and $I_{(2k)\pi}$) are determined by the intrinsic parities of the particles[3],

$$I_{\tilde{N}-N} = -1, \quad I_{(2k)\pi} = (-1)^{2k} = +1.$$

2. Annihilation into an arbitrary number of neutral π – mesons

$$5) \quad \tilde{p} + p \rightarrow k\pi^0 \quad (k = 4, 5 \ldots)$$

is allowed in triplet states with odd values of the orbital angular momentum and also in singlet states with even values of the orbital angular momentum. Since all the states of the system consisting only of π^0 – mesons are of even charge parity, the initial states of the system of $\tilde{p} - p$ annihilating each other must also be of even charge parity. The states of the system particle – antiparticle noted above are of just that kind (see Ref. 4). The selection rule under discussion is responsible for the smallness of the effect consisting of the annihilation of the triplet nucleon- antinucleon system into an arbitrary number of π^0 – mesons in the nonrelativistic approximation

$$\sigma^{tr}_{k\pi^0} = A_5 v_{\tilde{p}} / c.$$

3. The comparison of the two selection rules given above leads to the annihilation of the $\tilde{p} - p$ system in the state with zero orbital angular momentum into an even number of neutral π – mesons being forbidden. As a result of this in the nonrelativistic approximation the effective cross section for the reaction

$$6) \quad \tilde{p} + p \rightarrow (2k)\,\pi^0 \quad (k = 2, 3, \ldots)$$

is equal to

$$\sigma_{(2k)\pi^0} \approx \sigma^{tr}_{(2k)\pi^0} \approx A_6 v_{\tilde{p}} / c.$$

In conclusion, I wish to express my sincere thanks to Prof. V. L. Ginzburg for the interest shown in this work and for the discussion of results.

---

[1] S. Amati and B. Vitale, Nuovo Cimento **2**, 719 (1955).

[2] I. Brabant, Phys. Rev. **101**, 498 (1956).

[3] V. B. Berestetskii, J. Exptl. Theoret. Phys. (U.S.S.R.) **21**, 93 (1951).

[4] A. I. Akhiezer and V. B. Berestetskii, *Quantum Electrodynamics*, GITTL, 1953, p. 153.

Translated by G. M. Volkoff
18

Remarks on the Theory of Scattering of Particles with a Given Total Angular Momentum

V. T. KHOZIAINOV
Institute for Physical Problems,
Academy of Sciences, USSR

(Submitted to JETP editor February 24, 1956)
J. Exptl. Theoret. Phys. (U.S.S.R.) 31, 138-140
(July, 1956)

1. WE consider the scattering of two fermions interacting by means of a boson field, but, in contrast to the usual treatment of this problem, the initial and final states of the pair of fermions are specified as states with a certain given total angular momentum. It turns out that this approach to the problem presents a number of peculiarities.

It is convenient to separate the motion of the center-of-mass from the relative motion and then to examine the process in the system of coordinates in which the center-of-mass is at rest. The matrix element which corresponds to the simplest irreducible diagram (which is the only one we shall consider for the sake of brevity) may be written in the form

$$\overline{\psi}_{\sigma_1\sigma_2}(k)\,\Gamma^{(1)}D(k-k_0)\,\Gamma^{(2)}\psi_{\sigma_1^0\sigma_2^0}(k_0), \tag{1}$$

where D is the retarded interaction function, $\Gamma^{(i)}$ is the vertex part, the matrix of which operates on the indices of the ith particle; $k(\epsilon, \mathbf{k})$ is the 4-momentum of the particle in the system of coordinates under consideration ($\mathbf{k}_1=-\mathbf{k}_2=\mathbf{k}$); $\sigma_i = \pm ½$ define the spin states of the particles. We consider only the process of interaction which does not lead to the radiation or absorption of bosons and also the case of the absence of external fields. The diagrams which take into account the proper mass of the particles and which are not related to the interaction between the particles are also not taken into account.

The matrix elements of interest to us in the energy-angular momentum space may be most conveniently obtained from the matrix elements of type (1) by a suitable transformation which takes into account the spinor nature of the wave functions[1]

$$\mathfrak{M}^{jm\chi}_{j_0m_0\chi_0} = \sum_{\sigma_1,\sigma_2}\sum_{\sigma_1^0,\sigma_2^0}\iint (dk)\,(dk_0)\,A^{\chi}_{jm}A^{\chi^*}_{j_0m_0}M^{\sigma_1\sigma_2k}_{\sigma_1^0\sigma_2^0k_0}. \tag{2}$$

Here j and m are the quantum numbers of the total angular momentum and of its component, and the index χ characterizes the spin state of the pair of particles (singlet and triplet). The coefficients A^{χ}_{jm}, for example, in the simplest case of the singlet state, have the following form:

$$A^s_{jm} = \delta(k_4-\varepsilon)\,k^{-2}\delta \tag{3}$$

$$\times(|\mathbf{k}|-p)\,Y_{jm}(n_k)\,2\sigma_1\delta_{\sigma_1,-\sigma_2}/\sqrt{2}.$$

In the same way, one may define the coefficient for the triplet case which includes suitable spherical vectors and the required symmetric combinations of spin states (ϵ is the energy, p is the absolute magnitude of the momentum of the particles in the energy-angular momentum space).

By transforming in the manner indicated the matrix element of the zero order approximation to (1) (Möller scattering), for example for the transition singlet → singlet ($\chi = \chi_0 = s$), we obtain an expression of the form

$$e^2A(\varepsilon)\,Q_j(\Delta)\,\delta_{jj_0}\delta_{mm_0},$$

where the form of the function $A(\epsilon)$, which arises as a result of the summation in (2) [similar to (6), see below] depends on the explicit form of the interaction and on the kind of Bose particles, but does not depend on j and m. The argument of Q_j (Legendre function of the second kind) is the quantity $\Delta = 1 + \mu^2/2p^2$ where $p = |\mathbf{k}|$ is the absolute magnitude of the momentum of the particles, and μ is the mass of the boson responsible for the interaction.

In the case of electrodynamics the integration in (2) cannot be carried out formally (if one considers the particles in the initial and final states to be free) since $Q_j(1)$ diverges. For bound states $k^2 \neq m^2$ and the function Δ will contain the binding energy of the particles.

For large $j \gg l$ we have

$$Q_j(1+\mu^2/2p^2) \approx K_0(\mu j/p).$$

Therefore, for not too large initial energies

$\mu j/p \gg 1$ and then $K_0(\mu j/p) \approx \sqrt{\pi p/2j\mu}\, e^{-j\mu/p}$.

As may be seen, the magnitude of the scattering amplitude in this case depends exponentially on the mass of the bosons responsible for the interaction, which makes scattering by means of heavy particles improbable. For energies so large that $j\mu/p \ll 1$ we have $K_0(j\mu/p) \approx \ln(p/j\mu)$, i. e., the scattering amplitude increases logarithmically.

2. Within the framework of perturbation theory the transformation (2) permits one to separate the divergences in a unique way without carrying out the evaluation of the corresponding integrals.

As an example, let us consider the correction to the matrix element which takes into account the loop corresponding to polarization of the vacuum. In the case of electrodynamics, for example, we have

$$e^4\overline{\psi}_{\sigma_1\sigma_2}(k)\,\gamma_\mu^{(1)}\,D_{\mu\sigma}^{(0)}(q)\,T_{\sigma\tau}(\hat{q})\,D_{\tau\nu}^{(0)}(q)\,\gamma_\nu^{(2)}\,\psi_{\sigma_1^\circ\sigma_2^\circ}(k_0); \quad (4)$$

$$D_{\mu\nu}^{(0)} = (\delta_{\mu\nu} - \hat{q}^{-2}q_\mu q_\nu)\,\hat{q}^{-2}; \quad \hat{q} = \hat{k} - \hat{k}_0;$$

$$T_{\sigma\tau}(\hat{q}) = \mathrm{Sp}\int \gamma_\sigma \frac{1}{\hat{q} - \hat{\varkappa} - M}\,\gamma_\tau\,\frac{1}{\hat{\varkappa} - M}\,(d\varkappa).$$

Using the transformation (2) we shall obtain ($\chi = \chi_0 = s$)

$$e^4\int \frac{Y_{jm}^*(\mathbf{n})\,Y_{j_0m_0}(\mathbf{n}_0)}{(\hat{k} - \hat{k}_0)^2} \quad (5)$$

$$\times\, T(\hat{k} - \hat{k}_0)\,\Phi_{jm,\,j_0m_0}^{(\chi,\chi_0)}(k,\ k_0)\,d\mathbf{n}\,d\mathbf{n}_0,$$

where the integration is carried out over the directions of the momenta of the particles; $(\hat{k} - \hat{k}_0)^2 = -2p^2(\Delta - \mathbf{nn}_0)$, $T = 1/3\,T_{\mu\mu}$, and the symbol Φ denotes the sum

$$\Phi = \left(\delta_{\mu\nu} - \frac{q_\mu q_\nu}{\hat{q}^2}\right) \quad (6)$$

$$\times \sum_{\sigma_1,\,\sigma_2}\ \sum_{\sigma_1^\circ,\,\sigma_2^\circ} 2\sigma_1\,\frac{\delta_{\sigma_1,\,-\sigma_2}}{\sqrt{2}}\,2\sigma_2^\circ\,\frac{\delta_{\sigma_1^\circ,\,-\sigma_2^\circ}}{\sqrt{2}}\,(\gamma_\mu)_{k_0\sigma_1^\circ}^{k,\,\sigma_1}\,(\gamma_\nu)_{-k_0,\,\sigma_2^\circ}^{-k,\,\sigma_2}.$$

It may easily be shown that Φ does not depend on the angular variables of integration in (5) which permits one to take Φ outside the integral sign.

Further, we have[2]

$$3T(\hat{q}) = 2(\hat{q}^2 + 8M^2)\,I(\hat{q}) - 12\,I_{\mu\mu}(\hat{q}), \quad (7)$$

$$I_{(\ \ ,\,\mu\mu)}(\hat{q}) = \int \frac{(1,\ \varkappa^2)\,(d\varkappa)}{[(\hat{\varkappa} + \hat{q}/2)^2 - M^2]\,[(\hat{\varkappa} - \hat{q}/2)^2 - M^2]}.$$

Carrying out the integration over the angles (5) under the integral sign (7) (for which we temporarily restrict the region of integration), we shall obtain, taking into account

$$\int \frac{Y_{jm}^*(\mathbf{n})\,Y_{j_0m_0}(\mathbf{n}_0)\,d\mathbf{n}\,d\mathbf{n}_0}{(a - \mathbf{nn}_0)\,(b - \mathbf{nn}_0)\,(c - \mathbf{nn}_0)} \quad (8)$$

$$= 4\pi\left[\frac{Q_j(a)}{(a - b)\,(a - c)} + \frac{Q_j(b)}{(b - a)\,(b - c)} + \frac{Q_j(c)}{(c - a)\,(c - b)}\right]\delta_{jj_0}\delta_{mm_0},$$

the following expression [for example, for $I(q)$]:

$$4\pi Q_j(\Delta)\,I(0) + I_{jR}(\Delta,\ \Delta_\varkappa,\ \alpha), \quad (9)$$

where $I(0)$ is a logarithmically divergent integral and the quantity

$$I_{jR} = \frac{8\pi}{p^4}\int \frac{(d\varkappa)}{\alpha}\int_{-1}^{+1}\left[\frac{Q_j(\Delta_\varkappa + \Delta)}{\Delta_\varkappa} \quad (10)\right.$$

$$\left. - \frac{O_j(\Delta_\varkappa + \Delta - \alpha t)}{\Delta_\varkappa - \alpha t}\right]\frac{dt}{t}$$

($\Delta_\varkappa = -2(\hat{\varkappa}^2 - m^2)/p^2,\ \alpha = 2|\varkappa|/p$) turns out to be finite.

3. Further, let us examine the complete scattering amplitude (1) considering the functions D and Γ to have been renormalized. If the interaction occurs by means of particles of mass μ, then the following representation holds[3]

$$D(\hat{q}^2) = \int \frac{\rho(\lambda^2)\,d\lambda^2}{\hat{q}^2 - \lambda^2 + i\varepsilon}; \quad (11)$$

$$\rho(\lambda^2) = \delta(\lambda^2 - \mu^2) + \sigma(\lambda^2);$$

$$\sigma(\lambda^2) \geqslant 0; \quad \sigma(\lambda^2) = 0 \text{ for } \lambda^2 \leqslant \mu^2; \ \varepsilon \to 0^+.$$

The transformation of the matrix element which contains the function D into the space of the angular momenta is here carried out similarly to the earlier case, so that replacing the upper limit of the integral (11) by a certain quantity Λ^2, and then integrating over the angles under the integral sign we shall find that the matrix element turns out to be proportional to the quantity

$$\int_0^{\Lambda^2} \rho(\lambda^2)\,Q_j(\Delta - \lambda^2/2p^2)\,d\lambda^2.$$

The existence of the scattering amplitude as an observable imposes certain conditions on the function $\rho(\lambda^2)$ in order to guarantee the convergence of the integral. In the case of the angular momentum j the integrand for large values of λ^2 turns out to be proportional to $\rho(\lambda^2)/(\lambda^2)^{j+1}$. Thus only for $j = 0$ is the commonly used condition[4] necessary that $\int \lambda^{-2}\rho(\lambda^2)\,d\lambda^2$ should not diverge at the upper limit. For a collision with an angular momentum $j > 0$ the requirements imposed on the function $\rho(\lambda^2)$ may be relaxed.

---

[1] V. T. Khoziainov, J. Exptl. Theoret. Phys. (U.S.S.R.) 27, 275 (1954).

[2] R. Feynmann, Phys. Rev. 76, 769 (1949).

[3] N. Lehmann, Nuovo Cimento 11, 342 (1954).

[4] Lehmann, Symanzik and Zimmermann, Nuovo Cimento 12, 425 (1955).

Translated by G. M. Volkoff
19

On the Reduction of Wave Equations for Spin 0 and 1 to the Hamiltonian Form

F. I. FEDOROV
The Institute of Physics and Mathematics, Academy of Sciences, Byelorussian SSR

(Submitted to JETP editor February 29, 1956)
J. Exptl. Theoret. Phys. (U.S.S.R.) 31, 140-142 (July, 1956)

RECENTLY Schrödinger[1] and Case[2] have shown that equations for particles of spin 0 and 1

$$(\beta_k \nabla_k + \varkappa)\,\psi = 0, \tag{1}$$

the matrices β_k in which satisfy the well-known conditions of Duffin

$$\beta_i\beta_k\beta_l + \beta_l\beta_k\beta_i = \delta_{ik}\beta_l + \delta_{kl}\beta_i \tag{2}$$

may be reduced to the Hamiltonian form

$$H\psi = i\dot{\psi}, \tag{3}$$

where H is the Hamiltonian operator which has the form

$$H = \gamma_\alpha p_\alpha + \varkappa\gamma_4 \quad (\alpha = 1, 2, 3), \tag{4}$$

while the matrices γ_k ($k = 1, 2, 3, 4$) also satisfy conditions (2). To Eq. (3) we must also add the initial condition of the form

$$(H\gamma_4 - \varkappa)\,\psi = 0, \tag{5}$$

which, in consequence of (3), holds at any arbitrary instant of time. These results are evidently of interest, in particular because they allow one to formulate a theory of particles with spin 0 and 1 (to a large extent by analogy with the well-developed theory of Dirac). In the work by Schrödinger[1] and Case[2] the Hamiltonian form (3) is obtained by resolving Eqs. (1) into their components for a certain specific choice of the matrices β_k. Such a noninvariant method of derivation is unnecessarily awkward and requires separate calculations for spin 0 and spin 1. Moreover, the connection between the matrices γ_k and the initial matrices β_k remains unclear in this method of procedure. The object of the present note consists of showing the method by means of which the reduction to the form (3)-(5) may be carried out simultaneously for spin 0 and 1 without introducing components, and solely on the basis of Eq. (1) and the algebra (2). In the course of the derivation the relation between the matrices γ_k and β_k is also established. The results are generalized to the case of zero rest mass.

Let us write (1) in the form $(\beta_\alpha \nabla_\alpha + \beta_4 \nabla_4 + \varkappa)\psi = 0$ and multiply it by $(1 - \beta_4^2)$ and by β_4^2. Taking into account the fact that $\beta_4\beta_\alpha\beta_4 = 0$ we shall obtain

$$[((\beta_4\beta_\alpha - \beta_\alpha\beta_4)\,\nabla_\alpha + \varkappa\beta_4)\,\beta_4 - \varkappa]\,\psi = 0, \tag{6}$$

$$\beta_4\,[((\beta_4\beta_\alpha - \beta_\alpha\beta_4)\,\nabla_\alpha + \varkappa\beta_4) + \nabla_4]\,\psi = 0. \tag{7}$$

On the basis of (2) it is easily seen that the matrices

$$\gamma_\alpha = i\,(\beta_4\beta_\alpha - \beta_\sigma\beta_4), \quad \gamma_4 = \beta_4 \tag{8}$$

satisfy the same conditions (2) as do β_k and are likewise Hermitian. We note that (8) is easily solved with respect to β_α and gives $\beta_\alpha = -i(\gamma_4\gamma_\alpha - \gamma_\alpha\gamma_4)$. Evidently (6) can be rewritten with the aid of (8) in the form (5) where H is defined by (4) and $p_\alpha = -i\nabla_\alpha$. Thus the initial condition (5) is the result of multiplying (1) by $(1 - \beta_4^2)$. The relation (7) takes on the form

$$\gamma_4\,(H + \nabla_4)\,\psi = 0. \tag{9}$$

We operate on (5) by the operator $\nabla_4 = -i\,\partial/\partial t$, on (9) by the operator H and subtract the results. Taking into account that

$$H\gamma_4 H = \varkappa H, \tag{10}$$

we shall obtain the fundamental Eq. (3).

The method presented above may also be extended to the generalized wave equations of Lehmann[3]

$$(\beta_k \nabla_k + \beta_0)\psi = 0, \quad |\beta_0| = 0 \tag{11}$$

for particles with zero rest mass and with spin 0 and 1. The matrices β_k of these equations satisfy conditions (2), while the matrix β_0 may always be chosen in a projective form: $\beta_0^2 = \beta_0$ (see Ref. 3). For spin 0, Eqs. (11) take on the form

$$\nabla_i \psi_i = 0, \quad \nabla_i \psi_0 + \psi_i = 0 \tag{12}$$

and for spin 1 (Maxwell's equations)

$$\nabla_k \psi_{ik} = 0, \quad \nabla_k \psi_i - \nabla_i \psi_k + \psi_{ik} = 0 \tag{13}$$

[see Ref. 3, Eqs. (8) and (10)]. It is easy to show that in these cases β_0 has the following properties:

$$\beta_0\beta_k + \beta_k\beta_0 = \beta_k; \quad \beta_0\beta_k = \beta_k(1-\beta_0); \tag{14}$$

$$(1-\beta_0)\beta_k = \beta_k\beta_0;$$

from this and from $\beta_0^2 = \beta$ the following relations are also obtained

$$\beta_0\beta_k\beta_0 = 0, \quad \beta_0\beta_i\beta_k = \beta_i\beta_k\beta_0. \tag{15}$$

Multiplying, as before, (11) by $(1-\beta_4^2)$ and by β_4^2, we will correspondingly obtain [taking into account (14) and (15)],

$$[(\gamma_\alpha p_\alpha + \beta_0\gamma_4)\gamma_4 - \beta_0]\psi = 0, \tag{16}$$

$$\gamma_4[(\gamma_\alpha p_\alpha + \gamma_4\beta_0) + \nabla_4]\psi = 0. \tag{17}$$

Here γ_k are defined by (7), and therefore $\beta_0\gamma_\alpha = \gamma_\alpha\beta_0$, $\beta_0\gamma_4 = \gamma_4(1-\beta_0)$. Further,

$$(\gamma_\alpha p_\alpha + \beta_0\gamma_4)(17) - \nabla_4(16) \rightarrow (\gamma_\alpha p_\alpha + \nabla_4)\beta_0\psi = 0. \tag{18}$$

On the other hand,

$$(1-\beta_0)(16) \rightarrow \gamma_\alpha p_\alpha \gamma \beta_0 \psi = 0. \tag{19}$$

We introduce the notation

$$\beta_0\psi = \psi_0, \tag{20}$$

$$\gamma_\alpha p_\alpha = H. \tag{21}$$

As a result of this, Eqs. (18) and (19) take on the form

$$H\psi_0 = i\dot{\psi}_0, \tag{22}$$

$$H\gamma_4\psi_0 = 0. \tag{23}$$

Since in this case

$$H\gamma_4 H = 0, \tag{24}$$

the initial condition (23) is maintained for all time in consequence of (22).

Thus also in the case of particles of zero rest mass one may obtain from Eqs. (11) the Hamiltonian form (22) with the initial condition (23), not for the complete wave function ψ but only for its part $\psi_0 = \beta_0\psi$.

The following circumstance is of interest. Evidently (11) cannot be obtained from (1) by equating to zero the constant $\varkappa = mc/h$ which is proportional to the mass of the particle, even though (11) [in contrast to (1)] describes particles of zero rest mass (see Ref. 4). The situation is different if we adopt a description by means of equations in the Hamiltonian form (3), (5) and correspondingly (21), (23). Indeed, (22) and (23) are directly obtained from (3) and (5) by setting $\varkappa = 0$ (and replacing ψ by ψ). The same also holds for relations (22) and (24),^{0} which are special cases of the corresponding relations (4) and (10) with $\varkappa = 0$.

By decomposing Eq. (22) for the case of spin 0 [see (12)], we shall obtain

$$-p_\alpha\psi_4 = \dot{\psi}_\alpha, \quad p_\alpha\psi_\alpha = \dot{\psi}_4, \tag{25}$$

while (23) gives identically zero, i.e., the initial conditions in this case disappear. It may be easily seen that the four equations (25) are equivalent to the five equations (12). Similarly, relation (22) for the case of Maxwell's equations (13) takes on the form

$$p_\alpha\psi_{\beta 4} - p_\beta\psi_{\alpha 4} = \dot{\psi}_{\alpha\beta}, \quad p_\beta\psi_{\alpha\beta} = \dot{\psi}_{\alpha 4}, \tag{26}$$

while (23) gives $p_\alpha \psi_{\alpha 4} = 0$. Introducing the three-dimensional notation $\mathbf{E} = (i\psi_{\alpha 4})$, $\mathbf{H} = (\psi_{\alpha\beta})$, we obtain for the Hamiltonian equations for the electromagnetic field curl $\mathbf{H} = \dot{\mathbf{E}}$, − curl $\mathbf{E} = \dot{\mathbf{H}}$ with the "initial condition" div $\mathbf{E} = 0$.

Note added in proof: After this letter had been submitted for publication the author learned of an analogous article by Case (see Ref. 5) in which, however, the case of zero rest mass is not considered.

---

[1] E. Schrödinger, Proc. Roy. Soc. (London) A229, 39 (1955).

[2] K. M. Case, Phys. Rev. 99, 1572 (1955).

[3] F. I. Fedorov, Dokl. Akad. Nauk SSSR 82, 37 (1952).

[4] H. J. Bhabha, Rev. Mod. Phys. 21, 451 (1946).

[5] K. M. Case, Phys. Rev. 100, 1513 (1955).

Translated by G. M. Volkoff
20

On the Theories of Multiple Meson Production

L. G. IAKOVLEV
Moscow State University

(Submitted to JETP editor March 9, 1956)
J. Exptl. Theoret. Phys. (U.S.S.R.) 31, 142-144
(July, 1956)

IN the calculations of effective cross sections for multiple production of mesons, integrations are carried out over the momenta (or over the energies) and over the angles of emergence of the product particles. Since exact calculations, taking into account all the conservation laws, are accompanied by great difficulties, various approximate methods of calculation are used. In such calculations the maximum limit for the energy of one of the particles is taken to be equal to the value $\epsilon_n = \mathcal{E} - \sum_{i=1}^{n-1} m_i$ ($\mathcal{E}$ is the total energy of colliding particles, Σm_i is the sum of the rest masses of all the product particles except the given one). The object of this article is to show that these values should be diminished as required by the laws of conservation of energy and momentum. The calculation of the maximum energy and momentum for each product particle is reduced to the problem of finding a conditional extremum.

We shall carry out the calculation in the system of the center of mass. We assume that after the collision n particles in all are formed. We denote the total energy, the momentum and the velocity of the ith product particle by ϵ_i, $\mathbf{k}_i$, v_i, and the corresponding quantities for the product particle being investigated we shall denote by the index n. Then the laws of the conservation of energy and momentum will take on the form:

$$\varepsilon_n + \sum_1^{n-1} \varepsilon_i = \mathcal{E}, \quad \mathbf{k}_n + \sum_1^{n-1} \mathbf{k}_i = 0. \tag{1}$$

It is evident that in order to make k_n a maximum it is necessary that the momenta of all the $(n - 1)$ particles should be directed opposite to the momentum $\mathbf{k}_n$; then

$$k_n = -\sum_1^{n-1} k_i. \tag{2}$$

Let us find v_n:

$$v_n = k_n / \varepsilon_n = \sum_1^{n-1} k_i / (\mathcal{E} - \sum_1^{n-1} \varepsilon_i). \tag{3}$$

It is necessary to find the maximum of the function $v_n(k_1, \ldots, k_{n-1})$ which is defined by Eq. (3) under the condition

$$\left[m_n^2 + \left(\sum_1^{n-1} k_i\right)^2\right]^{1/2} + \sum_1^{n-1} (m_i^2 + k_i^2)^{1/2} = \mathcal{E}, \tag{4}$$

which follows from (1) and from the relations $\epsilon_i = m_i^2 + k_i^2$. The problem is reduced to the solution of the system of equations

$$\partial F(k_1, \ldots, k_{n-1}) / \partial k_j = 0, \quad (j = 1, \ldots, n-1), \tag{5}$$

where $F \equiv v_n + \lambda \mathcal{E}$.

In its expanded form Eq. (5) takes on the form:

$$\frac{1}{\mathcal{E} - \Sigma\varepsilon_i} + \frac{v_j \Sigma k_i}{(\mathcal{E} - \Sigma\varepsilon_i)^2} + \lambda \left[\frac{\Sigma k_i}{\mathcal{E} - \Sigma\varepsilon_i} + v_j\right] = 0. \tag{6}$$

Since λ must satisfy all the equations of the system the equations must be satisfied identically; from this it follows that $v_1 = v_2 = \ldots = v_{n-1} = v$. Then the $(n - 1)$ particles may be considered as a single particle with the mass $M = \sum_{i=1}^{n-1} m_i$ and the velocity v.

From (4) we find

$$k_{n\,\max} = [(\mathcal{E}^2 - M^2 + m_n^2)^2 - 4m_n^2 \mathcal{E}^2]^{1/2} / 2\mathcal{E}, \tag{7}$$

$$\varepsilon_{n\,\max} = {}^1/_2 [\mathcal{E} - (M^2 - m_n^2) / \mathcal{E}],$$

$$v_{n\,\max} = [(\mathcal{E}^2 - M^2 + m_n^2)^2 - 4m_n^2 \mathcal{E}^2]^{1/2} / (\mathcal{E}^2 - M^2 + m_n^2).$$

Sternheimer[1] has calculated the maximum angle of recoil of the nucleon after a collision.

$$\operatorname{tg} \theta_{\max} = (1 - v_c^2)^{1/2} (v_c^2 / v_{\max}^2 - 1)^{-1/2} \tag{8}$$

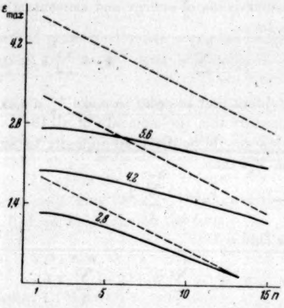

FIG. 1. Maximum energy of a π − meson formed as a result of a $\pi - N$ collision.

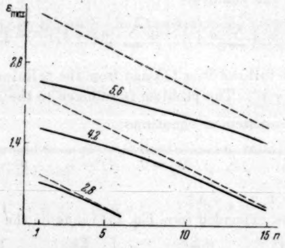

FIG. 2. Maximum energy of a π − meson formed as a result of an $N - N$ collision.

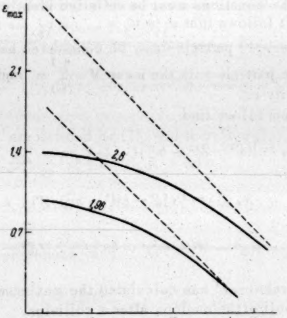

FIG. 3. Maximum energy of a π − meson formed as a result of the annihilation of a nucleon and an antinucleon.

(θ_{max} is the angle in the laboratory coordinate system, v_c the velocity of the system of the center-of-mass in the laboratory system). The author proposes to use θ_{max} as a criterion for identifying particles. Evidently the existence of a maximum angle for nucleon recoil should be taken into account during integration over the angle θ.

In Figs. 1-3 the solid curves represent maximum meson energies in certain reactions. The number of π − mesons produced is plotted along the horizontal axis; the numbers labeling the curves give the total energy of the system; the dotted curves represent results which take into account only the law of conservation of energy which, measured in the system of center-of-mass, is equal to 10^9 ev.

I express my thanks to Prof. D. Ivanenko for discussions.

---

[1] R. M. Sternheimer, Phys. Rev. 93, 642 (1954).

Translated by G. M. Volkoff
21

Polarization of Neutrons Scattered by Carbon Taking Nuclear Volume into Account

N. A. GULIEV
Moscow State University

(Submitted to JETP editor March 10, 1956)
J. Exptl. Theoret. Phys. (U.S.S.R.) 31, 144-146
(July, 1956)

EXPERIMENTS on the double scattering of high energy nucleons by nuclei indicate a considerable polarization of the primary scattered beam[1]. A comparison of the data for light elements (H, Be, He, C) shows that the polarization is independent of the kind of nucleus and shows that the angular distribution is practically unchanged for energies in the range 100-300 mev. One may assume that the scattered particle interacts with the nucleus as a whole. In order to explain polarization accompanying scattering by nuclei with spin 0 it is useful to take into account spin-orbit forces of the form

$$U_{s.o.} = (a / r)\,(dU_1 / dr)\,\sigma l. \tag{1}$$

The complete interaction potential between the nucleon and the nucleus may in such a case be written in the form

$$U(r) = U_1(r) + iU_2(r) + U_{\text{s. o.}}(r) \tag{2}$$

Calculations in which the interaction is represented in the form of a complex rectangular well have led, both in the quasi-classical approximation and also in the exact method of phases (in particular, for nucleons of energy 290 mev scattered by C^{12}), to the appearance in the angular distribution of the polarization coefficient $P(\vartheta)$ of a region in which the sign changes and which corresponds to the region of the first diffraction minimum in the angular distribution of the differential scattering cross section [see Ref. 2 in which the relation between $P(\vartheta)$ and $\sigma(\vartheta)$ is shown]. However, the measurements of polarization do not confirm the presence of a region in which the sign changes. It is, of course, possible that the region in which the sign of the polarization changes is so narrow that it is not accessible to observation at the present time. The measurements of the polarization for a wide group of elements (He, Be, C, Cu, Al) at energies of 100-300 mev have led to the conclusion that the possibly existing region in which the sign changes has been smoothed out. Some authors suppose that the discrepancy between the calculations and the experimental data may be explained by the form of the potential utilized. Because of the factor $(a/r)dU_1/dr$ in the spin-orbit term $\boldsymbol{\sigma}\cdot\mathbf{l}$ the polarization is predominantly an edge effect and the region in which the sign changes is very sensitive to the shape of $U_1(r)$. Apparently the rectangular potential well which was used earlier turns out to be only a rough approximation from the point of view of taking into account the edge effect. One would expect that the smoothing out of its edge, being a better representation of the actual nuclear potential, should give for $P(\vartheta)$ a better agreement with experiment.

Below we present the results of the calculation of the polarization carried out, utilizing a more realistic way of taking into account the influence of the form of the nuclear potential. The static scalar meson field which is a good approximation for the given problem is defined by the equation

$$(\nabla^2 - k_0^2)\varphi = -4\pi\rho. \tag{3}$$

The distribution of the nucleons inside the nucleus is chosen in accordance with the result of Ref. 3

$$\rho = \begin{cases} \rho_0 & \text{for} \quad r \leqslant R_0, \\ \rho_0 (R_0/r)^2 e^{-\alpha(r-R_0)} & \text{for} \quad r \geqslant R_0. \end{cases} \tag{4}$$

Taking into account (4) we obtain from (3)

$$\varphi_1 = a_1(e^{-k_0 r} - e^{k_0 r})/r + c_1 \quad \text{for} \quad r \leqslant R_0, \tag{5}$$

$$\varphi_2 = a_2 r^{-1} e^{-k_0 r} + b_2 r^{-1} e^{k_0 r} Ei(-[\alpha + k_0]r)$$

$$+ d_2 r^{-1} e^{-k_0 r} Ei(-[\alpha - k_0]r) \quad \text{for} \quad r \geqslant R_0,$$

where a_1, c_1, a_2, b_2, d_2 are constants depending on R_0, α, ρ, k_0, g. We assume the spin-orbit forces to be of the form

$$\begin{aligned} &(a/r)(d\varphi_1/dr)\,\boldsymbol{\sigma}\mathbf{l} \quad \text{for} \quad r \leqslant R_0, \\ &(a/r)(d\varphi_2/dr)\,\boldsymbol{\sigma}\mathbf{l} \quad \text{for} \quad r \geqslant R_0, \end{aligned} \tag{6}$$

where $a = \frac{1}{2}\lambda(\hbar/mc)^2$, $\lambda = 15$ as given by Heisenberg[4].

The functions φ_1 and φ_2 can be approximated with sufficient accuracy by the corresponding branches of the parabolas

$$y_1 = -0.248g + 0.029gr^2 \quad \text{for} \quad 0 \leqslant r \leqslant R_0, \tag{7}$$

$$y_2 = -0.41g + 0.183gr - 0.021gr^2 \quad \text{for} \quad R_0 \leqslant r \leqslant 6r_0,$$

where $R_0 = 1.602 \times 10^{-13}$ cm, $\alpha = 0.68 \times 10^{-13}$ cm and $k_0 = 0.675 \times 10^{13}$ cm^{-1}, $r_0 = 10^{-13}$ cm. The radial factor for the spin-orbit forces is replaced correspondingly by $0.058g$ and $-0.032g + 0.143\, g/r$. The coupling constant g varies from $3e$ to $5e$. Thus the total interaction potential between the neutron and the C^{12} carbon nucleus will be of the form

$$U_1(r) = gy_1(1 + i\varepsilon) + 0.058ag^2 \quad \text{for} \quad 0 \leqslant r \leqslant R_0, \tag{8}$$

$$U_{11}(r) = gy_2(1 + i\varepsilon)$$

$$- g^2(0.032 - 0.143r^{-1}) \quad \text{for} \quad R_0 \leqslant r \leqslant 6r_0,$$

$\bar{\epsilon} = 1$ (for energies of 300 mev).

The polarization is defined by the formula

$$P(\vartheta) = \{|f - ig| \tag{9}$$

$$- |f + ig|\} / \{|f - ig| + |f + ig|\};$$

$$f(\vartheta) = -\sum_{l=0}^{L} [(l+1)A_l^+ + lA_l^-] P_l^0(\cos\vartheta); \tag{10}$$

$$g(\vartheta) = -\sum_{l=0}^{L} (A_l^+ - A_l^-) P_l^1(\cos\vartheta),$$

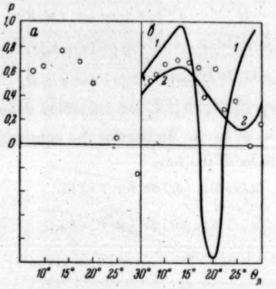

a – polarization of protons on He (E = 315 mev), *b* – the same on C (E = 290 mev). *1* – results of calculation with a rectangular well, *2* – the same, taking into account the volume distribution.

$$A_l^{\pm} = (\exp\{2i\delta_l^{\pm}\} - 1)/2i, \qquad (11)$$

$\delta_l^{\pm}$ is the phase shift for the partial wave with $J = l \pm 1/2$, which we calculate in the WKB approximation; P_l^0, P_l^1 are the Legendre polynomials. The results of the calculation of $P(\vartheta)$ are given by the graph, and show that, because of the more accurate description of the behavior of the potential at the edge of the nucleus by means of introducing a certain nucleon distribution inside it, we have succeeded in obtaining better agreement with experiment. This is explained by the inclusion of higher phases. The polarization remains approximately constant for g varying from $3e$ to $5e$ which can be understood from the nature of the phenomenon. A decrease in ϵ makes the agreement with experiment worse.

In conclusion, I express my thanks to Prof. D. Ivanenko for his continued interest in the work and for the discussion of results.

---

[1] Chamberlain, Wiegand, Segre, Tripp and Ypsilantis, Phys. Rev. 93, 1430 (1954); 95, 1105 (1954).

[2] I. I. Levintov, Dokl. Akad. Nauk SSSR 98, 373 (1954).

[3] N. N. Kolesnikov, Thesis, Moscow State Univ., 1955.

[4] W. Heisenberg, *Theory of the atomic nucleus* (Russian translation), 1953.

Translated by G. M. Volkoff
22

Calculation of Elastic Scattering of Slow Electrons in Hydrogen by the Integral Equation Method

V. I. OCHKUR AND IU. V. PETROV
Leningrad State University

(Submitted to JETP editor March 20, 1955)
J. Exptl. Theoret. Phys. (U.S.S.R.) 31, 146-148
(July, 1956)

THE problem of the elastic scattering of slow electrons by the hydrogen atom, taking exchange into account, was first solved by Morse and Allis[1] by means of a numerical integration of the corresponding integro-differential equation and later by Massey and Moiseiwitsch[2] by means of a variational principle. The object of the present calculation consisted of checking the effectiveness of the method of integral equations proposed by Drukarev[3].

We shall start with the same approximate representation of the wave function of the system "electron + hydrogen atom" which was used by Morse and Allis:

$$\Psi(r_1 r_2) = \psi(r_1) F^{\pm}(r_2) \pm \psi(r_2) F^{\pm}(r_1), \qquad (1)$$

where $\psi(r)$ is the function of the ground state of the hydrogen atom. $F^{+}(r)$ and $F^{-}(r)$ are considered to be spherically symmetric, which means that only s-scattering is taken into account.

With the choice of $\Psi(r_1 r_2)$ made above the functions $f^{\pm}(r) = rF^{\pm}(r)$ must satisfy the equation

$$\left(\frac{d^2}{dr^2} + k^2\right) f^{\pm}(r) = V(r) f^{\pm}(r) \pm 2u(r) \times \int_0^{\infty} u(r') f^{\pm}(r') \left\{\gamma(rr') + \varepsilon - \frac{k^2}{2}\right\} dr' \qquad (2)$$

and the boundary conditions

$$f^{\pm}(0) = 0, \qquad (3)$$

$$f^{\pm}(r) \sim \frac{1}{k} \sin kr + a^{\pm} e^{ikr}, \qquad (4)$$

where

$$V(r) = 2\left\{\int_0^{\infty} u^2(r') \gamma(rr') dr' - \frac{1}{r}\right\}, \qquad u(r) = r\psi(r),$$

$$\gamma(rr') = \begin{cases} 1/r & r \geqslant r' \\ 1/r' & r \leqslant r', \end{cases}$$

ε is the energy of the atom, k is the wave number of the incident electron.

We note that usually[2,4] in order to derive this equation the wave function (1) is substituted into Schrōdinger's equation and after multiplying it by $\psi(r_1)$, and integrating over r_1, Eq. (2) is obtained. In so doing it is generally overlooked that the Schrodinger equation cannot be exactly satisfied by any function of the form (1). However, Eq. (2) may be justified quite rigorously if one uses the variational principle formulated for collision problems.

Using the method indicated by Drukarev[3], Eq. (2) may, by taking (3) into account, be brought to the form of the following two integral equations:

$$X(r) = \varphi_1 + \int_0 K(rs)\, X(s)\, ds, \tag{5}$$

$$Y(r) = \varphi_2 + \int_0^r K(rs)\, Y(s)\, ds, \tag{6}$$

with

$$f^{\pm}(r) = \alpha_1 X(r) + \alpha_2 Y(r). \tag{7}$$

Here the following notation is used:

$$\alpha_1 = f'(0), \quad \varphi_1 = \frac{1}{k}\sin kr; \tag{8}$$

$$\varphi_2 = \frac{1}{k}\int_0^r \sin k(r-s)\, u(s)\, ds;$$

$$\alpha_2 = \int_0^\infty u(s)\, f(s)\left(\frac{1}{s} + \varepsilon - \frac{k^2}{2}\right) ds;$$

$$K(rs) = \frac{1}{k}\sin k(r-s)\, V(s)$$

$$\pm \frac{2}{k}\, u(s) \int_s^r \sin k(r-t)\, u(t)\left(\frac{1}{t} - \frac{1}{s}\right) dt.$$

Substituting (7) into (8) we shall obtain the equation relating α_1 to α_2.

$$\alpha_2 = \alpha_1 \int_0^\infty u(r')\, X(r')\left(\frac{1}{r} + \varepsilon - \frac{k^2}{2}\right) dr' \tag{9}$$

$$+ \alpha_2 \int_0^\infty u(r')\, Y(r')\left(\frac{1}{r'} + \varepsilon - \frac{k^2}{2}\right) dr.$$

This equation and the condition (4) allow us to find both constants and by this, together with (5) and (6), completely determine the solution.

In the antisymmetric case, one may simplify the calculations considerably if one takes into account that the complete wave function is invariant with respect to replacing $f(r) \to f(r) + Cu(r)$, where C is an arbitrary constant. On this basis one may consider either α_1 or α_2 to be arbitrary. In particular, setting $\alpha_1 = 0$ we shall obtain

$$f(r) = \alpha_2 Y(r). \tag{10}$$

Equation (9) then reduces to

$$\int_0^\infty u(r')\, Y(r')\left(\frac{1}{r'} + \varepsilon - \frac{k^2}{2}\right) dr' = 1.$$

Using (6) and the fact that

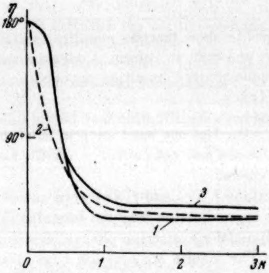

FIG. 1. The scattering phase for the symmetric case: *1* – numerical integration, *2* – variational method, *3* – method of integral equations.

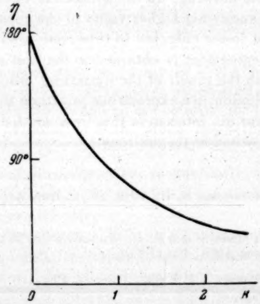

FIG. 2. The scattering phase in the antisymmetric case. The results of all three methods coincide within the scale of the drawing.

$$({}^1/r+\varepsilon)\,u=d^2u\,/\,dr^2,$$

it is not hard to show that this equality is satisfied identically, and that, therefore, it does not amount to some supplementary condition imposed on the function $Y(r)$.

An analogous simplification may be obtained by setting $\alpha_2=0$. But one must keep in mind that the iteration process may not converge equally rapidly in the two cases.

The functions $f^+(r)$ and $f^-(r)$ were calculated in the first approximation from the formulas (5)-(7), (9) and (10) and the scattering phases were found from them. The results are given in Figs. 1 and 2. For comparison, the results of a numerical integration[1] of Eq. (2) and the results a variational calculation[2] are also given there. In the antisymmetric case all three curves coincide within the scale of the drawing. In the symmetric case one obtains a somewhat higher value of the phase for $k>0.5$; at lower energies in this case also a complete agreement is obtained in the first approximation with the result of the numerical integration.

In conclusion, we express our gratitude to G. F. Drukarev for his interest in this work and for a number of valuable suggestions.

---

[1] P. M. Morse and W. P. Allis, Phys. Rev. **44**, 269 (1933).

[2] H. S. W. Massey and B. L. Moiseiwitsch, Proc. Roy. Soc. (London) A205, 483 (1950).

[3] G. F. Drukarev, J. Exptl. Theoret. Phys.(U.S.S.R.) **25**, 139 (1953).

[4] I. A. Erskin and H. S. W. Massey, Proc. Roy. Soc. (London) A212, 521 (1952).

Translated by G. M. Volkoff
23

On the Relation between the Distribution of a Quasi-Monochromatic Stationary Process and the Distribution of its Envelope

IA. I. LIKHTER
Institute for Scientific Research
in Terrestrial Magnetism, the Ionosphere,
and Radio Propagation

(Submitted to JETP editor March 21, 1956)
J. Exptl Theoret. Phys. (U.S.S.R.) **31**,
148-149 (July, 1956)

NOT long ago Blanc-Lapierre and others[1] showed that if the probability density $w_A(A)$ of the envelope of a quasi-monochromatic station-any stochastic process ξ is known, the characteristic function $f_\xi(u)$ of the process is

$$f_\xi(u)=\int_0^\infty w_A(A)\,J_0(Au)\,dA. \tag{1}$$

Rytov[2] continued the calculation and obtained the following formula:

$$w_\xi(\xi)=\frac{1}{\pi}\int_{|\xi|}^\infty \frac{w_A(A)}{\sqrt{A^2-\xi^2}}\,dA, \tag{2}$$

connecting the probability density $w_\xi(\xi)$ of a stationary stochastic process with $w_A(A)$. In the present note I wish to show another way of deriving Eqs. (1) and (2), whereby they are obtained as the zero-order approximation in neglecting the narrow passband width of an amplifier. The use in this derivation of the time average, correct in the case of a stationary stochastic process, gives the possibility of obtaining in a natural manner the correction terms accounting for the finite width of the passband.

A quasi-monochromatic stationary process can be written in the form $\xi(t)=A(t)\cos[\omega_0 t+\varphi(t)]$, where $A(t)$ and $\varphi(t)$ are functions of time varying slowly in comparison with $\cos\omega_0 t$. Then the characteristic function $f_\xi(u)$ is

$$f_\xi(u)=\lim_{T\to\infty}\frac{1}{T}\times\int_0^T \exp\{iuA(t)\cos[\omega_0 t+\varphi(t)]\}\,dt. \tag{3}$$

Let us break up the interval 0, T into N small intervals, each of length $\tau=2\pi/\omega_0$. Then

$$f_\xi(u)=\lim_{N\to\infty}\frac{1}{N}\sum_{m=1}^N\frac{1}{\tau}\times\int_{(m-1)\tau}^{m\tau}\exp\{iuA(t)\cos[\omega_0 t+\varphi(t)]\}\,dt. \tag{4}$$

Taking into account the smallness of the change of $A(t)$ and $\varphi(t)$ in the time τ, we expand the expression under the integral sign in a series in A and φ and limit ourselves to terms of the first order of smallness.

Then after simple transformations we obtain in place of Eq. (4),

$$f_\xi(u)=\lim_{N\to\infty}\frac{1}{N}\sum_{m=1}^{N}\frac{1}{\tau}\tag{5}$$

$$\times\int\limits_{(m-1)\tau}^{m\tau}\exp\{iuA_m\cos(\omega_0t+\varphi_m)\}\,dt$$

$$+\lim_{N\to\infty}\frac{1}{N}\sum_{m=1}^{N}\frac{1}{\tau}\int\limits_0^\tau iu\dot{A}_m\theta\cos(\omega_0\theta+\varphi_m)$$

$$\times\exp\{iuA_m\cos(\omega_0\theta+\varphi_m)\}\,d\theta$$

$$-\lim_{N\to\infty}\frac{1}{N}\sum_{m=1}^{N}\frac{1}{\tau}\int\limits_0^\tau iuA_m\dot{\varphi}\,\theta\sin(\omega_0\theta+\varphi_m)$$

$$\times\exp\{iuA_m\cos(\omega_0\theta+\varphi_m)\}\,d\theta.$$

Here A_m ; φ_m , $\dot{A}_m$, and $\dot{\varphi}_m$ are the values of $A(t)$, $\varphi(t)$, and their derivatives at the beginning of the m th interval. It is easy to see that the first of the sums in Eq. (5) gives Eq. (1); the other two sums give the correction depending on the finiteness of the rate of change of A and φ.

If we use the well-known expression determining the probability density of a stochastic variable in terms of its characteristic function, we obtain from Eq. (5),

$$w_\xi(\xi)=\frac{1}{2\pi}\int\limits_{-\infty}^{+\infty}f_\xi(u)\,e^{-iu\xi}\,du\tag{6}$$

$$=\overline{\frac{1}{\pi\sqrt{A^2-\xi^2}}\left(1+\frac{\dot{\varphi}}{\omega_0}\right)}$$

(In this transformation the second sum in Eq. (5) gives zero.)

In this way Eq. (6) agrees with Eq. (2) to the accuracy of the correction term

$$\overline{\dot{\varphi}/(\pi\omega_0\sqrt{A^2-\xi^2})}.\tag{7}$$

We note that although for a stationary process $\dot{\varphi}$ must be equal to zero, the average value, Eq. (7), may differ from zero, since in increasing the passband, A and $\dot{\varphi}$ in the general case are no longer independent random variables. It is interesting that the rate of change of the amplitude does not influence the probability density $w_\xi(\xi)$ in the first approximation.

We note in closing that in the case in which ξ is obtained by use of a narrow-band filter from a quasi-monochromatic stationary stochastic process, obeying the normal probability distribution law, the correction term in Eq. (6) disappears, and we are left with the correct formula, Eq. (2). This agrees with a well-known property of the normal distribution relating to the linear transformation of the spectral components.

---

[1] Blanc-Lapierre, Savelli and Tortrat, Ann. Télécomm. 9, 237 (1954).

[2] S. M. Rytov, J. Exptl. Theoret. Phys. (U.S.S.R.) 29, 702 (1955); Soviet Phys. JETP

Translated by C. W. Helstrom
24

Atomic Magnetic Moments of Ferromagnetic Metals and Alloys

F. M. GAL'PERIN

(Submitted to JETP editor March 29, 1956)
J. Exptl. Theoret. Phys. (U.S.S.R.) 31, 150-152
(July, 1956)

IN contemporary physics it is well known that on account of the difficulties associated with the many-electron problem, the relation for the quantitative calculation of the atomic magnetic moments m_φ and m_π, for the ferromagnetic and paramagnetic states of ferromagnetics, respectively, has not thus far been found. The relation proposed by us was obtained empirically.

1. *Pure metals.* It is well known that m is expressed as a fractional number of Bohr magnetons M_B (see Table I), and that this fraction is due to the exchange interaction between the s-electrons of the metal and the d- (or f-) electrons of the atoms, as a consequence of which m must somehow depend on the lattice parameter. On this basis we propose that in the equation for m, as well as in Eqs. (3)-(6), there enters the term

$$E=0.641\,[n_1(r_1-R)+n_2(r_2-R)]=E_0+\Delta E,\tag{1}$$

where n_1 is the number of nearest neighbors of an atom in the lattice, n_2 the number of next-nearest neighbors, r_1 and r_2 the corresponding interatomic distances, R an empirical constant characterizing the given transition element, E_0 the integral part of E, and ΔE the fractional remainder, $|\Delta E|<1$.

Let us first examine the first transition series of the periodic table of elements. For it*,

$$R=0.0325\,Z^2+\begin{matrix}30.6182-1.9175\,Z & \text{for} & Z\geqslant 26\\ 27.2382-1.7875\,Z & \text{for} & Z\leqslant 26,\end{matrix}\tag{2}$$

TABLE I. Atomic magnetic moments of ferromagnetic metals and alloys.

Metal	$N_{d(f)}$	$n_1(r_1, \text{Å})$	$n_2\,(r_2, \text{A})$	R, A	Group	$E\,(\Delta E)$	m, M_B calc.	m, M_B exptl.	Relative Error %
Ni φ	2	12 (2.4868)		2.4082	2	0.6 (0,6)	0.6	0.604	< 1
Ni π		12 (2.4868)				0.6 (0,6)	1,6	1.61	< 1
Co φ	3	6 (2.499)	6 (2.507) 6 (2,507)	2.5382	1	−0,27 (−0,27)	1,73	1.715	1
Co π		6 (2.499)				−0,27 (−0,27)	3,27	3,27	1
Fe φ	4	8 (2.4777)	6 (2.8610)	2.7332	1	−0,82 (−0,82)	2.18	2,217	1.6
Fe π		8 (2.4777)				−1.31 (−0,31)	3.31	3,37	2
Gd φ	1 (7)	6 (3,561)	6 (3,629)	3.566	1	0,22 (0,22)	7,22	7,12	1
Gd π		6 (3.561)				0,22 (0,22)	7.78	7.8—7,94	1
Dy φ	4	6 (3.506)	6 (3,585)	2.610	2	7,20 (0,20)	9,20	8,7*	3.8
Dy π		6 (3.506)				7,20 (0,20)	10.20	10.59	
Er φ	2	6(3.466)	6 (3.539)	2.325	2	9,06 (0,06)	9,06	>8.6	
Er π		6(3.466)				9,06 (0,06)	10.06	9,53	5
Mn (in MnAs)	5	2 (2.84)	6 (3.71)	2.8632	1	3,25 (0,25)	3.25	3.40	4.6
Mn (in MnBi)	5	2 (3.06)	6 (4.30)	2.8632	2	5,80 (0,80)	3,20	3,52	10
Mn (in $MnCu_2Al$)	5	12 (4.17)		2.8632	2	10,06 (0,06)	3,94	4.06	3
Cr (in CrTe)	4	2 (3.105)	6 (3.981)	3,0582	2	3.61 (0,61)	2.39	2,39	< 1
Cr (in CrSb)	4	2 (2,726)	6 (4.127)	3.0582	1	3,7 (0,7)	2.7	2.7	< 1
Cr (in CrO_2) φ	4	2 (2.86)	8 (3.429) 4 (4.41)	3.0582	1	5,1 (0,1)	2.1	2.07	< 1
Cr (in CrO_2) π					1	5,1 (0,1)	2.9	2.95	2
Fe (in Ni_3Fe)	4	$2.508 = r_{ab}$	6 (3,546)	2.7332	2	3.13 (0,13)	2.87		
Ni (in Ni_3Fe)	2	$2.489 = R_{ab}$	8 (2.508)	2.4082		0,51 (0,51)	$\frac{-0.49}{2.38^{**}}$ $\overline{m}$ =1,19***	[2,3] ±2.35 ± 0.20 1,21	max 8 2
Mn (in Ni_3Mn)	5	$2,543 = r_{ab}$	6 (3,596)	2,8632	2	2.82 (0,82)	3.18		
Ni (in Ni_3Mn)	2	$2,522 = R_a$	8 (2,543)	2.4082	2	0,69 (0,69)	$\frac{-0.31}{2.87^{**}}$ $\overline{m}$ =1,03***	[2,3] ±2.88 ± 0.20 1.01	max 8 2

* The moment for dysprosium depends on the field. Here the moment is given for the maximal field.

** The difference of the moments of the components of the alloy: $m_{Fe} - m_{Ni}$ and $m_{Mn} - m_{Ni}$.

*** The average moment per atom of the alloy.

where Z is the atomic number of the element.

For the series of elements under consideration, $R = R_s + R_d$ (to an accuracy of 1%), where R_s and R_d are the radii, respectively, of the s- and d-shells of the isolated atom, calculated in the manner of Slater. Let us assume that an analogous relation $R = R_s + R_f$ (R_f = radius of the f-shell of the isolated atom) holds also for Gd, Dy and Er (the third transition series), by the use of which R is calculated for these metals also.

The pure ferromagnetic metals can be divided into two groups: group 1 consists of Gd, Fe and Co, for which $r_1 < R$; group 2 consists of Ni, Dy and Er, for which $r_1 > R$. For the indicated groups

$$m_{\varphi\pi} = N_d + N_f - 2 + E_0 + \frac{i + \Delta E_\varphi}{1 + i \mp \Delta E_\pi}, \tag{3}$$

where N_d and N_f are the numbers of unpaired d- and f-electrons, respectively, in the atom; $i = 1$ for group 1, $i = 0$ for group 2. Here and in what follows, the upper signs in front of ΔE or E are for group 1, the lower signs for group 2. We note that in front of the quantity ΔE, related to the exchange interaction, the opposite sign appears in (3) for group 1. This recalls the change of the positive exchange integral to a negative one in the transition from the ferromagnetic state to the paramagnetic. The integer M_B in m_π is one unit larger than in m_φ

2. *Alloys.* All transition metals, which are paramagnetic in pure form, when entering into ferromagnetic alloys are considered as "pure ferromagnetic" metals (the non-transition elements in alloys are not considered). For them

TABLE II. Curie points of ferromagnetic metals.

Metal	n_1	$N_{d(f)}$	$\Theta_{d(f)}$°K	Θ°K		$\frac{d\Theta}{dP} \cdot 10^3 \cdot \frac{\text{deg}}{\text{atm}}$	
				calc.	exptl.	calc.	exptl.
Ni	12	2	576*	600	631	+0.40	0.35±0.01;[4] 0.441
Co	12	3	1296*	1409	1393	—0.18	—
Fe	8	4	1024*	1045	1043	—0.73	—
Gd	6	7	252	286	289	—1.22	—1.2∓0.05 [4]
Tb	6	6	216	—	200		
Dy	6	4	144	156	155		
Ho	6	3	108	—	—		
Er	6	2	72	80	80		
Tu	6	1	36	—	10?		

* $A = 230\,k$ (experiment: $220\,k$) for Ni, $184\,k$ (experiment: $183\,k$) for Fe, and $946\,k$ for Co. A for groups 1 and 2 corresponds to the increasing and decreasing branches of the curve $A(r_1/R)$.

$$m_{\varphi\pi} = N_d - 2 + \frac{i \pm \Delta E_\varphi}{1 \mp \Delta E_\pi}, \tag{4}$$

where $i = 0$ for group 1 and $i = 1$ for group 2.

The binary alloys are characterized by E_a, E_b and $E_{ab} = 0.641 n_{ab} \cdot (r_{ab} - R_{ab})$; $R_{ab} = c_a R_a + c_b R_b$, where c_a and c_b are the atomic concentrations of components a and b, respectively. For Ni_3Fe and Ni_3Mn, $E_{ab} = 0$ (Table I).

3. *Curie points Θ and their variation with pressure P.* Let us suppose that

$$\Theta_{d(f)} = n_1^2 N_d^2 (N_f^1); \tag{5}$$

$$\text{for Ni, Co and Fe: } A = (1 \pm \Delta E_\Phi) k \Theta_{d(f)},$$

where A = exchange integral, k = Boltzmann constant and n_1 is given in Table II. The change of the Curie point under pressure in units of 10^3 atm is

$$\Theta = \Theta_{d(f)}/1 - 0.1(1 \pm \Delta E);$$

$$\frac{d\Theta}{dP} \cdot 10^3 \frac{\text{deg}}{\text{atm}} = \mp (1 \pm \Delta E). \tag{6}$$

We note that ΔE in Eq. (6) is the same as in Eqs. (3)-(5). Ferrites, manganites and other ferromagnetics, for which $r_1 > R$, make up group 2; and therefore for them, as also for Ni, according to Eq. (6), it follows that one expects the positive sign of the effect; Gd, Fe, Co and invar alloys make up group 1 ($r_1 < R$), and therefore for them one expects the negative sign of the effect.

In Tables I and II data are presented for the calculations with Eqs. (1)-(6); the results agree satisfactorily with experiment, in particular with the data of neutronographic analysis of the magnetic structure of alloys[2,3].

---

* R is computed with the same accuracy (to the fourth decimal place) as r is given experimentally (cf. Ref. 1).

[1] S. V. Vonsovskii, *The Contemporary Study of Magnetism*, Moscow, 1953.

[2] C. G. Shull and M. K. Wilkinson, Phys. Rev. 97, 304 (1955).

[3] G. E. Bacon, *Neutron Diffraction*, Oxford, 1955.

Translated by C. W. Helstrom
25

On the Theory of the Hall Effect in Ferromagnetics

N. S. Akulov and A. V. Cheremushkina

(Submitted to JETP editor March 30, 1956)
J. Exptl. Theoret. Phys. (U.S.S.R.) 31, 152-153
(July, 1956)

IT has been shown that[1,2] the increase of the ohmic resistivity in the disordering of the alloys Fe_3Al is accompanied by a proportional increase in the Hall constant R, i.e., the relation

$$R - R_0 = a(\rho - \rho_0). \quad (1)$$

exists. An analogous relation was also found for the change of R and ρ in the dispersion hardening. In addition, the question has been posed[1,3] of the relation between R and ρ as the temperature T changes. Karplus and Luttinger[3], as a result of developing and making more precise the theory of Samoilovich and Kon'kov[4], found that R as a function of T is proportional to ρ^2. However, an examination of the existing experimental data did not support this conclusion of the theory: The exponent of degree n proved to be less than 2 and different for different elements[5]. Contrary to these results, the measurements given by us for the alloys Fe-Ni gave the following dependence (see the Figure)

$$a = a_0 + a_1\rho. \quad (2)$$

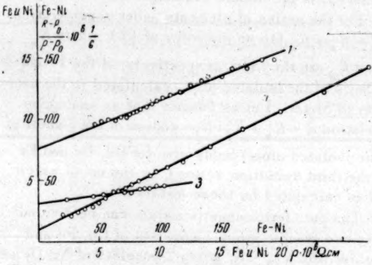

FIG. 1. *1*–Ni, 2–Fe, 3–46% Ni + 53.2% Fe.

In addition, the analysis of experimental data of other authors presented by us showed that the relations (1) and (2) are found to be in good agreement with experiment also for Fe and Ni in the interval from 100° K even to a temperature of the order of 0.8Θ (Θ = Curie point).

From Eqs. (1) and (2) it follows that, besides the Hall effect of the first kind, obeying the theory of Karplus and Luttinger, there exists a Hall effect of the second kind, for which a does not depend on ρ. Thus one can also explain the fractional values of n obtained empirically by the authors mentioned above.

A final solution of the question of the relation between R and ρ is made difficult, however, by the results on the changes of Hall effect at low temperatures, according to which there exists a region where $dR/dT < 0$. The quantum theory of electrical conductivity gives (taking into account the residual resistivity)

$$\rho = \rho_0 + bT^n, \quad (3)$$

where $n = 5$. Meanwhile, the presence of a region of the Hall effect for which $dR/dT < 0$ requires for R the relation

$$R = R_0 + b_1 T^{n_1} + b_2 T^{n_2}, \tag{4}$$

where $b_1 < 0$.

The presence of a negative term in Eq. (4), if it is supported, creates serious difficulties for the present quantum-mechanical theory of the Hall effect and for the establishment of a relation between ρ and R. In particular, it contradicts Eqs. (1) and (2); therefore, further careful investigations are necessary in the region of low temperatures for the resolution of the question of the reality of the existence of the anomalous Hall effect found in Ref. 6.

---

[1] N. S. Akulov and A. V. Cheremushkina, Dokl. Akad. Nauk SSSR 102, 45 (1955).

[2] N. S. Akulov and A. V. Cheremushkina, Dokl. Akad. Nauk SSSR 98, 35 (1954).

[3] R. Karplus and J. Luttinger, Phys. Rev. 95, 1154 (1954).

[4] A. G. Samoilovich and V. A. Kon'kov, J. Exptl. Theoret. Phys. (U.S.S.R.) 20, 783 (1950).

[5] J.–P. Jan, Helv. Phys. Acta 25, 677 (1952).

[6] J.–P. Jan and H. M. Gijsman, Physica 18, 339 (1952).

Translated by C. W. Helstrom
26

The Effect of Ordering on the Energy Spectrum of Phonons

I. M. LIFSHITZ AND G. I. STEPANOVA
Physico-technical Institute,
Academy of Sciences, Ukrainian SSR

(Submitted to JETP editor April 3, 1956)
J. Exptl. Theoret. Phys. (U.S.S.R.) 31, 156-157
(July, 1956)

A METHOD was set forth in Ref. 1 for the study of the vibration spectrum of solid solutions of isotopes. The method devoloped there can be applied to the determination of the spectral density of such solutions in the presence of long-range order. In the case considered, the lattice is divided into two sublattices, for which the probabilities P_i of finding the ith isotope are different and are given by the values

$$P_1^{\mathrm{I}} = 1 - c + \frac{s}{2}\,;\quad P_1^{\mathrm{II}} = 1 - c - \frac{s}{2}\,; \tag{1}$$

$$P_2^{\mathrm{I}} = c - \frac{s}{2}\,;\quad P_2^{\mathrm{II}} = c + \frac{s}{2}\,.$$

The indices I and II denote the types of sites, c = concentration of the second isotope and the quantity s characterizes the degree of order. The value $s = 1$ ($c = \frac{1}{2}$) corresponds to complete ordering of the crystal, the value $s = 0$ to complete disorder.

To make clear the peculiarities of the spectrum, we consider the case of a small difference in masses of the two isotopes. According to the results obtained[1], the spectral density of a system with random distribution of masses can be represented in the form

$$\nu(z) = \nu_0(z) - d\xi / dz, \tag{2}$$

where, for small mass differences,

$$\xi(z) = \frac{1}{N}\left\{ z\nu_0(z) \sum_{\mathbf{r}} \overline{\varepsilon}_{\mathbf{r}} \right. \tag{3}$$

$$+ z^2 \int\limits_{\omega^2(\mathbf{k})=z} \frac{d\Omega}{|\nabla\omega^2|} ⨍ \frac{d\mathbf{k}'}{z - \omega^2(\mathbf{k}')}$$

$$\left. \times \sum_{\mathbf{r},\mathbf{r}'} \overline{\varepsilon_{\mathbf{r}}\varepsilon_{\mathbf{r}'}} \exp\{2\pi i(\mathbf{k} - \mathbf{k}')(\mathbf{r} - \mathbf{r}')\} + \ldots \right\},$$

$$\varepsilon_{\mathbf{r}} = (\overline{m}_{\mathbf{r}} - m_{\mathbf{r}}) / \overline{m}_{\mathbf{r}}. \tag{4}$$

Here z is the square of the frequency, $m_{\mathbf{r}}$ is the value of the mass at site $\mathbf{r}$ ($\mathbf{r} = n_1\mathbf{a}_1 + n_2\mathbf{a}_2 + n_3\mathbf{a}_3$, n_i = an integer, $\mathbf{a}_i$ = lattice constants), the bar denotes averaging, N = total number of atoms, $d\Omega$ is an element of area on the surface $\omega^2(\mathbf{k}) = z$ over which integration is to be carried out, $\nabla\omega^2$ is the gradient in the space of the wave vector $\mathbf{k}$, ⨍ is the principal value of the integral, $\nu_0(z)$ is the unperturbed spectral density; the spectral density is normalized to unity. For a crystal with the distribution of Eq. (1), it is natural to use (for the unperturbed case) the spectral density $\nu_{0\,\mathrm{ord}}$ of a lattice with alternating masses

$$\overline{m}_{\mathrm{I}} = \overline{m}(1 - x),\quad \overline{m}_{\mathrm{II}} = \overline{m}(1 + x), \tag{5}$$

which represent the mean masses at sites of type I and II, respectively. Here $\overline{m} = (1 - c)m_1 + cm_2$, $x = s(m_2 - m_1)/2\overline{m} = s\epsilon/2$. Then

$$\overline{\varepsilon}_{\mathrm{I}} = \overline{\varepsilon}_{\mathrm{II}} = 0,\quad \overline{\varepsilon_{\mathrm{I}}^2} = \left(c - \frac{s}{2}\right)\left(1 - c + \frac{s}{2}\right)\varepsilon^2,$$

$$\overline{\varepsilon_{\mathrm{II}}^2} = \left(c + \frac{s}{2}\right)\left(1 - c - \frac{s}{2}\right)\varepsilon^2$$

and, in accord with (2) and (3), we have

$$\nu(z) = \nu_{0_{\mathrm{ord}}}(z) - \frac{d}{dz}\,\xi_{\mathrm{ord}}(z), \tag{6}$$

$$\xi_{\mathrm{ord}}(z) = \varepsilon^2\left\{ c(1-c) - \frac{s^2}{2}\right\} z^2 \nu_{0_{\mathrm{ord}}}(z) \int_0^{z_g^0} \frac{\nu_{0\mathrm{ord}}(z')}{z-z'}\,dz'. \tag{7}$$

Thus the fluctuating addition, defined by the departure of the actual masses from the mean values $\overline{m}_{\mathrm{I}}$ and $\overline{m}_{\mathrm{II}}$, is proportional to ϵ^2. It is easy to see that for complete order ($s = 1$, $c = \frac{1}{2}$), the additional contribution is zero.

For three-dimensional crystals and sufficiently small values of mass differences for the isotopes, complete ordering does not in general lead to a discontinuity in the frequencies, and, consequently, Eqs. (2) and (3) have meaning for all values of the frequency except the limit frequency z_g^0. When a discontinuity appears, (2) and (3) are not valid close to frequencies which bound the forbidden region. Expressions that are valid for all frequencies, and the displacement of the limiting frequencies, are easily determined by means of another decomposition, shown in Ref. 1.

In many cases, as a consequence of the basic symmetry of the coefficients of interaction, the function $\nu_{0\ \mathrm{ord}}$ can have singularities. For example, if the interaction is limited to nearest neighbors, the spectral density of a simple cubic lattice, for the sites I and II of which we have, respectively, sites with even and odd values of $(n_1 + n_2 + n_3)$, has (near the limit frequencies z_0) singularities of the form

$$\nu_{0\mathrm{ord}} \sim \sqrt{xz_0 / |z_0 - z|}. \tag{8}$$

The frequency gap in this case is

$$z_0^+ - z_0^- \sim 2xz_0. \tag{9}$$

In spite of the fact that (2) and (3) are not valid near z_0 (because of the singularities of $\nu_{0\ \mathrm{ord}}$) we can, with their help, still draw some conclusions on the spectrum of the crystal under investigation.

For complete order, according to the relations obtained, the fluctuating term is equal to zero and the behavior of the spectral density near the limiting frequencies $z_0^{\pm}$ is given by Eq. (8). The frequency gap is a maximum in this case.

With the appearance of disorder, as a result of the drawing together of m_{I} and m_{II}, the frequency gap decreases. Moreover, the increasing fluctuation contribution can materially affect the course of the spectral density near $z_0^{\pm}$. Near the limiting frequencies, the fluctuating term $\Delta\nu$, in accord with (3) and (8), has the form

$$\Delta\nu \sim \frac{\varepsilon}{s}\left\{c(1-c) - \frac{s^2}{4}\right\}\left(\frac{xz_0}{|z_0 - z|}\right)^{3/2}. \tag{10}$$

Hence it is evident that the role of the added term depends on the degree of order. For $xz_0/|z_0 - z \sim 1$, when the increase in $\nu_{0\ \mathrm{ord}}$ is already considerable, the fluctuating term remains small and cannot compensate for the increase if s is not small. For small s, on the other hand, compensation can take place.

In the case of complete disorder, $x = 0$ and the frequency gap vanishes.

---

[1] I. M. Lifshitz and G. I. Stepanova, J. Exptl. Theoret. Phys. (U.S.S.R.) 30, 938 (1956); Soviet Phys. JETP 3, 656 (1956).

Translated by R. T. Beyer
28

CONTENTS – *Continued*

Letters to the Editor:

Discrete Energy Losses of Electrons Reflected from a MoO_2 Surface . . . . N. B. Gornyi 131 31, 132

K-Shell Gamma Ray Internal Conversion Coefficients . . . . L. A. Sliv and I. M. Bank 133 31, 134
Selection Rules for Antiproton Annihilation into π–Mesons . . . I. M. Afrikian 135 31, 136
Remarks on the Theory of Scattering of Particles with a Given Total Angular Momentum . . . . V. T. Khoziainov 137 31, 138
On the Reduction of Wave Equations for Spin 0 and 1 to the Hamiltonian Form . . . . F. I. Fedorov 139 31, 140
On the Theories of Multiple Meson Production . . . . L. G. Iakovlev 141 31, 142
Polarization of Neutrons Scattered by Carbon Taking Nuclear Volume into Account . . . . N. A. Guliev 142 31, 144
Calculation of Elastic Scattering of Slow Electrons in Hydrogen by the Integral Equation Method . . . . V. I. Ochkur and Iu. V. Petrov 144 31, 146
On the Relation between the Distribution of a Quasi-Monochromatic Stationary Process and the Distribution of Its Envelope . . . . Ia. I. Likhter 146 31, 148
Atomic Magnetic Moments of Ferromagnetic Metals and Alloys . F.M. Gal'perin 147 31, 150
On the Theory of the Hall Effect in Ferromagnetics . . . . N. S. Akulov and A. V. Cheremushkina 150 31, 152
The Effect of Ordering on the Energy Spectrum of Phonons . . . . I. M. Lifshitz and G. I. Stepanova 151 31, 156

SOVIET PHYSICS JETP VOLUME 4, NUMBER 1 FEBRUARY, 1957

CONTENTS

The Translation Journals of the American Institute of Physics 1
Direct Measurement of Molecular Attraction of Solid Bodies. II. Method for Measuring the Gap. Results of Experiments . . . . I. I. Abrikosova and B. V. Deriagin 2 31, 3
Elastic Scattering of 310 MEV π^+-Mesons from Protons . . . . E. L. Grigoriev and N. A. Mitin 10 31, 37
On the Problem of Unquantized Relativistically Invariant Renormalized Equations for a Three-Dimensional Extended Particle . . . . Iu. M. Shirokov and D. G. Sannikov 13 31, 113
Temperature Dependence of the Viscosity of Liquid Nitrogen at Constant Density . . . . N. F. Zhdanova 19 31, 14
Production of Positive Pions in $(p-p)$ Collisions at 660 MEV . . V. M. Sidorov 22 31, 178
Investigation of the (d, p) Reaction in Phosphorous and Chlorine . I. B. Teplov 31 31, 25
The Coefficient of Volume Absorption of Second Sound and the Viscosity of the Normal Component of Helium II down to 0.83° K . . . . . . K. N. Zinov'eva 36 31, 31
The Theory of Galvanomagnetic Effects in Metals . . . . I. M. Lifshitz, M. Ia. Azbel' and M. I. Kaganov 41 31, 63
Structure of the Intermediate State of Superconductors . . . . B. M. Balashova and Iu. V. Sharvin 54 31, 40
π^+-Meson Energy Spectrum for $pp \to np\pi^+$ Reaction at 556 and 657 MEV . . . . M. G. Meshcheriakov, V. P. Zrelov, B. S. Neganov, I. K. Vzorov and A. F. Shabudin 60 31, 45
Variational Principles in Hydrodynamics . . . . V. I. Skobelkin 68 31, 317
The Dynamical Magnetic Moment of the Deuteron . . . . A. M. Korolev 73 31, 211
The Production of Charged Mesons by the Bombardment of Beryllium and Carbon with 660 MEV Protons . . . . M. G. Meshcheriakov, I. K. Vzorov, V. P. Zrelov, B. S. Neganov and A. F. Shabudin 79 31, 55
Solution of the Fundamental Diffusion Equation for Cosmic Ray Particles Emitted by a Constant Energy Concentrated Pulsed Source . . . . . . Iu. A. Popov 85 31, 80
The Application of Non Self-Adjoint Operators to Scattering Theory . . . . M. S. Livshits 91 31, 121
Interaction of Nitrogen Nucleus with Nuclei in an Emulsion . . . . D. M. Parfanovich and A. M. Semchinova 99 31, 188
Generalized Phase Analysis as a Corollary of the Unitary Property of the S-Matrix . . . . Iu. F. Gol'fand 103 31, 224
The Antiferromagnetism of Anhydrous Sulfates of Ni^{++}, Fe^{++}, Co^{++} and Cu^{++} . . . . A. S. Borovik-Romanov, V. R. Karasik and N. M. Kreines 109 31, 18
Cascade Showers Produced by Electrons and Photons in Light and Heavy Elements . . . . I. P. Ivanenko 115 31, 86

(*Contents continued on inside back cover*)